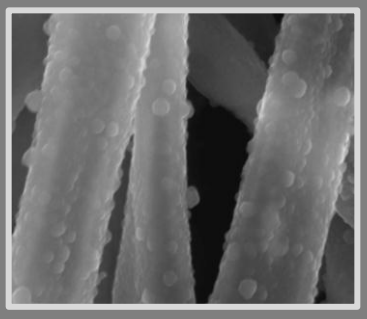
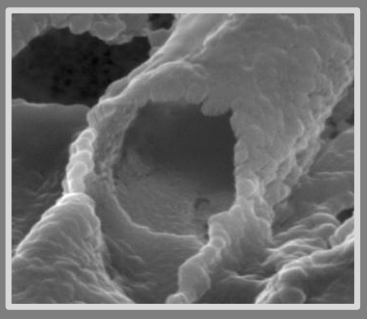
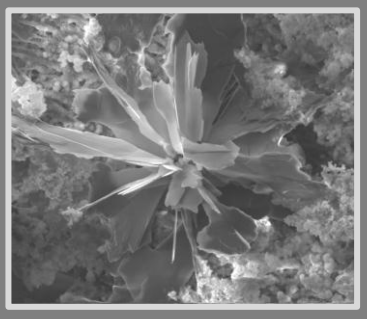
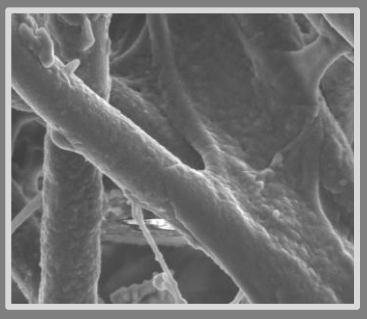

Design of Hybrid Fibers for Bone Tissue Engineering

Nadège Sachot

A thesis submitted for the obtention
of the degree of Doctor of Philosophy

Defence: June 2014

Doctoral Program: Materials Science and Engineering, Technical University of Catalonia, Barcelona

Thesis Supervisor: Dr. Oscar Castano

Department of Materials Science and Metallurgy, ETSEIB, Barcelona
Institute for Bioengineering of Catalonia, Barcelona

A ma maman,

"Damit das Mögliche entsteht, muss immer
wieder das Unmögliche versucht werden."
Hermann Hesse

Acknowledgments

Numerous scientific collaborations and several years of research were necessary to build this thesis. During the difficult moments, my friends and family constantly supported me. For this reason, I would like to express my gratitude to all the persons, scientists or not, who contributed to bring this thesis to an end.

Foremost, I would like to thank Prof. Josep Planell, former director of the Institute for Bioengineering of Catalonia (IBEC) in Barcelona and group leader of the "Biomaterials and Regenerative Therapies" group, for giving me the possibility to conduct my thesis in his laboratory. I particularly also thank Dr. Oscar Castano, supervisor of this thesis, for his guidance, his time, his scientific advices and for trusting in my work. His disponibility was greatly appreciated, as well as his precious help for preparing conferences and writing manuscripts. I further thank the senior researchers of the group, namely Dr. Miguel Angel Mateos Timoneda and Prof. Elisabeth Engel, who also regularly discussed with me the work performed in this thesis.

Some studies presented in the manuscript were partially financed by the European Commission and the "Agencia de Gestio d'Ajuts Universitaris I de Recerca" (AGAUR). These two institutions provided travel grants, enabling me to perform research in various countries and to collaborate with diverse research groups. For this reason, I kindly thank them. I deeply thank as well as all the scientists from the host laboratories who nicely welcomed me. This includes Prof. Malgorzata Lewandowska from the Technical University of Warsaw (WUT), Poland, and her team: Dr. Tomasz Brynk, Tomasz Jaroszewicz, Ewa Kijeńska, Emilia Choińska, Piotr Bazarnik, Dr. Marcin Rasinski and Dr. Agata Rguska. My aknowledgments also go to Prof. Joëlle Amédée from the "Institut National de la Santé et de la Recherche Médicale" (INSERM), Bordeaux, France and her team (Reine Bareille, Robin Siadous, Dr. Sylvain Catros and Dr. Hugo Oliveira) who introduced me to some *in vitro* and *in vivo* assays. I also thank Prof. Aldrik Velders for his kind supervision during my stay at the University of Wageningen (WU), Netherlands and his collaborators, in particular Dr. Junyou Wang, Rui Carvalho and Maria Oikonomou, who teached me how to use their devices and always find time to answer my questions.

More personally, I would like to thank the persons who cross my road during my research stays abroad and who simply became my friends (if not already listed above, i.e Emilia, Rui and Maria): Camille Ehret, Céline Charbonneau, Yunus Sariçay, Katarzyna Zalewska-Wierzbicka, Gosia Wlodarczyk-Biegun and Marcin Biegun.

Further acknowledgments are expressed to my labmates (Riccardo Levato, Aitor Sanchez Ferrero, Xavier Punet, Tiziano Serra, Laura Gomez Rubio, Dr. Arlyng Gonzalez and Dr. Soledad Perez) who shared with me these four years, their knowledge and most of all, their friendship. A huge thank you as well to Yassine Maazouz and David Pastorino who always found time for a short talk between their experiments and who often shared with me their free time.

It is also a pleasure to acknowledge the Gorska family (Gabriela, Michal, Pawel and Malgorzata) who hosted me at their home during my stay in Poland and became very close friends. My gratitude goes as well to Judit Roda and her daughter, Maria, for hosting me in Barcelona till the end of my PhD after my research stays abroad. Their support and kindness during the thesis writing were greatly appreciated. Thank you to all these persons for considering me as part of their family and daily caring about me.

With a particular attention, I would like to thank Ben and Norman for believing in me, supporting me in my professional decisions, providing me precious advices and being always ready to help me whenever I need. Thank you so much.

On the other hand, I am immensely thankful to my friends from Switzerland, namely Raphael, Gregory, Amaury, Andreas, Matthias and Nicolas, for visiting me in Barcelona, always caring about me despite the distance and for simply being such wonderful friends. From France, I would like to especially express my gratitude to Pierre-Alain, Nicolas, Ludwine, Elodie, Emilien, Marie, Guillaume, Pierre, Thomas, Geoffrey and Louise who not only supported me during my PhD but who encouraged me since the early beginning of my studies. Mathieu and Lucie are also particularly thanked for our regular diners when I came back home and for their unwavering friendship. Finally, I would like to say thank you to my other friends, Peter and Karin, Alex, Jong-Eun, Sebastien, Edouard and Sabine with who I spent unforgettable moments, who contributed to my happiness in Barcelona and who are keen to keep contact despite our different current locations.

Finally, these acknowledgements would not have been complete without thanking my family. I address special thanks to my brother, Adrien, and my sister, Charlène, for regularly sending me news from home and for encouraging me to persevere during studies struggles. Thanks also to my lovely nephews, Quentin and Valentin, for the time spend in front of the webcam, for their drawings and for their smiles when coming back in France. In addition, I thank Claude for being good supports for all of us. My ultimate acknowledgment is addressed to my wonderful mother. I thank her for her eternal care, for always finding the right words to motivate me and for being a perfect example of loyality, honesty, tenacity and so much more. More than acknowledgements, I am expresssing her all my admiration, gratitude and love. Maman, merci pour tout!

Abstract

Most of the conventional organic-inorganic composite materials developed for bone tissue engineering do not possess intimate interactions between their constituents. As a consequence, they generally degrade in a non-homogeneous manner and easily lose their integrity under mechanical load. On the other hand, their bioactive phase (i.e. inorganic) is often masked by the polymeric one, resulting in a non optimal bioactivity. To overcome these problems, hybrid materials can be produced. Hybrids are composites that exhibit an improved synergy between their compounds at the nanoscale. Using the sol-gel method and the electrospinning technique, it has been possible to deposit two kinds of hybrid fibers: one constituted by a silicon-calcium-phosphate bioactive glass and polycaprolactone, and the other by a titanium-calcium-phosphate-sodium bioactive glass and polylactic acid. Both biomaterials showed a promising potential for bone regeneration due to their inherent composition and ability to trigger specific cellular responses such as osteo and angiogenesis. However, the interactions between the phases in such hybrids are considered as "weak" because hybrids are simply prepared by blending the different compounds together. Therefore, a new protocol has been implemented to create hybrid fibers with strong chemical interactions between the glass and the polymer. This strategy is based on a coating approach and enables the fabrication of scaffolds with controllable properties (surface roughness, composition, stiffness). This protocol represents a significant step forward towards the development of functional artificial 3D biomaterials aimed for tissue engineering and opens valuable perspectives of work for the future, especially in terms of materials' design.

Keywords: bone tissue engineering, biomaterials, hybrid fibrous scaffolds, electrospinning, sol-gel method, bioactive glasses, synthetic polymers, osteogenesis, vascularization.

Introduction

Organs, muscles and fat of the human body are supported by the skeleton, which provides the structure of the organism. The skeleton is constituted by a hard tissue named "bone". In an adult, 206 bones are counted and they represent around 15% of the average adult's total body mass. Bones fulfill essential functions such as protection of internal organs, production of red and white blood cells, support of body structure, mobility, and storage of minerals, growth factors and fats. Bone is therefore a very important body constituent for the mechanism of the body's activity.

Unfortunately, bone can suffer from many injuries or defects that can arise from a variety of causes. This includes, for example, fracture non union, trauma, tumor removal or musculo-skeletal disorders. If the damage is small, bone possesses the remarkable ability to self-repair. But, when the damage is larger than a critical size, bone is no longer capable of self-healing. In this case, strategies have to be developed to help bone to recover its functionalities or even to regenerate. Currently, bone replacement surgeries are therefore performed. Most of them rely on the grafting of autologous bone (i.e. harvested from the patient own body); a graft considered as the "gold standard" for such procedure. However, it is associated to donor site morbidity and its supply is limited. As an alternative, allografts can be used (i.e. harvested from another patient) but they carry the risk of disease and infection transmission, and possible immunological response from the host. Consequently, a novel interdisciplinary research field as emerged to develop biomaterials for tissue regeneration. This field is known as "Tissue Engineering" and is devoted to the development of artificial materials able to trigger specific cellular responses involved in tissue formation. For bone tissue engineering, these materials should specifically trigger osteo and angiogenesis, while simultaneously providing a suitable mechanical support. They should ideally be bioactive, biocompatible, match the mechanical properties of natural bone and be progressively replaced by the new formed tissue. This way, a fully functional and healthy bone could be regenerated and no additional surgical procedure would be required to remove the implanted materials.

Many materials have been developed to produce these bioactive and biodegradable substitutes as, for example, polymers (synthetic or natural), ceramics and glasses. But, when implanted as single phases and processed with the required porosity, these materials did not appear to be 100% satisfactory because they did not exhibit bioactivity (polymers) or were very fragile (ceramics, glasses). Though, both the lack of bioactivity and suitable mechanical properties are important for the targeted application. Therefore, to overcome these limitations, composite materials have been designed with the aim to produce scaffolds with the combined properties of their constituents. In particular, sol-gel derived bioactive glasses associated to polymers (hybrid materials) have been shown to be promising as they yield to homogeneous materials that have an excellent compromise between bioactivity and toughness. This strategy enables

moreover the creation of templates with good phase interactions at the nano level and offers the possibility to precisely control these interactions. Materials with good stability and tailored degradation can be obtained by this way. Despite these advantages, such materials constitute a novel emerging concept and some optimizations are required. In fact, many of the hybrid materials developed up to date were based on the combination of a polymer and silica. As a result, even though presenting some bioactivity, the bioactive potential of these materials was restricted to a certain extent. It is only quite recently that researchers started to introduce calcium and phosphate in the glass network prepared by the sol-gel method to provide osteoinductivity to the biomaterial. On the other hand, the design of these materials has mainly been limited to the fabrication of foams and monoliths. Thus, the field of hybrid materials still offers various working perspectives for the development of materials able to improve the healing process of injured bone.

Numerous material considerations have to be taken into account to develop hybrid materials, especially because of their interactions with the surrounding biological environment. Indeed, the composition of the material, its mechanical properties and its architecture influence the cellular responses. Cell survival, signaling, proliferation and differentiation are directly affected by the physical and chemical cues that deliver the scaffold. These properties have also an impact on the mineralization process of the material. It is therefore very important to select properly the constituents of the material and the material fabrication technique. One of the most popular processing techniques is electrospinning. It allows the deposition of micro and nano fibers of a variety of materials and the production of templates that mimic the fibrous structure of the collageneous-based matrix of native bone. Using the sol-gel method and the electrospinning, it was believed that grafts with remarkable properties for bone tissue engineering could be furthermore developed, and biological performance of hybrid scaffolds even be enhanced. Given the socioeconomic consequences that could be induced by treating patients with injured bone, finding solutions for the critical defects that bone cannot repair by itself became particularly essential.

Objectives and thesis outlines

Knowing the importance of bone for the body's activity, restoring bone tissue functions or helping to its repair has become a major concern for the scientific community and biomedical companies. As this research field is relatively new, many improvements in the material development are expected to be done in the future. Therefore, this thesis focuses on the fabrication and characterization of novel hybrid scaffolds for bone tissue engineering; especially on the combinations of one of two synthetic polymers (polycaprolactone PCL and polylactic acid PLA) and one of two bioactive glasses (silicon- and titanium-based glasses). Three different materials are presented in this thesis. All were prepared by using the sol-gel method and the electrospinning technique.

In chapter 1, a literature review is made to provide the reader the essential information necessary to understand the concepts related to this thesis and the state of the art behind this work.

The chapter 2 reports the development of hybrid silicon-calcium-phosphate/PCL electrospun fibers, obtained through the preparation of a glass-polymer blend. This study aimed to fabricate homogeneous fibers with different compositions, to demonstrate the role of such scaffolds in the triggering of osteo and angiogenesis, and to optimize the electrospinning processing parameters to obtain a continuous fiber deposition.

The chapter 3 focuses on the development of hybrid titanium-calcium-phosphate-sodium/PLA electrospun fibers, also produced through the preparation of a glass-polymer blend. These fibers were fabricated to show that this glass, usually prepared by melting method, could be processed using the sol-gel method and be used in the same way than the other silicon-calcium-phosphate glass. In addition to its physicochemical and mechanical characterization, in parallel, the material biodegradation and biological performances were assessed.

The chapter 4 describes the development of novel fibers based on the silicon-calcium-phosphate/PLA glass system and prepared by a new material fabrication approach. The aim of this work was to implement a totally novel protocol to create materials that possess covalent bonding between their constituents and exhibit immediate good biological responses. This was achieved through the coating of polymeric fibers with different glass compositions. The fibers were investigated in terms of their physico-chemical and mechanical properties. Preliminary cellular assays were also conducted.

Finally, in chapter 5, the significance of the work and the contributions to the 'material science' and 'tissue engineering' fields are summarized. Its limitations are also discussed and the future perspectives of work that this thesis provides are described.

In the context of a rapidly but active ageing world population, the need of suitable synthetic materials is clear. The objectives of this thesis were therefore set according to the future demands on bone tissue engineering and the problems currently reported in the literature on artificial materials.

Table of Contents

List of Figures

CHAPTER 1
Literature review

CHAPTER 2
Electrospun hybrid fibers prepared with silicon-calcium-phosphate bioactive ORMOGLASSES and polycaprolactone

CHAPTER 3

Electrospun hybrid fibers prepared with a titanium-calcium-phosphate-sodium bioactive ORMOGLASS and polylactic acid

CHAPTER 4

Polylactic acid electrospun fibers covalently coated with silicon-calcium-phosphate bioactive ORMOGLASSES

CHAPTER 5

General discussion and conclusion

APPENDICES

List of Tables

List of Abbreviations

Ɛ Dielectric constant

ΔH_c Heat of cold crystallization

ΔH_m Heat of fusion

3D Three-dimensional

α-MEM Minimum essential Eagle medium

a.u Arbitrary unit

Ca^{2+} Calcium ion

T_g Glass transition temperature

T_m Melting transition temperature

AFM Atomic force microscopy

ALP Alkaline phosphatase

ANOVA Analysis of variance

APTES Aminopropyltriethoxysilane

CaSR Calcium sensing receptor

cDNA Complementary deoxyribonucleic acid

Col I Collagen I

COOH Carboxylic

DSC Differential scanning calorimetry

DMT Derjaguin–Muller–Toporov

ECM Extracellular matrix

EDS Energy dispersive X-Ray spectroscopy

EtOH Ethanol

EPC Endothelial progenitor cell

FESEM Field-emission scanning electron microscopy

FTIR Fourier transform infrared spectroscopy

GADPH Glyceraldehyde 3-phosphate dehydrogenase

HA Hydroxyapatite

HE Hematoxylin Eosin

HEPES 4-(2-hydroxyethyl)-1-piperazineethanesulfonic acid

MetEtOH Methoxyethanol

MSC Mesenchymal stem cell

MT Masson's trichrome

NMR Nuclear magnetic resonance

OH Hydroxyl

OPN Osteopontin

OCN Osteocalcin

ORMOGLASS Organically modified glass

PBS Phosphate buffered saline

PCL Poly (caprolactone)

PCR Polymerase chain reaction

PGA Poly (glycolic acid)

PLA Poly (lactic acid)

PLLA Poly (L-lactic acid)

PLDA Poly (D-lactic acid)

RIPA Radioimmunoprecipitation assay

RGD Arginine glycine aspartic acid

SBF Simulated body fluid

SEM Scanning electron microscopy

TEOS Tetraethylorthosilicate

TEP Tri-ethylphosphate

TGA Thermogravimetric analysis

UV Ultraviolet

VEGF Vascular endothelial growth factor

VEGFR Vascular endothelial growth factor receptor

vWF Von Willebrand factor

XRD X-ray diffraction

Chapter 1

Literature review

1.1. Bone Tissue: structure and physiology

Although constituted by cartilage, marrow, nerves and blood vessels, bone is mainly formed by a hard mineralized solid structure referred as "bone tissue" (or osseous tissue). Bone tissue is a strong and tough connective tissue that supports the skeleton rigidity and presents a complex and highly hierarchical organized structure [1]. Morphologically, it can be subdivided into two distinct bone types according to their porosity and unit microstructure: the cortical bone (also known as compact bone) and the trabecular bone (also called cancellous or spongy bone) [2]. The cortical bone is distinguished by its high density (low porosity and void spaces) and represents the higher mass percentage of the total bone mass of an individual (around 80%). It is typically forming the outer shell of most bones and supports the mechanical properties of the skeleton. The trabecular bone is defined by its low density and accounts for the other 20% of the total bone mass of an adult. It possesses a significantly high surface area and its high porosity allows room for blood vessels and bone marrow. Unlike cortical bone which provides the structural support, the trabecular bone, found in the internal part of bone extremities, is mainly involved in metabolic activity.

Cortical and trabecular bones are both made of nearly the same organic and inorganic components (**Figure 1-1**). The combination of these two phases of different nature makes of bone a composite tissue. Each component phase contributes to the unique mechanical properties of bone. These properties depend on the structural organization of each phase [2]. In a general point of view, it is commonly accepted that the organic part provides elasticity and flexibility to the bone, whereas the inorganic one provides rigidity and load-bearing strength [1]. The major organic constituents are collagens organized in fibril bundles that form a 3D nano scaled collageneous matrix network [2,3]. Proteoglycans, noncollageneous macromolecules (other proteins like osteocalcin, osteopontin, BMP-2…) [1] and cells complete the organic composition. The inorganic component is mainly constituted by carbonated hydroxyapatite; a calcium phosphate mineral with low amount of carbonate that nucleates and grows along the collagen fibrils epitaxially. Collagen and hydroxyapatite, among other minor components, form together the bone extracellular matrix (ECM) and provide structural support to the cells that are present in the bone structure. The microstructure of the bone matrix differs between the cortical and the trabecular bone. This explains the differences in terms of properties (stiffness, porosity, functions…) [2]. The cortical bone exhibits a parallel alignment of collagen layers. These concentric layers are called lamellae [1–3]. They form osteons and are densely packed. In the center of these cylindrical structures, in the Haversian's Canal, nerves and blood vessels are found. Blood vessels come from the Volkmann's canals that are connected to the Haversian's Canal and assure the transmission of the blood vessels from the periosteum (exterior layer of the cortical bone) into the bone. This enables the supply of the nutrients and oxygen to the cells and the removal of detritus. The microstructure of trabecular bone, in contrast, is rather formed by an interconnecting framework of individual trabecula (single osteons) and marrow filled cavities [1].

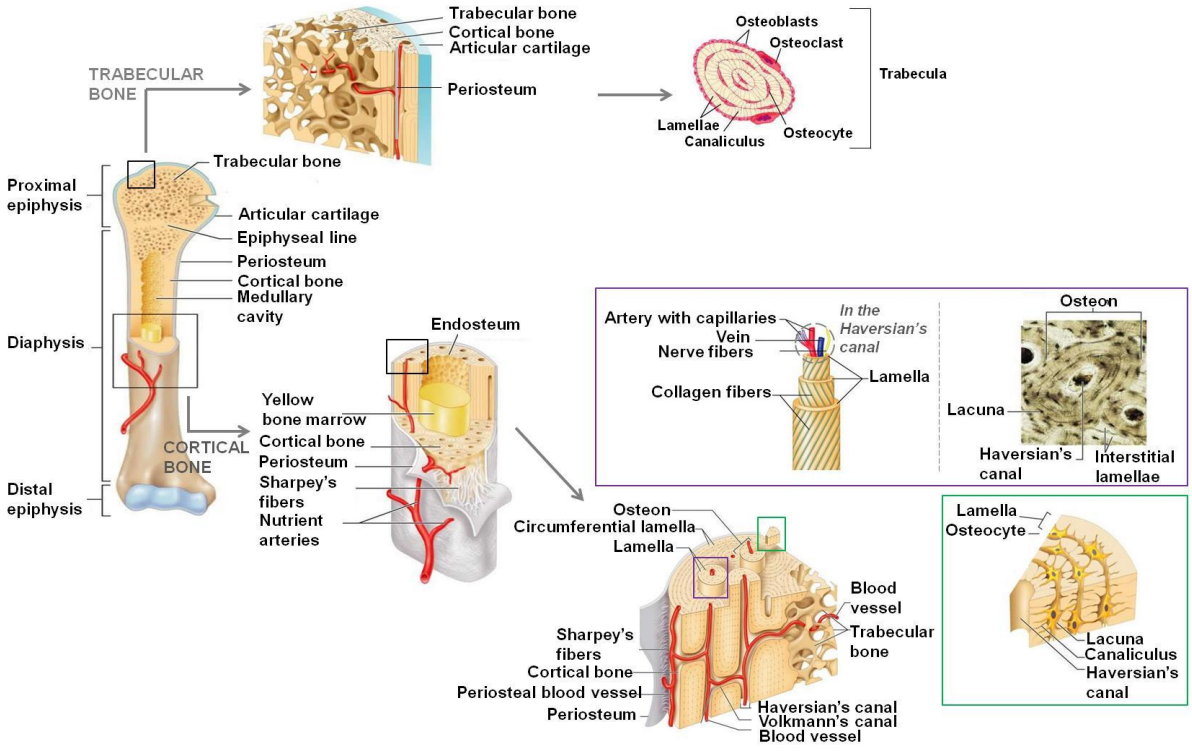

Figure 1-1. Microscopic structure of trabecular and cortical bones.

(scheme adapted from [4] *and* [5]*)*

Initially, bone extracellular matrix is not mineralized [6]. The mineralization occurs thanks to the activity of specific cells. The cellular response is achieved through precise signaling pathways provided by the extracellular matrix (ECM) (stiffness, structure, chemical environment…) [7,8]. In fact, cells continuously interact with the ECM and that results in the stimulation and upregulation of genes involved in the formation of bone. This phenomenon is particularly important for the mineralization process [9] but also for the constant remodeling of bone [10]. Bone formation and resorption are indeed characteristics of this dynamic tissue. Throughout life, bone is remodeled thanks to the activity of multiple cells in order to maintain the structure integrity of bone organ and repair microdamaged areas occurring from everyday stress (**Figure 1-2**).

Various cell types are classified in living bone. The first ones are osteoblasts. Osteoblasts are differentiated mesenchymal or stromal stem cells usually coming from the bone marrow and responsible for bone formation [11,12]. They produce an organic unmineralized matrix (osteid) that includes several specific proteins such as collagen type I (main proportion), osteopontin, osteocalcin, bone sialoprotein and others [1]. Osteoblasts are found on the surface of bones where non mineralized matrix has been newly created. As time goes by, these cells are able to mineralize the generated matrix through the deposition of minerals and they become entrapped [13]. At this point, osteoblasts are considered as mature bone cells and are called osteocytes [13,14]. In comparison to osteoblasts, osteocytes are quite inert cells. They are suggested to be mainly involved in the cellular communication between osteoblasts and osteoclasts, acting like a sensing and information transfer system [15,16]. To a lower extent, they also

play a role in bone formation, regulation of bone mass and mechano-sensing [14]. The place where osteocytes are located, between the lamellae, is known as lacuna and each lacuna is occupied by only one osteocyte. Osteocytes present a star shaped morphology with long cytoplasmic extensions that spread into a connected network formed by small canals named canaliculi [16]. The canaliculi enable thus the connections between adjacent osteocytes and serve also for the nutrient and oxygen supply from the newly formed bone to the older lamellae (from the exterior to the center of the osteons or trabeculae). Other cells, named bone lining cells (flat and elongated entities that cover bone surfaces), are also found but their nature and functions are not yet clearly determined and still argued in the literature [17]. However, what seems to be commonly accepted is their inactivity in terms of bone modeling and remodeling activity. They rather seem to play a role in the maintenance of the bone fluids and ions fluxes between bone fluid and interstitial fluid compartments for mineral homeostasis [17,18]. Finally, the last cell type constituting the bone cells family is represented by the osteoclasts. Osteoclasts are cells responsible for bone resorption [19,20]. In other terms, they promote the removal of the mineralized matrix and break down the organic one. The amount of bone is thus constantly balanced between the activity of osteoblasts and osteoclasts. Osteoclasts are multinucleated cells resulting from the fusion of cells of the monocyte-macrophage lineage [12,19,20]. They are located at the bone surface, as the osteoblasts, but in small cavities called Howship's lacunae (resorptive pits) [1]. These lacunae are formed by the osteoclasts themselves along with the bone resorbtion activity at the place they are situated. The dissolution of the mineralized bone is achieved through the local acidification of the resorptive cavity and the one of the collagen matrix through subsequent enzymatic metabolisms [21,22]. All degradation products are then evacuated towards extracellular space [22].

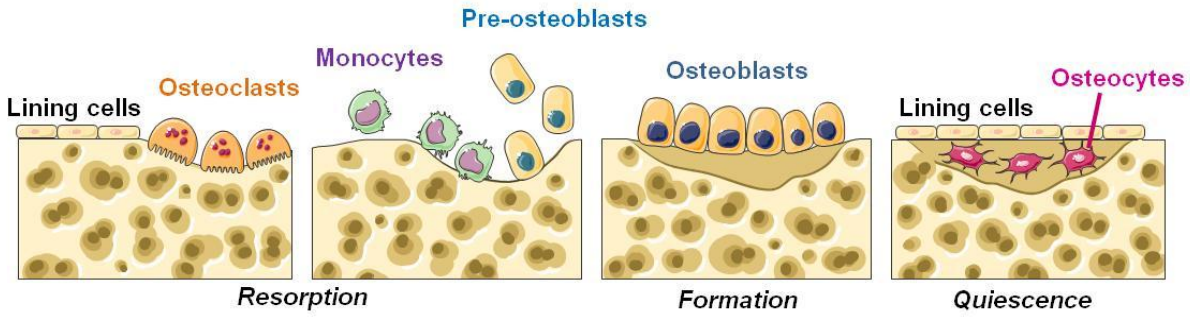

Figure 1-2. Bone remodelling cycle.
(scheme adapted from [23]*)*

In summary, bone is a complex biologic system that can be considered as three interconnecting parts [24]: the extracellular matrix, the cells attached to the matrix (or embedded in) and the environment within which the cells reside. It is a well organized composite tissue which components themselves, as well as their hierarchical structural organization, directly impact the mechanical properties. From the macro to the subnanoscale, the various levels of structural organization precisely define the rigidity, strength, flexibility and elasticity of bone. On the other hand, as aforementioned, bone presents the

particular ability of permanent remodeling. This involves number of cell types, signaling pathways and intra and extracellular molecules. Understanding the anatomy and physiology of bone is thus the starting point for the development of materials for bone tissue engineering.

1.2. Current bone replacement possibilities and bone tissue engineering

Despite its constant remodeling and ability to repair small damages in response to injury and mechanical stimulus, bone is not always able to achieve a complete regeneration of the injured area by itself. Its capacity of self-healing is sometimes limited, as it is the case, for example, for large bone defects. Tumor removal, trauma or infections often lead to skeletal defects with consequent size for which the auto-regeneration process is compromised. Such cases represent around 1 million patients every year in the United States for example [25]. With the increase in life expectancy and skeletal problems related to ageing, this number is even expected to rise in the future. Important socioeconomic consequences may be induced by these problems. Thus, finding solutions for these critical defects is a major concern for the scientific community and biomedical companies. To date, several bone-grafting procedures have been successfully implemented to achieve the union between two damaged surfaces. These procedures imply the use of natural or synthetic bone substitutes.

1.2.1. Natural bone substitutes

The first approach is based on the grafting of a bone fragment taken from a healthy part of the patient's own body. This kind of filler is called autologous bone graft and is considered as the gold standard of bone replacement. Autologous grafts can be harvested in the form of trabecular or cortical bone but trabecular bone remains the most grafted. It is generally harvested from the iliac crest of the patient (anterior or posterior) because of the relative easy access and large bone supply at this position [26]. The implantation success of autologous (or autogeneous) grafts is explained by the several essential elements that they content for bone regeneration: an osteoinductive matrix able to support ingrowth of new bone, osteoinductive factors and osteogenic cells [27]. These grafts are moreover able to integrate rapidly with the host environment [28,29], to support the efficient ingrowth of new blood vessels and infiltration of new osteoblasts, and to achieve ultimately strength equivalent to that of a cortical grafts after few months [30]. Their advantages are their non-immunogeneity, excellent success rate, histocompatibility and low risk of transmitting diseases. However, the amount of autografts is limited and the surgical procedures performed to extract the future graft is often associated to donor site morbidity [31]. It leads also frequently to various complications such as infection, fracture, nerve and vascular injuries, scar and chronic pain at the donor site [32].

To bypass the problem of low availability of autologous grafts, allografts rapidly became the second best alternative for surgeons. This approach consists in the harvesting of bone fragment from somebody else's body. They can be used as fresh, frozen or freezed-dried grafts but tissue processing and

sterilization are required before implantation to avoid strong immune response or viral disease transmission [33]. Moreover, these steps generally result in the elimination of the osteogenic cells (i.e loss of the osteogenic cellular properties) and affect the graft structural strength [34,35]. Other problems related to the delayed infiltration of capillaries into the implanted graft also limit the rate of osteointegration and the formation of new bone. Despite that, allografts have been proven to be ultimately effective bone replacements [26].

Xenografts, grafts taken from other species, can also be used to fill bone defects but their efficiency is still discussed because of their poor histocompatibility, low bone formation promotion and immunogenicity [36–38]. Moreover, their use is commonly associated to controversial procedures and ethical issues for example concerning the animal rights and religious or philosophical objections [39].

1.2.2. Synthetic bone substitutes

To overcome the limitations due to natural bone grafts listed above, synthetic substitutes were developed. These biomaterials are classified in three different families [40,41]: the first generation, the second generation and the third generation. Although each category clearly possesses distinct functions, all of them are still of interest for scientists as the choice of the biomaterials type directly depends on the targeted application.

1.2.2.1. First biomaterial generation

The first generation of biomaterials refers as bioinert materials that is to say biomaterials that do not induce important immune response and limit the foreign body reaction. Their main function is to replace the damaged part of bone by providing an immediate structural support. Metals, ceramics and polymers are used in that purpose. However, they present several disadvantages. Many metal alloys for example possess higher elastic modulus than natural bone. This means that, in load-bearing applications, the load will be rather taken by the implant and not by the natural bone after implantation. As a consequence, the natural bone might resorb because of the lack of mechanical stimulation [42,43]. Moreover, the osteointegration of metals is usually poor at the implantation site due to the usual invasion of fibrous tissue [43]. These two phenomena can lead to failure. To achieve a better anchorage of the implant with the surrounding tissue, the surface of metallic implants is often modified [44,45]. By this way, interactions between the biological environment and the implanted metal can be improved. For ceramics, the problem is their brittleness and consequent rapid failures. Studies on the processing conditions and design have been conducted to obtain tougher inorganic materials [46]. In polymers, wear occurs as time goes by and organic fragments can be released into the blood. This can result in osteolysis and bone resorption [42]. A constant attention is thus given to the abrasion, wear and friction properties when a synthetic organic material is aimed to be used.

1.2.2.2. Second biomaterial generation

The second generation of biomaterials includes bioactive and/or biodegradable materials. These materials are aimed to enhance the interactions between the host tissue and the implant and to degrade progressively along with the regeneration or healing of the new bone. Typical examples are bioactive glasses (silicon or metal based), calcium phosphate cements or composites that create a bond with the surrounding environment by the formation of a calcium-phosphate layer at the surface of the implant [47,48]. They can be implanted as a single phase or be used to coat inert metallic material, for example, in order to form a mechanically strong interface that cannot be achieved by the metal itself. Another example of this second generation of biomaterials is the use of polymers for the production of bioresorbable fixations and sutures [49].

1.2.2.3. Third biomaterial generation - Tissue engineering approach

The last generation of biomaterials is characterized by bioactive and biodegradable materials able to trigger specific cellular responses. The development of such materials is part of a quite novel research field called "tissue engineering". Tissue engineering is known as the "interdisciplinary field that applies the principles of engineering and life sciences toward the development of biological substitutes that restore, maintain, or improve tissue function or a whole organ" [50]. A variety of systems are currently investigated regarding their potential repair or regeneration [51–53]. The scientific advances made in materials science, biology and engineering have mainly contributed to a significant evolution in this research area. The need of specific requirements for different organs also pushed scientists to design substitutes with well-defined and accurate properties. Biomaterials of the third generation should, in fact, specifically activate the genes that stimulate the reconstruction of the targeted living tissue. Thanks to this genetic control, the activity of cells is guided towards particular behaviors necessary for tissue regeneration. For bone tissue engineering, this implies cell differentiation, osteoblast proliferation and synthesis of mineralizable extracellular matrix [40]. These responses are induced by the surface properties of the bioresorbable material (mechanical, topographical, chemical) [54] and by its dissolution products i.e ions or growth factors [55,56]. The regeneration process is thus based on the interplay between cells, material and signaling pathways. Two routes of repair are commonly considered in tissue engineering. First, the material can be designed to promote bone formation as an *ex situ* template on which cells are seeded and cultured (followed by a subsequent implantation) (**Figure 1-3**). Second, the material can be directly implanted to act as a bone formation promoting-substrate *in situ* [40]. Such scaffolds can be produced using diverse materials, as for the two other biomaterial generations (natural or synthetic polymers, bioactive glasses, ceramics…), but their production is particularly challenging due to the numerous expectations and requirements that they should satisfy.

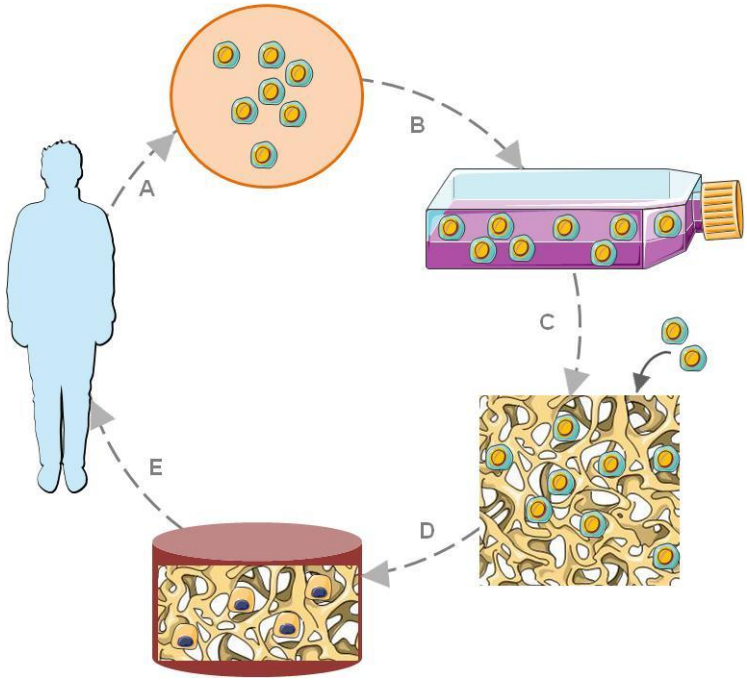

Figure 1-3. Tissue engineering principles involved in the *ex situ* approach of scaffolds implantation using a porous bioactive and biodegradable biomaterial on which cells are seeded. A: harvesting of cells from the patient, B: expansion of cells in *in vitro* conditions, C: cell seeding on a 3D-scaffold, D: maturation of the template in physiological conditions (cells proliferation and differentiation) and E: transplantation of the engineered template to repair or regenerate the damaged tissue. (nb: growth factors and cells can additionally be encapsulated in the matrix of the material [56,57]).
(*scheme designed using images from* [23]*)*

1.3. Scaffolds for bone tissue engineering: design considerations and material choice

From a general point of view, scaffolds should fulfill many criteria to be considered as good candidates for bone tissue engineering. They should [58]:

- be biocompatible and degrade without releasing toxic byproducts
- act as a 3D template to support cellular adhesion, proliferation and differentiation
- exhibit high porosity (interconnecting network) to favor cell migration towards the center of the structure and infiltration of fluids and blood vessels
- stimulate simultaneously osteogenesis and angiogenesis
- resorb at the same time than the new bone is formed
- possess suitable mechanical properties and keep a structural integrity at the beginning of the regeneration process
- be shaped to match the exact bone defect cavity
- be sterilizable

Multiple variables should thus be taken into account to design a suitable 3D scaffold as all these parameters will influence the cellular responses and the ability of the template to promote the growth of a healthy and fully functional bone. The selection of a relevant structure as well as the choice of a proper material is a key aspect in that sense. As explained previously, natural bone tissue is a composite material

mainly containing collagen (an organic phase) and hydroxyapatite (an inorganic phase). Based on these observations, it is naturally that researchers started to produce scaffolds made of polymers, ceramics, glasses and their composites.

1.3.1. Natural and synthetic polymers

Numerous studies in the literature report the use of natural polymers such as collagen, alginate, chitosan and hyaluronic acid [59–62] but also synthetic ones, namely polyglycolic acid, polylactic acid, polyanhydrides and polyorthoesthers [62–65]. Scaffolds prepared with naturally derived polymers are usually well biologically recognized and support positively cell adhesion and activity. However, they can contain pathogenic impurities and their mechanical and biodegradation properties are difficult to control [66]. Moreover, for some of them, the supply is limited. Synthetic polymers present several advantages over natural polymers. They can be produced at a large scale with controlled physical and mechanical properties, rate of degradation and also different shapes [66]. Their chemical versatility and processability vary according to their structure, making them a very interesting option for scaffold development for numerous applications. Currently, the attention is especially concentrated on synthetic polymers, which are involved in medical devices already approved by official agencies, such as the United State Food and Drug Administration (FDA) or the European Medicines Agency (EMA). Examples of those commercial devices in orthopaedics, among others, are sutures, screws and fixations [67]. These polymers are principally poly(**α**-hydroxy esters), such as polyglycolic acid (PGA) and polylactic acid (PLA), and aliphatic polyesters, such as polycaprolactone (PCL), as well as their copolymers [64]. They are biocompatible, can be degraded by hydrolysis, and are easily metabolized and excreted. The degradation of these materials occurs through a bulk erosion process (non enzymatic) by uptake of water [68]. When water penetrates into the specimen, it induces the hydrolytic cleavage of ester bonds resulting in the formation of carboxyl-end groups. These groups accelerate the rate of hydrolysis of the remaining ester bonds leading to the generation of oligomers in the specimen [69]. If these oligomers are located at the surface of the matrix, they can be removed before their total degradation. But if they are in the bulk, deep in the matrix, they cannot (or with difficulties) diffuse out. Consequently, a high acidic environment is forming inside the specimen, promoting the autocatalysis of further hydrolysis reactions. Thus, a degradation difference exists between the interior of the structure and its surface [68]. The degradation of poly(**α**-hydroxy esters) and aliphatic poly esters is described as heterogeneous and is attributed to reaction-diffusion processes [70]. During the biodegradation and, depending on the location considered in the sample, the molecular weight (bimodal distribution interior-surface) differs. The diffusion ability of the oligomers influences the degradation rate and resorption kinetics of the scaffold. The degradation of these polymers is accompanied by the release of byproducts, what explains the weight loss changes of the structure during its degradation. Globally, the degradation of these polymers is influenced by the polymer

chemical composition, its architecture, crystallinity, molar mass, processing history, chain orientation and porosity [67].

In spite of their good global biocompatibility and controllable biodegradation, synthetic polymers can induce an inflammatory response [42,71]. In addition, they are not efficiently osteoconductive nor osteoinductive. In other words, they do not efficiently support the ingrowth of capillaries and cells from the host into a 3D structure to form bone nor enable the repair in a location that would normally not heal if left untreated [54,72]. Finally, they are not bioactive and do not stimulate the desired cellular responses (i.e osteo and angiogenesis). These properties are though essential to develop a successful scaffold for bone engineering.

1.3.2. Ceramics, calcium phosphates and the particular potential of bioactive glasses

Ceramics, calcium phosphates and bioactive glasses are inorganic biocompatible compounds that are osteoconductive and are additionally able to develop a strong interface between the implant and the host tissue [48,73]. They directly bond to bone by creating a biologically active hydroxyl carbonate apatite layer (HCA). The precipitation and growth of this phase onto their surface is a particularly interesting property for a scaffold as HCA possesses similarities to the mineral phase of natural bone. Moreover, as mentioned previously, the implant-host tissue interactions are crucial for the anchorage of the implant and its success. These materials are therefore especially efficient in terms of bioactivity. They are also known for their excellent ability to support cell attachment, differentiation and proliferation of relevant cells [74,75]. However, due to differences in composition and processing, their dissolution and mechanical properties are rather different [76,77]. For example, calcium phosphates prepared as amorphous phases exhibit higher dissolution rates than ones prepared as crystalline compounds, and bioactive glass-ceramics materials generally show better mechanical properties than completely amorphous glasses [67]. Although, material dissolution affects the bioactivity and biological responses and, despite their lack of toughness and extreme fragility, bioactive glasses present a significant advantage over materials of different nature: they target specific cellular responses by activating genes responsible for osteogenesis [78,79]. This upregulation at the molecular level is the basis of tissue engineering and is thus a remarkable attractive feature that makes bioactive glasses one of the most studied materials in the last years. An investigation conducted by Oonishi *et al.* also revealed that bioactive glasses induced bone formation more rapidly than calcium phosphate based materials [80]. These valuable characteristics are mainly attributed to their dissolution properties and release of proper ions. Another key aspect regarding the use of bioactive glasses is the possibility to tune their resorption rate by controlling their chemical properties. This is especially true for glasses prepared by the sol-gel method [81]. For bioactive glasses prepared by the conventional quenching-melting method, this control is more difficult. This aspect will be described more precisely in a following section (see **1.4**).

The first and most popular bioactive glass was developed in 1969 by Prof. Larry Hench. This glass was named "bioglass®" and was synthesized in the SiO_2:Na_2O:CaO:P_2O_5 system. It refers as the specific composition 46.1 mol.% SiO_2, 24.4 mol.% Na_2O, 26.9 mol.% CaO and 2.6 mol.% P_2O_5, a composition that has been used to produce many novel materials and products commercially available nowadays [82]. The elaboration of this glass launched novel research lines such as the development of ceramics, glass-ceramics and other bioactive glasses derived from this silicon-based system [83]. Since the 90's, materials with diverse compositions (constituents and molecular ratios) have been indeed successfully produced [84]. Li *et al.* for example developed bioactive glass powders that do not contain Na_2O [85]. Uo *et al.* produced fine sheets of glass without SiO_2 [86]. Even glasses with novel constituents combination have been achieved through the incorporation or replacement of one the bioglass® initial compounds by ZnO, Fe_2O_3, MgO and others [87,88]. Among all these formulations, one glass has particularly been pointed out as another promising glass composition: the 44.5 mol.% CaO, 44.5 mol.% P_2O_5, 6 mol.% Na_2O and 5 mol.% TiO_2 system. This glass is known as "G5" and was developed in 2003 by Navarro *et al.*. Whereas silicate derived glasses can be produced by the sol-gel or the quenching-melting method, G5 is currently only prepared by the conventional melting-quenching method. As for silicon-based glasses, G5 has been demonstrated to possess suitable properties for bone tissue engineering applications while exhibiting a slower degradation rate [89,90]. This makes it more favorable for applications that require slow resorbable materials and also from the viewpoints of cell attachment, growth and differentiation [91]. More recently, this glass has been additionally demonstrated to act as an efficient vascularization promoter *in vitro* and *in vivo* conditions [92,93]. According to published studies [94,95], this property is also inferred to silicon-based glasses. However, the ability of silicate glasses to promote angiogenesis does not seem to be always optimal and the addition of growth factors such as vascular endothelial growth factor (VEGF) is often necessary to achieve a more satisfactory vascularization [96,97].

Although having intrinsic valuable properties for bone regeneration (i.e. mechanical toughness and strength or bioactivity), pure organic or inorganic phases do not satisfy all the desired requirements that a scaffold for bone tissue engineering should fulfill. In fact, templates produced using these materials individually are mechanically stable but have no inherent bioactivity (polymers) or are perfectly bioactive but not tough (inorganic compounds). Composite scaffolds have therefore been developed to overcome these limitations.

1.3.3. Composite materials

1.3.3.1. General description

The aim of composite materials is to obtain templates with suitable mechanical properties and bioactivity simultaneously. For bone regeneration, they are usually made by the association of an organic phase and an inorganic one. This material combination is an interesting approach for scaffold fabrication

as the nature of the selected constituents resembles the structure of natural bone. The organic part can mimic the collagen of the extracellular matrix while the inorganic one can mimic the hydroxyapatite (HA minerals). The global properties of the scaffold are aimed to be supported by both constituents. In other words, each family of compounds provides its own inherent properties [98,99]. Typical example of composites are scaffolds prepared by the incorporation of HA granules or fibers into a polymeric matrix [100–103]. Such studies revealed however that the contents of the inorganic and organic phases directly influence the bioactivity and mechanical properties of the scaffolds. In many cases, a template that is efficiently bioactive often has weak mechanical properties [104]. Thus, a compromise should be often found when developing composites to obtain a suitable balance between the two properties, considering also that inorganic compound shape, size, dispersion, orientation and mechanical features additionally play a role [98]. Furthermore, the scaffolds should have an appropriate structure with interconnected pores to enable cells attachment, migration into the scaffolds, and fluids and blood vessels infiltration [105–107]. Interestingly, composites can be shaped with diverse architectures and with different porosity [67,107]. This is possible thanks to the various processing technologies currently available such as solvent-casting and particulate leaching technique, gas foaming, additive manufacturing, and electrospinning. Another parameter that is also crucial regarding the final scaffold properties is the interactions between the organic phase and the inorganic one [108]. Composites commonly prepared with microsized inorganic particles for example often do not have a direct interface between their compounds (or very weak) (**Figure 1-4**). This may be caused by the manufacturing process selected to prepare the material (as for example, drawing method that may be responsible for the formation of void between the compounds – see **Figure 1-4, 1**) and/or non-optimal affinity between the compounds (**Figure 1-4, 2**). Usually, nanosized inorganic compounds are preferred to prepare composites (nanocomposites) because an enhancement in the interfacial interactions between the phases can be achieved [109]. The number of interfaces is increased due to the high surface area provided by nanoscaled compounds, what can lead to a better control on the mechanical and degradation properties. But this strategy is not completely optimal and the probability of crack initiation-propagation may be high due to these numerous interfaces. This may result finally in an ultimate depreciation of the mechanical properties [98,110]. To avoid that, and also a possible phase segregation [111], the polymer/inorganic nanofiller compatibility is often improved by modifying the surface of the nanofiller with organic molecules [112,113]. Despite that, the synergy between the two phases is still often not appropriate for the targeted application because of the heterogeneous degradation of the phases, the rapid loss of the composite mechanical properties or the inappropriate release rate of ions/monomers from the material [86,104]. Hence, composite materials with interactions at the molecular or nanometric level (also called hybrid materials) have been developed in order to produce more homogeneous templates with improved properties for bone regeneration (superior mechanical properties, homogeneous degradation and synergistic material). The fabrication of such materials usually involved a common versatile technique: the sol-gel method [114]. This method allows

the manipulation of the nanostructure of the materials at the molecular level and the control on the nature of the interfaces. Thus, it is a very powerful tool to develop hybrids (see **1.4**).

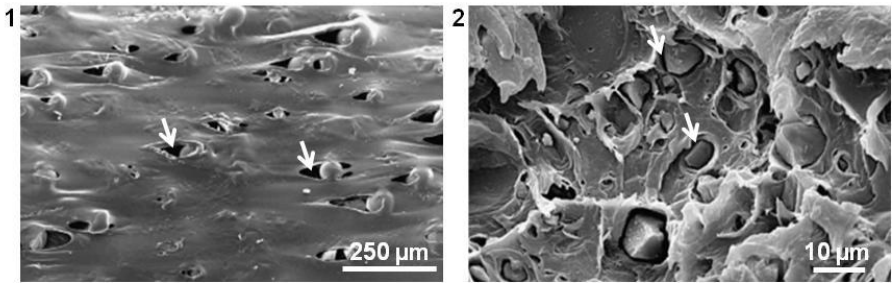

Figure 1-4. Typical examples of composites that possess limited intimate interactions between their inorganic constituent (microparticles) and polymeric matrix. Arrows point the presence of void between the phases (material shown on picture 1: extruded and drawn material – material shown on picture 2: extruded and compressed material).
(picture 1 is adapted from [104] *and picture 2 from* [115]*).*

1.3.3.2. Hybrid materials

Hybrids are classified in two categories depending on the nature of the intimate organic-inorganic interface [111,116]. The first family is the class I materials which possess weak interactions between their constituents (Van der Waals, electrostatic or hydrogen bonding interactions). The second one is the class II materials which exhibit strong interactions between their components (covalent or ionic bonding). Compared to traditional composites, hybrid scaffolds prepared with weak or strong phase interactions usually present better properties. But, a clear difference in the resulting properties of the scaffold is however noted between these two classes of hybrids.

Hybrids class I

Hybrid organic-inorganic materials of class I have been extensively investigated up to now for numerous applications. The interpenetration of the organic and inorganic network constitutes the basis of these materials and explain why class I hybrid scaffolds exhibit improved mechanical and degradation properties, when compared to traditional composites. In these materials, the two phases are nanoscopically separated but macroscopically uniform [117]. Considering bone tissue engineering, a representative example is the material developed by Martin *et al.* in 2004 [118]. Polyvinyl alcohol (PVA) was chosen for the organic part and bioactive glass for the inorganic one. They incorporated PVA during the synthesis of the bioactive glass, which was prepared by the sol-gel method. After gelation of this hybrid sol and an aging-drying process, class I hybrid monoliths were obtained. The study revealed that by controlling the experimental conditions, crack-free monoliths could be produced. The degradation as well as the bioactivity of the materials could be also tailored by changing, for example, the content of PVA, or adding extra-compounds in the initial glass composition (P_2O_5 in $CaO\text{-}SiO_2$ system). In their study, no mechanical tests were performed but another report by Landry *et al.* showed that organic-inorganic materials prepared by the *in situ* polymerization of silanes (tetraethylorthosilicate TEOS) in

polymers resulted in materials with enhanced mechanical properties [119]. This was attributed to the nature of the interactions between the two phases: the hydrogen bonds formed between the residual hydroxyls of the hydrolyzed TEOS molecules and the ones in the polymer, acted as crosslinkers [120]. However, this kind of bonding is weak and is not stable in aqueous medium as the water molecules may easily separate the chains [121]. For this reason, the degree of crosslinking and phases interpenetration is very important. If the nature of the precursors is not precisely selected and if the conditions of the hydrolysis reaction are not well controlled, the crosslinking and phase interpenetration may not be sufficient to tailor efficiently the degradation of the material. In the case of a too fast degradation, the degradation might not be suitable to support bioactivity for example [118]. Another drawback for the production of these materials is the phase separation that might occur due to incompatibilities between the phases. Once again, reaction conditions such as temperature and pH are of paramount importance to accomplish a homogeneous material and this should be perfectly controlled [119]. Although having some drawbacks, class I materials are promising materials considering the good global properties that they can exhibit if their design is properly tailored.

Hybrids class II

An increasing effort has been done in the last years to produce class II materials to overcome the problems resulting from the weak interactions between the material phases. The aim is to produce scaffolds with good stability and good performance under physiological conditions. Nevertheless, such materials are difficult to produce and only three materials involving biocompatible and biodegradable polymers are reported in the literature for bone regeneration. The three of them imply the use of coupling agents for functionalizing the polymer in order to subsequently covalently link the polymer to the inorganic part (pure silica network or silica network with incorporated calcium) [122–124]. Considering that there are only few examples of class II hybrid materials in the literature and that they show a high promising potential for the field, each one is briefly presented here.

The first material (disc shape) was developed by Tian *et al*. in the 90's [122]. This material was a PCL/silica hybrid prepared by the sol-gel method in which PCL was intimately incorporated into the silica network (TEOS reagent). The reaction consisted in the end-capping of hydroxyl PCL with isocyanatopropyltriethoxysilane (IPTES). The terminal hydroxyl groups of the polymer reacted with the isocyanate group of IPTES to form a urethane linkage, creating an IPTES end-capped PCL. After the substitution of the ethoxy ligands of IPTES by hydroxyl groups (hydrolysis), IPTES end-capped PCL condensated and linked to hydrolyzed TEOS molecules. As a result, a silica network containing polymeric fragments was created, in which IPTES acted as an intermediate covalent linker between the two phases. The reaction extent was mainly controlled by the molecular weight of the PCL as the length of the PCL chains directly influenced the number of available sites for reaction [125]. Consequently, the shorter the chains, the higher the number of available reactive terminal groups and the higher end-capping potential. In addition to the covalent bonding, these hybrids were demonstrated to be also linked by

hydrogen bondings: PCL ester groups interacted with residual hydrolyzed ethoxy groups of the silica network [125]. These two types of interactions contributed to the good stability of the polymeric phase in hybrids in comparison to pure PCL [125]. On the other hand, according to preliminary tests [126], it has been shown that these hybrids were also a suitable support for cell culture.

Several years after the development of these hybrids, Rhee *et al*. incorporated calcium (salt) in the system, with the aim to improve the hybrids bioactivity [127–129]. This was a very interesting idea since calcium ions (Ca^{2+}) play an important role in the bioactivity efficiency of materials and in the osteogenesis process. Later, Rhee published in fact a more detailed study in which he assessed the bone like apatite forming ability of this end-capped PCL/silica/calcium material depending on the PCL content in the hybrids [130]. Hybrids containing the lowest PCL content exhibited the best bioactive properties. This was explained by the presence of a higher number of silanol groups in the silica phase for the low PCL content hybrids and a stronger release of Ca^{2+} into the simulated body fluid (SBF) solution [128,130,131]. Indeed, it is well reported that silanols act as nucleation sites for apatite crystals, and Ca^{2+} ions released in the surrounding medium contribute to the supersaturation of the fluids and the deposition of a calcium phosphate precipitate [132,133]. The study showed that the PCL content also affected the mechanical properties of the materials, but all the materials possessed tensile strengths and Young's moduli in the range of trabecular bone. Moreover, *in vivo* tests revealed that the material directly induced bone formation on the surface of the scaffold without creating any fibrous tissue [131].

The second material (porous material) was developed by Poologasundarampillai *et al*. in 2010 [123]. In their study, they functionalized a biopolymer, poly(**γ** glutamic acid) (**γ**PGlu), with glycidoxypropyl trimethoxysilane (GPTMS). They used TEOS to create the inorganic network and added calcium into the network (a calcium salt). Unlike synthetic PCL, which degrades by random chain scissions from the bulk (potentially rapidly affecting the mechanical properties of the material), natural **γ**PGlu enzymatically degrades from the surface. This means that the bulk of the material can maintain its mechanical properties as long as the water does not infiltrate the matrix and catalyzes the degradation from the inside. It was thus expected that the use of **γ**PGlu would slow down the loss of the scaffold mechanical properties. But the degradation process is a complicated phenomenon, whose rate and mechanism is influenced by numerous factors (porosity, hydrophilicity, pH of surrounding fluid…). As no direct study has been performed to assess the loss of the mechanical properties and the role of **γ**PGlu, it is however not possible to certify that **γ**PGlu is an effective compound to better control the material degradation of class II hybrids. However, one of their complementary studies revealed the role of the degree of crosslinking in the dissolution of the polymer [134]. Hybrid materials with a high degree of crosslinking exhibited a slower polymer release than ones prepared with lower covalent coupling. As reported in their first synthesis study, the coupling of the two materials can be tailored by the amount of coupling agent used for reaction. A higher proportion of coupling agent resulted in an increase in the organic/inorganic interactions. On the other hand, they demonstrated that the amount of solvent used in such reactions impacts the reaction rate, and the nanostructure and nanoporosity of the materials. As for

the end-capped PCL/silica/calcium material, these hybrids exhibited good bioactivity. Calcium has been pointed out as an essential element for the formation of the hydroxyl carbonated apatite. The incorporation of calcium in the network was therefore required to promote bioactivity. Knowing that high degree of crosslinking in the hybrids leads to more compact structures and consequently to relatively slow dissolution rate of calcium, the working reaction conditions should be carefully selected in order to reach a proper bioactivity. About mechanical properties, compressive mechanical testings demonstrated that the toughness of the hybrids was improved in comparison to glass alone. Finally, cellular assay (live/dead test) showed that Saos-2 cells attached and spread on the material surface without suffering of any cytotoxic effects.

The third material (foamed structure) was developed by Mahony *et al*. in 2010 [124]. It is also prepared with a biopolymer (gelatin) and the same coupling agent than the previous material (GPTMS). TEOS was also used to form the silica network but the materials did not contained calcium. The main aim of this study was to demonstrate that tough materials could be created by preparing class II materials. As for the other two materials, the study showed that the percentage of gelatin and degree of crosslinking affected the mechanical properties of the scaffolds. Degree of porosity was influenced by the concentration of surfactant used during the material foaming. This directly also impacted the mechanical strength of the scaffolds but globally, all materials produced were considered as stiff substrates (based on the approximate stiffness of various tissues). In addition, they had remarkable elastic properties and tailorable dissolution properties. Finally, according to cell morphological observations (mesenchymal stem cells), the materials were shown to be biocompatible and non-cytotoxic independent of the reagent contents or chemical control performed on the reactions (degree of crosslinking and surfactant amount).

Although the hybrids described above seem to be the unique class II materials found in the literature, it should be noticed that, shortly, other polymers may be also covalently functionalized to be incorporated within an inorganic network. Indeed, Maeda *et al*., for example, already achieved the first step of polymer functionalization with PLA and aminopropyltriethoxysilane (APTES) as coupling agent [135]. However, they did not exploit this finding to create a real organic/inorganic material in which the functionalized polymer is intimately incorporated in a silica network. The material was simply formed through the reaction of functionalized PLA chains with other functionalized PLA chains. No reagent such as TEOS was used to introduce a high content of inorganic network in the hybrid. Therefore, the inorganic content was restricted to the quantity of APTES molecules efficiently linked to the PLA chains and it cannot be more controlled than by changing the molecular weight of the polymer. From a general point of view, this material could be considered as a class II hybrid because it possesses a strong covalent bond between its organic and inorganic phases. However, it does not exactly enter this category because no inorganic network was really introduced in the material (except the part of the organosilane). For this material, the classification is rather subjective and is controversial [121,136]. Some scientists might already consider this material as class II materials while some other might not. Anyhow, such functionalized polymers might be the starting point for the production of additional class II hybrids in the

future, as it has been actually the case for the GPTMS functionalized gelatin prepared by Ren *et al.* [136,137] in 2001 and the subsequent work described above, performed by Mahony *et al.* in 2010.

Summarizing, the class II hybrid materials described in this section appear to be valuable systems for bone tissue engineering due to their biodegradable constituents, remarkable bioactivity and good mechanical properties. The possibility to tune material structure (foams and discs with different porosity) and properties (toughness, bioactivity) by controlling the material preparation (chemical reactions and reagents contents) is a very interesting point as different applications require different materials properties. Material design could be adapted to a specific application. However, only preliminary assays have been performed with cells to demonstrate the biocompatibility of the structures. No extensive studies seem to have been performed to evaluate in more details the adhesion, proliferation, differentiation and potential of these scaffolds to trigger specific cellular responses. If *in vitro* and *in vivo* studies effectively demonstrated that these materials efficiently promote osteogenesis, they could definitely be confirmed as promising grafts for bone regeneration. But, such materials represent a relatively new concept in biomaterials and their development is just starting. No doubt that other materials made of diverse polymers, coupling agents and inorganic phases may be fabricated in the future and that extensive studies relating the cellular responses induced by these materials will be reported in the literature in the coming years.

1.4. The sol-gel process

Known since the late 1800's, the sol-gel process has gained a considerable popularity in the last 40 years regarding the fabrication of materials and its relevant use in diverse research fields (optics, electronics, magnetism…). As mentioned previously, this method is particularly interesting for preparing hybrid polymer-glass materials for biomedical applications as it enables to manipulate the structure of the glass at a molecular level and to additionally control the nature of the interfaces in the hybrid [114]. Based on the studies described in the "hybrid materials" section, it is clear that these possibilities are crucial for the ultimate scaffolds properties that are aimed to be achieved (mechanical properties, bioactivity). The sol-gel technology offers the possibility to find the precise material preparation conditions that allow the production of materials for specific applications; that is to say with tailored particular properties [99]. It enables moreover the fabrication of biocompatible, bioactive, resorbable and porous materials with an intrinsic high interconnectivity [138,139]. Unlike glasses prepared by the usual melting-quenching method, the sol-gel approach is also a low temperature process that does not require high temperature treatments and the materials obtained are more pure and homogeneous [140]. They also have a high surface area and nanoporosity [141,142]. All these advantages have contributed to make this technology an ideal option for the development of biomaterials.

Specifically, the sol-gel technology relies on the hydrolysis of organic molecules followed by their polycondensation to form a polymeric structure [143]. It usually involves the use of metal alkoxides

precursors [144], which determine the composition of the glass. The sol is the colloidal suspension obtained just after the hydrolysis of the alkoxides. The gel is formed when the created particles constituting the colloidal suspension assemble into a network through the condensation step. In most of the cases, hydrolysis and condensation (competitive processes) occur simultaneously once the hydrolysis reaction has been initiated. Metal alkoxides are compounds in which the metal is surrounded by electronegative OR ligands (generic molecular structure $M\text{-}(OR)_n$ where R is an organic ligand). As a consequence, the metal possesses a positive charge and it can be attacked by a nucleophile, as for example, water. In this kind of reaction, the water donates its electron pair to the metal to form a chemical bond and the R groups of the alkoxides are replaced (leaving groups). Depending on the nature of the metal, the hydrolysis process is more or less rapidly initiated. Among other parameters, basic or acid catalysts can therefore be used to control the hydrolysis time scale [145]. Schematically, the nucleophilic attack that undergoes alkoxides in the sol-gel method occurs as follows [143]:

$$M\text{-}(OR)_4 + H_2O \xrightarrow{\text{catalyst}} HO\text{-}M\text{-}(OR)_3 + R\text{-}OH \qquad \textit{Partial Hydrolysis (R: } CH_3, CH_2CH_3 \textit{...)}$$

$$M\text{-}(OR)_4 + 4H_2O \rightarrow M\text{-}(OH)_4 + 4R\text{-}OH \qquad \textit{Complete Hydrolysis}$$

Once hydrolyzed, alkoxides molecules link together:

$$(OR)_3\text{-}M\text{-}OH + HO\text{-}M\text{-}(OR)_3 \rightarrow (OR)_3\text{-}M\text{-}O\text{-}M\text{-}(OR)_3 + H_2O \qquad \textit{Condensation}$$

$$\text{or} \quad (OR)_3\text{-}M\text{-}OR + HO\text{-}M\text{-}(OR)_3 \rightarrow (OR)_3\text{-}M\text{-}O\text{-}M\text{-}(OR)_3 + R\text{-}OH \qquad \textit{Condensation}$$

The quantity of water and catalyst introduced to start the process control the degree of hydrolysis. The condensation process liberates byproducts, water and/or alcohol, which are incorporated in the internal pores of the prepared glass [99,146]. If the condensation process continues to take place, large polymeric chains can eventually form, leading to the creation of macromolecules. This reaction, known as the ageing, can go on until a final stage is reached and contributes to the increase of the stiffness of the glass [147,148]. In addition to ageing, the glass also undergoes a drying process which is characterized by the evaporation of the liquids (alcohol, eventual remaining water and solvents used) contained in the glass and the formation of small interconnected pores ranging from 1 to 30 nm [141]. Drying is often associated to the appearance of cracks in the glass, affecting its structural integrity and mechanical properties. To avoid that, an attention should be particularly given to the drying and gelation time for examples as they directly impact on the cracking of the gels [99]. Gels obtained can be furthermore stabilized i.e. additionally dried at higher temperatures. **Figure 1-5** illustrates the different processes involved in the formation of glasses using the sol-gel method.

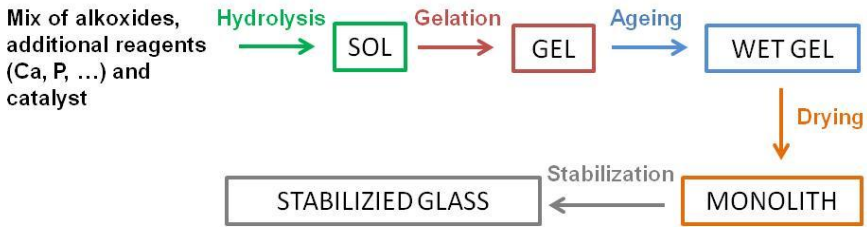

Figure 1-5. Scheme of the sequence of processes involved in the sol-gel synthesis.

(scheme adapted from [149]*)*

The reaction mechanisms involved in the sol-gel process are influenced by many parameters [99,145]. The main ones are the pH, the structure of the alkoxide precursors, the catalysts used and the gelation time. But, changing these parameters also affects the microstructure of the final glass and consequently its properties (structural, mechanical) [114]. Therefore, although the chemistry implied in the reaction mechanisms appears to be simple, the determination of the optimized working conditions is a very delicate task. However, finding these parameters is the pathway to follow to be able to produce a glass with suitable properties and to subsequently tune the organic-inorganic interfaces in hybrids.

The preparation of hybrids using the sol-gel method may be achieved in various ways [99,150] but there are two main ones [144]. The first one consists in the dissolution of organic molecules such as polymers in a sol-gel hydrolyzed suspension. If the inorganic compound does not have reactive organic groups, the interactions between the organic and inorganic phases are weak. This kind of material is called “blend” and it is a class I material. The main advantage of this preparation method is the simplicity of the approach. But, it has also a consequent drawback: a possible phase separation between the compounds, resulting in an inhomogeneous material. This can be avoided if the organic-inorganic interactions are improved e.g. by modifying the glass properties in changing its preparation conditions for example or if the interactions between both constituents are of the same nature than ones present in the inorganic or organic phase. Even though considering carefully this issue and the eventual successful fabrication of homogeneous materials, such hybrids usually present a short-term stability because of their weak interactions. The other possibility is to use an inorganic precursor that possesses reactive organic groups which can be used to create chemical bonds with the organic part of the hybrid, as described in details in the previous section. This way, class II materials can thus be produced and a better control on the material stability can be achieved. These materials are usually obtained by reacting the inorganic and organic precursor at the same time. Both material synthesis presented here are commonly performed in liquid state. It is therefore essential to find a suitable solvent for both the organic and inorganic compounds. It should be moreover selected according to its compatibility with the sol-gel reactions. Without these considerations, the fabrication of materials using these approaches is not possible. But once all parameters related to the glass and the whole system glass/organic phase have been properly set, the hybrid can be processed in many shapes (foams, fibrous membrane, monoliths) [118,151,152] (**Figure 1-6**). This is an additional advantage inherent to the sol-gel process.

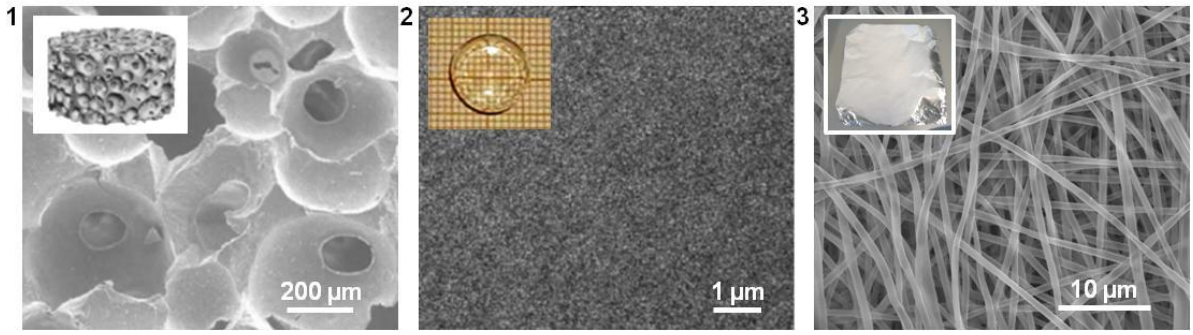

Figure 1-6. Examples of hybrid scaffolds prepared using the sol-gel method (from left to right): foams, monoliths, fibers. *(Picture 1 is adapted from* [58] *and from* [81], *picture 2 from* [118], *picture 3 from the author's own propriety)*

In summary, the sol-gel method is a very powerful technology that provides tremendous possibilities of combination of different properties in one material. It can be applied to numerous glass systems, mainly silicate based networks but for titanium based glasses (i.e G5), the sol-gel approach does not seem to have been implemented yet to produce hybrid materials. One of the interesting points of using the sol-gel method to produce hybrids is the possibility to tailor the interfaces between the organic and inorganic phases. However, despite being based on apparent simple chemistry, many critical issues regarding the synthesis of the glass have first to be faced. Consequently, finding the proper working conditions to match a material with specific features is not easy. Besides these difficulties, the sol-gel method enables the fabrication of hybrids that can be shaped under different forms due to its versatile processing ability. This is a valuable benefit of using this process as it is demonstrated that scaffolds characteristics influence cellular responses.

1.5. Scaffold properties and their effect on cellular behavior

Adhesion, proliferation and differentiation of cells cultured on a scaffold constitute the basis of tissue engineering approaches. It is well known that cell-cell interactions direct cellular activity towards these behaviors and contribute to the fate determination of uncommitted stem cells [153,154]. But they are not the only one to influence the biological response. The material properties also directly affect the cell functions. In fact, the material properties can be efficiently used to control cellular processes through chemical and physical guidance. The key design factors to develop a biomaterial aimed to trigger specific cellular responses are its chemical and mechanical surface properties, and its architecture (**Figure 1-7**). Together, all these material properties coordinate the interplay between intrinsic and extrinsic determinants of stem cell fate to produce a desired phenotype [155]. The relation between cells and the 3D microenvironment is described in this section.

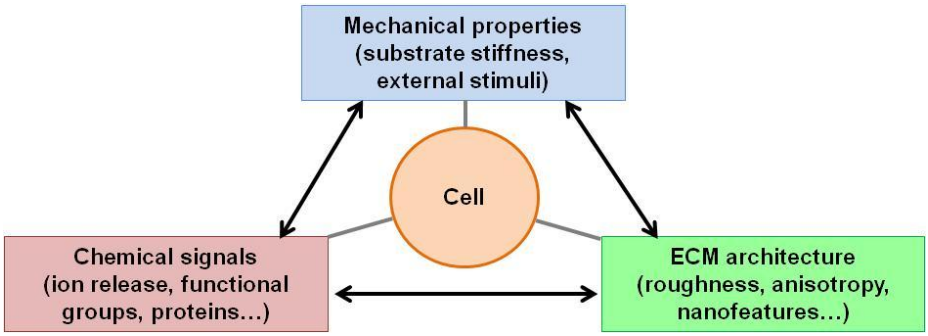

Figure 1-7. Scheme representing the dynamic dependence between the various features of 3D scaffolds on cells and involved in the regulation of the material biological performance.

(scheme adapted from [156]*)*

1.5.1. Material chemical surface properties

Scaffold chemical surface properties depend on the compounds selected to prepare the material (composition), its processing method and an eventual functionalization step that can be performed on its surface subsequently to its fabrication. Each biomaterial possesses therefore specific surface properties, as for examples wettability, electric charge, protein adsorption ability and bioactivity, which regulate the biological performance of the scaffold. One of the factors that can be considered to explain these differences in properties and in cellular response induced by the material is the nature of the functional groups present on its surface. Hence, Lee *et al.* demonstrated that the functionalization of polyethylene substrates with different organic functional groups (COOH, CH_2OH, $CONH_2$, CH_2NH_2) resulted in a better cellular adhesion [157]. This was explained by a better wettability of the functional groups-grafted surfaces in comparison to non-grafted ones. They also showed that the chemistry of the functional groups itself was important as they modify the electric charge of the polymeric surface. Negatively charged substrates showed a poor cell adhesion, whereas the positive ones exhibited the best one. On neutral surfaces (-CH_2OH and $CONH_2$ groups), cells adhered better on hydroxyl-grafted substrates, possibly because of specific hydrogen bonding created between the surface hydroxyl groups of the polymer and the polar groups of the cell surfaces [158,159]. Though, the adhesion was still lower than on positively charged materials. Cell multiplication followed the same tendency than the cell adhesion assay: the more hydrophilic the material, the better the proliferation. Finally, they demonstrated that substrates inducing the best proliferation were not systematically associated to the best cellular spreading. Cells, indeed, significantly spread on the neutral surfaces, despite proliferating a little bit less than the positively charged surfaces. Authors suggested therefore that the compatibility between the cells and the surface chemistry plays a direct role in cellular spreading. Other research groups described as well the general observations made by Lee *et al.* and even give evidence that the nature of functional groups can also trigger osteoblastic differentiation [160,161].

Other studies reported in the literature showed moreover that cell behavior can be influenced by these functional groups in an indirect manner: the surface properties that functional groups provide to the

material affect protein adsorption and consequently the cellular response [162–164]. Arima *et. al.* for example examined the kinetics of protein adsorption on materials having different functional groups and correlated it to cell adhesion [165]. Results showed that depending on the chemistry of the functional groups exposed at the materials' surface, non cell-adhesive proteins such as bovine serum albumin (BSA) previously adsorbed on self-assembled monolayers of alkanethiols (SAMs), were more or less rapidly replaced by cell-adhesive proteins (fibronectin, vitronectin, …). This induced difference in cell adhesion: SAMs terminated with COOH groups supported a better cell adhesion than ones having NH_2 groups. This was explained by the slower proteins displacement process for NH_2-terminated materials. Thus, the efficiency of the proteins displacement (rate and amount of replaced proteins) ultimately modulated the cells adhesion, as it is well known that cell-adhesive proteins, natural or engineered, adsorbed or covalently linked to materials, facilitate cell adhesion [162,166]. Currently, the grafting of biomolecules (peptides or proteins) is in fact an approach extensively used in tissue engineering to guide cellular adhesion and activity [167,168]. In this case, ligand identity, conformation and density are key parameters to develop the materials [155,169] because they regulate for examples the efficiency of integrin-mediated cell adhesion [170], modulate the matrix deposition by osteogenic cells [171] and control the cell-type specificity of these responses [172].

The last factor related to the surface that can be considered to develop smart artificial materials is the ions dissolution that occurs along with the material resorption [173]. Bioactive glasses are nowadays one of the most attractive materials able to stimulate osteogenesis and angiogenesis due to its ion release ability [93–95,174,175]. The dissolution products of bioactive glasses (calcium, silicon, titanium, phosphate or other element used as doping constituent) modify the chemical physiological environment of biological entities and consequently mediate the cell metabolism. Extracellular Ca^{2+} for example is known for interacting with bone cells by affecting their calcium-sensing receptors (CaSR) and directly activating intracellular mechanisms [176]. Concretely, one study performed by Honda *et al.* demonstrated that extracellular calcium increases the expression of IGF-II, an insulin-like growth factor that mediates the subsequent increase in human osteoblast proliferation [177]. Other studies revealed as well that cell migration, proliferation and differentiation may be controlled by the activation of various CaSR-mediated intracellular signaling pathways [178,179]. Ca^{2+} is therefore very important regarding bone remodeling and can be used in scaffolds for bone tissue engineering to serve as an extracellular messenger that guides the cell behavior of osteoblastic cell lineage. In fact, it is already commonly accepted that calcium ions (and also silicon ions) released from silicon-based bioactive glasses play a critical role in that sense. Xynos *et al.* were the first in 2001 to demonstrate that ion products of bioactive glass dissolution have a direct effect on the gene-expression profile of human osteoblasts; more precisely on genes relevant to osteoblast metabolism and bone homeostasis [78]. More recently, an osteogenic glass based on titanium network has also been demonstrated to act as a gene-expression regulator able to stimulate the activation of genes involved in angiogenesis [180]. The up-regulation of gene-expression that can be achieved by the use of bioactive glasses in tissue engineering is thus a very promising approach to control cellular

activity towards desired responses. However, it should be specified that the concentrations of these ions is critical and that a precise control on the material dissolution rate should be reached in order not to induce cytotoxicity [181]. The ion concentration and release kinetics of bioactive glasses can be controlled by the material composition itself [89] or by fabricating polymer/bioactive glasses constructs [67]. Though, in some cases, it is still extremely delicate to monitor precisely the features of the ion release of the inorganic phase in a predetermined manner as it is often embedded in the organic matrix. This affects the dissolution of the bioactive glass and consequently its ability to trigger the desired cellular response (cell adhesion, spreading, proliferation, differentiation and migration) [180,182]. This problem also affects the mineralization potential of the materials [104,183]. For all these reasons, the tailoring of the chemical material surface properties is essential.

1.5.2. Material mechanical properties

In addition to the influence that chemical material surface properties have on cellular activity, there is significant evidence that physical properties of the substrates also contribute to stem cell fate determination. One of them is the material mechanical properties e.g. stiffness, or elasticity. The local mechanical interactions between the cells and its microenvironment regulate cell shape, organization and differentiation [184,185]. This observation is valid for natural environment as well as for artificial 3D structures. Cells are able to discriminate different ranges of stiffness of their microenvironement and to respond to this stimulus by pulling on the extracellular matrix. The contractile forces that exert cells on the matrix result in tensile stresses in the cytoskeleton. This phenomenon occurs through the transmission of force between the cell and the cellular cytoskeleton by means of focal adhesions (cell-extracellular matrix contacts) [156]. The pathway of force transmission from inside the cell to the elastic matrix is provided by actin structures that are in turn linked to focal adhesions [186,187], and by well-known signaling proteins such as Rho GTPase associated with the focal adhesion complexes to act as mechano-transducers [188,189]. These intracellular forces regulate the signaling pathways involved in the fundamental processes that determine cell functions. A very popular study conducted by Engler *et al.* with gels has indeed demonstrated that the elastic modulus of the matrix plays a role in directing stem cell lineage specifications [190]. Contractile forces in the cytoskeleton are suggested to be driven by actin-myosin action and to regulate human stem cell differentiation. Soft substrates mimicking the stiffness of the brain tissue induced cell differentiation towards a neurogenic lineage, whereas cells cultured on substrates with intermediate and higher stiffness mimicking the one of muscle and bone tissues, respectively evolved towards myogenic and osteogenic cells. They additionally showed that cells adjust their internal stiffness to match the one of the substrate. Stiffer matrices in fact produced stiffer and increasingly tensed cells. Solon *et al.* made similar observations with fibroblasts using soft elastic substrates [191].

Although it is recognized that the stiffness of materials has an effect on cell behavior, it should be emphasized that the stiffness alone does not seem to always be an efficient cell differentiation parameter. For example, Rowlands *et al.* showed that, unlike in Engler and coworkers' work, the substrate stiffness alone was not sufficient to achieve osteogenic differentiation of mesenchymal stem cells (MSCs) in the stiffness range that they investigated [192]. The coating of the gel with molecules (collagen, fibronection or laminin) was necessary to induce this phenotype. The type of molecules present on the materials surface, in fact, modulated the differentiation process for a given substrate stiffness. Their study demonstrated thus that there is a feedback mechanism between the material stiffness and the adhesive ligand, considering osteogenic differentiation. For myogenic differentiation, this observation is also valid but the interplay of these two extracellular environmental factors appeared to be less obvious. This difference was attributed to a predisposition of MSCs to differentiate into myogenic lineage in comparison to osteogenic lineage when cultured on the studied substrates.

The two studies mentioned here highlighted thus the difficulties to clearly define how each material parameter, in an individual manner, can be responsible for the triggering of specific cell phenotype. Such assays often lead to controversial discussion because the conditions in which the material is investigated usually differ from one group to another (cell type used, cell badge, parameters set for the assay, material conditioning…). Nevertheless, it is commonly accepted that, combined with other factors or not, the material mechanical properties play an important role in the determination of cell behaviors. This is particularly clear when looking at the numerous studies reported in the literature on cells and mechanosensing, mechanotransduction and mechanoresponse [184,189,193].

1.5.3. Material architecture

The choice of a suitable fabrication technique to produce three dimensional structures is a significant hurdle for the improvement of tissue-engineering treatment. The architecture of the material fabricated should, in fact, not only have suitable mechanical properties, but also enable an optimal mass and fluid transport through the whole template [107]. In other words, the substrate prepared should exhibit a suitable porosity to ensure an efficient colonization of the material by cells, enable the supply of nutrients and oxygen, the evacuation of detritus and support the invasion of blood vessels. All these phenomena will contribute to the performance of the material and ultimately, to the formation of a fully functional and healthy bone. An appropriate porosity is thus required for bone regeneration [194].

As seen in **Figure 1-6**, materials can be shaped under different forms depending on the processing techniques used to fabricate scaffolds (foaming, sintering, salt leaching, additive manufacturing…). Each technique leads to the production of materials with specific pore size and interconnectivity, which can be controlled by varying the experimental parameters [195]. Porosity can be considered at three levels: the macro, the meso and micro one. The macroporosity refers to pores having a size larger than 50 nm, the mesoporosity to ones having a size between 2 and 50 nm and the

microporosity to ones having a size smaller than 2 nm [196]. The macroporosity is considered as the most significant factor that influences cell behavior, bone growth and vascularization. For example, Valerio *et al.* demonstrated that bioactive glass macroporous structures with pores ranging from 100 µm to 500 µm (prepared by the sol-gel method and foaming technique) support cell migration towards the inside of the scaffold [75]. Sepulveda *et al.* and Xynos *et al.* additionally showed that foams with large pores (diameters between 10 and 500 µm) enhanced cellular differentiation and proliferation, as well as bone formation and vascularization [141,197]. According to Hulbert *et al.*, the minimum for macropores size requirement is around 100 µm [198]. In their study in dogs, they showed that samples with pores comprised between 75 µm to 100 µm induced only little bone ingrowth, whereas samples with pore size ranging from 100 µm to 150 µm promoted a better bone ingrowth and apparition of calcified tissue. Samples with pores smaller than 75 µm were infiltrated by fibrous connective tissue only. The samples with the larger pores of the study (150-200 µm) exhibited the best results in terms of calcification, vascularization and presence of unmineralized bone within the pores. They justified the relevance of their results by correlating their observations with the diameter of the normal harverian systems (100-200 µm). This showed the critical importance of macroporosity on cellular response considering osteo and angiogenesis. However, depending on the testing conditions (load bearing or non load bearing conditions), the critical pore size mentioned by Hulbert and coworkers appear not to be universal [199,200]. Also, results differ between *in vitro* and *in vivo* assays, what makes difficult to define precise criteria on macropores size. In *in vitro* conditions, a low porosity can stimulate osteogenesis by suppressing cell proliferation and forcing cell aggregation while, in *in vivo* conditions, a higher porosity and pore size promoted a better bone ingrowth due to a good vascularization and oxygenation, favoring thus osteogenesis [107]. Moreover, the optimal, or range of optimal, pore size required for bone regeneration has been suggested to be dependent on each distinct cell types and also demonstrated to possess an upper limit to be efficiently functional [201]. Finally, the interconnectivity of pores is essential for bone regeneration as it enables the infiltration of bone, the development of an efficient blood vessels network and the promotion of cell-cell interactions [75,194,202].

On the other hand, the meso and microporosity also affects the cellular response. The presence of these very small pores increases the surface area of the scaffold. It promotes the adsorption of biological metabolites such as proteins and enhances cell adhesion [203,204]. The roughness created by these small pores favors the anchorage of cells and improves the proliferation and differentiation of bone cell lineage [204,205]. In parallel, it contributes to a better ion exchange and bone-like apatite formation by dissolution and re-precipitation process (in the case of biodegradable materials) [206]. Simon *et al.* showed that geometrical parameters (pore size and spatial arrangement of pores) affect the pattern of bone ingrowth [207]. The ability to vary and control the level of the different types of porosity (i.e. the meso, the micro and the macroporosity) is thus a key factor in the development of scaffolds for bone tissue engineering. As explained previously, the sol-gel technology appears to be a remarkable method to tailor the cellular response by varying porosity because it enables to control the macroporosity of materials by

using different fabrication methods and tune their texture at the meso and micro level [141,147]. It should be however noticed that the porosity of the material always has to be compromised between biological behavior and mechanical properties, as a too high void volume may provide good vascularization and osteointegration but significantly decrease the scaffold resistance to mechanical failure [208].

Another major research topic regarding the optimization of bone tissue repair is the ability to control cell-ECM interactions and to optimize cellular responses by producing materials with features tailored at the micro and nanoscale. If roughness can be achieved through the fabrication of meso-microporous scaffolds, it can also be tailored by engineering the surface of materials using various techniques. The texturing and patterning of a material surface can be performed using blasting [209], electropolishing [210], chemical treatments [211], lithography [212] and others. It is well known that micro and nanofeatures (roughness for example) created on the material surface positively affect cellular response (adhesion, detachment, proliferation, differentiation, spreading), in comparison to materials prepared with a smooth topography [210,213]. Materials having nanofeatures are even thought to be more suitable than ones with microfeatures because they may be more biomimetic and consequently better guide cell behavior [214]. The basement membranes of various tissues are composed of complex mixtures of nanoscale pits, pores, striations, particles, fibers and protrusions [213]. Based on a study conducted by Palin *et al.*, the replication of the nanoscale bone roughness on material surface indeed induced greater bone-forming cell adhesion and proliferation [215]. Other researchers have shown as well that, for some materials, the smaller the nanofeatures, the better the cell adhesion and differentiation [216–219]. However, it is difficult to establish a limit range of nanotopographic scale, in which bone regeneration is positively affected due to the diversity in topographic characteristics associated to the different studies mentioned above (size, uniformity and shape). What is clear is that nanotopography controls cell behavior through the regulation of focal adhesion formation and cytoskeleton contractility, and activation of processes taking place at the sub-cell level (genes upregulation, cell signaling, cell metabolism) [212,214,219].

But the physical surface patterning or texturing approach is not only used to modify the nanotopography of a material in terms of depth, pattern size or shape. It also enables to control the anisotropy of the material surface, a property to which cells are highly sensitive too. Cells cultured on grooved substrates for example elongate and align in the direction of the groove [220,221] (**Figure 1-8, 2**). The degree of alignment seemed to be directly related to the depth of the grooves [221], what demonstrated once again the importance of the roughness and the interplay of various physical factors for cellular activity. The spatial arrangement of fibers produced by electrospinning also induced similar responses [222,223]. When cultured on aligned fibrous mats, cells oriented themselves in the direction of the anisotropy (**Figure 1-8, 3**). In contrast, on non-woven mats, cells spread following the multi-directions of the random fiber organization. In addition to that physical guidance, electrospun fibers

present numerous particular advantages for bone tissue engineering. These benefits, as well as the explanation of the electrospinning process, are described in the following section.

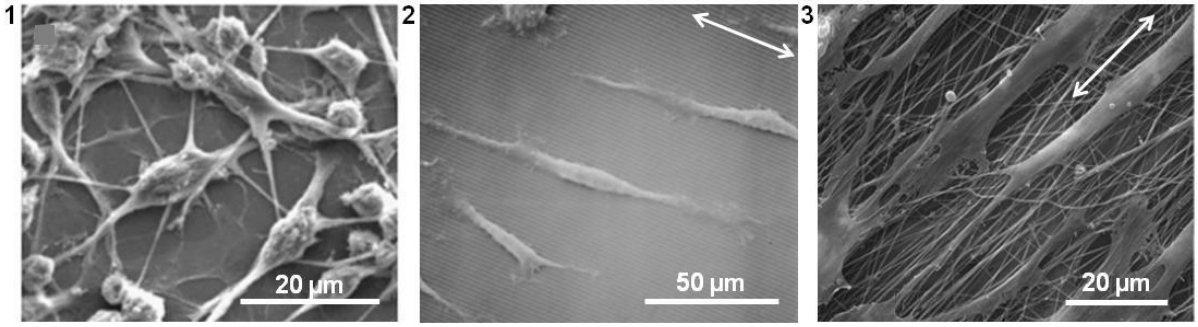

Figure 1-8. Examples of morphology of cells cultured on 1) tissue culture plate, e.g not patterned or textured surface, 2) grooved substrate and 3) aligned electrospun fibers. Arrows symbolize the direction of the anisotropy.
(Picture 1 is adapted from [222], *picture 2 from* [220], *picture 3 from* [224]*).*

In summary, material properties directly influence bone formation in tissue engineering. Both physical and chemical cues play a role in the targeting of specific cellular responses required for the regeneration of a fully healthy functional bone (osteo and angiogenesis). Choice of material constituents, nature of the functional groups present at the material surface, stiffness, roughness, nanofeatures and topography, among others, are as many parameters that interfere in that mechanism. It is however difficult to investigate the role of each factor in an independent manner as all of them are related. It is although clear that bone formation is the results of a dynamic dependence between numerous properties and that, with the cell-cell interactions and external mechanical stimulus, the cell-biomaterial interactions account as an essential part in the regeneration process. Given the diversity of the materials currently produced, it is necessary to specify that each material possesses a unique combination of properties and that each template will require specific improvements in order to achieve the proper biological performance. This should especially be achieved by finding a good compromise between all the criteria that an ideal scaffold should fulfill (mechanical properties, biological response, sterilizability…). Up to now, no ideal material has been developed - even though some are promising - and the design of biomaterials remains a challenging field of research with many and various perspectives of development.

1.6. Electrospinning technique

Among the various fabrication methods available to produce 3D scaffolds, electrospinning technique is nowadays one of the most used techniques. It is based on electrostatic principles and enables the deposition of micro and nano-scaled fibers. Its advantages are numerous and the fibers produced by this technique are commonly recognized as a suitable template for bone tissue engineering. The main benefit of producing electrospun fibrous substrates is the possibility to mimic the nanofibrous structure of the collagen matrix of natural bone [3,225,226]. It is moreover a cost-effective technique that does not

require sophisticated equipments and that can be used with an impressive variety of compounds [225,227].

Basically, the electrospinning process is simple. The set up consists in a syringe pump, a voltage source and a metallic collector (**Figure 1-9**). The principle behind the fibers formation relies on the competition between the electrostatic forces formed in a polymeric solution (melt or dissolution solutions) when it is subjected to a high voltage and its surface tension. When a voltage is applied to a liquid drop, the fluid charges, and as a result, repulsive electrostatic forces appear. The liquid however maintains its confinement (drop shape) up to a certain voltage thanks to its surface tension. If the intensity of the voltage is sufficiently increased up to a critical point, repulsive forces overcome the surface tension and a liquid jet rises from the drop (appearance of a Taylor cone [228]). The more the jet travels from the drop, the more elongated and thinner becomes the jet. This is explained by the instability of the jet which starts to whip and then bend and stretch [229,230]. These processes are represented in **Figure 1-10**. During this whipping process, solvent evaporates and solidification of the jet occurs. Fibers are then collected on a grounded metallic support. The flying time of the jet should thus be long enough to enable the complete drying of the jet. Fibers are deposited either as random or aligned mats, by using immobile or rotary collector respectively [231,232]. Fibers can be obtained from numerous synthetic polymers such as PLA, PCL, PGA, but also natural ones, as for examples silk, chitosan, gelatin and collagen [226]. To control the fibers production and the final fibers features, several variables can be manipulated. Processing parameters such as solution intrinsic properties (viscosity, solvent dielectric constant), ambient factors (humidity, room temperature) and set up conditions (liquid dispensing rate, voltage applied, tip-to-collector distance) influence the electrospinning procedure [233,234]. For example, fibers prepared using a solution with low viscosity will lead to the formation of thinner fibers than ones prepared with a higher viscosity solution [235]. One of the reasons of this is that viscosity and polymer chain entanglement are important criterion for the fiber deposition [236]. Similarly, fibers prepared with a low voltage will result in the fabrication of fibers with bigger diameter than ones deposited at a higher applied field [237]. High electric fields seem to favor the charge repulsion and promote the fiber slimming. So, although the basic principles of electrospinning appear to be simple, the setting of proper experimental parameters that enables the deposition of fibers with well defined features is usually laborious. This is particularly true, knowing that undesired phenomenon such as beads formation often occurs. Also, the continuity of the fiber deposition is easily disrupted and the process efficiency is consequently affected. Achieving the fabrication of homogeneous and continuous fibers is thus very challenging in electrospinning.

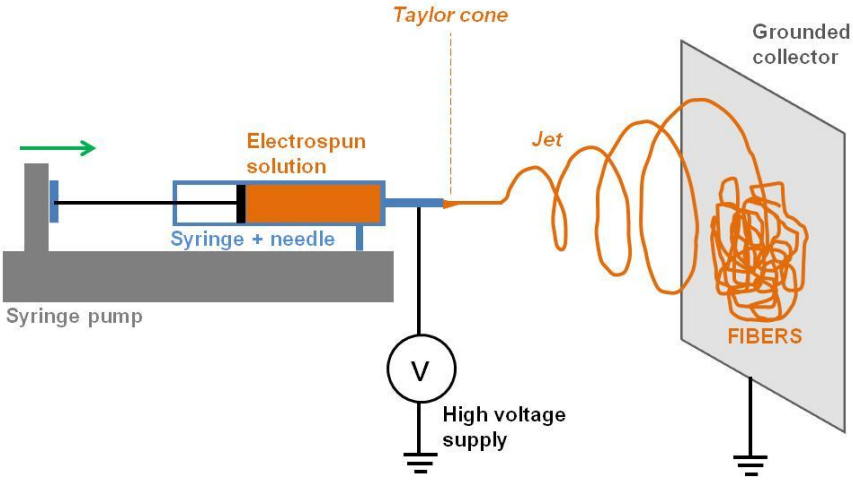

Figure 1-9. Scheme representing the electrospinning set-up.

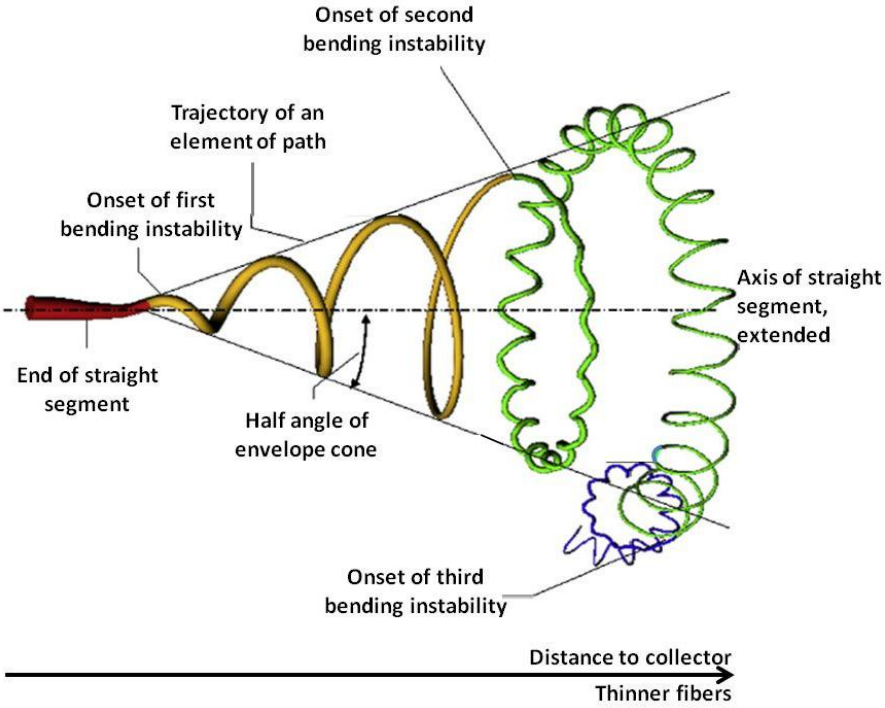

Figure 1-10. Path of an electrospinning jet that undergoes bending instabilities, solvent evaporation and slimming. *(image adapted from* [238])

Regarding biological concerns, composite electrospun fibers are the most interesting materials. In fact, bioactive compounds are generally added in the polymeric solution to provide bioactivity to the organic substrate. To do so, bioactive nanoparticles are frequently used. They are incorporated in the polymeric solution before starting the electrospinning. Typically, these nanoparticles are hydroxyapatite or silica xerogel [239,240]. Due to their high surface-to-volume ratio, these composites usually show good cellular adhesion and activity [226,227,241]. As explained previously, the nanotexture (i.e. nanoroughness induced by the nanosized fibers) that provides such electrospun fibers is particularly attractive for cells. They are also particularly interesting as they have been demonstrated to promote mineralization. But it is not always the case for all of the nanocomposites. Some of them possess limited

bioactivity or cellular responses due to a common critical problem: the bioactive phase is embedded in the polymer. Consequently, this phase is not detected by cells nor contributes to the supersaturation of bioactive ions at the interface of the biomaterial and the biological environment, a mechanism necessary to induce calcium-phosphate precipitation and involved in cell signaling [242]. An interesting study reported by Tong *et al.* demonstrated that the exposition of the particles can be controlled by changing the nanoparticles size and by controlling precisely the experimental parameters of the electrospinning process [183]. However, even though researchers seem to be aware that the encapsulation of the bioactive phase is a critical issue, very few studies that focus on that problem are found in the literature. To overcome this challenge as well as the limitations related to conventional composites (inhomogeneous degradation rate of the compounds, very low or inexistent cohesion between them, limited strength), hybrid organic-inroganic fibers prepared by the sol-gel method have gained interest in the last five years. Song and coworkers were for example some of the firsts to introduce this concept in bone tissue engineering and electrospinning [243]. In 2008, they reported the development of gelatin-siloxane nanofibers produced with intimate interactions between their compounds (hydrogen bonding). The siloxane introduced in the gelatin acted as a bridging agent for the polymer chains and resulted in a crosslinking effect. The fibers exhibited a good stability and were able to form bone mineral. They were also able to efficiently support cell adhesion, spreading and proliferation, and to elicit significant osteoblastic activity. This hybrid appeared to be a promising material for bone regeneration. This study highlighted thus the potential of the sol-gel technology to prepare hybrid scaffolds using electrospinning and the necessity to produce a synergic hybrid blend. This way, scaffolds with remarkable properties can be produced. Though, in comparison to the nanocomposites approach, hybrid fibers did not attract the attention of many research groups. Therefore, hybrid fibrous scaffolds prepared by the sol-gel method and the electrospinning technique have been chosen as research topic to carry out this thesis. Consequently, the work reported in this manuscript focuses on the development of bioactive and biodegradable fibrous hybrid grafts (class I and class II) prepared via these two methods, and the characterization of these biomaterials in terms of physico-chemical, mechanical and biological properties.

1.7. References

[1] Clarke B. Normal bone anatomy and physiology. Clinical Journal of the American Society of Nephrology 2008;3:131–9.

[2] Rho J-Y, Kuhn-Spearing L, Zioupos P. Mechanical properties and the hierarchical structure of bone. Medical Engineering & Physics 1998;20:92–102.

[3] Olszta MJ, Cheng X, Jee SS, Kumar R, Kim Y-Y, Kaufman MJ, et al. Bone structure and formation: A new perspective. Materials Science and Engineering: R: Reports 2007;58:77–116.

[4] http://classes.midlandstech.edu/carterp/Courses/bio210/chap06/lecture1.html 2014.

[5] http://fau.pearlashes.com/anatomy/Chapter%209/Chapter%209.htm 2014.

[6] Caetano-lopes J, Canhão H, Fonseca JE. Osteoblasts and bone formation. Acta Reumatologica Portuguesa 2007;32:103–10.

[7] Geiger B, Bershadsky A, Pankov R, Yamada KM. Transmembrane extracellular matrix–cytoskeleton crosstalk. Nature Reviews Molecular Cell Biology 2001;2:793–815.

[8] Guilak F, Cohen DM, Estes BT, Gimble JM, Liedtke W, Chen CS. Control of stem cell fate by physical interactions with the extracellular matrix. Cell Stem Cell 2009;5:17–26.

[9] Murshed M, Harmey D, Millán JL, Mckee MD, Karsenty G. Unique coexpression in osteoblasts of broadly expressed genes accounts for the spatial restriction of ECM mineralization to bone. Genes & Development 2005;19:1093–104.

[10] Damsky CH. Extracellular matrix-integrin interactions in osteoblast function and tissue remodeling. Bone 1999;25:95–6.

[11] Yamaguchi A, Komori T, Suda T. Regulation of Osteoblast Differentiation Mediated by. Endocrine Reviews 2000;21:393–411.

[12] Katagiri T, Takahashi N. Regulatory mechanisms of osteoblast and osteoclast differentiation. Oral Diseases 2002;8:147–59.

[13] Franz-Odendaal TA, Hall BK, Witten PE. Buried alive: how osteoblasts become osteocytes. Developmental Dynamics 2006;235:176–90.

[14] Dallas SL, Bonewald LF. Dynamics of the transition from osteoblast to osteocyte. Annals of the New York Academy of Sciences 2010;1192:437–43.

[15] Matsuo K, Irie N. Osteoclast-osteoblast communication. Archives of Biochemistry and Biophysics 2008;473:201–9.

[16] Bonewald LF. Establishment and characterization of an osteocyte-like cell line, MLO-Y4. Journal of Bone and Mineral Metabolism 1999;17:61–5.

[17] Miller SC, Jee W. The bone lining cell : a distinct phenotype ? Calcified Tissue International 1987;41:1–5.

[18] Miller SC, de Saint-Georges L, Bowman BM, Jee WS. Bone lining cells: structure and function. Scanning Microscopy 1989;3:953–60.

[19] Väänänen HK, Zhao H, Mulari M, Halleen JM. The cell biology of osteoclast function. Journal of Cell Science 2000;113:377–81.

[20] Miyamoto T, Suda T. Differentiation and function of osteoclasts. The Keio Journal of Medicine 2003;52:1–7.

[21] Teitelbaum SL, Abu-Amer Y, Ross FP. Molecular mechanisms of bone resorption. Journal of Cellular Biochemistry 1995;59:1–10.

[22] Väänänen K. Mechanism of osteoclast mediated bone resorption - rationale for the design of new therapeutics. Advanced Drug Delivery Reviews 2005;57:959–71.

[23] http://www.servier.fr/servier-medical-art 2014.

[24] Szpalski C, Wetterau M, Barr J, Warren SM. Bone tissue engineering : current strategies and techniques — part I : scaffolds. Tissue Engineering : Part B 2012;18:246–57.

[25] Yaszemski MJ, Oldham JB, Lu L, Currier BL. Clinical needs for bone tissue engineering technology. In: Squared T em, editor. Bone engineering, 2000, p. 541–7.

[26] Finkemeier CG. Bone-grafting and bone-graft substitutes. The Journal of Bone and Joint Surgery 2002;84-A:454–64.

[27] Gazdag A, Lane J, Glaser D, Forster R. Alternatives to autogenous bone graft : efficacy and indications. The Journal of the American Academy of Orthopaedic Surgeons 1995;3:1–8.

[28] Burwell RG. Studies in the transplantation of bone. The Journal of Bone and Joint Surgery 1964;46-B:110–40.

[29] Heslop BF, Zeiss IM, Nisbet NW. Studies on transference of bone. British Journal of Experimental Pathology 1960;41:269–87.

[30] Burchardt H. The biology of bone graft repair. Clinical Orthopaedics and Related Research 1983:28–42.

[31] Younger EM, Chapman MW. Morbidity at bone graft donor sites. Journal of Orthopaedic Trauma 1989;3:192–5.

[32] Dimitriou R, Mataliotakis GI, Angoules AG, Kanakaris NK, Giannoudis P V. Complications following autologous bone graft harvesting from the iliac crest and using the RIA : a systematic review. Injury, International Journal of the Care of the Injured 2011;42:S3–15.

[33] Giannoudis P V, Dinopoulos H, Tsiridis E. Bone substitutes: an update. Injury, International Journal of the Care of the Injured 2005;36S:S20–7.

[34] Palmer SH, Gibbons CL, Athanasou NA. The pathology of bone allograft. The Journal of Bone and Joint Surgery British Volume 1999;81-B:333–5.

[35] Pelker RR, Friedlaender GE. Biomechanical aspects of bone autografts and allografts. The Orthopaedic Clinics of North America 1987;18:235–9.

[36] Poumarat G, Squire P. Comparison of mechanical properties of human, bovine bone and a new processed bone xenograft. Biomaterials 1993;14:337–40.

[37] Taschieri S, Del Fabbro M, Testori T, Weinstein R. Efficacy of xenogeneic bone grafting with guided tissue regeneration in the management of bone defects after surgical endodontics. Journal of Oral and Maxillofacial Surgery 2007;65:1121–7.

[38] Develioglu H, Unver Saraydin S, Kartal U. The bone-healing effect of a xenograft in a rat calvarial defect model. Dental Materials Journal 2009;28:396–400.

[39] Caplan AL. Ethical issues raised by research involving xenografts. The Journal of the American Medical Association 1985;254:3339–43.

[40] Hench LL, Polak JM. Third-generation biomedical materials. Science 2002;295:1014–7.

[41] Navarro M, Michiardi A, Castaño O, Planell JA. Biomaterials in orthopaedics. Journal of the Royal Society, Interface 2008;5:1137–58.

[42] Bauer TW, Schils J. The pathology of total joint arthroplasty. II. Mechanisms of implant failure. Skeletal Radiology 1999;28:483–97.

[43] Southam J, Selwyn P. Structural changes around screws used in the treatment of fractured human mandibles. British Journal of Oral Surgery 1970;8:211–21.

[44] Lopez-Esteban S, Saiz E, Fujino S, Oku T, Suganuma K, Tomsia AP. Bioactive glass coatings for orthopedic metallic implants. Journal of the European Ceramic Society 2003;23:2921–30.

[45] Habibovic P, Barrère F, Van Blitterswijk CA, De Groot K, Layrolle P. Biomimetic hydroxyapatite coating on metal implants. Journal of the American Ceramic Society 2002;85:517–22.

[46] Gogotsi GA. Fracture toughness of ceramics and ceramic composites. Ceramics International 2003;29:777–84.

[47] Blencke B, Brömer H, Deutscher K, Hennig W. Untersuchungen über den histologischen und mechanischen Verbund von glaskeramischen Werkstoffen mit dem Implantatlager. Biomedizinische Technik Band 1978;23:360–1.

[48] Kotani S, Fujita Y, Kitsugi T, Nakamura T, Yamamuro T, Ohtsuki C, et al. Bone bonding mechanism of beta-tricalcium phosphate. Journal of Biomedical Materials Research 1991;25:1303–15.

[49] Rokkanen PU, Böstman O, Hirvensalo E, Mäkelä EA, Partio EK, Pätiälä H, et al. Bioabsorbable fixation in orthopaedic surgery and traumatology. Biomaterials 2000;21:2607–13.

[50] Lanza RP, Langer RS, Vacanti J. Principles of tissue engineering. 1997.

[51] Nieponice A, Soletti L, Guan J, Deasy BM, Huard J, Wagner WR, et al. Development of a tissue engineered vascular graft combining a biodegradable scaffold, muscle-derived stem cells and a rotational vacuum seeding technique. Biomaterials 2008;29:825–33.

[52] Subramanian A, Krishnan UM, Sethuraman S. Development of biomaterial scaffold for nerve tissue engineering: biomaterial mediated neural regeneration. Journal of Biomedical Science 2009;16:108–18.

[53] Whang K, Healy KE, Elenz DR, Nam EK, Tsai DC, Thomas CH, et al. Engineering bone regeneration with bioabsorbable scaffolds with novel microarchitecture. Tissue Engineering 1999;5:35–51.

[54] Davies JE (Ed.). The bone-biomaterial interface. 1991.

[55] Hoppe A, Güldal NS, Boccaccini AR. A review of the biological response to ionic dissolution products from bioactive glasses and glass-ceramics. Biomaterials 2011;32:2757–74.

[56] Lee K, Silva EA, Mooney DJ. Growth factor delivery-based tissue engineering: general approaches and a review of recent developments. Journal of the Royal Society, Interface 2011;8:153–70.

[57] Malafaya PB, Silva GA, Reis RL. Natural-origin polymers as carriers and scaffolds for biomolecules and cell delivery in tissue engineering applications. Advanced Drug Delivery Reviews 2007;59:207–33.

[58] Jones JR, Ehrenfried LM, Hench LL. Optimising bioactive glass scaffolds for bone tissue engineering. Biomaterials 2006;27:964–73.

[59] Li Z, Ramay HR, Hauch KD, Xiao D, Zhang M. Chitosan-alginate hybrid scaffolds for bone tissue engineering. Biomaterials 2005;26:3919–28.

[60] Yang C. Enhanced physicochemical properties of collagen by using EDC/NHS-crosslinking. Bulletin of Materials Science 2012;35:913–8.

[61] Ji Y, Ghosh K, Shu XZ, Li B, Sokolov JC, Prestwich GD, et al. Electrospun three-dimensional hyaluronic acid nanofibrous scaffolds. Biomaterials 2006;27:3782–92.

[62] Dhandayuthapani B, Yoshida Y, Maekawa T, Kumar DS. Polymeric scaffolds in tissue engineering application: a review. International Journal of Polymer Science 2011;2011:1–19.

[63] Middleton JC, Tipton AJ. Synthetic biodegradable polymers as orthopedic devices. Biomaterials 2000;21:2335–46.

[64] Gunatillake PA, Adhikari R. Biodegradable synthetic polymers for tissue engineering. European Cells & Materials 2003;5:1–16.

[65] Athanasiou KA, Agrawal CM, Barber FA, Burkhart SS. Orthopaedic applications for PLA-PGA biodegradable polymers. Arthroscopy: The Journal of Arthroscopic & Related Surgery 1998;14:726–37.

[66] Liu X, Ma PX. Polymeric scaffolds for bone tissue engineering. Annals of Biomedical Engineering 2004;32:477–86.

[67] Rezwan K, Chen QZ, Blaker JJ, Boccaccini AR. Biodegradable and bioactive porous polymer/inorganic composite scaffolds for bone tissue engineering. Biomaterials 2006;27:3413–31.

[68] Li S. Hydrolytic degradation characteristics of aliphatic polyesters derived from lactic and glycolic acids. Journal of Biomedical Materials Research 1999;48:342–53.

[69] Siparsky GL, Voorhees KJ, Miao F. Hydrolysis of polylactic acid (PLA) and polycaprolactone (PCL) in aqueous acetonitrile solutions: autocatalysis. Journal of Environmental Polymer Degradation 1998;6:31–41.

[70] Woodruff MA, Hutmacher DW. The return of a forgotten polymer -polycaprolactone in the 21st century. Progress in Polymer Science 2010;35:1217–56.

[71] Hutmacher DW. Scaffolds in tissue engineering bone and cartilage. Biomaterials 2000;21:2529–43.

[72] Burg KJ, Porter S, Kellam JF. Biomaterial developments for bone tissue engineering. Biomaterials 2000;21:2347–59.

[73] Hench LL, Splinter RJ, Allen WC, Greenlee TK. Bonding mechanisms at the interface of ceramic prosthetic materials. Journal of Biomedical Materials Research 1971;5:117–41.

[74] Bosetti M, Cannas M. The effect of bioactive glasses on bone marrow stromal cells differentiation. Biomaterials 2005;26:3873–9.

[75] Valerio P, Guimaráes MHR, Pereira MM, Leite MF, Goes AM. Primary osteoblast cell response to sol-gel derived bioactive glass foams. Journal of Materials Science Materials in Medicine 2005;16:851–6.

[76] Clèries L, Fernández-Pradas JM, Sardin G, Morenza JL. Dissolution behaviour of calcium phosphate coatings obtained by laser ablation. Biomaterials 1998;19:1483–7.

[77] Ducheyne P, Radin S, Heughebaert M, Heughebaert JC. Calcium phosphate ceramic coatings on porous titanium: effect of structure and composition on electrophoretic deposition, vacuum sintering and in vitro dissolution. Biomaterials 1990;11:244–54.

[78] Xynos ID, Edgar AJ, Buttery LD, Hench LL, Polak JM. Gene-expression profiling of human osteoblasts following treatment with the ionic products of Bioglass 45S5 dissolution. Journal of Biomedical Materials Research 2001;55:151–7.

[79] Jell G, Stevens MM. Gene activation by bioactive glasses. Journal of Materials Science: Materials in Medicine 2006;17:997–1002.

[80] Oonishi H, Hench LL, Wilson J, Sugihara F, Tsuji E, Matsuura M, et al. Quantitative comparison of bone growth behavior in granules of Bioglass, A-W glass-ceramic, and hydroxyapatite. Journal of Biomedical Materials Research 2000;51:37–46.

[81] Martin RA, Yue S, Hanna J V, Lee PD, Newport RJ, Smith ME, et al. Characterizing the hierarchical structures of bioactive sol-gel silicate glass and hybrid scaffolds for bone regeneration. Philosophical Transactions of the Royal Society - Series A, Mathematical, Physical, and Engineering Sciences 2012;370:1422–43.

[82] Hench LL. The story of bioglass. Journal of Materials Science Materials in Medicine 2006;17:967–78.

[83] Jones JR. Review of bioactive glass: from Hench to hybrids. Acta Biomaterialia 2013;9:4457–86.

[84] Gerhardt L-C, Boccaccini AR. Bioactive glass and glass-ceramic scaffolds for bone tissue engineering. Materials 2010;3:3867–910.

[85] Li R, Clark AE, Hench LL. An investigation of bioactive glass powders by sol-gel processing. Journal of Applied Biomaterials 1991;2:231–9.

[86] Uo M, Mizuno M, Kuboki Y, Makishima A, Watari F. Properties and cytotoxicity of water soluble Na2O-CaO-P2O5 glasses. Biomaterials 1998;19:2277–84.

[87] Choueka J, Charvet JL, Alexander H, Oh YH, Joseph G, Blumenthal NC, et al. Effect of annealing temperature on the degradation of reinforcing fibers for absorbable implants. Journal of Biomedical Materials Research 1995;29:1309–15.

[88] Zhang Y, Santos J. Crystallization and microstructure analysis of calcium phosphate-based glass ceramics for biomedical applications. Journal of Non-Crystalline Solids 2000;272:14–21.

[89] Navarro M, Ginebra M, Clément J, Martinez S, Avila G, Planell JA. Physicochemical degradation of titania-stabilized soluble phosphate glasses for medical applications. Journal of the American Ceramic Society 2003;86:1342–52.

[90] Navarro M, del Valle S, Martínez S, Zeppetelli S, Ambrosio L, Planell JA, et al. New macroporous calcium phosphate glass ceramic for guided bone regeneration. Biomaterials 2004;25:4233–41.

[91] Kiani A, Lakhkar NJ, Salih V, Smith ME, Hanna J V, Newport RJ, et al. Titanium-containing bioactive phosphate glasses. Philosophical Transactions of the Royal Society Series A, Mathematical, Physical, and Engineering Sciences 2012;370:1352–75.

[92] Aguirre A, Gonzalez A, Navarro M, Castano O, Planell JA, Engel E. Control of microenvironmental cues with a smart biomaterial composite promotes endothelial progenitor cell angiogenesis. European Cells and Materials 2012;24:90–106.

[93] Vila OF, Bagó JR, Navarro M, Alieva M, Aguilar E, Engel E, et al. Calcium phosphate glass improves angiogenesis capacity of poly(lactic acid) scaffolds and stimulates differentiation of adipose tissue-derived mesenchymal stromal cells to the endothelial lineage. Journal of Biomedical Materials Research Part A 2013;101:932–41.

[94] Gerhardt L-C, Widdows KL, Erol MM, Burch CW, Sanz-Herrera JA, Ochoa I, et al. The pro-angiogenic properties of multi-functional bioactive glass composite scaffolds. Biomaterials 2011;32:4096–108.

[95] Day RM. Bioactive glass stimulates the secretion of angiogenic growth factors and angiogenesis in vitro. Tissue Engineering 2005;11:768–77.

[96] Leach JK, Kaigler D, Wang Z, Krebsbach PH, Mooney DJ. Coating of VEGF-releasing scaffolds with bioactive glass for angiogenesis and bone regeneration. Biomaterials 2006;27:3249–55.

[97] Leu A, Stieger SM, Dayton P, Ferrara KW, Leach JK. Angiogenic response to bioactive glass promotes bone healing in an irradiated calvarial defect. Tissue Engineering Part A 2009;15:877–85.

[98] Wang M. Developing bioactive composite materials for tissue replacement. Biomaterials 2003;24:2133–51.

[99] Kickelbick G. Introduction to Hybrid Materials. Hybrid Materials. Synthesis, Characterization, and Applications, 2007, p. 1–48.

[100] Wei G, Ma PX. Structure and properties of nano-hydroxyapatite/polymer composite scaffolds for bone tissue engineering. Biomaterials 2004;25:4749–57.

[101] Thomson RC, Yaszemski MJ, Powers JM, Mikos AG. Hydroxyapatite fiber reinforced poly(alpha-hydroxy ester) foams for bone regeneration. Biomaterials 1998;19:1935–43.

[102] Martinez-Valencia AB, Carbajal-De laTorre G, Duarte Moller A, Esparza-Ponce HE, Espinosa-Medina MA. Study of bioactivity , biodegradability and mechanical properties of polyurethane/nano-hydroxyapatite hybrid composites. International Journal of the Physical Sciences 2011;6:6681–91.

[103] Kong L, Gao Y, Lu G, Gong Y, Zhao N, Zhang X. A study on the bioactivity of chitosan/nano-hydroxyapatite composite scaffolds for bone tissue engineering. European Polymer Journal 2006;42:3171–9.

[104] Niemelä T, Niiranen H, Kellomäki M. Self-reinforced composites of bioabsorbable polymer and bioactive glass with different bioactive glass contents. Part II: In vitro degradation. Acta Biomaterialia 2008;4:156–64.

[105] Mastrogiacomo M, Scaglione S, Martinetti R, Dolcini L, Beltrame F, Cancedda R, et al. Role of scaffold internal structure on in vivo bone formation in macroporous calcium phosphate bioceramics. Biomaterials 2006;27:3230–7.

[106] Murphy CM, O'Brien FJ. Understanding the effect of mean pore size on cell activity in collagen-glycosaminoglycan scaffolds. Cell Adhesion & Migration 2010;4:377–81.

[107] Karageorgiou V, Kaplan D. Porosity of 3D biomaterial scaffolds and osteogenesis. Biomaterials 2005;26:5474–91.

[108] Gan YX. Effect of interface structure on mechanical properties of advanced composite materials. International Journal of Molecular Sciences 2009;10:5115–34.

[109] Misra SK, Mohn D, Brunner TJ, Stark WJ, Philip SE, Roy I, et al. Comparison of nanoscale and microscale bioactive glass on the properties of P(3HB)/Bioglass composites. Biomaterials 2008;29:1750–61.

[110] Etcheverry M, Barbosa SE. Glass fiber reinforced polypropylene mechanical properties enhancement by adhesion improvement. Materials 2012;5:1084–113.

[111] Mammeri F, Bourhis E Le, Rozes L, Sanchez C. Mechanical properties of hybrid organic–inorganic materials. Journal of Materials Chemistry 2005;15:3787.

[112] Lee K-H, Rhee S-H. The mechanical properties and bioactivity of poly(methyl methacrylate)/SiO2-CaO nanocomposite. Biomaterials 2009;30:3444–9.

[113] Liu A, Hong Z, Zhuang X, Chen X, Cui Y, Liu Y, et al. Surface modification of bioactive glass nanoparticles and the mechanical and biological properties of poly(L-lactide) composites. Acta Biomaterialia 2008;4:1005–15.

[114] Gupta R, Kumar A. Bioactive materials for biomedical applications using sol-gel technology. Biomedical Materials 2008;3:034005(15pp).

[115] Blaker JJ, Bismarck A, Boccaccini AR, Young AM, Nazhat SN. Premature degradation of poly(alpha-hydroxyesters) during thermal processing of Bioglass-containing composites. Acta Biomaterialia 2010;6:756–62.

[116] Valliant EM, Jones JR. Softening bioactive glass for bone regeneration: sol–gel hybrid materials. Soft Matter 2011;7:5083–95.

[117] Kickelbick G. Concepts for the incorporation of inorganic building blocks into organic polymers on a nanoscale. Progress in Polymer Science 2003;28:83–114.

[118] Martín AI, Salinas AJ, Vallet-Regí M. Bioactive and degradable organic–inorganic hybrids. Journal of the European Ceramic Society 2005;25:3533–8.

[119] Landry CJ., Coltrain BK, Brady BK. In situ polymerization of tetraethoxysilane in poly(methyl methacrylate): morphology and dynamic mechanical properties. Polymer 1992;33:1486–95.

[120] Landry CJ., Coltrain BK, Wesson JA, Zumbulyadis N, Lippert JL. In situ polymerization of tetraethoxysilane in polymers: chemical nature of the interactions. Polymer 1992;33:1496–506.

[121] Valliant EM, Jones JR. Softening bioactive glass for bone regeneration: sol–gel hybrid materials. Soft Matter 2011;7:5083–95.

[122] Tian D, Dubois P, Jeromet R. A new poly(epsilon-caprolactone) containing hybrid ceramer prepared by the sol-gel process. Polymer 1996;37:3983–7.

[123] Poologasundarampillai G, Ionescu C, Tsigkou O, Murugesan M, Hill RG, Stevens MM, et al. Synthesis of bioactive class II poly(γ-glutamic acid)/silica hybrids for bone regeneration. Journal of Materials Chemistry 2010;20:8952–61.

[124] Mahony O, Tsigkou O, Ionescu C, Minelli C, Ling L, Hanly R, et al. Silica-gelatin hybrids with tailorable degradation and mechanical properties for tissue regeneration. Advanced Functional Materials 2010;20:3835–45.

[125] Tian D, Dubois PH, Jerome R. Biodegradable and biocompatible inorganic – organic hybrid materials. I. synthesis and characterization. Journal of Polymer Science Part A: Polymer Chemistry 1997;35:2295–309.

[126] Tian D, Dubois P, Grandfils C, Robert J, Viville P, Lazzaroni R, et al. A novel biodegradable and biocompatible ceramer prepared by the sol-gel process. Chemistry of Materials 1997;9:871–4.

[127] Rhee S-H, Choi J-Y, Kim H-M. Preparation of a bioactive and degradable poly(ε-caprolactone)/silica hybrid through a sol-gel method. Biomaterials 2002;23:4915–21.

[128] Rhee S-H. Effect of calcium salt content in the poly(ε-caprolactone)/silica nanocomposite on the nucleation and growth behavior of apatite layer. Journal of Biomedical Materials Research Part A 2003;67:1131–8.

[129] Rhee S-H, Lee Y-K, Lim B-S, Yoo JJ, Kim HJ. Evaluation of a novel poly(ε-caprolactone)-organosiloxane hybrid material for the potential application as a bioactive and degradable bone substitute. Biomacromolecules 2004;5:1575–9.

[130] Rhee S-H. Bone-like apatite-forming ability and mechanical properties of poly(ε-caprolactone)/silica hybrid as a function of poly(ε-caprolactone) content. Biomaterials 2004;25:1167–75.

[131] Yoo JJ, Lee JE, Kim HJ, Kim S, Lim JH, Lee SJ, et al. Comparative in vitro and in vivo studies using a bioactive poly(ε-caprolactone)-organosiloxane nanohybrid containing calcium salt. Journal of Biomedical Materials Research Part B: Applied Biomaterials 2007;83B:189–98.

[132] Ohtsuki C, Kokubo T, Yamamuro T. Mechanism of apatite formation on $CaO\text{-}SiO_2\text{-}P_20_5$ glasses in a simulated body fluid. Journal of Non-Crystalline Solids 1992;143:84–92.

[133] Kokubo T, Kushitani H, Ohtsuki C, Sakka S, Yamamuro T. Chemical reaction of bioactive glass and glass-ceramics with a simulated body fluid. Journal of Materials Science: Materials in Medicine 1992;3:79–83.

[134] Poologasundarampillai G, Yu B, Tsigkou O, Valliant E, Yue S, Lee PD, et al. Bioactive silica–poly(γ-glutamic acid) hybrids for bone regeneration: effect of covalent coupling on dissolution and mechanical properties and fabrication of porous scaffolds. Soft Matter 2012;8:4822–32.

[135] Maeda H, Kasuga T, Hench LL. Preparation of poly(L-lactic acid)-polysiloxane-calcium carbonate hybrid membranes for guided bone regeneration. Biomaterials 2006;27:1216–22.

[136] Ren L, Tsuru K, Hayakawa S, Osaka A. Synthesis and characterization of gelatin-siloxane hybrids derived through sol-gel procedure. Journal of Sol-Gel Science and Technology 2001;21:115–21.

[137] Ren L, Tsuru K, Hayakawa S, Osaka A. Novel approach to fabricate porous gelatin-siloxane hybrids for bone tissue engineering. Biomaterials 2002;23:4765–73.

[138] Pereira MM, Hench LL. Mechanisms of hydroxyapatite formation on porous gel-silica substrates. Journal of Sol-Gel Science and Technology 1996;7:59–68.

[139] Sepulveda P, Jones JR, Hench LL. In vitro dissolution of melt-derived 45S5 and sol-gel derived 58S bioactive glasses. Journal of Biomedical Materials Research 2002;61:301–11.

[140] Schmidt H. Chemistry of material preparation by the sol-gel process. Journal of Non-Crystalline Solids 1988;100:51–64.

[141] Sepulveda P, Jones JR, Hench LL. Bioactive sol-gel foams for tissue repair. Journal of Biomedical Materials Research 2002;59:340–8.

[142] Jones JR, Gentleman E, Polak J. Bioactive glass scaffolds for bone regeneration. Elements 2007;3:393–9.

[143] Brinker CJ, Scherer GW. Sol-gel science, the physics and chemistry of sol-gel processing. 1990.

[144] Schubert U, Husing N, Lorenz A. Hybrid inorganic-organic materials by sol-gel processing of organofunctional metal alkoxides. Chemistry of Materials 1995;7:2010–27.

[145] Meixner DL, Dyer PN. Influence of sol-gel synthesis parameters on the microstructure of particulate silica xerogels. Journal of Sol-Gel Science and Technology 1999;14:223–32.

[146] Jones JR. New trends in bioactive scaffolds: the importance of nanostructure. Journal of the European Ceramic Society 2009;29:1275–81.

[147] Brinker CJ, Sehgal R, Hietala SL, Deshpande R, Smith DM, Loy D, et al. Sol-gel strategies for controlled porosity inorganic materials. Journal of Membrane Science 1994;94:85–102.

[148] Hench LL, West JK. The sol-gel process. Chemical Reviews 1990;90:33–72.

[149] Saravanapavan P, Hench LL. Mesoporous calcium silicate glasses. I. Synthesis. Journal of Non-Crystalline Solids 2003;318:1–13.

[150] Podbielska H, Ulatowska-Jarza A. Sol-gel technology for biomedical engineering. Bulletin of the Polish Academy of Sciences: Technical Sciences 2005;53:261–71.

[151] Pereira MM, Jones JR, Hench LL. Bioactive glass and hybrid scaffolds prepared by sol–gel method for bone tissue engineering. Advances in Applied Ceramics 2005;104:35–42.

[152] Shin S-H, Purevdorj O, Castano O, Planell JA, Kim H-W. A short review: Recent advances in electrospinning for bone tissue regeneration. Journal of Tissue Engineering 2012;3:2041731412443530.

[153] Stains JP, Civitelli R. Cell-cell interactions in regulating osteogenesis and osteoblast function. Birth Defects Research Part C, Embryo Today : Reviews 2005;75:72–80.

[154] Stapor PC, Azimi MS, Ahsan T, Murfee WL. An angiogenesis model for investigating multi-cellular interactions across intact microvascular networks. American Journal of Physiology Heart and Circulatory Physiology 2013;304:H235–45.

[155] Saha K, Pollock JF, V. SD, E. HK. Designing synthetic materials to control stem cell phenotype. Current Opinion in Chemical Biology 2007;11:381–7.

[156] Provenzano PP, Keely PJ. Mechanical signaling through the cytoskeleton regulates cell proliferation by coordinated focal adhesion and Rho GTPase signaling. Journal of Cell Science 2011;124:1195–205.

[157] Lee JH, Jung HW, Kang IK, Lee HB. Cell behaviour on polymer surfaces with different functional groups. Biomaterials 1994;15:705–11.

[158] Lee JH, Pazk JW, Lee HB. Cell adhesion and growth on polymer surfaces with hydroxyl groups prepared by water vapour plasma treatment. Biomaterials 1991;12:443–8.

[159] Curtis ASG, Forrester J V, McInnes C, Lawrie F. Adhesion of cells to polystyrene surfaces. The Journal of Cell Biology 1983;97:1500–6.

[160] Arima Y, Iwata H. Effect of wettability and surface functional groups on protein adsorption and cell adhesion using well-defined mixed self-assembled monolayers. Biomaterials 2007;28:3074–82.

[161] Nakaoka R, Yamakoshi Y, Isama K, Tsuchiya T. Effects of surface chemistry prepared by self-assembled monolayers on osteoblast behavior. Journal of Biomedical Materials Research Part A 2010;94:524–32.

[162] Webb K, Hlady V, Tresco PA. Relative importance of surface wettability and charged functional groups on NIH 3T3 fibroblast attachment, spreading, and cytoskeletal organization. Journal of Biomedical Materials Research 1998;41:422–30.

[163] Wilson CJ, Clegg RE, Leavesley DI, Pearcy MJ. Mediation of biomaterial-cell interactions by adsorbed proteins: a review. Tissue Engineering 2005;11:1–18.

[164] Cai K, Frant M, Bossert J, Hildebrand G, Liefeith K, Jandt KD. Surface functionalized titanium thin films: zeta-potential, protein adsorption and cell proliferation. Colloids and Surfaces B: Biointerfaces 2006;50:1–8.

[165] Arima Y, Iwata H. Effects of surface functional groups on protein adsorption and subsequent cell adhesion using self-assembled monolayers. Journal of Materials Chemistry 2007;17:4079–87.

[166] Punet X, Mauchauffé R, Giannotti MI, Rodríguez-Cabello JC, Sanz F, Engel E, et al. Enhanced cell-material interactions through the biofunctionalization of polymeric surfaces with engineered peptides. Biomacromolecules 2013;14:2690–702.

[167] Hersel U, Dahmen C, Kessler H. RGD modified polymers: biomaterials for stimulated cell adhesion and beyond. Biomaterials 2003;24:4385–415.

[168] Delaittre G, Greiner AM, Pauloehrl T, Bastmeyer M, Barner-Kowollik C. Chemical approaches to synthetic polymer surface biofunctionalization for targeted cell adhesion using small binding motifs. Soft Matter 2012;8:7323–47.

[169] Lutolf MP, Hubbell JA. Synthetic biomaterials as instructive extracellular microenvironments for morphogenesis in tissue engineering. Nature Biotechnology 2005;23:47–55.

[170] Massia SP, Hubbell JA. An RGD spacing of 440 nm is sufficient for integrin alphaV beta3-mediated fibroblast spreading and 140 nm for focal contact and stress fiber formation. The Journal of Cell Biology 1991;114:1089–100.

[171] Rezania A, Healy KE. The effect of peptide surface density on mineralization of a matrix deposited by osteogenic cells. Journal of Biomedical Materials Research 2000;52:595–600.

[172] Lewandowska K, Pergament E, Sukenik CN, Culp LA. Cell-type-specific adhesion mechanisms mediated by fibronectin adsorbed to chemically derivatized substrata. Journal of Biomedical Materials Research 1992;26:1343–63.

[173] Hoppe A, Güldal NS, Boccaccini AR. A review of the biological response to ionic dissolution products from bioactive glasses and glass-ceramics. Biomaterials 2011;32:2757–74.

[174] Hench LL. Genetic design of bioactive glass. Journal of the European Ceramic Society 2009;29:1257–65.

[175] Charles-Harris M, Koch MA, Navarro M, Lacroix D, Engel E, Planell JA. A PLA/calcium phosphate degradable composite material for bone tissue engineering: an in vitro study. Journal of Materials Science: Materials in Medicine 2008;19:1503–13.

[176] Marie PJ. The calcium-sensing receptor in bone cells: a potential therapeutic target in osteoporosis. Bone 2010;46:571–6.

[177] Honda Y, Fitzsimmons RJ, Baylink DJ, Mohan S. Effects of extracellular calcium on insulin-like growth factor II in human bone cells. Journal of Bone and Mineral Research 1995;10:1660–5.

[178] Chattopadhyay N, Yano S, Tfelt-Hansen J, Rooney P, Kanuparthi D, Bandyopadhyay S, et al. Mitogenic action of calcium-sensing receptor on rat calvarial osteoblasts. Endocrinology 2004;145:3451–62.

[179] Choudhary S, Wadhwa S, Raisz LG, Alander C, Pilbeam CC. Extracellular calcium is a potent inducer of cyclo-oxygenase-2 in murine osteoblasts through an ERK signaling pathway. Journal of Bone and Mineral Research 2003;18:1813–24.

[180] Aguirre A, González A, Planell JA, Engel E. Extracellular calcium modulates in vitro bone marrow-derived Flk-1^+ $CD34^+$ progenitor cell chemotaxis and differentiation through a calcium-sensing receptor. Biochemical and Biophysical Research Communications 2010;393:156–61.

[181] Maeno S, Niki Y, Matsumoto H, Morioka H, Yatabe T, Funayama A, et al. The effect of calcium ion concentration on osteoblast viability, proliferation and differentiation in monolayer and 3D culture. Biomaterials 2005;26:4847–55.

[182] Navarro M, Engel E, Planell JA, Amaral I, Barbosa M, Ginebra MP. Surface characterization and cell response of a PLA/CaP glass biodegradable composite material. Journal of Biomedical Materials Research Part A 2008;85A:477–86.

[183] Tong H-W, Wang M, Li Z-Y, Lu WW. Electrospinning, characterization and in vitro biological evaluation of nanocomposite fibers containing carbonated hydroxyapatite nanoparticles. Biomedical Materials 2010;5:054111 (13pp).

[184] Vogel V, Sheetz M. Local force and geometry sensing regulate cell functions. Nature Reviews Molecular Cell Biology 2006;7:265–75.

[185] Wozniak MA, Chen CS. Mechanotransduction in development: a growing role for contractility. Nature Reviews Molecular Cell Biology 2009;10:34–43.

[186] Beningo KA, Dembo M, Kaverina I, Small J V, Wang Y-L. Nascent focal adhesions are responsible for the generation of strong propulsive forces in migrating fibroblasts. The Journal of Cell Biology 2001;153:881–7.

[187] Tamada M, Sheetz MP, Sawada Y. Activation of a signaling cascade by cytoskeleton stretch. Developmental Cell 2004;7:709–18.

[188] Ingber DE. Mechanical signaling and the cellular response to extracellular matrix in angiogenesis and cardiovascular physiology. Circulation Research 2002;91:877–87.

[189] Bershadsky AD, Balaban NQ, Geiger B. Adhesion-dependent cell mechanosensitivity. Annual Review of Cell and Developmental Biology 2003;19:677–95.

[190] Engler AJ, Sen S, Sweeney HL, Discher DE. Matrix elasticity directs stem cell lineage specification. Cell 2006;126:677–89.

[191] Solon J, Levental I, Sengupta K, Georges PC, Janmey PA. Fibroblast adaptation and stiffness matching to soft elastic substrates. Biophysical Journal 2007;93:4453–61.

[192] Rowlands AS, George PA, Cooper-White JJ. Directing osteogenic and myogenic differentiation of MSCs: interplay of stiffness and adhesive ligand presentation. American Journal of Physiology Cell Physiology 2008;295:C1037–44.

[193] Ingber DE. Cellular mechanotransduction: putting all the pieces together again. FASEB Journal: Official Publication of the Federation of American Societies for Experimental Biology 2006;20:811–27.

[194] Kuboki Y, Takita H, Kobayashi D, Tsuruga E, Inoue M, Murata M, et al. BMP-induced osteogenesis on the surface of hydroxyapatite with geometrically feasible and nonfeasible structures: topology of osteogenesis. Journal of Biomedical Materials Research 1998;39:190–9.

[195] Tai H, Mather ML, Howard D, Wang W, White LJ, Crowe JA, et al. Control of pore size and structure of tissue engineering scaffolds produced by supercritical fluid processing. European Cells & Materials 2007;14:64–77.

[196] Rouquerol J, Avnir D, Fairbridge CW, Everett DH, Haynes JM, Pernicone N, et al. Recommendations for the characterization of porous solids. Pure and Applied Chemistry 1994;66:1739–58.

[197] Xynos ID, Hukkanen MVJ, Batten JJ, Buttery LD, Hench LL, Polak JM. Bioglass 45S5 stimulates osteoblast turnover and enhances bone formation in vitro: implications and applications for bone tissue engineering. Calcified Tissue International 2000;67:321–9.

[198] Hulbert SF, Young F A, Mathews RS, Klawitter JJ, Talbert CD, Stelling FH. Potential of ceramic materials as permanently implantable skeletal prostheses. Journal of Biomedical Materials Research 1970;4:433–56.

[199] Itälä AI, Ylänen HO, Ekholm C, Karlsson KH, Aro HT. Pore diameter of more than 100 microm is not requisite for bone ingrowth in rabbits. Journal of Biomedical Materials Research (Applied Biomaterials) 2001;58:679–83.

[200] Harris WH, Jasty M. Bone ingrowth into porous coated canine acetabular replacements: the effect of pore size, apposition, and dislocation. Hip 1985:214–34.

[201] O'Brien FJ, Harley BA, Yannas I V, Gibson LJ. The effect of pore size on cell adhesion in collagen-GAG scaffolds. Biomaterials 2005;26:433–41.

[202] Murphy WL, Dennis RG, Kileny JL, Mooney DJ. Salt fusion: an approach to improve pore interconnectivity within tissue engineering scaffolds. Tissue Engineering 2002;8:43–52.

[203] Yuan H, Kurashina K, de Bruijn JD, Li Y, de Groot K, Zhang X. A preliminary study on osteoinduction of two kinds of calcium phosphate ceramics. Biomaterials 1999;20:1799–806.

[204] Lampin M, Warocquier-Clérout R, Legris C, Degrange M, Sigot-Luizard MF. Correlation between substratum roughness and wettability, cell adhesion, and cell migration. Journal of Biomedical Materials Research 1997;36:99–108.

[205] Kawai N, Niwa S, Sato M, Sato Y, Suwa Y, Ichihara I. Bone formation by cells from femurs cultured among three-dimensionally arranged hydroxyapatite granules. Journal of Biomedical Materials Research 1997;37:1–8.

[206] Daculsi G, LeGeros RZ, Heughebaert M, Barbieux I. Formation of carbonate-apatite crystals after implantation of calcium phosphate ceramics. Calcified Tissue International 1990;46:20–7.

[207] Simon JL, Roy TD, Parsons JR, Rekow ED, Thompson VP, Kemnitzer J, et al. Engineered cellular response to scaffold architecture in a rabbit trephine defect. Journal of Biomedical Materials Research Part A 2003;66:275–82.

[208] Hollister SJ. Porous scaffold design for tissue engineering. Nature Materials 2005;4:518–24.

[209] Lüthen F, Lange R, Becker P, Rychly J, Beck U, Nebe JGB. The influence of surface roughness of titanium on beta1- and beta3-integrin adhesion and the organization of fibronectin in human osteoblastic cells. Biomaterials 2005;26:2423–40.

[210] Larsson C, Thomsen P, Aronsson BO, Rodahl M, Lausmaa J, Kasemo B, et al. Bone response to surface-modified titanium implants: studies on the early tissue response to machined and electropolished implants with different oxide thicknesses. Biomaterials 1996;17:605–16.

[211] Montanaro L, Arciola CR, Campoccia D, Cervellati M. In vitro effects on MG63 osteoblast-like cells following contact with two roughness-differing fluorohydroxyapatite-coated titanium alloys. Biomaterials 2002;23:3651–9.

[212] Chen W, Sun Y, Fu J. Microfabricated nanotopological surfaces for study of adhesion-dependent cell mechanosensitivity. Small 2013;9:81–9.

[213] Flemming RG, Murphy CJ, Abrams GA, Goodman SL, Nealey PF. Effects of synthetic micro- and nano-structured surfaces on cell behavior. Biomaterials 1999;20:573–88.

[214] Yim EKF, Pang SW, Leong KW. Synthetic nanostructures inducing differentiation of human mesenchymal stem cells into neuronal lineage. Experimental Cell Research 2007;313:1820–9.

[215] Palin E, Liu H, Webster TJ. Mimicking the nanofeatures of bone increases bone-forming cell adhesion and proliferation. Nanotechnology 2005;16:1828–35.

[216] Lim JY, Hansen JC, Siedlecki C a, Runt J, Donahue HJ. Human foetal osteoblastic cell response to polymer-demixed nanotopographic interfaces. Journal of the Royal Society, Interface 2005;2:97–108.

[217] Dalby MJ, Childs S, Riehle MO, Johnstone HJH, Affrossman S, Curtis ASG. Fibroblast reaction to island topography: changes in cytoskeleton and morphology with time. Biomaterials 2003;24:927–35.

[218] Dalby MJ, Giannaras D, Riehle MO, Gadegaard N, Affrossman S, Curtis A. SG. Rapid fibroblast adhesion to 27nm high polymer demixed nano-topography. Biomaterials 2004;25:77–83.

[219] Dalby MJ, Yarwood SJ, Riehle MO, Johnstone HJH, Affrossman S, Curtis ASG. Increasing fibroblast response to materials using nanotopography: morphological and genetic measurements of cell response to 13-nm-high polymer demixed islands. Experimental Cell Research 2002;276:1–9.

[220] Sun H, Wirsén A, Albertsson A-C. Electron beam-induced graft polymerization of acrylic acid and immobilization of arginine-glycine-aspartic acid-containing peptide onto nanopatterned polycaprolactone. Biomacromolecules 2004;5:2275–80.

[221] Clark P, Connolly P, Curtis ASG, Dow JAT, Wilkinson CDW. Cell guidance by ultrafine topography in vitro. Journal of Cell Science 1991;99:73–7.

[222] Gupta D, Venugopal J, Prabhakaran MP, Dev VRG, Low S, Choon AT, et al. Aligned and random nanofibrous substrate for the in vitro culture of Schwann cells for neural tissue engineering. Acta Biomaterialia 2009;5:2560–9.

[223] Xu CY, Inai R, Kotaki M, Ramakrishna S. Aligned biodegradable nanofibrous structure: a potential scaffold for blood vessel engineering. Biomaterials 2004;25:877–86.

[224] Klumpp D, Horch Raymund E, Beier Justus P. Tissue Engineering of Skeletal Muscle. Tissue Engineering for Tissue and Organ Regeneration, 2011.

[225] Ma Z, Kotaki M, Inai R, Ramakrishna S. Potential of nanofiber matrix as tissue-engineering scaffolds. Tissue Engineering 2005;11:101–9.

[226] Jang J-H, Castano O, Kim H-W. Electrospun materials as potential platforms for bone tissue engineering. Advanced Drug Delivery Reviews 2009;61:1065–83.

[227] Li W-J, Laurencin CT, Caterson EJ, Tuan RS, Ko FK. Electrospun nanofibrous structure: a novel scaffold for tissue engineering. Journal of Biomedical Materials Research 2002;60:613–21.

[228] Taylor G. Electrically driven jets. Proceedings of the Royal Society of London Series A, Mathematical and Physical Sciences 1969;313:453–75.

[229] Reneker DH, Yarin AL, Fong H, Koombhongse S. Bending instability of electrically charged liquid jets of polymer solutions in electrospinning. Journal of Applied Physics 2000;87:4531–47.

[230] Hohman MM, Shin M, Rutledge G, Brenner MP. Electrospinning and electrically forced jets. I. Stability theory. Physics of Fluids 2001;13:2201–20.

[231] Lu H, Zhang T, Wang XP, Fang QF. Electrospun submicron bioactive glass fibers for bone tissue scaffold. Journal of Materials Science Materials in Medicine 2009;20:793–8.

[232] Li W-J, Mauck RL, Cooper JA, Yuan X, Tuan RS. Engineering controllable anisotropy in electrospun biodegradable nanofibrous scaffolds for musculoskeletal tissue engineering. Journal of Biomechanics 2007;40:1686–93.

[233] Pham QP, Sharma U, Mikos AG. Electrospinning of polymeric nanofibers for tissue engineering applications: a review. Tissue Engineering 2006;12:1197–211.

[234] Matabola KP, Moutloali RM. The influence of electrospinning parameters on the morphology and diameter of poly(vinyledene fluoride) nanofibers - effect of sodium chloride. Journal of Materials Science 2013;48:5475–82.

[235] Mo XM, Xu CY, Kotaki M, Ramakrishna S. Electrospun P(LLA-CL) nanofiber: a biomimetic extracellular matrix for smooth muscle cell and endothelial cell proliferation. Biomaterials 2004;25:1883–90.

[236] Shenoy SL, Bates WD, Frisch HL, Wnek GE. Role of chain entanglements on fiber formation during electrospinning of polymer solutions: good solvent, non-specific polymer–polymer interaction limit. Polymer 2005;46:3372–84.

[237] Buchko CJ, Chen LC, Shen Y, Martin DC. Processing and microstructural characterization of porous biocompatible protein polymer thin films. Polymer 1999;40:7397–407.

[238] Reneker DH, Yarin AL. Electrospinning jets and polymer nanofibers. Polymer 2008;49:2387–425.

[239] Prabhakaran MP, Venugopal J, Ramakrishna S. Electrospun nanostructured scaffolds for bone tissue engineering. Acta Biomaterialia 2009;5:2884–93.

[240] Choi S, Lee SG, Im SS, Kim SH, Joo YL. Silica nanofibers from electrospinning/sol-gel process. Journal of Materials Science Letters 2003;22:891–3.

[241] Huang Z-M, Zhang Y-Z, Kotaki M, Ramakrishna S. A review on polymer nanofibers by electrospinning and their applications in nanocomposites. Composites Science and Technology 2003;63:2223–53.

[242] Hoppe A, Güldal NS, Boccaccini AR. A review of the biological response to ionic dissolution products from bioactive glasses and glass-ceramics. Biomaterials 2011;32:2757–74.

[243] Song J-H, Yoon B-H, Kim H-E, Kim H-W. Bioactive and degradable hybridized nanofibers of gelatin-siloxane for bone regeneration. Journal of Biomedical Materials Research Part A 2008;84:875–84.

Chapter 2

Electrospun hybrid fibers prepared with silicon-calcium-phosphate bioactive ORMOGLASSES and polycaprolactone

This chapter is divided into two parts. The first one is mainly devoted to the biological response induced by hybrid fibers made of polycaprolactone and silicon-calcium-phosphate bioactive organically-modified glasses (ORMOGLASSES). These fibers were partially previously developed by the host laboratory in which this thesis was conducted. For this reason, the production of the fibers was initially performed following experimental conditions already set before the start of this thesis. But, given the interesting properties of these fibers and the difficulties to electrospin the hybrid blend with these parameters, a study was done afterwards to optimize the deposition of the fibers. This is reported in the second part of the chapter.

The study on the biological performance of the material was carried out in collaboration with the "Biomaterials and Tissue Engineering Lab" of the Dankook University, South Korea. The experimental optimization of the electrospinning process was fully conducted at the institute for Bioengineering of Catalonia.

2.1. Chapter summary

Bioactive glasses in the system silicon-calcium-phosphate (from now on abbreviated as Si-Ca-P_2 system[1]) are very well known for bone tissue engineering due to their biological properties. The remarkable potential of these materials to trigger osteo and angiogenesis is suggested to be mainly due to its ion dissolution. Calcium cation (Ca^{2+}) in particular is believed to act as an angiogenic promoter through the stimulation of the calcium sensing receptor; a receptor found at the cellular membrane of various cells. Hybrid fibers containing an organically modified glass (ORMOGLASS) based on this system were also expected to lead to suitable cellular responses. Si-Ca-P_2 ORMOGLASS/polycaprolactone fibers were thus electrospun with different glass compositions in order to assess the influence of glass composition on the cellular behavior. Results showed that depending on the Ca^{2+} release profile (rate and concentration) of the material, changes in biological properties occurred. The material with the higher and more rapid Ca^{2+} release had a better osteo and angiogenic potential than others fibers prepared with lower calcium content. Additional assays such as Z-Potential measurements and fibers morphology investigation performed using Atomic Force Microscopy have also pointed it out this material as the more potentially successful template due to its more positive surface charge and nanoroughness. This study demonstrated thus that Si-Ca-P_2 ORMOGLASS/PCL fibers are a good option for the fabrication of smart materials and that the composition of the ORMOGLASS plays a critical role in the promotion of efficient vascularized bone regeneration.

In terms of material production however, the efficiency of the electrospinning process appeared not to be optimal when performing the fiber deposition with the conditions previously set by the laboratory. In fact, many experimental factors can affect the formation and collection of the fibers

[1]The abbreviation was defined in accordance with an oxide based nomenclature (oxides used to prepare the ORMOGLASS system): Si in reference to silicon oxide SiO_2, P_2 in reference to phosphorous oxide P_2O_5, and Ca in reference to calcium oxide CaO *[Hench et al., Journal of Biomedical Materials Research 1971; 5, 117-141]*.

(solution viscosity, solvent dielectric constant, voltage, temperature…), that is why the selection of the processing parameters is of critical importance. Moreover, fibers were only produced in the microscale, while to mimic the collageneous fibrous structure of native bone, the nanoscale should be reached. Therefore, the influence of the solvent used, the polymer concentration, the glass content and the glass hydrolysis level on fiber deposition was assessed. The fiber morphology and thickness were determined as well. Results showed that controlling the blend parameters, fibers with regular diameter could be produced without particular difficulties when 2,2,2-trifluoroethanol was used as solvent. The homogeneous fibers had a diameter ranging from 360 nm to 620 nm diameter depending on the conditions considered to prepare the blend. Blend preparation had a direct effect on the fibers features. This experimental optimization of the electrospinning process provides thus useful information for the efficient deposition of hybrid nanofibers with regular shape and promising biological performance.

2.2. Introduction

The role of smart materials for bone tissue engineering is to stimulate or trigger specific cellular responses involved in bone regeneration. It is commonly accepted that the Si-Ca-P_2 glass system promotes osteogenesis but, as explained in the introduction chapter, the angiogenesis potential of the materials prepared with this system is argued in the literature. Though, vascularization is essential if the formation of a fully and functional bone is aimed to be achieved. Angiogenesis consists in the formation of blood vessels from preexisting ones. This process is necessary for the correct cell migration, cell signaling, oxygen and nutrient supply, and residue elimination [1]. Materials that do not exhibit this property have therefore high chances to fail during the implantation. Recently, it has been demonstrated that composite materials containing a glass and a synthetic polymer (precise system already known for its osteogenic properties) could trigger angiogenic response by providing the suitable biochemical and mechanical cues to the cells [2]. The interplay of these factors activates two synergistic pathways in the angiogenesis process. The first one implies the stimulation of calcium sensing receptors (CaSRs) [3] and the second one the regulation of the mechanosensing [4,5]. These signals promote together endothelial progenitor cells (EPCs) homing, differentiation and tubulogenesis by activating the production of vascular endothelial growth factor (VEGF) and controlling the VEGFR-2 receptor expression. Ca^{2+} is moreover thought to be an efficient osteoinductive promoter, also by acting through the CaSR, and promoting the proliferation and differentiation of endothelial and osteoblastic cell lineage [6,7]. Several previous *in vivo* studies additionally indicated that bone marrow progenitor cells are recruited to high calcium concentration environments, suggesting that a CaSR-mediated chemotaxis took place [8,9]. This implicitly suggested that calcium releasing biomaterials could be used to control the healing bone matrix microenvironment, offering thus new pathways for potential and promising new therapies based on osteo and angiogenic-promoting scaffolds for engineering stem/progenitor cell tissue.

Up to now, and especially in the last years, many materials and material processing strategies have been considered for the development of bioactive 3D scaffolds that mediate bone regeneration through the chemical and physical microevironment [10]. Electrospinning is one of the techniques that have recently gained widespread interest for the design of these scaffolds due to its efficiency in producing micro and nanoscaled fibers. The creation of this biomimicking artificial matrix is well known in the field, as it constitutes a suitable substrate for cell adhesion, proliferation and differentiation [11]. More than being used as a biocompatible bioactive template, electrospun fibers should also degrade in physiological conditions and be metabolized by the body. For example, byproducts gradually released to the bloodstream along with the material degradation contribute to the success of the scaffolds only if this process is well controlled. This implies that the byproducts should be non toxic, be excreted easily by metabolic pathways and, especially in the case of bioactive byproducts, be delivered to the cells in a non-harmful concentration and rate. Among a high number of material combinations available to prepare scaffolds, composites having a ceramic or glass particles embedded in a biodegradable polymer have shown excellent results [12,13]. However, in these materials, each constituent degrades at a different rate and consequently provokes the release of the domains in a non-homogeneous manner. That can happen because the two compounds do not have intimate interactions between each other. Thus, the improvement of these interactions is necessary to better control the release of the key agents in particular [14]. This can be achieved through the formation of a covalent or ionic bonding, or the use of surfactants to enhance the adherence between the phases [15–17]. Another solution is to develop a material in which both compounds are of similar nature. In other words, if the phases possess a good surface affinity and good interactions due to the presence of organic fragments in the inorganic network, the final composite is expected to have a more homogeneous and controlled degradation. Therefore, this approach was thought to be a good option for the control of the release of bioactive ions such as Ca^{2+}, and for the assessment of the potential of synthetic biomaterials to serve as instructive grafts.

2.3. Fiber preparation and characterization

In this part of the chapter, the possibility of producing blends made of organometallic-modified amorphous glasses (ORMOGLASSES) and a biodegradable polymer is evaluated to subsequently investigate the biological response of these novel hybrid materials. The sol-gel method was selected to develop the organometallic networks by means of the hydrolysis of alkoxide precursor solutions. Polycaprolactone was chosen as the biodegradable polymer. Implementing this strategy, we aim to join the both domains at a nanometric level [18] and to obtain a tuned ion release suitable for the promotion of cell homing and enhancement of osteo and angiogenesis using the Si-Ca-P_2 system.

2.3.1. Materials and methods

2.3.1.1. Blend preparation and electrospinning

The preparation of the ORMOGLASS involved a mix of metal alkoxide precursor solutions. These precursors were prepared in the laboratory under inert atmosphere as follows: metallic calcium was refluxed in anhydrous 2-methoxyethanol (Sigma-Aldrich 99%) to obtain the calcium precursor, and phosphorous pentoxide (P_2O_5, Sigma-Aldrich 97%) was refluxed in absolute ethanol (Sigma-Aldrich >99%) to obtain the phosphorous one. The preparation of these precursors was already reported in the literature [19,20]. To make sure they were well prepared, each single precursor was assessed using the nuclear magnetic resonance (NMR) technique (see appendices A-1 and B-1). Silicon precursor was commercially acquired as tetraethylorthosilicate (TEOS, Aldrich, 98%). The three precursor solutions were mixed homogeneously with three different molar ratios under strong stirring. A previous work performed by our South Koreans collaborators showed that fibers prepared with a Ca/P ratio equal to 5 exhibited promising bioactivity and osteogenic potential [21]. For these reasons, the ORMOGLASS compositions were carefully set to maintain this Ca/P ratio value while the silicon content was changed. The three compositions targeted and the names of the fibers associated to these compositions are reported in **Table 2-1**. Once the mix has been done, a water catalyst (Si:H_2O = 1:3 molar ratio) was added to partially hydrolyze the solution and to produce a viscous ORMOGLASS sol. Only a partial hydrolysis was performed in order to make sure that the ORMOGLASS sol did not reach an advanced gel state; otherwise, it would not have been possible to blend it with the polymeric solution if it became too viscous. In parallel, a polymeric solution of polycaprolactone 16 % w/w (PCL, Sigma-Aldrich, MW = 70 000-90 000 KDa) in tetrahydrofuran (THF, Sigma-Aldrich, 99%) was prepared. Then, the ORMOGLASS sol and the polymeric solution were blended according to a ORMOGLASS:polymer ratio of 20:80 (v:v) in order to obtain the electrospinnable blends. The blends, as well as the pure polymeric solution, were finally loaded in a syringe and electrospun using a conventional electrospinning setup with a grounded flat collector. Fibers were thus deposited as randomly distributed fibrous mats. The processing parameters were the followings: 12 kV applied voltage, 1 ml/h blend dispensing rate and 15 cm distance tip-collector [22]. Images of the setups used to prepare the fibers (alkoxide preparation, precursor mix and blend preparation, electrospinning device) can be seen in appendix A-2.

Table 2-1. Compositions of the ORMOGLASS precursor mix prepared to produce the hybrid fibers (nominal composition - molar ratio percentage).

	PCL-S40	PCL-S52	PCL-S70
Si	40	52	70
Ca	50	40	25
P_2	10	8	5

2.3.1.2. Fiber morphological characterization and composition determination

Field Emission Scanning Electron Microscopy (FESEM, see appendix B-2) was used to assess the morphology of the fibers (Nova™-Nano SEM-230; FEI Co.). Energy Dispersive Spectroscopy (EDS) analysis was done to determine the exact fibers composition (Quanta 200 XTE 325/D8395; FEI Co.). For these two techniques, samples were previously coated with a thin carbon layer before analysis. Using FESEM pictures, the thickness of the fibers was also measured by means of ImageJ open source software [23]. 25 fibers were randomly selected for each material. Their fiber sizes were averaged and the standard deviations were calculated.

2.3.1.3. Fiber wettability

The wettability of the samples was evaluated by water contact angle using the sessile drop method for the pure hydrophobic PCL fibers and the captive bubble method for the hydrophilic hybrid fibers [24]. The captive bubble method is used to evaluate the wettability of highly hydrophilic samples that cannot be assessed by the conventional sessile method (see appendix B-3). In this case, material is reversely immersed in ultra-pure deionized water and a 3 µl air bubble is generated at the bottom of the water-receptacle. The contact angle between the fibers and the liquid is the result of the difference between 180° and the measured bubble angle. Measurements were carried out with a contact angle device coupled with a digital camera (Contact Angle System OCA15plus, Dataphysics) and were analyzed with the SCA20 Dataphysics software.

2.3.1.4. Atomic force microscopy measurements

Fibers stiffness (DMT modulus [25]) and roughness (R_q) were investigated using Atomic Force Microscopy (AFM, MultiMode 8 Atomic Force Microscope, Bruker - see appendix B-4) in PeakForce tapping mode in air. A thin layer of fibers were previously deposited on an adhesive substrate. Image treatment and data analysis were performed with Gwyddion, an open source software for scanning probe microscopy data analysis [26].

2.3.1.5. Electrostatic potential evaluation

The electric potential of the fibers surface was determined by the measurement of the Z-Potential (ZP, see appendix B-5). In fact, it is associated to the electric field generated at the solid-liquid interface when a liquid is forced to flow between two pieces of a material. These measurements were carried out using a SurPASS apparatus and acquired via the VisioLab software (Anton Paar Ltd.). All the measurements were performed using an adjustable gap cell, at a dynamic pH of electrolyte (KCl 1 mmol, pH ranging from 7.5 to 2.2) and samples with size of 10 x 20mm.

2.3.1.6. pH and calcium release measurements

Continuous Ca^{2+} concentration was monitored during the first hours of fibers immersion in water. Measurements were done using a Crison Ca^{2+} selective electrode and an Ag/AgCl reference electrode. They were carried out in 1 ml of a 0.02 M KCl and 2.5 mM $CaCl_2$ saline solution, with constant ionic strength. The initial pH of the solution was precisely adjusted to 7.4 before the immersion of each sample. The pH measurements were carried out using a Crison GLP22+ pH-meter and a Crison pH microelectrode. In addition to that assay, discrete pH and Ca^{2+} release measurements were collected at different time points, up to 14 days. The same setup was used but 4-(2-hydroxyethyl)-1-piperazineethanesulfonic acid (HEPES) was added to the saline solution in order to better simulate the buffering effect that naturally occurs in the body over a long period of time. Before starting, pH was also adjusted to 7.4. At each time point, the liquid was removed for the measurements and renewed.

2.3.1.7. In vitro assays

MC3T3-E1 cells were seeded on the materials (specimen cut from the electrospun fibrous layer) to assess the morphology, proliferation and differentiation of cells on the developed fibers.

2.3.1.7.1. Cell morphology assessment

Cells were seeded at a density of 5 000 cells/specimen (size of specimen: 10 mm diameter) and their morphology was assessed using SEM (Hitachi 3000) after 7 days. For that purpose, samples with cells were fixed during 10 min at room temperature in a phosphate buffered saline (PBS) solution with 2.5% of glutaraldehyde. The fixed samples were then dehydrated for 5 min using aqueous ethanol solutions with increasing concentrations of ethanol (75%, 95% and 100%). Afterwards, a critical-point drying was applied to the dehydrated samples. Finally, the samples were coated with a thin layer of gold and examined by SEM at an accelerating voltage of 10.0 kV. Cells present at the fibers' surface were colored artificially in orange on the SEM images and the filopodia in blue in order to evaluate and quantify the area occupied by the cells and the filopodia. The analysis was performed by means of the ImageJ software [23] and the results were reported as occupied percentage of the total picture area.

2.3.1.7.2. Cell proliferation assay

Cell proliferation (MC3T3-E1 cells) was evaluated using a cell counting kit, a colorimetric assay, involving tetrazolium salt WST-8 (CCK-8, Dojindo Molecular Technologies Inc.). Measurements were performed following the manufacturer's instructions. The cells were seeded on each scaffold in the same conditions than the previous test (density of 5 000 cells/specimen, 10 mm diameter specimen). At precise time points (1, 3, 5 and 7 days), 10 µl of the CCK-8 solution was added to each sample and incubated at 37˚C for 3 h. The absorbance was read at 450 nm using a microplate reader (Molecular Devices).

2.3.1.7.3. Cell differentiation assay – alkaline phosphatase activity

The osteoblastic differentiation of the MC3T3-E1 cells was determined by measuring the alkaline phosphatase (ALP) activity expressed by the cells on the scaffolds. The cells were seeded at a density of 12 500 cells/specimen (size of specimen: 25 mm diameter) and cultured up to 21 days in an osteogenic medium, a minimum essential Eagle medium (α-MEM) supplemented with 10% FBS, 50 μg/mL sodium ascorbate, 10 mM β-glycerol phosphate and 10 nM dexamethasone. At 7, 14, and 21 days, 20 μg of total protein was added to 50 μL of a p-nitrophenyl phosphate solution (Bio-Rad). This solution was incubated for 60 min with the cellular samples and the enzymatic activity of ALP was quantified by measuring the absorbance of the p-nitrophenol (compound formed by the hydrolysis of the p-nitrophenyl phosphate) at 405 nm using the Elisa Microplate Reader.

2.3.1.7.4. *In vitro* cell differentiation assay – Western blot

Western blot assay was performed at 21 days to assess the degree of osteogenesis on each sample. Osteopontin (OPN) and glyceraldehyde 3-phosphate dehydrogenase (GAPDH) were considered for that assay. Cell lysis and protein solubilization was achieved by immersing the cellular samples in a RIPA (Radio-ImmunoPrecipitation Assay) buffer. Lysates were centrifuged at 12 000 rpm for 10 min at 4°C and protein concentrations were determined by the Bradford method. Subsequently, proteins were separated by using 10% sodium dodecylsulfate polyacrylamide gel electrophoresis and transferred electrophoretically to polyvinylidene difluoride membrane. Nonspecific binding was blocked by immersing the membrane in 5% non-fat dry milk for 1 h at room temperature. The membrane was then incubated with primary antibodies against OPN (1:1000; Abcam) and GAPDH (1:1000; Santa Cruz Biotechnology Inc.) at 4˚C overnight. The membrane was washed and further incubated with horseradish peroxidase-conjugated anti-rabbit IgG (1:5000; Santa Cruz Biotechnology Inc.). The blots were developed using the enhanced chemiluminescence method (Amersham Pharmacia Biotech Inc.).

2.3.1.7.5. *In vitro* cell differentiation assay - quantitative real-time polymerase chain reaction

At 7, 14, and 21 days, the expression of the bone-associated genes, i.e ALP, osteopontin (OPN), collagen type I (Col I), and osteocalcin (OCN) was determined by quantitative real-time polymerase chain reaction (PCR). The first complementary DNA (cDNA) strand was synthesized from the total ribonucleic acid (RNA, 1 μg) using a SuperScript first strand synthesis system for real-time PCR (Invitrogen). This was done following the manufacturer's instructions. The reaction mixture was made up to 50 μl. Real-time PCR was performed using SYBR GreenER qPCR SuperMix reagents (Invitrogen). The relative transcript quantities were calculated using the ΔΔCt method with GAPDH as the endogenous reference

gene amplified from the samples. The primer sequences of the genes are summarized in the appendix A-3.

2.3.1.8. Biocompatibility in vivo tests

Male Sprague Dawley rats (250–300 g) were used for *in vivo* study. Animals were housed under standard conditions of temperature (23 ± 1°C), a 12 h light/dark cycle and fed with a standard pellet diet and water ad libitum. The protocols were approved by the Dankook University Institutional Animal Care and Use Committee, South Korea.

Round shape membranes, cut from the electrospun fibrous layers, with a diameter of 16 mm were implanted on the backs of the rats. The animals were anesthetized by intramuscular injection with a mixture of Ketamine HCl (80 mg/kg body weight) and Xylazine (10 mg/kg body weight). The back area of rats was shaved and prepared with alcohol and betadine solution. A 2 cm long incision was made on the mid-portion of the back. Four small pockets were formed subcutaneously with baby metzenbaum scissors on the backside in a lateral direction from the spine of each rat and the membranes were inserted. Each animal received one type of scaffold composition (PCL, PCL-S40 or PCL-S52 membranes). PCL-S70 fibers were not assessed in this section. The incision was subsequently closed with 4-0 non-absorbable monofilament suture material (Prolene). After 4 weeks, the animals were euthanized and implanted membranes were extirpated for histological analysis. Four samples per membrane were used for the *in vivo* biocompatibility study. The tissues surrounding the implanted membranes were placed in 4% buffered formaldehyde for 24 h at room temperature. Then, they were serially dehydrated in a graded ethanol, paraffin embedded, sectioned and stained with hematoxylin and eosin (HE) or Masson's Trichrome (MT) stain. Samples were examined with light microscopy. Histological scoring was done from the both stained slides. The scoring includes the extent of inflammatory response, thickness of fibrous capsule, presence of blood vessel, and proliferation of fibroblasts (from absence to severe, score from 0 to 3, 0: not observed or very low number of infiltrated inflammatory cells, 1: low number of infiltrated inflammatory cells/mild changes, 2: intermediate number of infiltrated inflammatory cells/moderate changes, 3: numbers of infiltrated inflammatory cells/severe changes). Tissue sections were immunostained for von Willebrand factor (vWF), a protein present in blood vessel basement membranes, and imaged by light microscope. In order to determine the quantity of the newly formed blood vessels, indicated by vWF staining, the number of vessels was manually counted (microscope magnification: x200), and normalized to membrane area with the use of Scion Image Software (Scion Corporation, Frederick, MD).

Complementary information about cellular and *in vivo* assays can be found in appendix B-6.

2.3.1.9. Statistical analysis

Results are shown as the mean ± standard deviation and analyzed via one-way analysis of variance (ANOVA). A value of $p < 0.05$ was considered statistically significant (*) and $p < 0.002$ highly statistically significant (**).

2.3.2. Results

2.3.2.1. Fiber surface properties and composition

FESEM images of the three different silicon content samples can be observed in **Figure 2-1**. No segregation of inorganic phases was observed even at higher magnifications, suggesting a good homogeneity between the ORMOGLASS and the PCL matrix. However, some beads and irregularities were present.

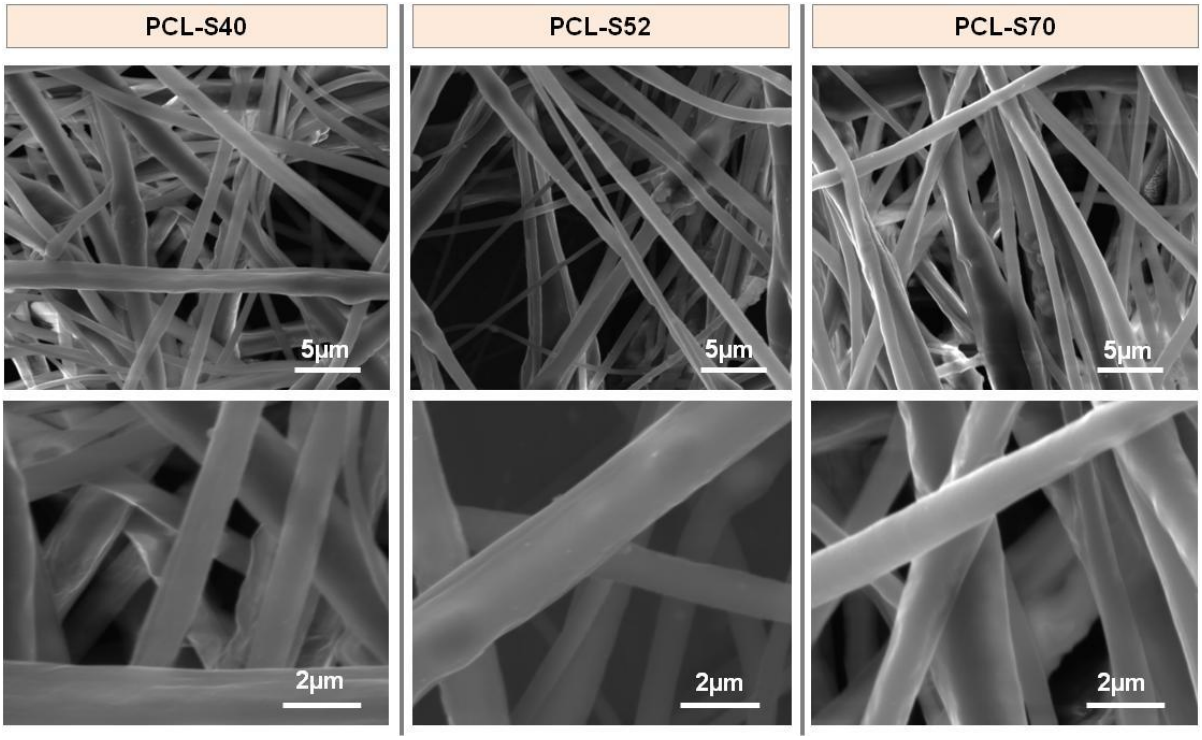

Figure 2-1. FESEM images of the hybrid fibers showing the morphology of the fibers.

The fiber compositions as well as their thicknesses and wettability are reported in **Table 2-2**. Fiber compositions were close to the ones targeted (nominal one). Fiber thicknesses did not change significantly between all the fibers. Their diameters were around 2 µm. Contact angle measurements revealed that the hydrophilicity of the fibrous membranes increased when the silicon content was increased. Water contact angles of all hybrid samples dramatically dropped compared to the one of pure PCL fibers (130.3 ± 0.8°, sessile drop measurement).

Table 2-2. Nominal and measured percentage of the hybrid fiber compositions, the fiber averaged thicknesses, water contact angle, roughness and stiffness.

	PCL-S40		PCL-S52		PCL-S70	
Fiber composition	*Nominal*	*Measured*	*Nominal*	*Measured*	*Nominal*	*Measured*
Si	40.0	43.3 ± 2.5	52.0	50.3 ± 1.5	70.0	66.3 ± 1.7
Ca	50.0	45.5 ± 2.5	40.0	40.4 ± 1.9	25.0	28.3 ± 0.9
P_2	10.0	11.7 ± 0.1	8.0	9.3 ± 0.4	5.0	5.5 ± 0.7
Diameter (µm)	2.1 ± 0.4		1.9 ± 0.3		2.2 ± 0.3	
Contact angle (°)	33.6 ± 0.4		27.1 ± 2.3		20.9 ± 1.9	
R_q (nm)	5.5 ± 0.5		7.0 ± 1.0		7.7 ± 0.6	
DMT Modulus (MPa)	64.4 ± 2.7		33.7 ± 1.1		18.8 ± 0.2	

2.3.2.2. Fiber topography

Fiber topography and stiffness (DMT modulus) assessments performed by AFM are presented in **Figure 2-2** and **Table 2-2** respectively. AFM 3D images and R_q values revealed that the fibers had a rough nanostructured surface and that roughness was increased towards the fibers having compositions with the higher silicon contents. This nanotopography was attributed to the presence of spherulites that oriented perpendicularly to the direction of the fiber. Spherulites correspond to regions where the polymer are semi-crystalline and composed of highly ordered lamellae, themselves connected by amorphous domains [27]. The folds due to the lamellae provided the nanoroughness. On the other hand, DMT modulus showed that the stiffness of the fibers were much lower for the hybrids than for pure PCL fibers (comparison with value from the literature [28]). There was also a clear difference between the hybrids: the lower the silicon content, the stiffer the material. Finally, this assay confirmed that the PCL and the ORMOGLASS were homogeneously blended as no heterogeneous areas were detected by AFM.

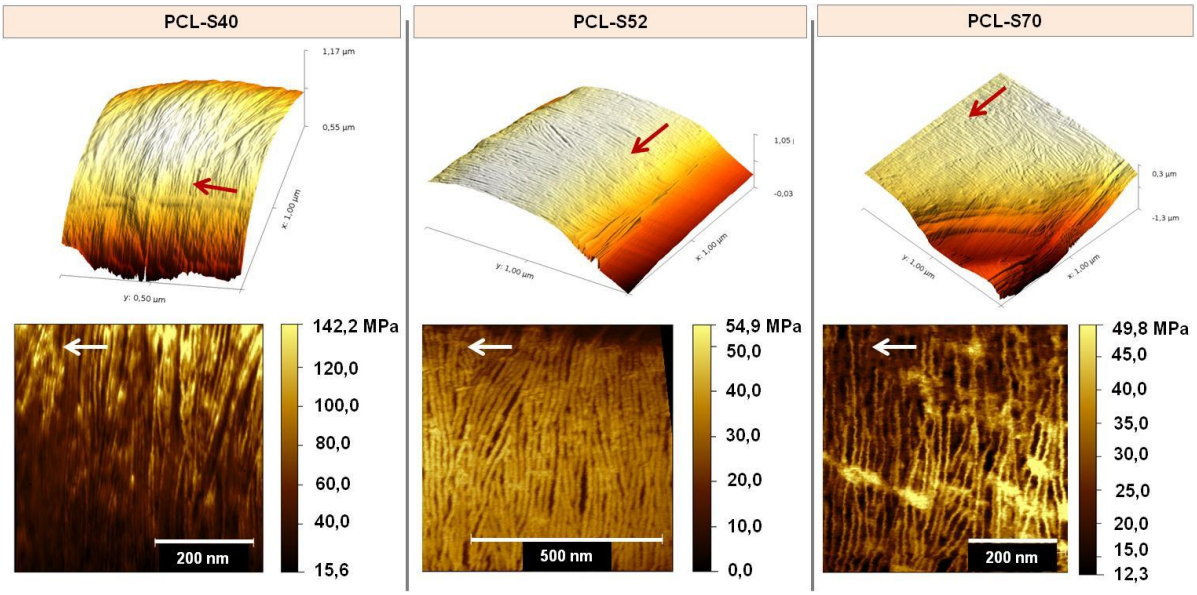

Figure 2-2. 3D plots of topographic images and DMT modulus maps of the hybrid fibers obtained by AFM. Arrows show the direction of the fiber length.

2.3.2.3. Fiber surface charge

ZP curves obtained for the hybrid fibers and pure PCL ones are plotted in **Figure 2-3** as a function of pH. PCL had the most negative value (-52.7 mV) at physiological pH 7.4. PCL-S70 and PCL-S52 have slightly less negative electrostatic potentials (-51.4 and -48.7 mV respectively). Surprisingly, PCL-S40 exhibited a value significantly more positive (-34.4 mV). Moreover, the isoelectric point (pH for which the potential is equal to zero) of PCL-S40 fibers (pH = 2.6) was lower than the other membranes (3.0, 2.7 and 2.9 for PCL, PCL-S70 and PCL-S52 fibers respectively).

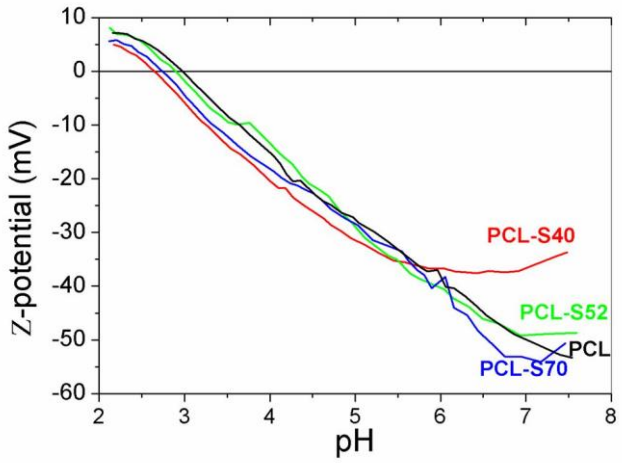

Figure 2-3. Plot of the Z-potential of the hybrid and pure PCL fibers, as a function of pH.

2.3.2.4. pH and calcium release measurements

pH and calcium release measurements were performed in aqueous solutions initially adjusted at pH 7.4 in order to simulate the pH of the blood. Because the aim of the continuous measurements was to determine precisely what happens at the material interface, this assay was performed without using any buffer. In this way, the effect of the material on the surrounding fluid can be better revealed as no buffer is present to moderate this effect. Moreover, calcium was added to the aqueous solutions to obtain solutions without buffer but with ions contained in conventional simulated body fluid (SBF) [29]. For the three kinds of hybrid fibers, a decrease in the Ca^{2+} concentration is observed after few minutes of immersion, suggesting that some of the Ca^{2+} released and/or already present in the solution were absorbed by the material (**Figure 2-4, 1**). This decrease is followed by an increase of the Ca^{2+} concentration in all the cases. But for the PCL-S40 fibers, this increase appeared earlier and it reached a higher concentration than the two others. These results are in accordance with what could be expected based on the composition of the fibers: the fibers with the lower silicon content, i.e. with the higher calcium content, released more calcium. About pH, all the values significantly increased at the initial stage of the immersion and ultimately reached values comprised between 9.3 and 9.7.

Discrete pH and calcium release measurements were acquired also in aqueous solutions with Ca^{2+} and the pH initially set at 7.4. But, in this test, HEPES was added as buffer to simulate the buffering effect that occurs in the body when the material is implanted for a longer time than the previous assay in continuous. Results are reported in **Figure 2-4, 2**. PCL-S40 fibers were the fibers that maintain the higher concentration of Ca^{2+} over time. PCL-S52 and PCL-S70 fibers showed the strongest burst release between the start and the second day of the assay (around half of its initial release concentration ability). Afterwards, Ca^{2+} concentrations decreased in a less drastic manner for these fibers. The discrete measurements were in agreement with the continuous ones: the lower the silicon content, the higher the Ca^{2+} release. Discrete pH results also showed coherence with the discrete Ca^{2+} release measurements. After the increase of pH occurring just after the material immersion, pH values tended to decrease and to stabilize at pH~7.4 with time. Over a long period, less calcium was released with time so the pH was less affected than at the early stages.

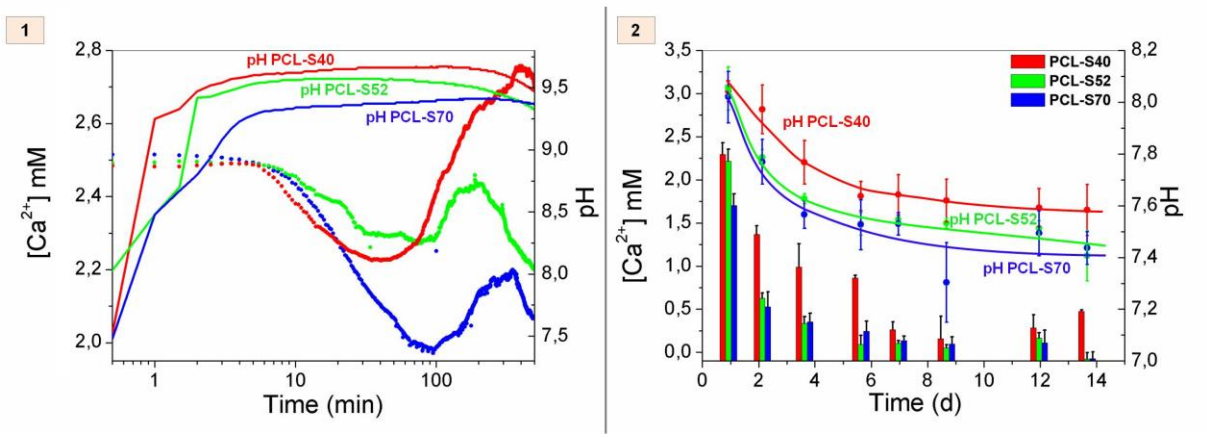

Figure 2-4. pH and Ca^{2+} release assessed by continuous (1: short term monitoring) and discrete (2: long term monitoring) measurements.

2.3.2.5. Cell adhesion, proliferation and differentiation

Representative SEM pictures of fixed MC3T3-E1 cells cultured on the different membranes are presented in **Figure 2-5**. All scaffolds were well populated by cells after 7 days. To better determine in which extent the cells adhered and spread on the scaffolds, the surface occupied by cells was quantified. All hybrid fibers showed a higher relative occupied surface (cell area) than PCL ones. This is especially true for the PCL-S40 fibers that exhibited the higher occupied surface in comparison to the rest. About the filopodia, they were found almost in the same quantity for the three hybrid samples, but clearly in a higher amount on these fibers than on PCL ones (**Figure 2-5, graphic**).

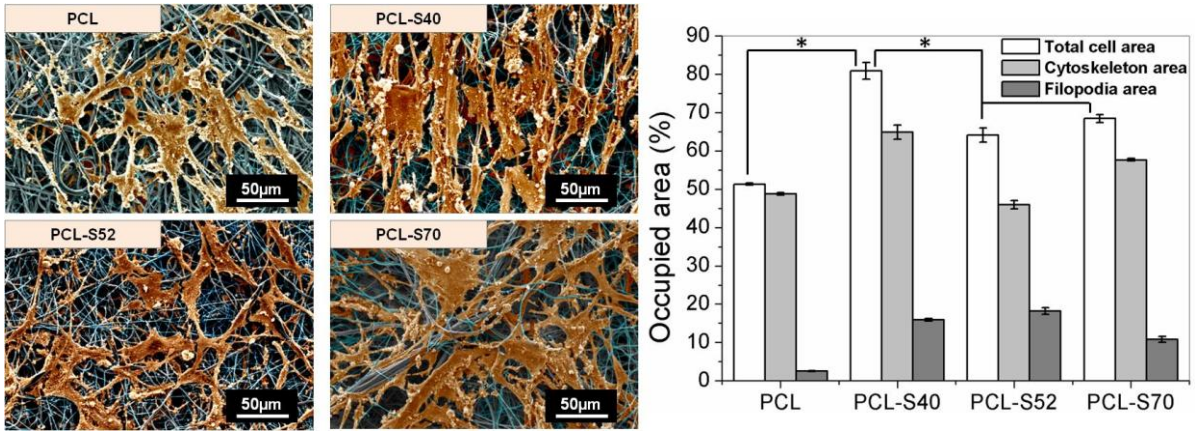

Figure 2-5. FESEM images showing the adhesion of cells cultured on the hybrid scaffolds after 7 days and histogram showing the quantification of area occupied by cells. Cells were artificially colored in order to improve the contrast between the fibers and the cells, and for the quantification of surface area percentage occupied by cells (*: statistical difference $p < 0.05$).

Results of proliferation and ALP activity tests are plotted in **Figure 2-6**. The proliferation was improved for all hybrid fibers in comparison to PCL ones (used as a control). More precisely, cells on PCL-S40 fibers proliferated better than ones cultured on the other fibers. At the end of the assay (7d), PCL-S40 fibers were the templates on which cells showed a significantly better proliferation in

comparison to the others. Results about ALP activity showed that from day 7 to day 14, the ALP activity increased for all the mats and from day 14 to 21, it decreased. PCL-S40 fibers are the fibers that induced the more pronounced increase in ALP activity between the day 7 and the day 14, and an ultimate higher level of activity. At day 14 and 21, the differences between PCL-S40 material and the others were even highly significant. Western blot assay confirmed these observations. The ratio OPN/GAPDH is also statistically significant for the PCL-S40 fibers (**Figure 2-7**). Both the protein and the enzyme were found to be present in a significant amount when cells were cultured on these fibers.

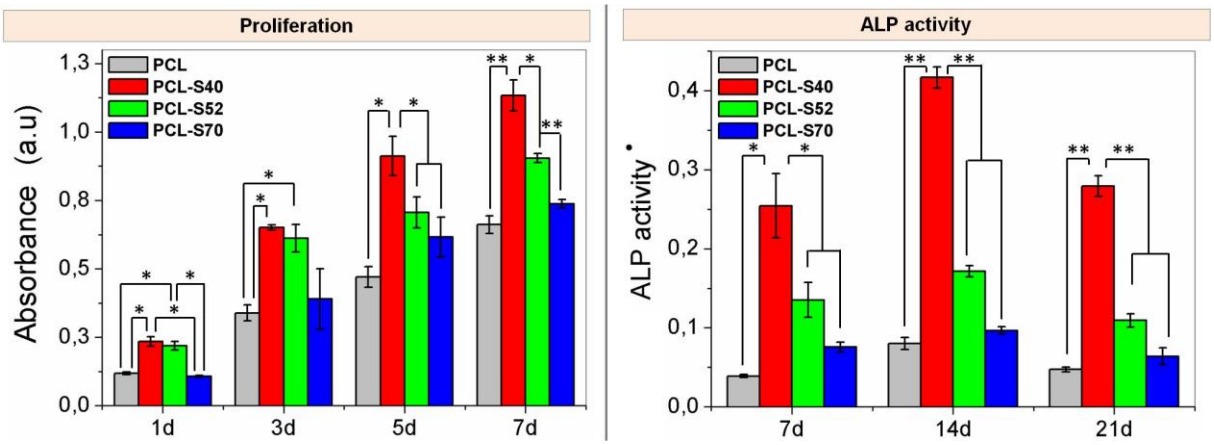

Figure 2-6. Quantification of proliferation and ALP activity of cells cultured on PCL and hybrid fibers (•: normalized to total protein - *: statistical difference $p < 0.05$ - **: statistical difference $p < 0.002$).

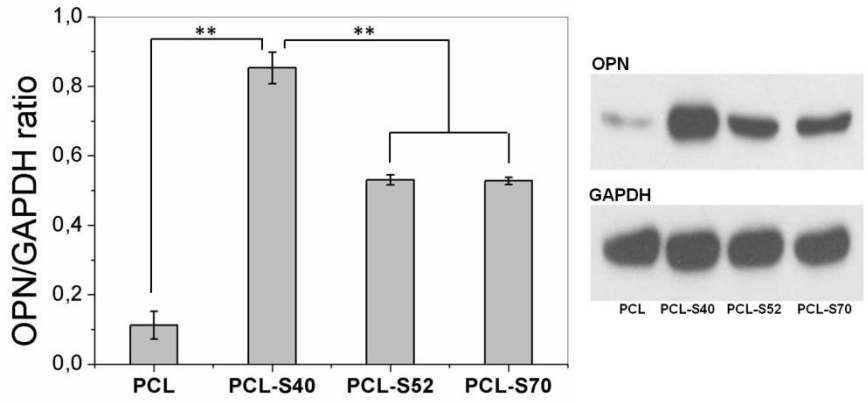

Figure 2-7. OPN/GAPDH ratio related to cells cultured on PCL and hybrid fibers. The pictures additionally show the western blot results enhanced with a chemiluminescence method (**: statistical difference $p < 0.002$).

The expression of the different bone-associated genes is shown in **Figure 2-8**. PCL-S40 is the sample that has the higher expression in all the markers, including the ALP one. This confirmed the results described here above. As aforementioned, the maximum of expressions of ALP occurred at 14 days of cell culture, in the early stages of differentiation. COL I expression also reached a maximum at this time point. For OPN and OCN genes, the maximum of expressions occurred at the third week, in the early stage of mineralization.

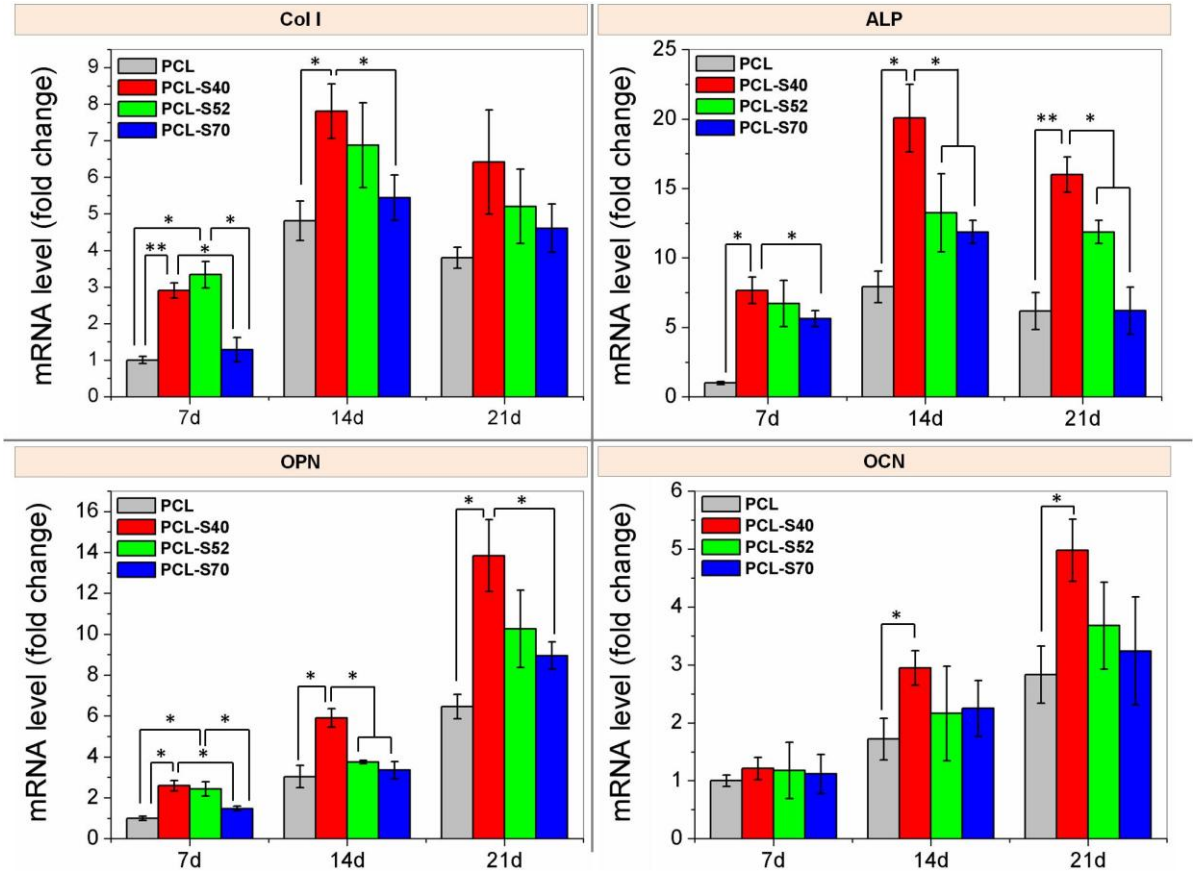

Figure 2-8. Expression of the bone-associated genes (Col I, ALP, OPN and OCN) measured by quantitative real-time PCR method (*: statistical difference $p < 0.05$ - **: statistical difference $p < 0.002$).

2.3.2.6. In vivo assays

Macroscopic evaluation

The tissue responses to the three membrane types (PCL, PCL-S40 and PCL-S52) implanted subcutaneously in dorsal region of rats were evaluated. Each animal received four scaffolds. The recovery from the anesthesia was uneventful. After implantation, all animals showed normal healing process without inflammation and remained in good health during the period of the study. The incision sites healed normally and no inflammatory signs and material related complications were observed. In summary, the membranes used in this study resulted in satisfactory healing.

After four weeks of implantation, all membranes were explanted at 4 weeks after implantation along with the tissues surrounding the implant. At harvesting, the samples and surrounding tissues showed no macroscopic redness or inflammation.

Microscopic evaluation

Pure PCL membranes were considered as a control for the assessment of inflammatory tissue responses at the microscopic level. Pictures of the histological cut sections are shown in **Figure 2-9** and biological responses analysis (presence of fibrous capsule, blood vessels, fibroblasts, formation of new

fibrous tissue and evaluation of inflammatory response [30]) are summarized in **Table 2-3**. No significant immune response was observed for the pure PCL fibers but the presence of fibrous capsule was clearly noticed. Fibroblasts arranged around the membrane and approximately 15-20% of the fibrous membrane was changed to fibrous tissue with fibroblasts infiltration. Few vessels were also observed within the infiltrated fibrous tissue and the surrounding area. PCL-S40 fibers exhibited a similar biological behavior than PCL fibers in term of biocompatibility. No significant immune response was seen after 4 weeks of subcutaneous implantation. A fibrous capsule was however observed but approximately 50% of membrane was changed to fibrous tissue with fibroblast and vessel infiltration. Concerning PCL-S52 fibers and their inflammatory response, the observations were nearly the same than for the other fibers (limited number of infiltrated inflammatory cells). A fibrous capsule was observed, as for PCL-S40 fibers, but fibrous tissue infiltrated significantly better than in the PCL and PCL-S40 samples. Approximately 85% of the fibrous membrane was changed to fibrous tissue with fibroblasts and blood vessels.

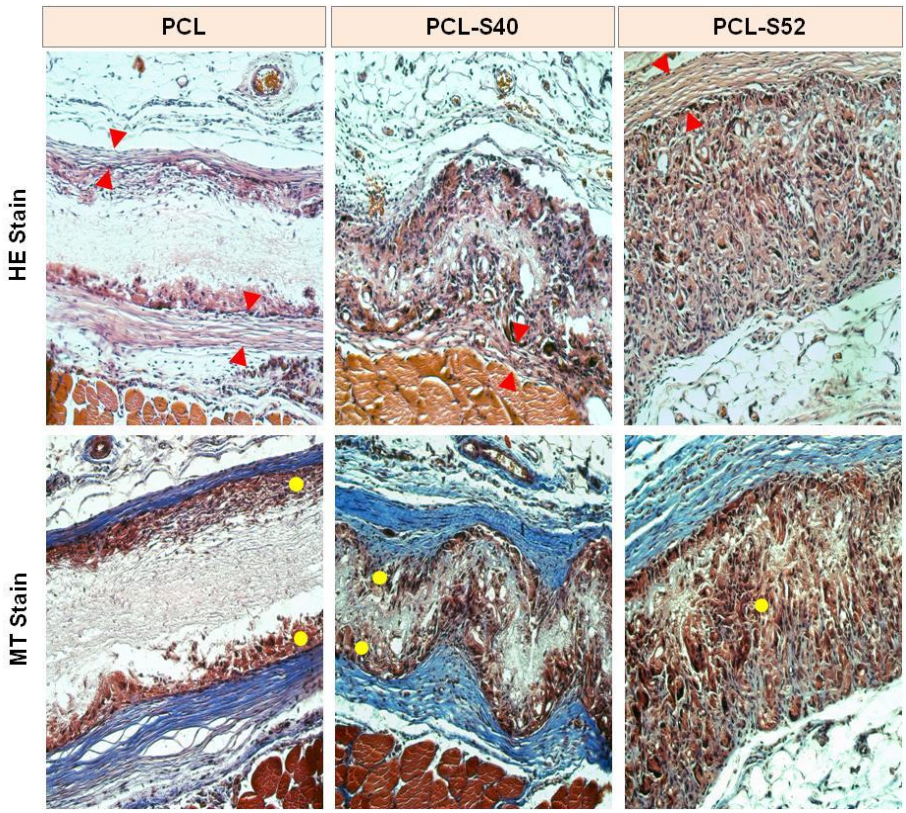

Figure 2-9. Images of rat subcutaneous tissue responses to the implanted membranes after four weeks of implantation: HE and MT stainings (microscope magnification x200 – red arrows denote the fibrous capsule and yellow dots denote the cells infiltrating the membranes).

Table 2-3. Histopathologic assessment after subcutaneous implantation of PCL and hybrid membranes after four weeks of implantation in rats. Each matrix has been rated according to the cell number/intensity of the lesions. 1: low number of infiltrated inflammatory cells/mild changes, 2: intermediate number of infiltrated inflammatory cells/moderate changes, 3: numbers of infiltrated inflammatory cells/severe changes.

	PCL				PCL-S40				PCL-S52			
	FC	IR	BV	F	FC	IR	BV	F	FC	IR	BV	F
No1	2	0	1	1	1	1	1	2	1	1	2	2
No2	2	1	1	1	1	1	2	2	1	1	3	3
No3	1	0	1	1	1	1	2	1	1	1	2	3
No4	2	0	1	1	1	1	1	2	1	1	2	2

FC: fibrous capsule, IR: inflammatory response, BV: blood vessel, F: fibroblasts

To quantify the enhancement in blood vessel formation obtained with the hybrid artificial membranes, immunohistochemical staining of the blood vessel endothelial specific marker vWF was performed (**Figure 2-10**). Using the Scion Image software, it has been possible to normalize the number of counted blood vessels to the membrane area. As already seen on the histological pictures, significant differences were observed between the pure PCL specimen and the hybrid ones. PCL-S40 (0.338 ± 0.147) and PCL-S52 (0.282 ± 0.1) groups demonstrated more prominent angiogenesis ratio than PCL group (0.048 ± 0.017). PCL-S40 and PCL-S52 groups had similar angiogenic potential and did not show significant difference. In both samples, the newly formed blood vessels were distributed homogeneously in the membranes. This assay also confirmed that PCL-S40 ($p = 0.004$) and PCL-S52 ($p = 0.003$) groups induced the formation of a significantly higher blood vessels than PCL groups.

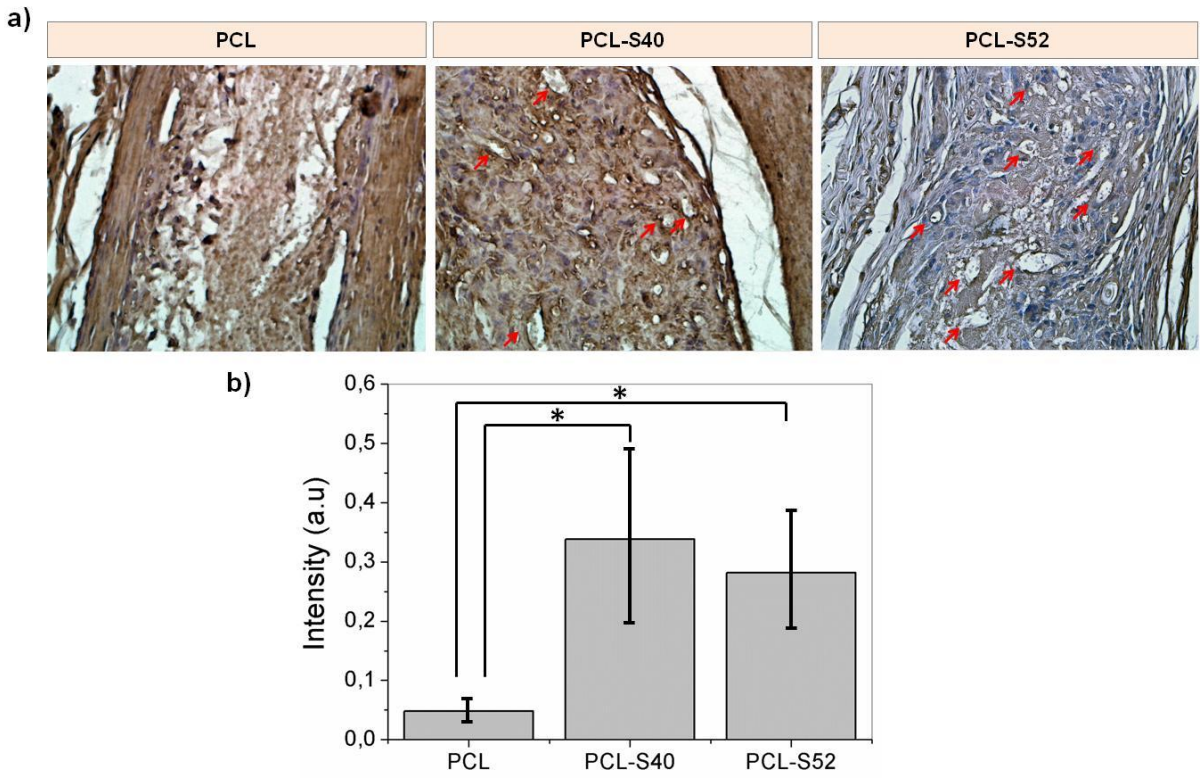

Figure 2-10. a) Images of the extracted fibrous membranes after 4 weeks of implantation: vWF staining (microscope magnification: x400 - Red arrows point the newly formed vessels within the membrane area). b) Quantification of the blood vessels number (normalization to the membrane area – *: statistical difference $p < 0.05$).

2.3.3. Discussion

ORMOGLASS/PCL blends were prepared with three different compositions and were successfully used to produce hybrid fibers by electrospinning (**Figure 2-1**, **Table 2-2**). Fibers with diameters of approximately 2 μm were collected and the measured compositions satisfied the targeted ones. Fibers exhibited some irregularities and beads in their morphology, suggesting that an effort should be made to improve the electrospining process. As the experimental parameters are known to affect the fibers deposition [31], it is believed that changing the processing conditions (the solvent or the level of hydrolysis of the glass for examples), the morphology and the fiber deposition continuity could be improved.

Despite these morphological and processing imperfections, the produced fibers induced good cellular responses due to the inherent material properties. In fact, the hybrid fibers obtained showed a good wettability in comparison to the pure PCL ones (**Table 2-2**). The addition of the ORMOGLASS in the polymeric matrix greatly improved the hydrophilicity in the three cases. Charles-Harris *et al.* demonstrated that osteoblast-like cells prefer to adhere to a hydrophilic calcium phosphate glass than to a hydrophobic synthetic polymer (polylactic acid, PLA) [32], which had similar hydrophobic properties than PCL [33]. Also Serra *et al.* observed that, on PLA scaffolds containing dispersed particles of this glass, rat mesenchymal stem cells better spread on the composite than on pure PLA scaffolds [34]. The

hydrophilicity of the fibrous hybrids therefore surely contributed to the good adhesion of cells on the membranes. In particular, PCL-S40 fibers exhibited the higher total surface area occupied by cells (**Figure 2-5**), suggesting that they constituted the most suitable templates for cell attachment. This could be seen on the FESEM pictures as well. This behavior might be explained by the surface charge of these fibers. Even though being negative at physiological pH, the value of the surface charge of the PCL-S40 fibers was indeed significantly more positive than the ones of the other fibers (**Figure 2-3**). As a recent study showed, cells have a better affinity with positively charged matrices in terms of cell adhesion and shape [35]. The fact that PCL-S40 fibers were the most positive substrate of the study can partly explain why a better cell adhesion is achieved for these fibers.

On the other hand, the surface roughness can also affect this behavior. According to AFM analysis, the fibers exhibited a nanotopography (**Table 2-2, Figure 2-2**) due to the presence of polymer spherulites [36]. Nanostructured surfaces are known to improve the cellular adhesion of bone-forming cells [37,38] and fibroblasts [39]. Such surfaces seem in fact to influence the cell-extracellular matrix contacts (i.e focal adhesion) by modulating integrin-mediated cell adhesion, spreading and cytoskeleton organization [40]. The nanoroughness of the three hybrid fibers appeared to be suitable for a good cellular adhesion, in *in vitro* as in *in vivo* conditions. However, a slight difference can be noticed between the roughnesses of the three fiber types: the roughness was decreased with the decrease of the silicon content in the fibers. This can be explained by a lower separation between the lamellae of the polymer spherulites [41]. This means that the spherulites of the low silicon-content fibers exhibited more densely packed molecules than the two other compositions. Thus, it can be concluded that the ORMOGLASS composition had an influence on the spherulization and consequently on the fiber roughness. One possible explanation is that ORMOGLASSES with different compositions induced different modifications in the molecular weight of the PCL chains, a parameter that directly controls the nucleation density of the spherulites [42]. According to Chen *et al.*[42], the fact that PCL-S40 fibers exhibited a higher nucleation density could signify that the molecular weight of the PCL was less reduced in this blend than in the others. Therefore, this demonstrates that the polymer-ORMOGLASS interactions can be tailored by changing the ORMOGLASS composition.

In addition to nanotopography, hydrophilicity and surface charge, material stiffness is also considered as an essential regulator for cell behavior. The determination of the DMT modulus by AFM showed that the stiffness of the fibers increased with the decrease of the silicon content of the fibers (**Figure 2-2**, **Table 2-2**). This can be attributed to the densification of the spherulites, as revealed by the roughness measurements, and the stronger intermolecular interactions within the lamellae. As a consequence, it can be inferred that ORMOGLASS composition not only affected the roughness but also the stiffness of the material. These mechanical differences might have played a role in the angiogenic promotion of the developed materials. However, the mechanism by which mechanical signals integrate with other microenvironmental cues (e.g. chemical ones) to regulate neovascularization remains unknown [43]. It is thus clear that, to effectively establish the role of the stiffness of these hybrid fibers on the

material angiogenic potential, another study, in which the variable of the calcium release in particular is eliminated, should be performed. But, changing one variable of the studied system might lead to significant modifications of most of the general material features listed above (as suggested by the changes of roughness and stiffness when different ORMOGLASS compositions are used for example), and consequently have an impact on the ultimate cellular response. Therefore, the assessment of these mechanical changes on angiogenesis is particularly complex in the case of such hybrids. It can be however specified that, based on the literature, substrates having a stiffness in the range of kPa seem to be suitable to promote angiogenesis [43]. The hybrid fibers developed here showed stiffness far from this range (GPa). Given the excellent biological performance of the scaffolds produced, this higher stiffness values did not seem to be negative regarding the angiogenic properties of the hybrids. In fact, it is believed that the calcium released by these fibers is the most relevant factor that explains the material angiogenic potential. For the mineralization of the material however, the stiffness of these hybrids seems to be appropriate [44].

The immersion of the fibers in the aqueous solution used to measure the pH and the calcium release (in the form of $Ca(OH)_2$) led to an immediate drastic increase in pH (**Figure 2-4**). After some minutes, the pH stabilized at around 9.5. The initial increase in pH did not seem to be immediately associated to a high release in Ca^{2+}. In fact, changes in Ca^{2+} concentration are not instantaneously detected by the calcium electrode. This means that other agents are responsible for the high basic pH measured. It is hypothesized that, just after the material immersion, silicon species (basic pH) may be released in the solution [45]. Once calcium starts to be released from the material, the pH surprisingly still remains stable. This might be due to the balance between the release of the basic Ca^{2+} and acidic phosphate compounds. The release of P^{5+} in the form of H_3-xPO_4 probably compensated the increase of pH due to the release of calcium. This suggested that during this stage, Ca^{2+} and PO^{4-} were simultaneously released in a way that their different amounts compensate the modifications in pH that each ion induced. On the other hand, calcium release assay demonstrated that the fibers with the lower silicon content (i.e higher calcium content) were the fibers that released the more Ca^{2+}. It also showed that their Ca^{2+} release started before the other fibers. Between the three fiber compositions, the calcium release of these fibers appeared to the most suitable to promote osteo and angiogenic properties. It is clear that the Ca^{2+} released from these fibers promoted the proliferation (**Figure 2-6**), differentiation and expression of bone-associated genes *in vitro* (ALP, OPN, Col I, OCN) (**Figure 2-7**, **Figure 2-8**), and the formation of blood vessels *in vivo* (**Figure 2-9**, **Figure 2-10**). Angiogenesis may be achieved by activating the production of VEGF through the CaSR for example. CaSR is indeed recognized by the scientific community as a key actor related to multiple behaviors in bone lineage and endothelial cells: stimulation of proliferation [46], migration [3,8,46], differentiation [3,47], adhesion [8] and mineralization [47] by regulating the expression of mitogenic genes [48], inducing chemotaxis [3] and increasing the production of growth factors [49], for example. Recently, Aguirre *et al.* have also demonstrated that calcium released from biomaterials (solvent-casting fabrication method), among other

factors, can be used to trigger these cellular functions [2]. CaSR is in fact a trans-membrane protein receptor able to detect extracellular calcium already contained in media and the calcium released by the biomaterial at the material-fluid interface.

Based on the excellent *in vitro* and *in vivo* results obtained with the fibers described in this chapter, this study made us conclude that the novel microscaled nanostructured fibers provided the right signals to the cells for the expression of angiogenic growth factors and osteogenic markers in therapeutic levels. Indeed, the Ca^{2+} release profile of the novel fibers, combined with their hydrophilicity, nanoroughness, surface charge and stiffness, seem to activate the essential cellular functions necessary to a successful material implantation and bone regeneration through synergetic pathways. This work showed, thus, that other types of smart materials than the one reported by Navarro *et al.* (i.e bioactive glass microparticles-polymer materials) [2,50], for example, can be developed by using a completely different approach and processing method (sol-gel and electrospinning). On the other hand, in comparison to other materials described in the literature, these novel hybrid fibers present several advantages. First, sol-gel derived biomaterials based on silicon-calcium-phosphate systems are usually prepared with calcium nitrate and triethylphosphate [51,52]. As demonstrated by Pereira *et al.*, the use of soluble salts in the sol-gel process leads to the formation of non-homogeneous and non-consolidated glasses [53]. The problem of using calcium nitrate is that it is progressively incorporated into the silicon network only at increasing temperatures above 400°C. If this step is not properly controlled, calcium does not correctly diffuse into the network and consequently, inhomogeneous regions (in composition) are formed [54]. To obtain more homogeneous glasses, calcium nitrate can be replaced by calcium methoxyethoxyde [53]. In this way, only alkoxide precursors are used. However, this alkoxide route seemed to have been implemented only for producing monolith glasses and hybrids [20,53]. In this thesis, we have successfully used the alkoxide route to prepare ORMOGLASSES and to produce electrospun polymer-ORMOGLASSES (blend) scaffolds. Unlike the conventional sol-gel glasses, the preparation of the ORMOGLASSES, in the case of our materials, does not require ageing and stabilization processes. This represents a significant gain of time and it does not involve temperature treatments that usually last several hours at high temperatures (from 60°C to 700°C) [52,54]. To prepare our blends, ORMOGLASSES can simply be obtained at ambient temperature and be immediately mixed with the polymer. Another advantage of the reported material fabrication method is that hybrids with a low content of silicon can be prepared. Commonly, sol-gel silicon-based glasses possess indeed a high percentage of silicon oxide (typically more than 50%) [21,52,55]. Lower silicon contents were achieved only for melt-derived glasses [56]. With our approach, we have achieved the fabrication of materials having silicon oxide content equal to 40% (and even 22% - data not shown here). Thus, this enabled us to produce materials with higher phosphate and calcium oxides contents. Martin *et al.* reported that the increase of P_2O_5 content made difficult the syntheses of Si-Ca-P_2/polyvinyl alcohol hybrids (formation of cracks) [57]. For our hybrids, no particular problems were observed when preparing the blends having the higher amount of P_2O_5, in comparison to the blends having the lower amount of P_2O_5. Concerning calcium, it is

interesting to increase its content if the developed material is aimed to be used for the triggering of specific cellular responses [2]. Indeed, according to the results reported in this chapter, the fibers that had the higher sustained calcium release (i.e. fibers with the higher calcium content) were the ones that showed the better biological performance. In other words, this means that the fabrication of these fibers may be a powerful tool that could be further used to assess the potential of calcium-releasing biomaterials. Finally, in the future, the blend could be used to prepare other scaffold architectures by using various fabrication methods, as for example rapid prototyping. This way, the material architecture could be adapted to match the structure of other specific applications that can possibly be targeted. This would be especially valuable for the applications that require the infiltration and formation of a blood vessel network.

Before concluding, a general comment should be added regarding the use of MC3T3-E1 cells and the *in vitro* characterization of the material. MC3T3-E1 cells are osteoprogenitor cells with a high propensity for osteoblast differentiation (cell lines) [58,59]. They are well known in the field as they can be used to assess the potential of scaffolds to trigger osteoblast phenotype by monitoring the level of alkaline phosphatase expression [60,61]. However, they are not "neutral" cells: they are already oriented cells (predisposition to evolve towards osteoblast lineage) and they may consequently not be the most suitable cell lines to effectively assess the differentiation potential of scaffolds. They may rather be used to study the differentiation of bone cells and mechanism of biological calcification [58,62] but not to evaluate the differentiation in a "neutral" way. Instead, mesenchymal stem cells are recommended for such assays (primary cells). They are multipotent cells and signals delivered by the materials are critical to trigger specific cell lineage [63]. Therefore, they may be more suitable in the sense that if the material does not effectively provide specific signals, they may not differentiate into osteoblast lineage at all. Thus, the use of mesenchymal stem cells appeared to be a more valuable model to assess the real potential of the materials. Hence, for the other *in vitro* studies presented in the next chapters, mesenchymal stem cells will be used. However, this comment about the use of MC3T3-E1 cells does not imply that the *in vitro* results discussed in this chapter are not reliable. In fact, many researchers commonly use these cells to biologically characterize the materials that they developed [51,59]. But, as it has been thought that mesenchymal stem cells would be more relevant, it has been decided to continue the *in vitro* assays in the future with these cells only and not with the MC3T3-E1 anymore.

2.3.4. Conclusion

A new family of hybrid bioactive fibers has been developed. Unlike the conventional hybrid materials containing a polymer and a pure inorganic glass, these novel fibers were made of a polymer and an organically modified glass (ORMOGLASS). The production of such materials is possible if alkoxide precursors are used to prepare the glass (organometallic network). The hybrid fibers produced showed

excellent osteo and angiogenic properties due to their inherent features such as good hydrophilicity, proper composition (Si-Ca-P_2 system, release of bioactive ions), nanoroughness and stiffness. The calcium released from the hybrid fibers is suggested to be one of the most crucial factors that affect the ultimate biological responses. This release is thought to be controlled by the intrinsic amount of calcium found in the ORMOGLASS but also by the content of silicon. Indeed, different calcium release curves were obtained for the different compositions. Not only the concentration was affected, but also the rates and the profiles, suggesting that silicon might act as a calcium release regulator by being part of the organometallic glass network. However, it is perfectly accepted that the other material properties also contributed to the final biological response. From the three hybrid mats studied, PCL-S40 fibers were the substrates that induced the best biological performance. The calcium release rate and concentration associated to these fibers appeared to be the most appropriate for the efficient stimulation of the CaSR and the subsequent formation and vascularization of tissue. In other words, these novel fibers appeared to be a good platform for the triggering of cellular responses required for bone regeneration. Thus, this study confirmed that it is possible to control the biological performance of scaffolds by precisely tuning the material mechanical, chemical and physical properties. It also highlighted the potential of organic/organically modified glass hybrids. In summary, this work opens a new door for the development of novel and smart biomaterials based on ORMOGLASSES.

2.4. Fiber preparation: optimization of the experimental process

This part of the work is dedicated to the improvement of the fiber deposition using electrospining. The improvements are evaluated by considering the efficiency of the fiber production (continuity of the process) and the enhancement in the fiber morphology (avoiding the formation of beads or irregular shape). Also, the ability to control the fiber diameters was investigated. In other words, this study aimed to optimize the fiber fabrication to enable a less problematic fiber fabrication, and to determine the blend conditions that lead to the formation of homogeneous nanofibers. Given the reported promising properties for vascularized bone tissue regeneration, this study appeared necessary for the production of the membranes in higher quantity. This is necessary to perform, for example, further biological studies and to enhance potentially the biological performance of this system by producing a better biomimicking material (nanostructure). For that purpose, fibers were prepared under different experimental parameters.

2.4.1. Materials and methods

2.4.1.1. Blend preparation and electrospinning

The blend preparation is achieved in the same way as the method described in the previous part of this chapter: the sol-gel method is applied to the glass precursor solution (same metal alkoxides system) and the sol obtained is blended with polycaprolactone. However, the solvent was changed, as well as the polymer concentration, the ORMOGLASS:polymer volume ratio and the degree of hydrolysis of the

precursor mix. These experimental conditions are summarized in **Table 2-4**. Even though the processing conditions (distance tip-to-collector, voltage applied…) could be also investigated to control the fiber deposition, this work was only focusing on the influence of the blend features. As a new solvent was used to produce the fibers, the processing parameters were initially adjusted and changed in comparison to the previous settings. They were fixed for all the fibers to: 7.5 kV applied voltage, 0.5 ml/h blend dispensing rate and 12 cm distance tip-collector. Because of these processing parameter changes, hybrid fibers with the three previous compositions were nevertheless produced using the old solvent (THF), but under the new setup conditions to serve as a control. On the other hand, it can be surprising that this optimization study was performed with the S52 glass composition whereas, according to the biological responses reported above, the S40 one seemed to be the most promising. This is explained by a time shift between the conception of the new experiments (experimental optimization of the fibers deposition) and the obtaining of the biological results reported in the first part of the chapter[2].

Polycaprolactone pellets (PCL) and tetrahydrofuran (THF) were purchased from Aldrich. The new solvent used, trifluoroethanol (TFE), was purchased from Panreac. All reagents used to prepare the glass sol were prepared as previously described and commercially acquired from the same suppliers (Ca metallic: Sigma-Aldrich 98%, 2-methoxyethanol anhydrous: Sigma-Aldrich 99.8%, P_2O_5: Sigma-Aldrich 99.99%, absolute ethanol: Panreac 99.8%, TEOS: Sigma-Aldrich 99.8%).

Table 2-4. Summary of the different blend parameters considered to produce the fibers (in italic: the changed parameters).

	Glass composition	**Solvent**	**Polymer concentration**	**Ormoglass:polymer volume ratio**	**Si:H_2O hydrolysis molar ratio**
Fibers (control)	S70, S52, S40	THF	16%	20:80	1:3
Influence of polymer concentration	S52	TFE	*8%, 10%, 12%, 14%, 15%, 16%*	20:80	1:3
Influence of ormoglass:polymer content	S52	TFE	10%	*5:95, 10:90, 20:80, 30:70, 40:60, 50:50*	1:3
Influence of hydrolysis level	S52	TFE	10%	20:80	*1:1, 1:2 1:3, 1:4, 1:5, 1:6, 1:10*

[2]The optimization study was started before the end of all the biological assays. Despite the fact that the good osteo and angiogenic features of PCL-ORMOGLASS fibers appeared already clearly, the remarkable properties of the PCL-S40 fibers were not totally demonstrated at this time. For this reason, S52 composition was arbitrarily selected to perform the study (as the intermediate composition).

2.4.1.2. Fiber morphological characterization

Scanning electron microscopy (SEM, Quanta Q200, FEI Co.) was used to assess the morphology of the fibers. A piece of the fibrous layer deposited on a flat collector covered with aluminum was cut, and fixed on the conventional metallic support used for SEM observations. Fibers were then sputtered with a thin layer of carbon to improve the conductivity of the samples and ensure that pictures with good quality could be obtained.

2.4.1.3. Fiber diameter measurements

SEM pictures were opened in ImageJ software and fibers diameters were determined using this application [23]. At least 10 diameter measurements were performed to obtain an averaged value of thickness for each type of the produced fibers.

2.4.2. Results

2.4.2.1. Fibers prepared with THF and three glass compositions

Figure 2-11 shows the morphology of the fibers obtained with THF as solvent and three different glass compositions. Pictures revealed that fibers were successfully produced under the new processing conditions. Fibers had however imperfections, as when they were produced with the previous setting parameters. They were not regular and beads were seen in the three cases. The fibers had different diameter (**Table 2-5**) but these differences were not significant between them. Their thickness ranged from 1.4 to 1.5 µm. The irregularity in fibers shape was particularly well represented by the high standard deviations of the average of the measurements.

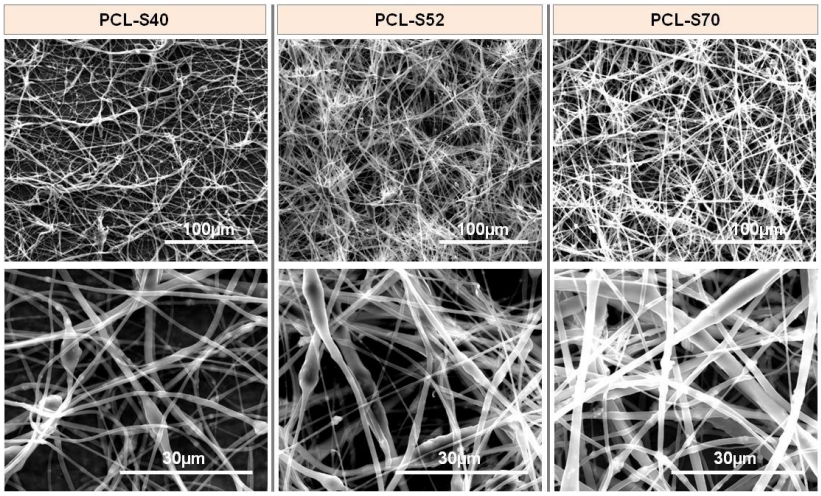

Figure 2-11. Morphology of the hybrid fibers prepared with THF as solvent and with three different glass compositions.

Table 2-5. Diameter of the hybrid fibers prepared with THF as solvent in function of their composition.

Label	Nominal composition	Fiber diameter (µm)
PCL-S40	40Si-50Ca-10P_2	1.4 ± 0.4
PCL-S52	52Si-40Ca-8P_2	1.4 ± 0.6
PCL-S70	70Si-25Ca-5P_2	1.5 ± 0.3

2.4.2.2. Fibers prepared with different polymer concentrations

Hybrid fibers were produced with different polymer percentages (8%, 10%, 12%, 14% and 15% solutions – w/w PCL/TFE ratio) using TFE as solvent (**Figure 2-12**). Fiber diameter average clearly increased with the increase in polymer concentration. Up to 12% PCL solution, submicron scaled fibers were obtained and their thicknesses were quite homogeneous. For the higher polymer contents, the fiber shape was more difficult to obtain and the fiber fabrication was particularly difficult. In fact, the high standard deviation of the fiber thickness associated to the 14 and 15% PCL solutions showed that the fibers were highly irregular (only the areas where fibers were well distinguished were taken into account for the measurement of the fibers' diameter). In the case of the 16% solution, fibers could not have been produced at all.

In order to have a comparison, pure PCL fibers were produced with different polymer percentages (8%, 10%, 12% and 14%). Fiber thickness measurements revealed that, as for the hybrid fibers, the fiber diameters increased with the polymer concentration (**Figure 2-13**). Measurements related to the hybrid and the pure polymeric fibers were coherent between each other. This validated the fiber diameter tendency that occurred when the polymer content was increased. On the other hand, it can be noticed that hybrid fibers prepared with a certain polymer concentration exhibited thinner fiber diameter than ones prepared with the same concentration but without the glass.

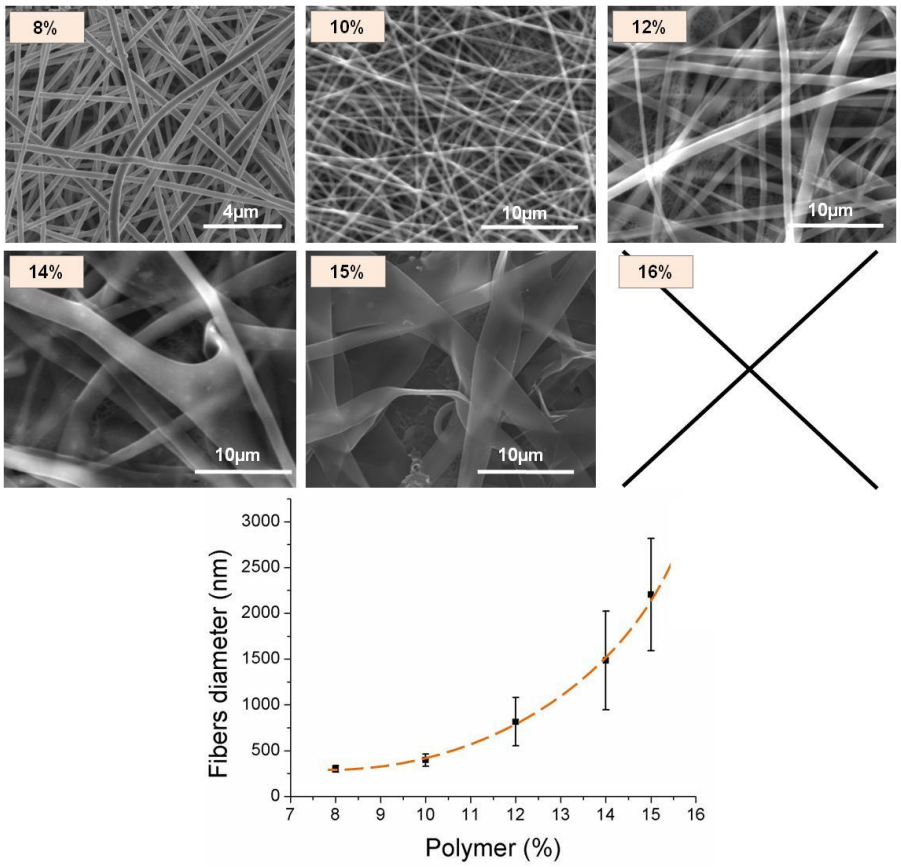

Figure 2-12. *Influence of polymer concentration on hybrid S52 fibers.* Morphology and thickness of hybrid PCL-S52 fibers obtained with TFE as solvent and different polymer concentrations (the orange dotted line shows the results' tendency).

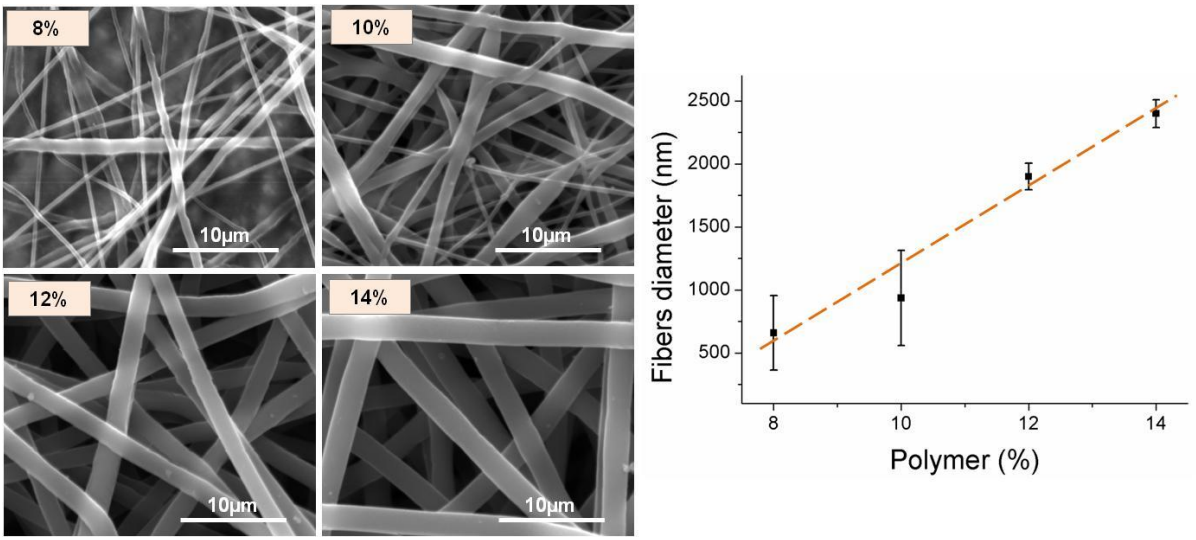

Figure 2-13. *Influence of polymer concentration on pure PCL fibers.* Morphology and thickness of pure PCL fibers obtained with TFE as solvent and different polymer concentrations (the orange dotted line shows the results' tendency).

2.4.2.3. Fibers prepared with different precursor contents

According to SEM pictures, regular fibers were obtained for all precursor contents, except for the 50:50 v/v blends (**Figure 2-14**). Up to the 40:60 ratios, fibers with thicknesses around 400 nm were produced and no imperfections were observed. This was confirmed by the low standard deviation of fiber diameter measurements. In this range of ORMOGLASS:polymer ratio, the electrospinning set-up and blend conditions seemed suitable for an appropriate scaffold fabrication. No problem with the fiber deposition continuity was noticed. For the 50:50 blends however, fibers with larger diameter and more heterogeneous geometry were obtained. Their deposition was not critical but anyway a little bit more difficult than the others.

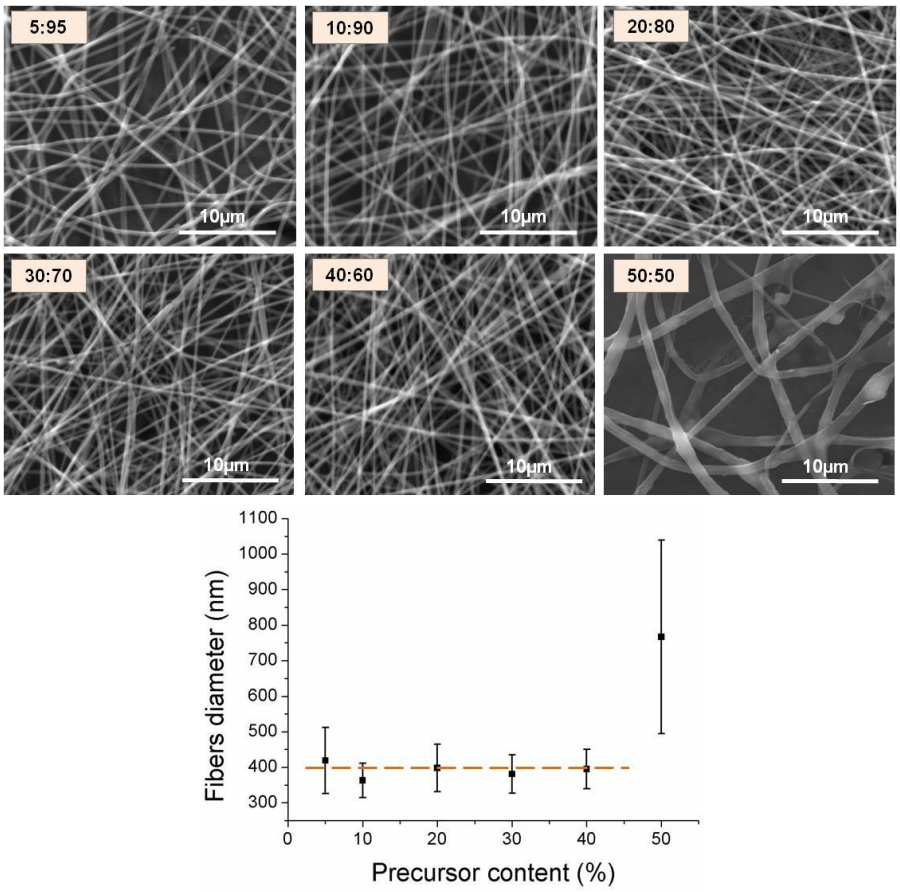

Figure 2-14. *Influence of ormoglass content on hybrid S52 fibers.* Morphology and thickness of hybrid PCL-S52 fibers obtained with TFE as solvent and different ormoglass contents (the orange dotted line shows the results' tendency).

2.4.2.4. Fibers prepared with different hydrolysis levels of the glass precursor mix

Changes in the hydrolysis level of the ORMOGLASS precursor mix resulted in the formation of fibers with different diameters (**Figure 2-15**). Up to hydrolysis ratios of 1:5, fibers with diameters below 600 nm were produced. Fibers showed regular shape, as reflected by the low standard deviation associated to their thickness measurements. Conversely, fibers produced with hydrolysis ratios of 1:6 and

1:10 exhibited a less homogeneous morphology and higher thicknesses. Moreover, their deposition was difficult in comparison to the others. Imperfections were clearly visible on the SEM pictures.

Another observation that can be made regarding the influence of the hydrolysis level is that from 1:3 to 1:10 ratio, fiber diameters increased. With ratios of 1:1 and 1:2, the diameters decreased. Fibers prepared with a hydrolysis ratio equal to 1:3 seemed to have the lower diameter.

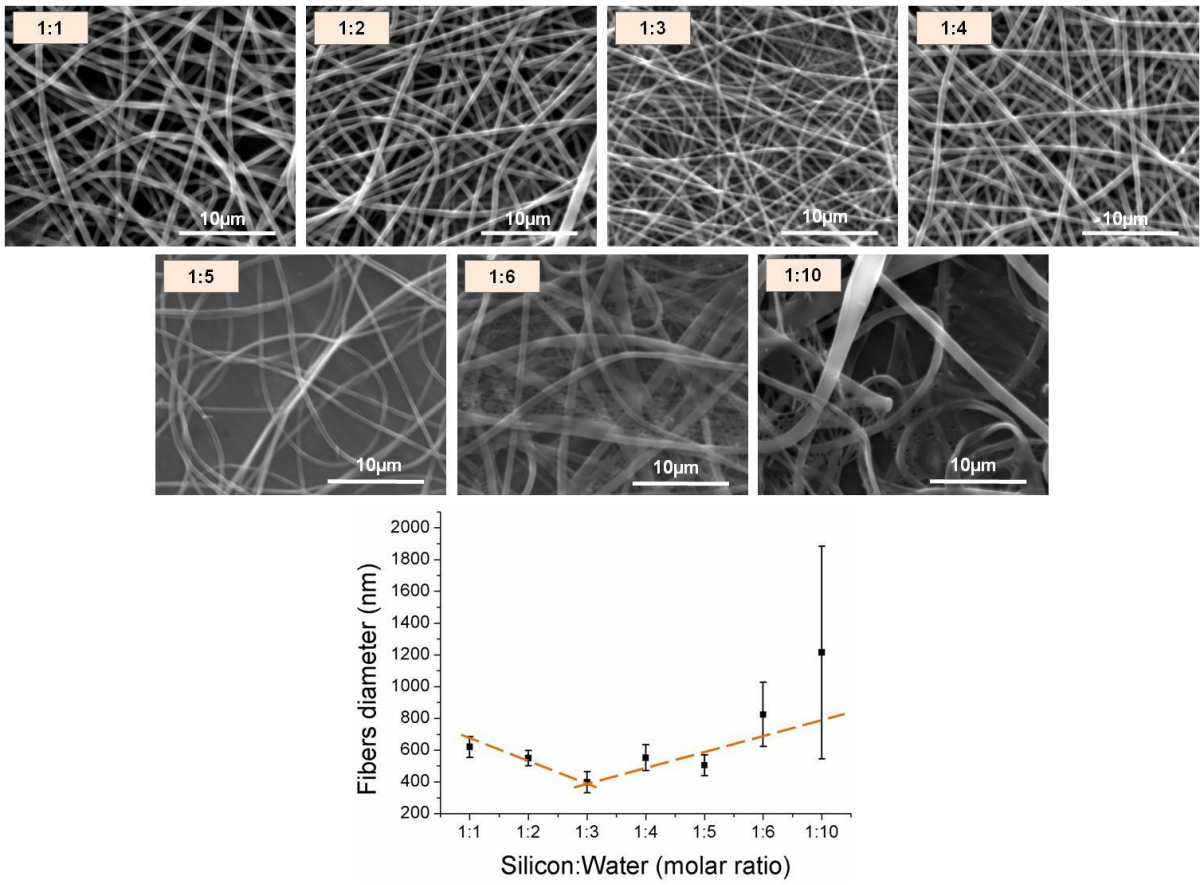

Figure 2-15. *Influence of glass hydrolysis degree on hybrid S52 fibers.* Morphology and thickness of PCL-S52 hybrid fibers obtained with TFE as solvent and different ormoglass hydrolysis ratios (the orange dotted line shows the results' tendency).

2.4.3. Discussion

Hybrid PCL-(Si,Ca,P_2) ORMOGLASS fibers were produced under new electrospinning setup and blend conditions. A preliminary study demonstrated that hybrid fibers could be electropun using THF as solvent, even with the new electrospinning parameters selected for this study. However, these fibers exhibited numerous imperfections such as irregularities in shape and presence of beads (**Figure 2-11**). The differences in fiber thicknesses were particularly well represented by the high standard deviation of the fiber diameter averages. The production of fibers with different thicknesses can be explained by the splitting of the primary jet into smaller jets that in turns, led to the drying of thinner fibers and a multimodal size distribution [64]. Torres-Giner *et al.* for example reported this behavior with a mix of natural/synthetic polymer (PLA/collagen) [65]. Patlolla *et al.* also published a study in which bimodal

fibers were obtained from a PCL/HA/TCP composite solution [66]. Regarding the electrospinning, the observed irregularities and beads meant that the conditions in which the fibers were electrospun were not optimal for the fabrication of a homogeneous scaffold in terms of geometry. In fact, the presence of beads may be explained by the instability of the jet initiation due to inappropriate polymer solution properties (surface tension, viscosity, dielectric constant…) and low force to pull the polymer jet [67]. Together, these problems affect the efficiency of the fiber deposition, eventually leading to the interruption of the electrospinning process. Therefore, it was necessary to improve the electrospinning process in order to obtain good continuity in the fiber deposition and more homogeneous fibers - if possible in the nanoscale.

Based on the results obtained with the fibers produced with THF as solvent, it seemed that the use of different ORMOGLASS compositions did not significantly affect the fibers morphology, nor the fibers diameter average (**Table 2-5**). This suggested that a change in the glass composition was not a critical parameter for the fibers fabrication. This implied that the optimization study could have been performed with S40 or S70 compositions instead of the S52 one. In other words, the arbitrary selection of one composition is not thought to affect the results: all the conclusions resulting from this study for one specific composition would be also obtained if other compositions were used. For this reason, it is assumed that the optimized experimental factors that were set in the present study would be also valid for the other compositions.

Fibers were afterwards prepared with the S52 composition and one blend parameter at a time was modified. The first parameter that was changed was the solvent. THF was replaced by TFE. In fact, as already mentioned, even if Si-Ca-P_2 fibers were obtained with THF as solvent, the fiber fabrication was difficult. The liquid drop at the tip of the syringe rapidly solidified, leading to the clogging of the needle. This prevented the fibers to be formed in a continuous manner and a regular cleaning of the tip was necessary to unblock the dispensing of the drop. It was hypothesized that this problem could be overcome by changing the solvent. TFE appeared to be more efficient for the electrospinning process due to its higher dielectric constant and polarizability (TFE: dielectric constant ε = 7,58 at 25°C [68], THF: ε = 26,14 at 25°C [69]). TFE possesses also a lower vapor pressure and slightly higher boiling temperature (vapor pressure P_v = 9,3 kPa at 25°C [70], boiling temperature T_b = 74°C at 1 atm [68]) than THF (P_v = 26.0 kPa at 25°C [69], T_b = 66°C at 1 atm [69]); in other words, it is less volatile. In the electrospinning process, the charges in the jet carry the liquid polymer to the collector thanks to the applied high voltage. The evaporation of the solvent has a direct impact on the mechanism of forces transfer through the jet because it affects its viscoelasticity [71,72]. A solvent with lower vapor pressure and higher boiling temperature exhibits thus a better mass flow velocity as it evaporates slower. Therefore, TFE has been selected to improve the processability of the blends due to its intrinsic electrical and thermodynamic properties. Globally, it has been indeed noticed that the fiber deposition was easier with this solvent than with THF.

Investigation of the influence of the polymer concentration on the fiber size demonstrated that the fiber diameters increased with the polymer content (**Figure 2-12**). This was in agreement with other

published studies [31,67,73]. This tendency is explained by the increase of the solution viscosity [31]. In our case, if hybrid nanofibers are intended to be produced, a 8% or 10% polymer solution should be used. With these concentrations, the fibers obtained were very homogeneous and did not have defects. They were, in fact, more regular than hybrid fibers prepared with other polymer contents and than pure PCL fibers prepared with similar concentrations. On the other hand, it was noticed that the incorporation of the glass suspension led to fibers with smaller diameter than pure PCL ones (**Figure 2-13**). This diameter reduction can be inferred to a decrease in viscosity of the PCL solution when the ORMOGLASS sol is added. Indeed, if low viscosity solution is used to perform the electrospinning, fibers with thinner diameters are obtained in comparison to ones prepared with a higher viscosity solution. The blends seemed therefore to be less viscous than a pure PCL solution.

Most of the fibers prepared with different precursor contents were produced with homogeneous morphologies (**Figure 2-14**), suggesting that the blend conditions and processing parameters were satisfactory for the fabrication of homogeneous scaffolds. Nevertheless, regular fibers have been only obtained up to a ratio of 40:60. With glass content equal to 50%, the fibers became heterogeneous and beads tended to appear. In fact, in this case, the content of the glass was too high to achieve a proper glass/PCL blend. The glass was segregated from the polymer. As a consequence, the glass dropped from the tip when the electrospinning was processed because it was not properly incorporated to the PCL solution (or only partially). This means that instead of a synergic PCL-glass blend, only (or mainly) the polymeric phase was electrospun. Therefore, it is assumed that the size of the fibers obtained for this ratio is principally determined by the viscosity of the polymeric solution itself. As viscous solutions (i.e polymeric ones) lead to thicker diameter than ones with lower viscosity (in our case, the blends), this would explain why there is a significant difference between the diameter of the low glass sol content fibers (up to 40%) and the ones containing 50% (or more) of ORMOGLASS.

About the hydrolysis level of the glass precursor solution, results showed that homogeneous bead-free nanofibers could be obtained up to a hydrolysis ratio of 1:5 and that from 1:3 ratio to 1:10 ratio, fibers diameters increased (**Figure 2-15**). For the sol-gel method, the water introduced to perform the hydrolysis has a direct influence on the sol prepared. The water quantity is, in fact, the most important parameter that determines the degree of condensation of the sol. For this reason, instead of colloidal suspensions, gels could be have been also obtained if a higher quantity of water was added to the ORMOGLASS precursor mix [74]. Therefore, the higher the degree of hydrolysis, the more viscous the glass suspension (or gel). As described previously, the addition of the glass into the PCL solution lowered the viscosity of the polymer solution. Thus, the more viscous the ORMOGLASS suspension, the lower the decrease in the viscosity. This is what happened here: by adding more water in the glass mix, the condensation process was more advanced. In other words, a more viscous ORMOGLASS was obtained and consequently, a more viscous blend. Thus, thicker fibers were produced when increasing the hydrolysis ratio.

This experimental optimization study has been successfully conducted. Hybrid PCL-ORMOGLASS fibers have been produced using TFE as solvent under new processing parameters. Blend conditions have been identified for the production of homogeneous, regular and defect-free nanofibers. The determination of specific parameters to collect fibers with well-defined size was important for the fabrication of biomimicking substrates. Achieving a continuous fiber deposition was also essential for the carrying out of further biological studies, as such assays commonly require a large amount of samples. Thanks to this work, PCL-ORMOGLASS fibers can from now on be produced without any particular problems.

2.4.4. Conclusion

PCL-Si,Ca,P_2 ORMOGLASS bioactive glass blends were prepared under different conditions in order to assess the effect of solution preparation (glass hydrolysis, polymer concentration, glass content) on the morphology and diameters of electrospun fibers. Results showed that the use of TFE was a more suitable solvent than THF in terms of fibers deposition efficiency and fibers regularity. Several blends prepared were appropriate for the production of fibers with homogeneous thicknesses. However, to obtain nanosized fibers, polymer solutions with low concentration, blends with ORMOGLASS contents inferior to 40% (volume percentage) and hydrolysis performed with Si:H_2O ratios up to 1:5 should be preferred. In summary, it has been globally demonstrated that the solution parameters directly influence the aspect of the fibers. This study provides therefore valuable experimental information for the fabrication of nanotextured substrates made of a synthetic polymer and an organically modified glass. This information will be used in the future to produce more efficiently the scaffolds needed to perform additional biological assays to the ones reported in the first part of this chapter.

2.5. Chapter conclusion

The PCL-ORMOGLASS bioactive fibers presented in this chapter constitute a novel type of hybrid material. The organic and inorganic materials interact with each other at the nanometric level due to the use of the sol-gel method and the incorporation of organic fragments in the ORMOGLASS network. Thanks to these suitable interactions, these hybrids exhibited a calcium release profile that seemed to be suitable to promote osteo and angiogenesis. Other hybrid properties such as nanoroughness, stiffness and hydrophilicity also contributed to the excellent fibers biological performance. The development of these fibers confirmed that material mechanical, chemical and physical properties can be used to trigger specific cellular responses. It highlighted thus the importance of the cell-artificial ECM interactions. Initially prepared as microfibers, nanofibers were also produced. This was achieved by changing the electrospinning conditions, more precisely the solvent used and the features of the blend. These modifications were applied in a controlled way in order to obtain scaffolds that better mimic the nanostructure of the collageneous fibrils of native bone. Thanks to this improvement, fibers will be

produced more easily and an additional nanotexture is given to the scaffold, a property which cells are sensitive. In summary, this work opened a new door for the development of temporary instructive polymer-ORMOGLASS biomaterials.

2.6 Acknowledgments

I kindly thank all the scientists from the "Biomaterials and Tissue Engineering Lab" of the Dankook University (South Korea) who contributed to the biological characterization of these hybrid fibers, especially Prof H-W Kim, Dr. Guang-Zhen Jin, Dr. T-H Kim and Dr. J-H Kim. The European Commission and the Spanish Ministry of Economy and Competitiveness are also acknowledged for funding (European ERANET project PI11/03030 - NANGIOFRAC) and project MAT2011-29778-C02-01, respectively). This work was also partially supported by a fellowship (2009–0093829) from the Priority Research Centers Program of the National Research Foundation of Korea.

2.7 References

[1] Laschke MW, Harder Y, Amon M, Martin I, Farhadi J, Ring A, et al. Angiogenesis in tissue engineering: breathing life into constructed tissue substitutes. Tissue Engineering 2006;12:2093–104.

[2] Aguirre A, Gonzalez A, Navarro M, Castano O, Planell JA, Engel E. Control of microenvironmental cues with a smart biomaterial composite promotes endothelial progenitor cell angiogenesis. European Cells and Materials 2012;24:90–106.

[3] Aguirre A, González A, Planell JA, Engel E. Extracellular calcium modulates in vitro bone marrow-derived Flk-1^+ $CD34^+$ progenitor cell chemotaxis and differentiation through a calcium-sensing receptor. Biochemical and Biophysical Research Communications 2010;393:156–61.

[4] Ingber DE. Mechanical signaling and the cellular response to extracellular matrix in angiogenesis and cardiovascular physiology. Circulation Research 2002;91:877–87.

[5] Engler AJ, Sen S, Sweeney HL, Discher DE. Matrix elasticity directs stem cell lineage specification. Cell 2006;126:677–89.

[6] Brown EM, MacLeod RJ. Extracellular calcium sensing and extracellular calcium signaling. Physiological Reviews 2001;81:239–97.

[7] Marie PJ. The calcium-sensing receptor in bone cells: a potential therapeutic target in osteoporosis. Bone 2010;46:571–6.

[8] Adams GB, Chabner KT, Alley IR, Olson DP, Szczepiorkowski ZM, Poznansky MC, et al. Stem cell engraftment at the endosteal niche is specified by the calcium-sensing receptor. Nature 2006;439:599–603.

[9] Tommila M, Jokilammi A, Terho P, Wilson T, Penttinen R, Ekholm E. Hydroxyapatite coating of cellulose sponges attracts bone-marrow-derived stem cells in rat subcutaneous tissue. Journal of the Royal Society, Interface 2009;6:873–80.

[10] Rezwan K, Chen QZ, Blaker JJ, Boccaccini AR. Biodegradable and bioactive porous polymer/inorganic composite scaffolds for bone tissue engineering. Biomaterials 2006;27:3413–31.

[11] Jang J-H, Castano O, Kim H-W. Electrospun materials as potential platforms for bone tissue engineering. Advanced Drug Delivery Reviews 2009;61:1065–83.

[12] Zou B, Liu Y, Luo X, Chen F, Guo X, Li X. Electrospun fibrous scaffolds with continuous gradations in mineral contents and biological cues for manipulating cellular behaviors. Acta Biomaterialia 2012;8:1576–85.

[13] Xie J, Blough ER, Wang C-H. Submicron bioactive glass tubes for bone tissue engineering. Acta Biomaterialia 2012;8:811–9.

[14] González B, Colilla M, de Laorden CL, Vallet-Regí M. A novel synthetic strategy for covalently bonding dendrimers to ordered mesoporous silica: potential drug delivery applications. Journal of Materials Chemistry 2009;19:9012–24.

[15] Mahony O, Tsigkou O, Ionescu C, Minelli C, Ling L, Hanly R, et al. Silica-gelatin hybrids with tailorable degradation and mechanical properties for tissue regeneration. Advanced Functional Materials 2010;20:3835–45.

[16] Kim H, Lee H, Knowles JC. Electrospinning biomedical nanocomposite fibers of hydroxyapatite/poly(lactic acid) for bone regeneration. Journal of Biomedical Materials Research Part A 2006;79A:643–9.

[17] Dorozhkin SV. Biocomposites and hybrid biomaterials based on calcium orthophosphates. Biomatter 2011;1:1–54.

[18] Ogoshi T, Chujo Y. Organic–inorganic polymer hybrids prepared by the sol-gel method. Composite Interfaces 2005;11:539–66.

[19] Ali AF, Mustarelli P, Magistris A. Optimal synthesis of organo-phosphate precursors for sol-gel preparations. Materials Research 1998;33:697–710.

[20] Manzano M, Arcos D, Rodriguez Delgado M, Ruiz E, Gil FJ, Vallet-Regi M. Bioactive star gels. Chemistry of Materials 2006;18:5696–703.

[21] Kim H-W, Kim H-E, Knowles JC. Production and potential of bioactive glass nanofibers as a next-generation biomaterial. Advanced Functional Materials 2006;16:1529–35.

[22] Castano O, Sachot N, Xuriguera E, Engel E, Planell JA, Park J-H, et al. Angiogenesis in bone regeneration: tailored calcium release in hybrid fibrous scaffolds. ACS Applied Materials & Interfaces 2014:just accepted manuscript.

[23] Rasband WS. Image J. US National Institute of Health, Bethesda, USA, Http://imagej.nih.gov/ij/ 1997:2014.

[24] Drelich J, Miller JD, Good RJ. The effect of drop (bubble) size on advancing and receding contact angles for heterogeneous and rough solid surfaces as observed with sessile-drop and captive-bubble techniques. Journal of Colloid and Interface Science 1996;179:37–50.

[25] Derjaguin B V, Muller VM, Toporov YP. Effect of contact deformations on the adhesion of particles. Journal of Colloid and Interface Science 1975;53:314–26.

[26] Nečas D, Klapetek P. Gwyddion: an open-source software for SPM data analysis. Central European Journal of Physics 2011;10:181–8.

[27] Gránásy L, Pusztai T, Tegze G, Warren JA, Douglas JF. On the growth and form of spherulites. Physical Review E, Statistical, Nonlinear, and Soft Matter Physics 2005;72:011605 (15 p).

[28] Hartman O, Zhang C, Adams EL, Farach-carson MC, Petrelli J, Chase BD, et al. Biofunctionalization of electrospun PCL-based scaffolds with perlecan domain IV peptide to create a 3-D pharmacokinetic cancer model. Biomaterials 2010;31:5700–18.

[29] Oyane A, Kim H-M, Furuya T, Kokubo T, Miyazaki T, Nakamura T. Preparation and assessment of revised simulated body fluids. Journal of Biomedical Materials Research Part A 2003;65:188–95.

[30] Anderson JM, Rodriguez A, Chang DT. Foreign body reaction to biomaterials. Seminars in Immunology 2008;20:86–100.

[31] Deitzel J., Kleinmeyer J, Harris D, Beck Tan N. The effect of processing variables on the morphology of electrospun nanofibers and textiles. Polymer 2001;42:261–72.

[32] Charles-Harris M, Koch MA, Navarro M, Lacroix D, Engel E, Planell JA. A PLA/calcium phosphate degradable composite material for bone tissue engineering: an in vitro study. Journal of Materials Science: Materials in Medicine 2008;19:1503–13.

[33] Biresaw G, Carriere CJ. Correlation between mechanical adhesion and interfacial properties of starch/biodegradable polyester blends. Journal of Polymer Science Part B: Polymer Physics 2001;39:920–30.

[34] Serra T, Planell JA, Navarro M. High-resolution PLA-based composite scaffolds via 3-D printing technology. Acta Biomaterialia 2013;9:5521–30.

[35] Kim J, Kim D-H, Lim KT, Seonwoo H, Park SH, Kim Y-R, et al. Charged nanomatrices as efficient platforms for modulating cell adhesion and shape. Tissue Engineering: Part C 2012;18:913–23.

[36] Zhang J-B, Ma D, Zhong H, Luo X-L. Atomic force microscopy studies of polycaprolactone ringed spherulites. Chinese Journal of Polymer Science 2000;18:569–72.

[37] Webster TJ, Siegel RW, Bizios R. Osteoblast adhesion on nanophase ceramics. Biomaterials 1999;20:1221–7.

[38] Palin E, Liu H, Webster TJ. Mimicking the nanofeatures of bone increases bone-forming cell adhesion and proliferation. Nanotechnology 2005;16:1828–35.

[39] Dalby MJ, Yarwood SJ, Riehle MO, Johnstone HJH, Affrossman S, Curtis ASG. Increasing fibroblast response to materials using nanotopography: morphological and genetic measurements of cell response to 13-nm-high polymer demixed islands. Experimental Cell Research 2002;276:1–9.

[40] Arnold M, Cavalcanti-Adam EA, Glass R, Blümmel J, Eck W, Kantlehner M, et al. Activation of integrin function by nanopatterned adhesive interfaces. ChemPhysChem: A European Journal of Chemical Physics and Physical Chemistry 2004;5:383–8.

[41] De Oliveira RRL, Albuquerque DAC, Cruz TGS, Yamaji FM, Leite FL. Measurement of the nanoscale roughness by atomic force microscopy: basic principles and applications. Atomic force microscopy - Imaging, measuring and manipulating surfaces at the atomic scale, 2012.

[42] Chen H, Li L-J, Ou-Yang W-C, Hwang JC, Wong W. Spherulitic crystallization behavior of poly(ε-caprolactone) with a wide range of molecular weight. Macromolecules 1997;30:1718–22.

[43] Mammoto A, Connor KM, Mammoto T, Yung CW, Aderman CM, Mostoslavsky G, et al. A mechanosensitive transcriptional mechanism that controls angiogenesis. Nature 2009;457:1103–8.

[44] Mulder L, Koolstra JH, den Toonder JMJ, van Eijden TMGJ. Relationship between tissue stiffness and degree of mineralization of developing trabecular bone. Journal of Biomedical Materials Research Part A 2007;84:508–15.

[45] Jones JR, Ehrenfried LM, Saravanapavan P, Hench LL. Controlling ion release from bioactive glass foam scaffolds with antibacterial properties. Journal of Materials Science Materials in Medicine 2006;17:989–96.

[46] Yamaguchi T, Chattopadhyay N, Kifor O, Butters RR, Sugimoto T, Brown EM. Mouse osteoblastic cell line (MC3T3-E1) expresses extracellular calcium (Ca^{2+}_o)-sensing receptor and its agonists stimulate chemotaxis and proliferation of MC3T3-E1 cells. Journal of Bone and Mineral Research 1998;13:1530–8.

[47] Yamauchi M, Yamaguchi T, Kaji H, Sugimoto T, Chihara K. Involvement of calcium-sensing receptor in osteoblastic differentiation of mouse MC3T3-E1 cells. American Journal of Physiology Endocrinology and Metabolism 2004;288:E608–E616.

[48] Chattopadhyay N, Yano S, Tfelt-Hansen J, Rooney P, Kanuparthi D, Bandyopadhyay S, et al. Mitogenic action of calcium-sensing receptor on rat calvarial osteoblasts. Endocrinology 2004;145:3451–62.

[49] Honda Y, Fitzsimmons RJ, Baylink DJ, Mohan S. Effects of extracellular calcium on insulin-like growth factor II in human bone cells. Journal of Bone and Mineral Research 1995;10:1660–5.

[50] Navarro M, Ginebra MP, Planell JA, Barrias CC, Barbosa MA. In vitro degradation behavior of a novel bioresorbable composite material based on PLA and a soluble CaP glass. Acta Biomaterialia 2005;1:411–9.

[51] Jo J-H, Lee E-J, Shin D-S, Kim H-E, Kim H-W, Koh Y-H, et al. In vitro/in vivo biocompatibility and mechanical properties of bioactive glass nanofiber and poly(ε-caprolactone) composite materials. Journal of Biomedical Materials Research Part B: Applied Biomaterials 2009;91B:213–20.

[52] Li R, Clark AE, Hench LL. An investigation of bioactive glass powders by sol-gel processing. Journal of Applied Biomaterials 1991;2:231–9.

[53] Pereira MM, Clark AE, Hench LL. Calcium phosphate formation on sol-gel-derived bioactive glasses in vitro. Journal of Biomedical Materials Research 1994;28:693–8.

[54] Lin S, Ionescu C, Baker S, Smith ME, Jones JR. Characterisation of the inhomogeneity of sol–gel-derived SiO_2–CaO bioactive glass and a strategy for its improvement. Journal of Sol-Gel Science and Technology 2009;53:255–62.

[55] Zhong J, Greenspan DC. Processing and properties of sol-gel bioactive glasses. Journal of Biomedical Materials Research 2000;53:694–701.

[56] Hench LL. The story of bioglass. Journal of Materials Science Materials in Medicine 2006;17:967–78.

[57] Martín AI, Salinas AJ, Vallet-Regí M. Bioactive and degradable organic–inorganic hybrids. Journal of the European Ceramic Society 2005;25:3533–8.

[58] Sudo H, Kodama H-A, Amagai Y, Yamamoto S, Kasai S. In vitro differentiation and calcification in a new clonal osteogenic cell line derived from newborn mouse calvaria. The Journal of Cell Biology 1983;96:191–8.

[59] Gibon E, Batke B, Jawad MU, Fritton K, Rao A, Yao Z, et al. MC3T3-E1 osteoprogenitor cells systemically migrate to a bone defect and enhance bone healing. Tissue Engineering Part A 2012;18:968–73.

[60] Brakefield AC, Prieto EM, Guelcher SA. A characterization of three groups of MC3T3-E1 pre-osteoblastic cells to aid in testing of polyurethane-bone scaffolds for wound healing. Young Scientist, a High School Research Journal (Vanderbilt University) 2011;1:3–5.

[61] Elgendy HM, Norman ME, Keaton AR, Laurencin CT. Osteoblast-like cell (MC3T3-E1) proliferation on bioerodible polymers: an approach towards the development of a bone-bioerodible polymer composite material. Biomaterials 1993;14:263–9.

[62] Quarles LD, Yohay D a, Lever LW, Caton R, Wenstrup RJ. Distinct proliferative and differentiated stages of murine MC3T3-E1 cells in culture: an in vitro model of osteoblast development. Journal of Bone and Mineral Research 1992;7:683–92.

[63] Caplan AI. Mesenchymal stem cells. Journal of Orthopaedic Research 1991;9:641–50.

[64] Reneker DH, Yarin AL, Fong H, Koombhongse S. Bending instability of electrically charged liquid jets of polymer solutions in electrospinning. Journal of Applied Physics 2000;87:4531–47.

[65] Torres-Giner S, Ocio MJ, Lagaron JM. Development of active antimicrobial fiber based chitosan polysaccharide nanostructures using electrospinning. Engineering in Life Sciences 2008;8:303–14.

[66] Patlolla A, Collins G, Livingston Arinzeh T. Solvent-dependent properties of electrospun fibrous composites for bone tissue regeneration. Acta Biomaterialia 2010;6:90–101.

[67] Mo XM, Xu CY, Kotaki M, Ramakrishna S. Electrospun P(LLA-CL) nanofiber: a biomimetic extracellular matrix for smooth muscle cell and endothelial cell proliferation. Biomaterials 2004;25:1883–90.

[68] Mukherjee LM, Grunwald E. Physical properties and hydrogen bonding in the system ethanol-2,2,2-trifluoroethanol. Journal of Physical Chemistry 1958;62:1311–4.

[69] Coetzee JF, Chang T-H. Purification of solvents for electroanalysis: tetrahydrofuran and dioxane. Pure and Applied Chemistry 1985;57:633–8.

[70] Chaudhari SK, Patil KR, Allepfs J, Coronas A. Measurement of the vapor pressure of 2,2,2-trifluoroethanol and tetraethylene glycol dimethyl ether by static method. Fluid Phase Equilibria 1995;108:159–65.

[71] Reneker DH, Chun I. Nanometre diameter fibres of polymer produced by electrospinning. Nanotechnology 1996;7:216–23.

[72] Megelski S, Stephens JS, Chase DB, Rabolt JF. Micro- and nanostructured surface morphology on electrospun polymer fibers. Macromolecules 2002;35:8456–66.

[73] Demir MM, Yilgor I, Yilgor E, Erman B. Electrospinning of polyurethane fibers. Polymer 2002;43:3303–9.

[74] Brinker CJ, Scherer GW. Sol-gel science, the physics and chemistry of sol-gel processing. 1990.

Chapter 3

Electrospun hybrid fibers prepared with a titanium-calcium-phosphate-sodium bioactive ORMOGLASS and polylactic acid

This chapter is divided in two parts. The first one reports the development of hybrid fibers made of polylactic acid and a titanium-calcium-phosphate-sodium bioactive ORMOGLASS. The physico-chemical properties of these fibers were investigated by means of various material characterization techniques. In vitro and in vivo assays were also carried out to investigate the biological performance of the scaffold. The other part discusses about the in vitro degradation of these fibers in simulated physiological conditions.

Most of the assays presented in the first part of the chapter were performed at the institute for Bioengineering of Catalonia. Only the in vivo assay was conducted in another center - the national institute for Health and Biomedical Research (INSERM, France) - in the frame work of the Nangiofrac European project and a 2 months research stay. The degradation study was performed at the Warsaw University of Technology (WUT, Poland); also in relation to the Nangiofrac project (3 months research stay).

3.1. Chapter summary

Although titanium-calcium-phosphate-sodium glasses (from now on abbreviated as Ti-Ca-P_2-Na_2 system[1]) are new bioactive glasses compared to silicon-based ones, they have been already demonstrated to possess great potential for bone tissue engineering. Lately, composites made of a synthetic polymer and a particular composition of a titanium glass (molar percentage: 5 Ti - 44.5 Ca - 44.5 P_2 - 6 Na_2, named G5) have been demonstrated to trigger osteo and angiogenesis. As many of the hybrid materials developed today usually promote osteogenesis but lack of ability to induce vascularization, this material combination appeared to be a good option for development of instructive scaffolds. Up to now, polymer-G5 materials have been produced only as bulk material or well-ordered structure (rapid prototyping architecture) and by implementing the melting-quenching method to prepare the glass. In this study, PLA-ORMOGLASS fibers (with G5-like composition) have been produced by means of the electrospinning technique in order to fabricate substrates for cells that promote simultaneously bone formation and vascularization, and additionally mimic the fibrous structure of the extracellular matrix of natural bone. Moreover, the sol-gel method (already known as an effective alternative to the conventional melting-quenching approach) was used to process the glass. Non-woven and aligned fibers were collected with two different glass contents. Physico-chemical characterization performed using scanning electron microscopy, contact angle measurements and tensile tests demonstrated that the scaffolds obtained exhibited homogeneous morphology, good hydrophilicity and good mechanical properties. Preliminary *in vitro* assays with MSCs (cells able to differentiate into osteoblastic lineage) and EPCs (cells involved in blood vessels formation) also showed that cells attached and proliferated on the materials. However, for

[1]The abbreviation was defined in accordance with an oxide based nomenclature (oxides used to prepare the ORMOGLASS system): Ti in reference to titanium oxide TiO_2, Ca in reference to calcium oxide CaO, P_2 in reference to phosphorous oxide P_2O_5, and Na_2 in reference to sodium oxide Na_2O *[Navarro et al., Journal of the American Ceramic Society 2003; 86, 1342-52]*.

the EPCs, these processes seemed to be a little bit more difficult than for the MSCs. The bioactivity and biocompatibility of these fibers were however demonstrated for both cell types *in vitro* and also *in vivo*. These novel fibers appeared thus to be a suitable option for the design of functional materials for tissue engineering applications. They constitute a significant improvement regarding the development of bioinspired structures.

The biodegradation behavior of the fibers is very important regarding the success of the scaffold implantation as this success relies on the ability of the material to interact properly with the biological environment. This behavior mainly depends on the design of the graft and more precisely on its capacity to biodegrade in a well defined manner (nature of ions released, dissolution profile of this release, rate of material resorption, preservation of mechanical properties). The assessment of the biological behavior of temporary templates is therefore very important in tissue engineering, especially for composites which usually exhibit complicated degradation behaviors. Therefore, the produced fibers have been incubated up to four weeks in physiological simulated conditions and their morphological, topographical and chemical changes have been investigated. The results showed that a significant loss of inorganic phase occurred at the beginning of the immersion and that the glass maintained afterwards a stable composition along the degradation period. Globally, the scaffolds underwent a fast and heterogeneous degradation. This study revealed thus that an effort should be made regarding the development of the material in order to avoid the initial drastic ORMOGLASS dissolution and that, according to the *in vitro* assay, the material durability may not be suitable for long term applications.

3.2. Introduction

The development of materials for tissue engineering has for a long time focused on implants aimed to simply replace non functional or damaged organs. But scaffolds design has considerably evolved in the last years and biomaterials from the third generation have been developed [1,2]. These materials are able to stimulate specific cellular responses, being bioactive and bioabsorbable [3–5]. Regarding bone regeneration, many material fabrication approaches have been implemented for the production of functional substrates able to interact and properly integrate with the host tissue and/or trigger cell differentiation towards osteoblastic lineage. But, the obtained scaffolds generally do not promote angiogenesis, a vascularization process essential for the formation of a fully functional living new tissue [6]. Several studies performed by our group have previously demonstrated that composites made of polylactic acid (PLA) and Ti-Ca-P_2-Na_2 bioactive glass have the potential to efficiently promote bone formation and to integrate with bone tissue [7,8]. More recently, another study pointed the formation of tube-like structure when endothelial progenitor cells (responsible of vessels formation) where cultured on this material [9]. The good biological performance of these scaffolds was mainly attributed to their stiffness and the ions released from the glass, as well the material intrinsic surface properties [9,10]. The combination of PLA with this bioactive glass appeared therefore to be a promising material association.

Up to date, this material has been only shaped by using the salt leaching-solvent casting method and the rapid prototyping technique [11,12]. As not only the chemistry but also the structure of a scaffold influences cellular response, the choice of appropriate scaffold architecture is critical. Biomimicking scaffolds are nowadays extensively investigated for this reason. Results reported in the chapter 2 particularly showed the potential of electrospun mats to support cell adhesion, proliferation and differentiation. It also revealed the importance of developing materials with specific features (composition for example) and validated the use of Si-Ca-P_2 ORMOGLASSES to prepare hybrid. However, to approve more generally and definitely the use of ORMOGLASSES for tissue engineering, the fabrication of hybrids involving other systems (i.e. other constituents) is required.

On the other hand, as part of the so-called "third generation" of materials, smart scaffolds should additionally degrade at a suitable rate that enables the triggering of specific cellular responses along the material progressive resorption [13]. This is particularly true if the material is intended to be implanted as an acellular template aimed to bond to the host tissue, mineralize and recruit cells by itself [14]. The final goal of designing such materials is that only the newly formed functional tissue remains at the end of the regeneration process and no additional surgical procedures are necessary to remove the implanted construct. The biodegradability of a substrate is therefore a very important concept that can even be critical regarding the effectiveness of the graft to promote the body's inherent capacity to heal and self-repair and act as cell-homing promoter. If toxic byproducts are released during material degradation for example, the local healthy tissue is not preserved and tissue regeneration will not occur properly. Scar tissue can consequently be formed attesting of non appropriate interactions between the template and the host tissue [15,16].

Many parameters such as architecture, porosity, hydrophilicity, crystallinity and chemical composition can affect the biodegradation mechanisms of a material [17–19]. This depends thus on its design and more precisely on its constituents and fabrication method (structure features: shape, size, interconnected porosity…). Depending on the clinical use and tissue targeted (soft or hard), different material properties are needed. For bone engineering, hybrid materials made of synthetic or biodegradable polymer and bioactive glasses are interesting composites as they are able to form a stable implant-host tissue interface. They even trigger the desired cellular responses by dissolving and releasing ions in the surrounding fluid (i.e osteogenesis and angiogenesis) [8,9]. Thus, by combining PLA and G5 glass together, fully bioresorbable scaffolds with remarkable mechanical and bioactive properties can be produced [20,21]. However, degradation is a complex mechanism influenced by several biological connected factors as for examples pH and fluid infiltration, oxygen supply and enzyme activity [22,23]. An exact control on the degradation process is therefore difficult to achieve, especially if this control is aimed to satisfy precise expectations like specific degradation rate or time scaled product release. Despite these drawbacks, it is essential to assess the degradation behavior of a scaffold as it will closely control the future of the template after implantation (changes in mechanical properties, induced cellular response) and consequently determine its success.

3.3. Fiber preparation and characterization

The study reported in this part of the chapter was carried out to prepare hybrids containing PLA and a titanium based ORMOGLASS (G5 composition) as fibrous mats in order to produce osteo and angiogenic biomimicking scaffolds. The ability to apply the sol-gel method to the G5 glass composition was also assessed in order to establish a new glass preparation protocol. The fiber production is based on the preparation of a PLA-G5 blend. The fabrication of these fibers was also aimed to approve the use of ORMOGLASSES for titanium based systems regarding biomedical applications. Therefore, the produced fibers were characterized and their biological responses were investigated. It was believed that producing PLA-titanium based ORMOGLASS composites as hybrid fibers would constitute a better environment for cellular activity (bioinspired structure) [24] and that the interactions between the phases could be improved in comparison to the over materials already prepared with these two families of compound.

3.3.1. Materials and methods

3.3.1.1. Blend preparation and electrospinning

The preparation of the glass involved a mix of metal alkoxide precursor solutions. This mix contained the same calcium and phosphorous precursors as the ones described in the previous chapter. The titanium precursor was prepared by dissolving titanium isopropoxide (Alfa Aesar 97%) in ethanol (Sigma-Aldrich >99%) and the sodium precursor by refluxing sodium metallic (Panreac) in methoxyethanol (Sigma-Aldrich 99%). To make sure they were well prepared, the single precursor were assessed using the nuclear magnetic resonance (NMR) technique (see appendix A-1 and B-1). The precursor solutions were mixed homogeneously under strong stirring according to the composition of G5 glass (molar ratio): 44.5 P_2 - 44.5 Ca - 5 Ti - 6 Na_2. Once the mix was ready, a basic catalyst (Ti:H_2O:NH_3:isopropanol catalyst with molar ratio of 1:60:4.5:100) was added to partially hydrolyze the solution and produce a viscous ORMOGLASS gel. The hydrolysis lasted three days and was performed at 4°C. In parallel, polymeric solutions of polylactic acid 3% and 4% w/w (PLA, 70/30 L-lactide/DL-lactide copolymer, Purasorb PLDL 7038) in trifluoroethanol (TFE, Panreac) were prepared. Then, the ORMOGLASS gel and the polymeric solution were blended according to a glass:polymer ratio of 10:90 and 20:80 (v:v) in order to obtain the electrospinnable blends. The fibers were labeled as PLA, T5 10-90 and T5 20-80. Before being blended with the PLA solution, the ORMOGLASS gel was left some minutes at room temperature to reach the same temperature as the polymeric solution. The blends, as well as the pure polymeric solution, were finally electrospun using a conventional electrospinning setup with a grounded flat or a rotary collector covered with aluminum. Fibers were thus deposited as randomly distributed or aligned fibrous mats. The processing parameters were the followings: 8 kV applied voltage, 0.5 ml/h blend dispensing rate, 18 cm distance tip-collector and 1000 rpm rotating speed (aligned fibers only). In order to minimize differences in the fibers composition due to the preparation of the ORMOGLASS (mix), one blend was used to produce two fibers types: the same blend for the fibers T5

10-90 aligned and random, and the same blend for the fibers T5 20-80 aligned and random. Images of the setups used to prepare the fibers (alkoxide preparation, precursor mix and blend preparation, electrospinning device) can be seen in appendix A-2.

3.3.1.2. Blend viscosity

In order to assess the effect of the addition of the ORMOGLASS gel on the polymeric solution, viscosity measurements of the blends were performed (vibroviscometer SV10, Malvern Instruments – see appendix B-7). Continuous measurements were done to make sure that the viscosity of the blends was stable over time. These continuous measurements were done for the T5 20:80 blends because these blends had the higher ORMOGLASS content and were therefore the more exposed to undergo viscosity changes (in comparison to the 10-90 ones). Moreover, punctual measurements were performed after mixing the two compounds to verify that the viscosity of the blends was suitable for the electrospinning process.

3.3.1.3. Fiber morphology and composition

Small pieces of the electrospun mats were obtained by cutting the fibrous layers at different places. The areas were selected randomly. After removing the aluminum foil, the pieces were fixed on a metallic support and coated with carbon. Support was then introduced in a Field Emission Scanning Electron Microscope (FESEM, Nova™-Nano SEM-230; FEI Co.) to assess the fibers arrangement and morphology.

To determine the exact composition of the fibers, the samples used for FESEM observations were loaded in a SEM device coupled with EDS (Quanta 200 XTE 325/D8395; FEI Co.). Even if pictures of the fibers could have been taken from this SEM-EDS coupled machine (see appendix B-2), the FESEM device was preferred as it enables to acquire images with better quality and higher magnifications. The measured compositions were averaged from elemental quantifications of three different points on the samples.

3.3.1.4. Fiber wettability

Contact angle measurements were performed using the sessile drop method to evaluate the wettability of the scaffolds (OCA 20 system, Dataphysics, GmbH – see appendix B-3). It consists in the deposition of an ultra pure water drop (3µl) on the material and the determination of the angle between this drop and the materials surface. The contact angle was determined by using the ImageJ software [25]. This approach enables the determination of the degree of hydrophilicity of the materials: the lower the contact angle values, the more hydrophilic the material. For the aligned fibers, pictures of the water drop on the fibers were taken perpendicular to the orientation of the fibers. For the random ones, no specific

positioning of the sample has been done as the contact angle values were not influenced by any defined fiber orientation (appendix A-4, A.4.1).

3.3.1.5. Fiber surface charge

Zeta potential (ZP) technique was used to assess the surface charge of the fibers (see appendix B-5). ZP measurements were performed in a 1 mM KCl electrolyte solution using the "adjustable gap cell" set-up (electrokinetic analyzer SurPASS, Anton Paar Ltd. Austria). The pH of the electrolyte was titrated from the basic region (pH ~ 8) to the acid one (pH ~ 2.5) by adding HCl 0.1M using the device pump. The electrolyte was forced to pass between two thin layers of fibers using a pressure program of maximum 300 mbar. The isoelectric points (IEP) and ZP values at pH = 7.4 were taken into account to compare the charge surface changes after the treatments.

3.3.1.6. Polymer thermal properties

Differential Scanning calorimetry (DSC, Q2000 TA) was used to determine the effect of the addition of the ORMOGLASS in the polymeric solution on the thermal properties of the produced fibers (see appendix B-8). As for FESEM, small pieces of the mats were cut at random areas of the electrospun layer (~ 1.2 mg sample). Samples were then place in aluminum pans and subjected to two heating ramps and one intermediate cooling: samples were first heated from -20°C to 180°C, cooled, and heated again. The heating rate for both ramps was fixed at 10°C/min and nitrogen was used as a purge gas. Crystallization and melting properties of the polymer were assessed by analyzing the curve of the first heating ramp. The glass transition (T_g) was determined considering the second heating cycle and using the inflexion point method (TA Universal Analysis software, v4.7A).

3.3.1.7. Thermogravimetry

Thermoanalyzer (TGA Q5000 TA) was used to determine the mass of the inorganic phase that is contained in the fibers and assess the stability of the polymeric phase (evaluation of decomposition temperatures) (see appendix B-9). Samples of ~ 10mg were placed on platinum pans and heated from room temperature (25°C) up to 700°C at a heating rate of 10°C/min in air. TGA coupled with FTIR (Nicolet 8700 Thermo Scientific) was also operated to identify the gaseous byproducts that decomposed and/or vaporized during the fibers degradation. In this case, measurements were performed in the same other conditions than simple TGA but in nitrogen. However, only the T5 20:80 fibers were selected for that assay. As they had the higher ORMOGLASS content, it was assumed that better infrared signals related to eventual degradation products from the ORMOGLASS could be reached (in comparison to fibers containing a smaller ORMOGLASS quantity). TGA curves were analyzed with the TA Universal

Analysis software (v4.7A) and FTIR spectra acquired using the OMNIC 8.2 software (Thermo Scientific).

3.3.1.8. Mechanical properties

Fibers strips (1cm width) were clamped by the grips of the tensile device (Tytron 250 Microforce Testing System) and elongated using a force load of 50 N (see appendix B-10). The MultiPurpose TestWare® software was used to acquire the strain-stress data curves. The Young's Modulus was calculated as the slope of the linear region of the curve. The thickness of the fibers layer was measured with ImageJ [25] software using FESEM pictures of the strips in transversal view (appendix A-4, A.4.2). The initial sample length (distance grip to grip) was set to 2 cm. For the aligned fibers, strain was applied along the fibers orientation. Results were considered statistically significant for $p < 0.05$ and highly significant for $p < 0.002$ (Student's t-test).

3.3.1.9. Protein adsorption

Protein adsorption test was performed to evaluate the ability of the fibers (PLA and hybrids) to support protein anchorage. 1 cm x 1 cm pieces were cut from the fibrous layers and immersed during 1 hour at room temperature in deionized water. Afterwards, fibers were transferred to a 24 well-plate and 1 mL of PBS solution containing 0.5 mg of bovine albumin serum (BSA, Sigma-Aldrich) was added to each well. Fibers were incubated for 30 min at 37°C. After this time, the membranes were rinsed gently three times with deionized water and allowed to dry at room temperature. The adsorption of the protein was qualitatively assessed by FTIR (Nicolet 8700 Thermo Scientific – see appendix B-11).

3.3.1.10. pH measurements

When performing preliminary tests for *in vitro* assays, it has been noticed that the medium used turned yellow instead of staying pink, its usual color. This indicated that the pH changed once the fibers were immersed in culture medium. To evaluate these changes, pH was measured (Crison GLP22+ pH-meter and Crison pH microelectrode). The possibility to control these changes was evaluated by immersing the fibers in four different solutions: deionized water, SBF, culture medium (advanced Dulbecco's modified Eagle medium, adv. DMEM, Gibco®) and culture medium supplemented with 20 mM of 4-(2-hydroxyethyl)-1-piperazineethanesulfonic acid (HEPES). Before starting the test, the medium containing HEPES was stabilized with sodium hydroxide at pH 7.4. This assay was conducted with the T5 20-80 fibers. Because these fibers had the higher ORMOGLASS content (in comparison to the other fibers of the study), they were expected to induce the most critical changes in pH. It was therefore hypothesized that, if the pH changes were controlled for these fibers, it would be also the case for the fibers with lower ORMOGLASS amount, as the pH changes would be more buffered.

3.3.1.11. In vitro assays

3.3.1.11.1. Material conditioning and cell seeding

Mesenchymal stem cells (MSCs) and endothelial progenitor cells (EPCs) obtained from rat bone marrow were used for this study. These two types of cells were chosen according to published results that demonstrated the potential of the titanium-based system to promote mesenchymal stem cell differentiation into osteoblastic cell lineage and endothelial progenitor cell differentiation towards phenotype involved in vascularization [26–28]. Medium for MSCs was prepared with advanced DMEM supplemented with 10% FBS, 1% of L-Glutamine, 1% Sodium pyruvate and 1% penicillin/streptomycin. Medium for EPCs was prepared with M199 supplemented with 20% FBS, 1% Glutamine, 1% penicillin/streptomycin and the growth factors (VEGF, IGF, EGF, bFGF, heparine and ascorbic acid) for the EPCs. HEPES (20 mM) was additionally added in both medium to make sure that the pH was maintained stable during the assay. Cells were grown on culture flasks in the incubator (37°C, 5% CO_2) and trypsinized just before seeding on the materials. Squares were cut from the electrospun fibrous layers to fit in a 24 well-plate, sterilized for 15 min under UV radiation, pre-incubated for 2 h in complete medium at 37°C and rinsed with PBS before seeding. Cells were seeded at a density of 10 000 cells/disc in 24 well-plates (500 µL medium/well).

3.3.1.11.2. Fluorescence staining

After 1 day and 10 days, cells were fixed using a paraformaldehyde-sacarose-H_2O-PBS solution to observe them thanks to fluorescent staining. 4,6-diamidino-2-phenylindole (DAPI) was used to stain the nuclei and green phalloidin for the actin cytoskeleton. Fluorescent images were collected using a confocal microscope with a x63 objective lens (oil immersion).

3.3.1.11.3. Cell fixation for FESEM imaging

Cells were also fixed using a glutaraldehyde-PBS solution and then lyophilized before carbon coating to be observed under FESEM. Pictures with cells fixed on the scaffolds were obtained with the same device and under the same conditions than the images of the fibers without cells.

3.3.1.11.4. Cell proliferation

Cell culture was carried out up to 14 days, changing the medium every two days, to quantify cell proliferation. At defined time points (1d, 3d, 7d, 10d, 14d), the medium was replaced with fresh medium containing 10% of Alamar Blue® (Thermo Scientific, TREK diagnostic systems). Plates were then incubated at 37°C during 4 h. Five replicates for each material were used for statistical analysis. Quantification of cellular proliferation using Alamar blue® implies the reduction of non fluorescent molecules to fluorescent molecules through cell metabolism. The intensity of the fluorescent is

proportional to the number of cells. After the 4 h hours of incubation, 100 µL of the reacted solution was transferred to a 96 well/plate and the fluorescence was measured. The measurements were performed at 590 nm with a microplate reader (Infinite M200 Pro, Tecan). The remaining mix medium/Alamar Blue® was removed and cells were washed with PBS. 500 µL of fresh medium was finally added to the wells and cells were furthermore cultured until the next measurement.

3.3.1.12. In vivo assay

In vivo assays were carried out to determine the biocompatibility of these novel fibers and to evaluate their potential for vascularization. The procedures and animal handling followed the principles of Laboratory Animal Care described by the National Society for Medical Research, and approved by the Animal Care and Experiment Committee of the University of Bordeaux Segalen. Experiments were carried out in accredited animal facilities according to European recommendations for laboratory animal care (directive 86/609 CEE of 24/11/86). Swiss Strain mice (females, 3 months) were used for this study. Mice were housed in individually ventilated cages on a 12-hour light-dark cycle at 21-23 ºC and 40-60% humidity, and allowed free access to irradiated standard rodent diet and sterilized water.

Round shape membranes, cut from the electrospun layers with a diameter of 1 cm, were implanted in the dorsus of the mices (subcutaneous implantation). Before implantation, membranes were sterilized by UV and incubated for 24 h in PBS. The animals were anesthetized using isoflurane and one small incision was made, with scissors, on each side of the dorsus. Each animal received two specimens of aligned fiber type (PLA, T5 20-80 or T5 10-90 membranes), in the left and right dorsal sites. Three animals were used for each fiber type for histological assays. This corresponds to 6 samples per material. The incision was closed using chirurgical staples. After one and four weeks, the animals were euthanized and implanted membranes were extirpated for histological analysis. The membranes and the tissues surrounding the implanted membranes were placed in 4% buffered formaldehyde solution for 24 h, at 4°C. Then, they were immersed during 3 days at 4°C in a sucrose solution (30%) and afterwards, immersed during 2 h in a sucrose solution (30%) containing 7% of gelatin, at 37ºC. The samples embedded in gelatin were snap frozen using liquid nitrogen and 8 µm sections were cut using a cryosection device (Leika, Germany). Hematoxylin and Eosin staining (HE) was performed in order to assess developed inflammation (formation of fibrous capsule), cell penetration into the materials and angiogenesis. CD31 immunostaining was additionally performed to confirm the presence of endothelial cells and to quantify more precisely the degree of angiogenesis. The number of micro vessels was determined for both stainings using 8 slices per sample (i.e. 42 sections per material type) and normalized using the area of the corresponding materials.

Complementary information about cellular assays and *in vivo* tests can be found in appendix B-6.

3.3.1.13. Statistical analysis

Using the Graphpad Prism 5.0 software, the D'Agostino and Pearson omnibus normality test was used in order to verify if data obeyed to a Gaussian distribution. Statistically significant differences between the groups were analyzed by the non-parametric Kruskal-Wallis test, followed by a Dunn post-test. Results were considered statistically significant for p value lower than 0.05.

3.3.2. Results

3.3.2.1. Blend viscosity

The viscosity values of PLA-ORMOGLASS blends measured continuously are presented in **Figure 3-1**. Measurements revealed that, after some minutes of stabilization, the viscosity of the blend is maintained over time. Initially, the ORMOGLASS was mixed with a 3% PLA solution but it has been noticed later that the viscosity of that blend (around 140 cP) was not optimal for the fabrication of the fibers (too low). The ORMOGLASS has been therefore mixed afterwards with a 4% solution and punctual viscosity measurements are reported for that polymer percentage. Results showed that after addition of the ORMOGLASS, the viscosity of the polymeric solution decreased (**Table 3-1**). The blend containing the higher ORMOGLASS quantity was the less viscous. Though, both slurries had an appropriate viscosity that enabled the fabrication of fibers by the electrospinning technique.

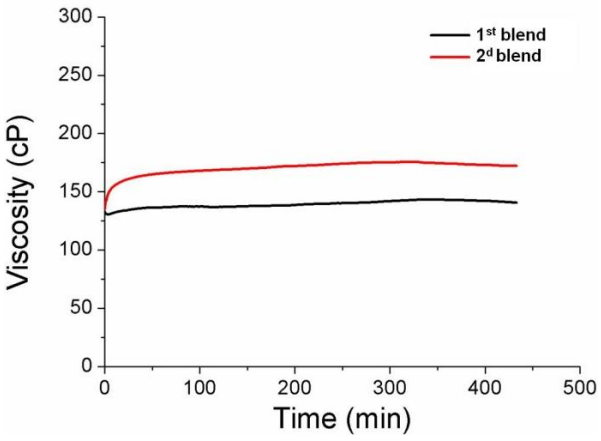

Figure 3-1. Viscosity of T5 20:80 blends (3% polymeric solution) measured in continuous.

Table 3-1. Viscosity of the PLA solution and hybrid blends (4% polymeric solution) after few minutes of homogenization.

	Viscosity (cP)	**Temperature (°C)**
PLA	665	24.6
T5 10-90	369	25.4
T5 20-80	284	25.1

3.3.2.2. Fiber morphology and composition

Figure 3-2 shows the morphology of the fibers and **Table 3-2** their composition. Random and aligned fibers were successfully produced without major imperfections (beads or aggregates for examples). Compositions of the fibers were close to the targeted G5 one for both fibers with both ORMOGLASS contents.

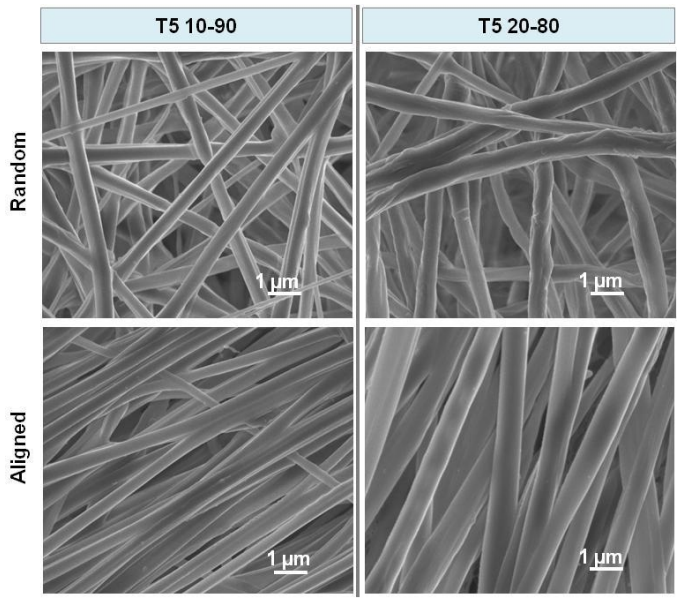

Figure 3-2. Morphology of the hybrid fibers (FESEM pictures).

Table 3-2. Composition of the hybrid fibers (molar percentages).

%	T5 10-90	T5 20-80
Ti	5.49 ± 0.81	5.66 ± 0.86
Ca	45.53 ± 1.61	44.08 ± 1.8
P_2	44.51 ± 0.44	45.16 ± 1.8
Na_2	4.47 ± 1.19	5.10 ± 0.85

3.3.2.3. Contact angle measurements

As observed on **Figure 3-3**, the incorporation of the glass gel improved the wettability of the scaffolds. In comparison to the contact angle values of PLA fibers (higher than 100°), hybrid fibers exhibited lower values for both ratios and both fiber distributions.

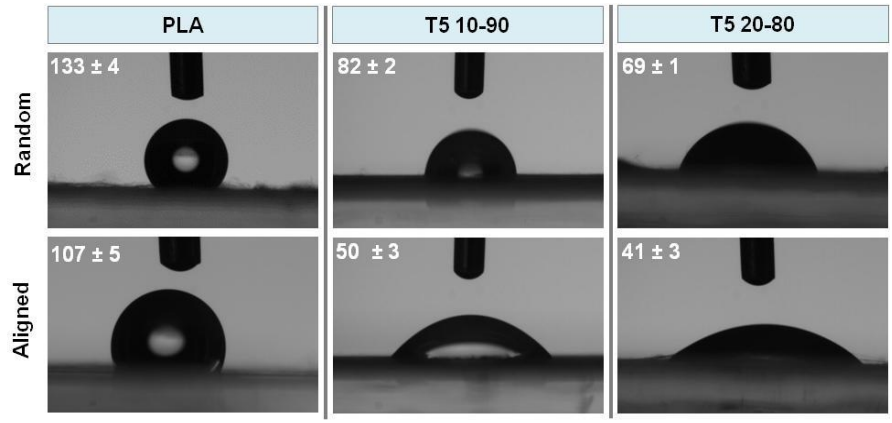

Figure 3-3. Contact angle pictures and measurements performed on PLA and hybrid fibers.

3.3.2.4. Fiber surface charge

The surface electrostatic potential of the fibers was evaluated by measuring the ZP. **Figure 3-4** shows the curves obtained. **Table 3-3** summarizes the isoelectric point values (IEP, pH value at ZP = 0) and ZP values after for pH = 7 (indicative value chosen for comparison). Globally, the produced fibers were less electronegative than the PLA ones. At pH = 7, the IEP values of the hybrids were very close to each other. At this pH however, the fibers with the higher ORMOGLASS content (T5 20-80 fibers) appeared to be the less electronegative.

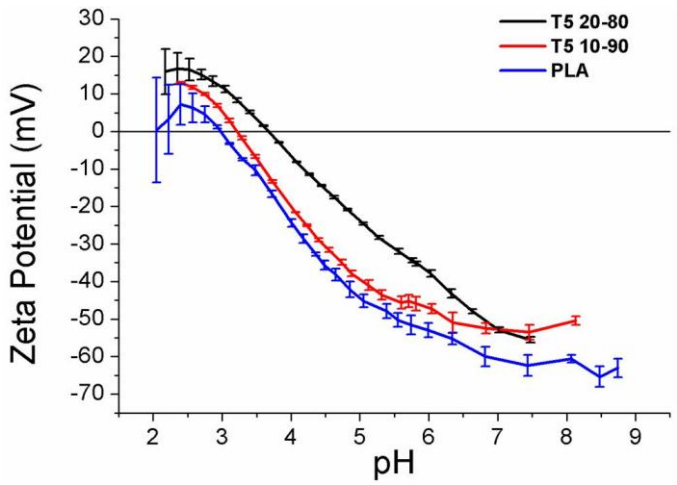

Figure 3-4. pH dependence of the zeta potential of the PLA and hybrid fibers.

Table 3-3. Electrostatic potential (ZP) at pH = 7.4 and isoelectric point (IEP) values of the fibers surface.

	ZP (mV)	IEP
PLA	-61	2.97
T5 10-90	-52	3.21
T5 20-80	-51	3.67

3.3.2.5. Polymer thermal properties

Figure 3-5 displays the DSC thermograms obtained for PLA and hybrid fibers (first and second heating ramps). Neither crystallization peak nor evident melting peak (only very small bump, not considered as significant to conclude anything on melting properties) were observed on the first heating ramp curve. It should be also specified that the sharp peak observed at ~122°C on the curve of the T5 20-80 fibers corresponds to a measurement artifact and should not be taken into consideration for data interpretation (appendix A-4, A.4.3). For the glass transition temperature, results showed that the T_g values were slightly shifted towards lower values when ORMOGLASS was incorporated in the polymeric fibers. The higher was the amount of ORMOGLASS in the fibers, the lower was the T_g. Though, these differences were very slight.

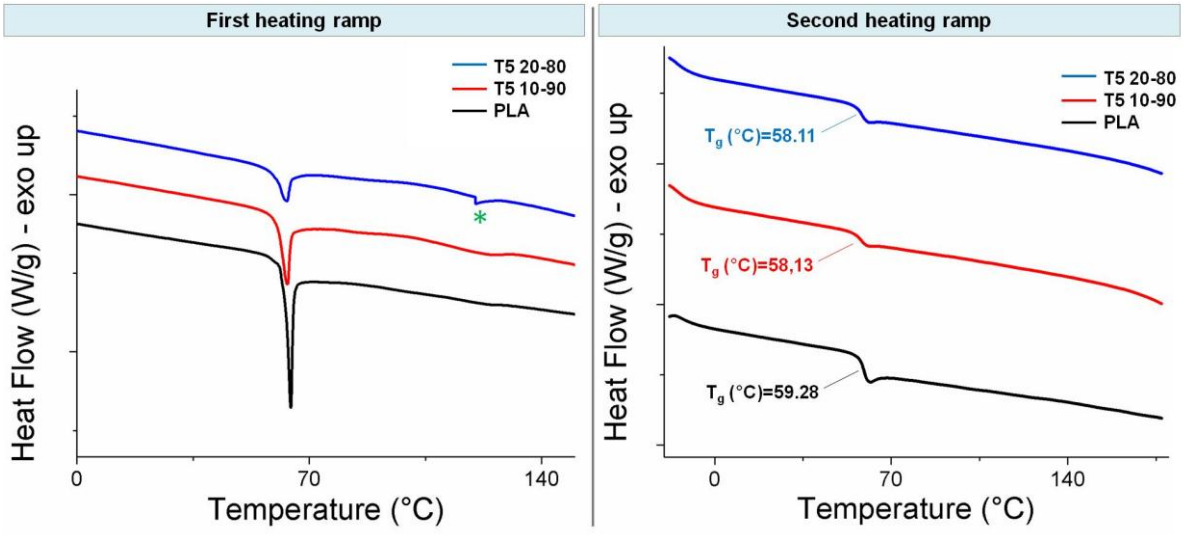

Figure 3-5. Thermograms of PLA and hybrid fibers obtained by DSC (first and second heating ramps, *: measurement artifact).

3.3.2.6. Thermogravimetry

Figure 3-6 shows the TGA thermograms, i.e. the weight and derivative weight (DTA) graphics, associated to the degradation of the fibers. The sample weight revealed that the final inorganic compound remaining after thermal treatment constituted 15.5% of the sample (in mass) for the T5 10-90 fibers and 24.3% for the T5 20-80 ones. However, these values did not represent the exact ORMOGLASS weight of the fibers as two other weight losses attributed to the presence of the ORMOGLASS during the degradation were identified. Considering that, the percentage of ORMOGLASS weight contained in the fibers T5 10-90 was increased to 25,5% and for the T5 20-80 ones to 40,8%. These two weight losses that occurred between 150 and 280°C were related to alkylphosphates; as revealed by the analysis of the vaporized gaseous products (appendix A-4, A.4.4) and based on studies reported in the literature [29,30]. Differences in the degradation temperatures of PLA were also observed for the hybrid fibers (**Table 3-4**). While PLA fibers had degradation temperature (max peak) of 360°C, hybrid fibers exhibited lower

values: 355°C for the T5 10-90 and 341°C for the T5 20-80. The higher was the ORMOGLASS content, the earlier the degradation of PLA occurred.

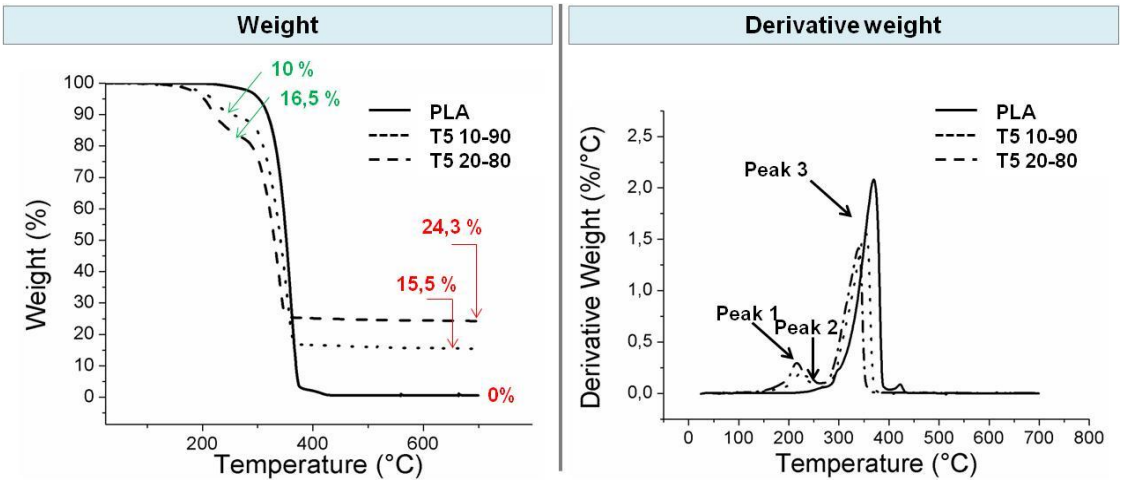

Figure 3-6. TGA curves of the hybrid fibers and their associated derivative curves (DTA). The percentages in red represent the amount of inorganic ORMOGLASS remaining at the end of the assay. The percentages in green correspond to the weight loss associated to the degradation of alkylphosphate molecules (peak 1 and 2) in the hybrid fibers.

Table 3-4. Table summarizing the thermal characteristics of the PLA and hybrid fibers obtained by TGA (*: calculated considering the weight associated to peaks 1 and 2).

	T Peak 1 (°C)	T Peak 2 (°C)	T Peak 3 (°C)	Remaining Weight (%)	Fibers Glass content (%)*
PLA	-	-	360	0	0
10-90	217	245	355	15.5	25.5
20-80	223	245	341	24.3	40.8

3.3.2.7. Tensile tests

As shown in **Figure 3-7,** the hybrid fibers exhibited the higher mechanical properties. Both, Young's Modulus and Yield Strength were improved in comparison to PLA fibers. The higher was the content of the ORMOGLASS, the higher was the Young's modulus. However, Yield strength appeared not to be affected by the content of ORMOGLASS itself. The same values were calculated for both compositions. Moreover, aligned fibers exhibited better mechanical properties than the random ones. Aligned fibers had for example a Young's modulus more than two-fold the one of random ones. Aspect of the samples after the tensile assay can be found in the appendix A-4, A.4.5.

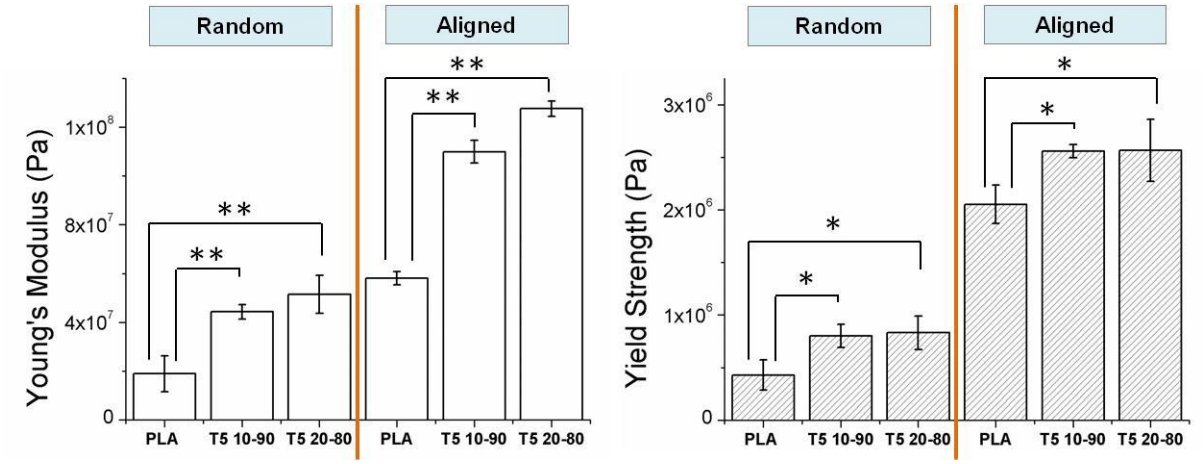

Figure 3-7. Histograms displaying the Young's Modulus and Yield Strength of PLA and hybrid fibers (tensile test measurements - *: statistical difference $p < 0.05$, **: statistical difference $p < 0.002$).

3.3.2.8. Protein adsorption

Qualitative measurements performed with FTIR revealed that BSA adsorbed better on the hybrid fibers than on the PLA ones (**Figure 3-8**). Indeed, after immersion in the protein solution, both hybrids exhibited signals of the amide I and II (chemical groups of the BSA molecule) [31,32], attesting of the presence of BSA on the fibers. To the contrary, these signals were not observed for the polymeric fibers.

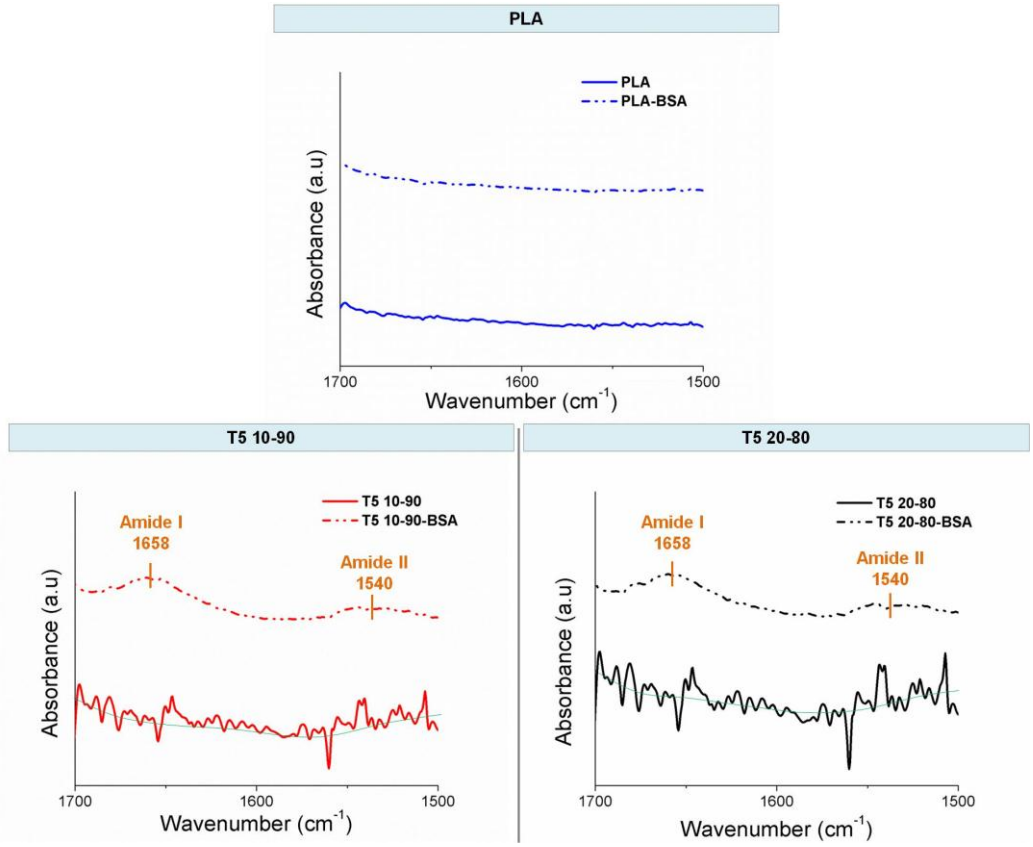

Figure 3-8. FTIR spectra obtained for PLA and hybrid fibers before and after the protein adsorption test.

3.3.2.9. pH measurements

Initially pink, the culture medium turned yellow when T5 20-80 fibers were immersed in it. pH measurements indeed clearly demonstrated that immediately after the fiber immersion, the pH of the medium critically dropped (**Figure 3-9**). For comparison, the measurements were also performed in SBF. The pH drop was even higher in this case. However, because SBF and medium are known to act as buffer of the pH, the measurement was additionally performed in water to evaluate the real pH changes in a solution that does not influence the pH. pH dropped from 7.4 to 2.7 in water. A significant pH decrease would be critical for cells and would lead to cytotoxicity [33]. Therefore, it was necessary to add a buffer in the medium in order to control the pH. Based on the pH curved obtained in medium containing 20 mM of HEPES, it can be seen that the pH remained quasi stable. In fact, according to the pictures, the color of the medium did not change significantly, suggesting that this HEPES concentration was suitable for cellular assays.

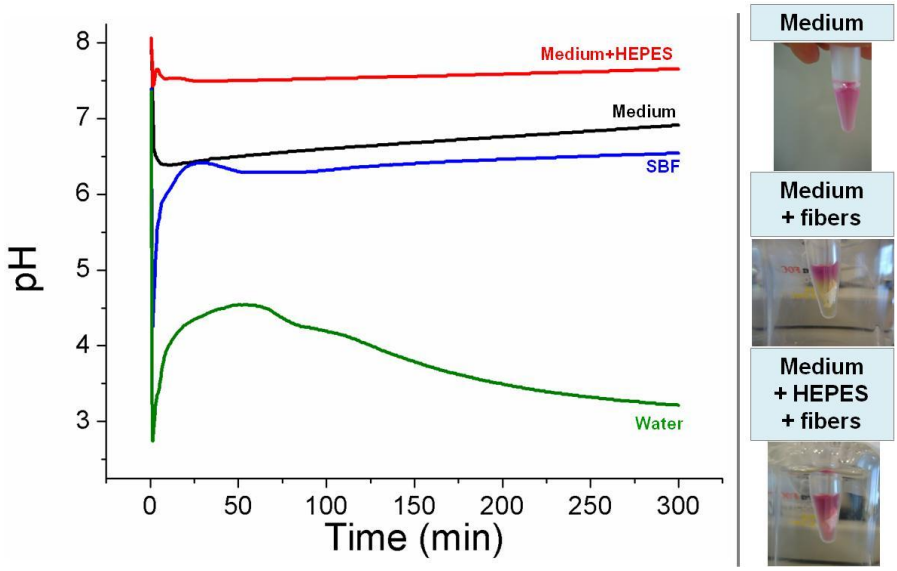

Figure 3-9. Evolution of pH after T5 20-80 fiber immersion in different solutions. Pictures show the color changes observed when fibers were immersed in medium.

3.3.2.10. *In vitro assays*

Pictures obtained thanks to the fluorescent staining and the cell fixation for FESEM imaging are presented in **Figure 3-10** (MSCs) and **Figure 3-11** (EPCs). Additional FESEM pictures can be seen in appendix A-4, A.4.6. After one day, MSCs greatly spread on the hybrids with both compositions. Moreover, on aligned fibers, cells tended to elongate in one direction whereas on random ones, they spread and attached in every direction. Based on FESEM images, it is clear that cells spread following the fiber length and the isotropy of the material. After 10 days, cells covered all the membranes. In comparison to the MSCs, EPCs spread less on the hybrids after one day. Some cells elongated but some were round. Even though some were elongated, their spreading was significantly less important than the

MSCs. This was confirmed by FESEM images on which round cells can be also seen. After 10 days, EPCs proliferated but the proliferation seemed to be less efficient than for the MSCs.

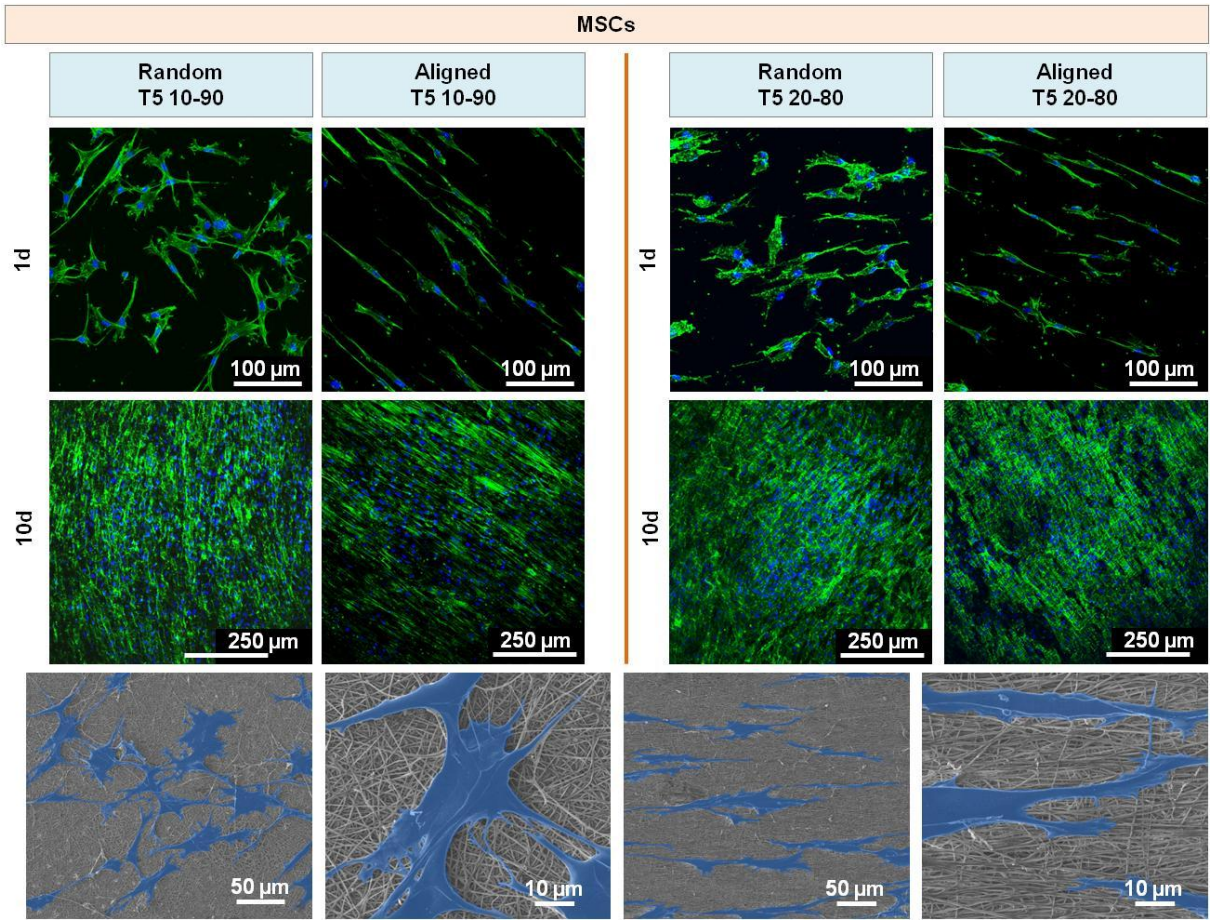

Figure 3-10. Pictures obtained thanks to fluorescent staining (microscope images) and cell fixation (FESEM images) of MSCs after 1d and 10d of culture on hybrid fibers. On the FESEM pictures, cells are artificially colored in blue to better visualize the cells on the material.

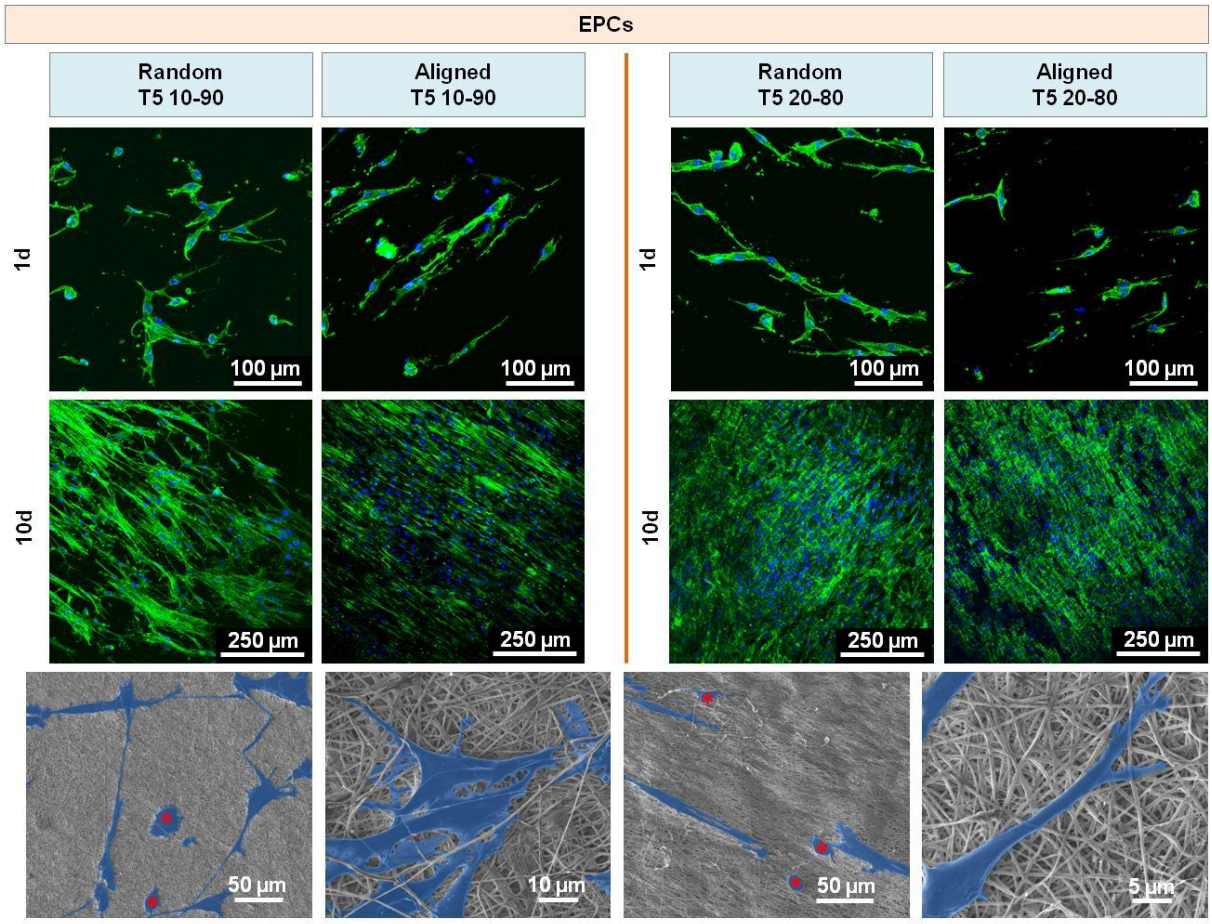

Figure 3-11. Pictures obtained thanks to fluorescent staining (microscope images) and cell fixation (FESEM images) of EPCs after 1d and 10d of culture on hybrid fibers. On the FESEM pictures, cells are artificially colored in blue to better visualize the cells on the material and red stars point the round cells.

In order to quantify cell proliferation, the number of cells present on the hybrids was determined at different time points of cell culture. These results are shown in **Figure 3-12** for both cell types. MSCs proliferated on all membranes. No evident conclusions can be extracted from this assay. In fact, the results were not statistically different between each other, not between samples with different compositions neither between samples with different fibrous arrangement. The only observation that can be done is that the proliferation on fibrous mats efficiently started after three days. For EPCs, proliferation occurred on all samples but very slowly compared to the one of the MSCs. While the cells reached confluence at the end of the assay for the control, EPCs on the fibrous mats seemed to have had difficulties to proliferate. This confirmed the results obtained with fluorescent staining. Finally, it can be seen that EPCs seemed to better proliferate on random fibers than on aligned ones. They even seemed to proliferate a little bit better on the random hybrids than on the random PLA ones. Though, the lack of statistical differences between the samples did not able to certify this comment. Further assays are required.

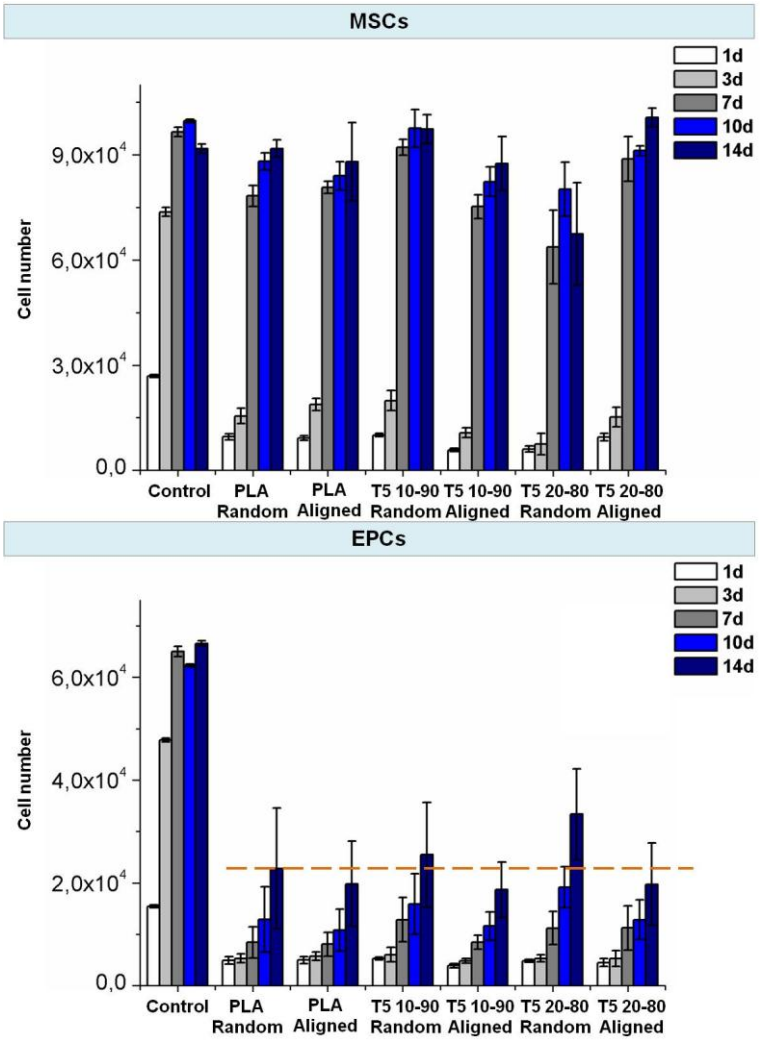

Figure 3-12. Proliferation quantification of MSCs and EPCs cultured on tissue culture plate (control), PLA and hybrid fibers – random and aligned. To facilitate the comparison with the hybrids, the higher number of EPCs on PLA membranes was delimited by an orange dot line (results were not statistically significant).

3.3.2.11. In vivo assay

Figure 3-13 displays the pictures of the slides after HE staining and the associated blood vessel quantification. As seen on **Figure 3-13 a**, a mild inflammatory response was observed for all tested materials. About cellular infiltration, no significant differences were seen between the PLA and the T5 10-90 fibers. In comparison with the other tested materials, the T5 20-80 material showed an increased cell infiltration at 7 and 28 days. Quantification of blood vessels revealed that after one week, all formulations exhibited the same amount of blood vessels per area of material (**Figure 3-13 b**, no statistical differences). After four weeks, the PLA and T5 10-90 fibers materials showed equivalent blood vessel density. However, a significant higher blood vessel density was observed for the T5 20-80 material, in comparison with PLA alone.

CD31 immunostaining confirmed that the hybrid fibers, in particular the T5 20-80 ones, promoted better angiogenesis than the PLA ones. As seen on **Figure 3-14 a**, for the T5 20-80 fibers, blood vessels already formed after one week. For the T5 10-90 however, no significant differences were seen at this time point in comparison to PLA material. But, after 28 days, the density of blood vessels was significantly improved for both formulations of the hybrid fibers. Compared with PLA fibers, the hybrid fibers induced a clear improvement in vascularization **Figure 3-14 b**.

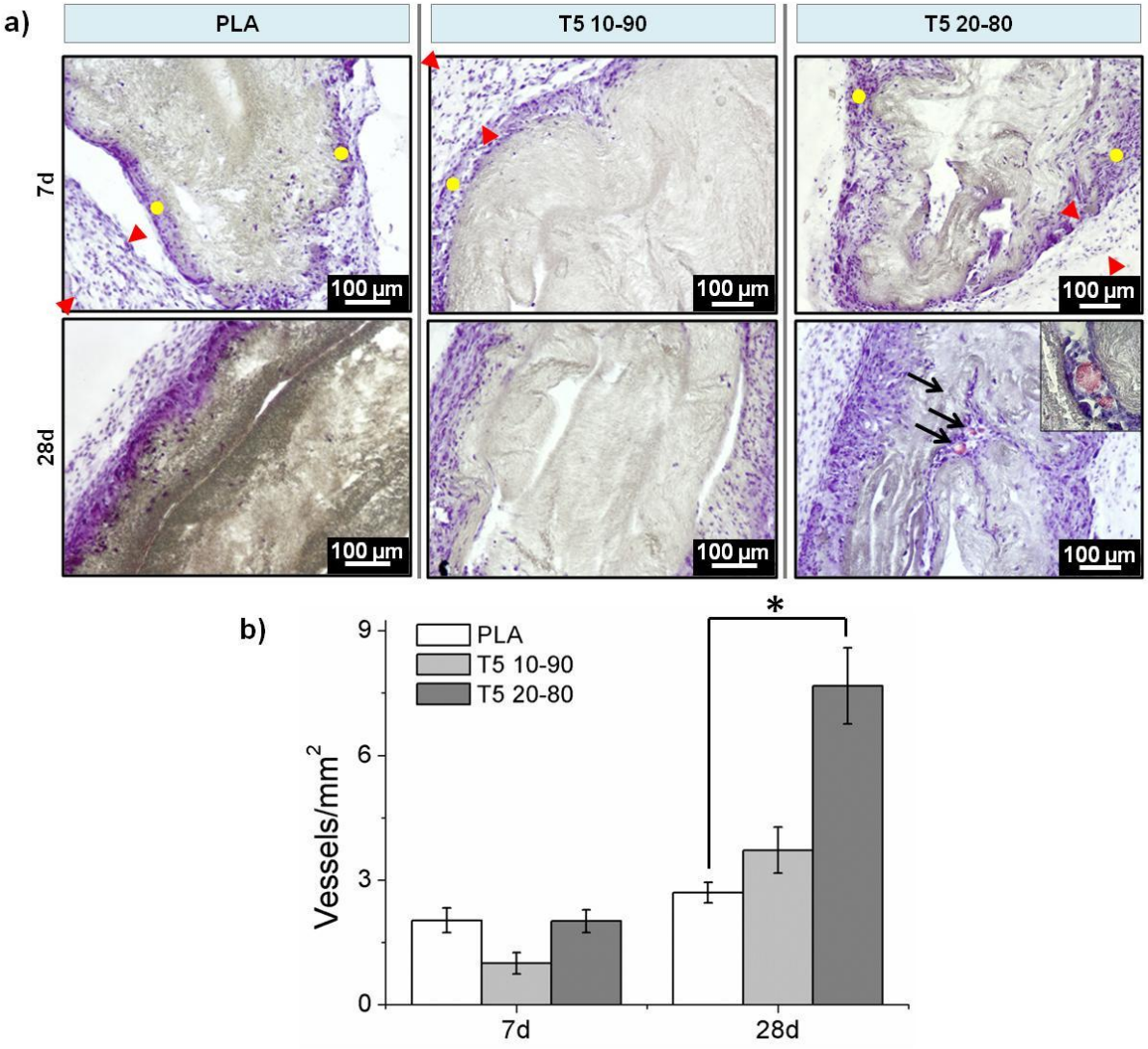

Figure 3-13. a) Histological analysis by HE staining and b) blood vessel density quantification of PLA, T5 10-90 or T5 20-80 membranes, after 7 and 28 days of subcutaneous implantation (n = 6; *: $p < 0.05$). Red arrows denote the presence of fibrous capsule (mild inflammatory response). Yellow dots point the cells penetrating the scaffolds. Black arrows show the presence of blood vessels. Blood vessels were identified by the staining of red blood cells (insert in the picture related to T5 20-80 fibers at 28d).

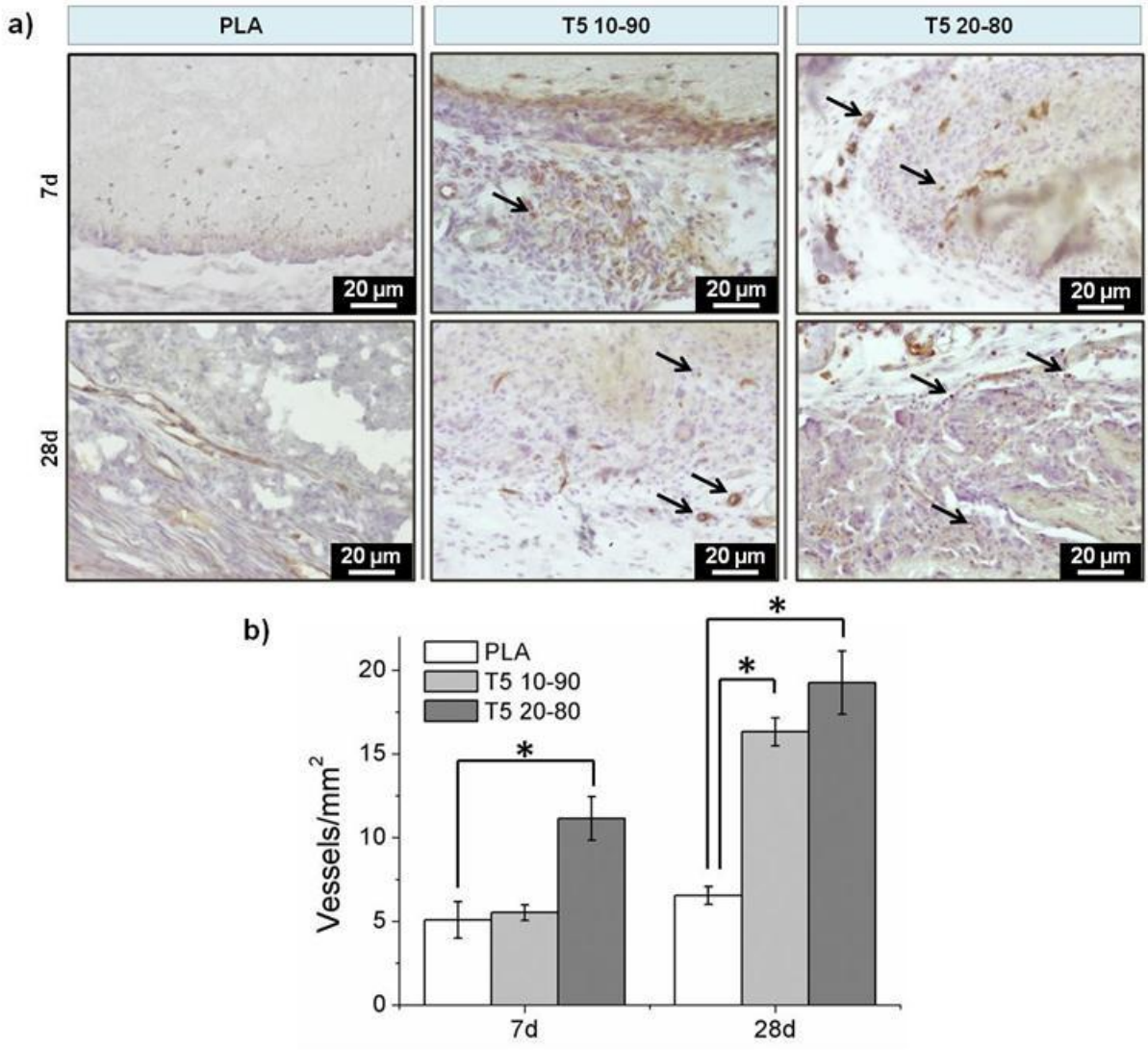

Figure 3-14. a) Histological analysis by CD31 immunostaining and b) blood vessel density quantification of PLA, T5 10-90 or T5 20-80 membranes, after 7 and 28 days of subcutaneous implantation (n = 6; *: $p < 0.05$). Black arrows point the presence of endothelial cells and blood vessels.

3.3.3. Discussion

Titanium-based ORMOGLASS/PLA blends were prepared with the G5 composition and with two different ORMOGLASS contents. The blends were used to produce hybrid fibers by electrospinning (**Figure 3-2**, **Table 3-2**). Fibers without imperfections were efficiently produced as random and aligned mats, suggesting that the processing parameters were well set and that the main problems encountered during the protocol elaboration were successfully overcome (appendix A-4, A.4.7). Moreover, the protocol established to prepare these homogeneous fibers is perfectly reproducible. This work demonstrates that titanium-based ORMOGLASS can be prepared by the sol-gel method and that this sol-gel derived ORMOGLASS can be used to produce hybrid fibers.

To produce fibers by electrospinning, many parameters have to be optimized before obtaining a continuous fiber fabrication. Numerous processing conditions influence indeed the fiber deposition and

the final fiber aspect (the voltage applied or the distance tip-collector for examples [34]). The viscosity of the solution is another crucial factor. Without a proper viscosity (too low or too high), the formation of fibers does not properly occur [35]. It was thus essential to prepare a blend with a suitable viscosity to ensure the fiber deposition. At the beginning of this work, it was not possible to electrospin the prepared blends because the PLA underwent alcoholysis when the ORMOGLASS was added. This occurred even with polymeric solutions having high polymer concentrations. As a result, the blends' viscosity dramatically decreased and they could not be used for the fabrication of fibers. The preparation of the blends was thus improved taking this problem into account. Finally, suitable blends parameters were set (by determining the amount of water to introduce for a suitable hydrolysis of the ORMOGLASS and finding the proper temperature and time of hydrolysis) and electrospinning could have been performed. With the considered blend preparation, even when the addition of the ORMOGLASS gel into the polymeric solution induced a decrease in the viscosity, the viscosity of the solution was in an appropriate viscosity range and remained stable over time (**Figure 3-1**, **Table 3-1**). Hence, the fibers were collected in the same conditions from the beginning to the end of the process. Otherwise, fibers with different features could have been produced during the electrospinning process if the viscosity changed with time (size and morphology). This was the first time that a glass with the G5 composition was processed using the sol-gel method and that PLA-T5 ORMOGLASS blends were used to collect fibers. Before, G5 glass was used only to prepare non-fibrous and non-hybrid composites [8,12].

Wettability of all hybrid fibers produced was improved in comparison to the one of PLA fibers (**Figure 3-3**). This result is in accordance with the other composites prepared with this glass for which the addition of the glass, highly hydrophilic, enhanced the wettability of the polymeric scaffolds [10,12]. In our case, it can be also noticed that aligned fibers had a lower contact angle than the random ones. However, to explain this difference, the way of performing the measurements should be taken into consideration for interpretation. Indeed, unlike for random fibers for which measurements can be performed in any direction, the positioning of aligned fibrous samples (parallel or perpendicular to the camera when taking the pictures) influences the water contact angle evaluation due to the anisotropy of the materials (appendix A-4, A.4.1). A picture taken perpendicularly to the fibers alignment revealed, in fact, a better hydrophilicity than a picture taken in the direction of the fiber length cross section. As aligned and random fibers were prepared from the same blend, the difference in contact angle values can be explained only by the anisotropic effect of the topography.

Differential scanning calorimetry results showed that the thermal properties of the polymer were globally not affected by the incorporation of the ORMOGLASS. In fact, the thermograms of the hybrid fibers associated to the first heating ramp were similar to the one of PLA fibers. Moreover, based on the second heating ramps, no significant differences in the T_g were observed for the PLA and the hybrid fibers (**Figure 3-5**). Concretely, this revealed that the polymer chains motion was quasi not restricted by the presence of the ORMOGLASS and that no strong chemical interactions seemed to have been created between the two phases. This observation is in agreement with what could be expected from a simple

PLA-ORMOGLASS mix prepared by the sol-gel method. Interactions at the nanometric level can be created thanks to the intrinsic advantages of the fabrication method [36], but no strong chemical interactions, able to induce significant modifications in the T_g, were formed.

Apart from that, thermograms obtained from thermogravimetric analysis revealed that when subjected to high temperatures, the physico-chemical properties of the materials differed in terms of degradation. It was seen for example that the degradation temperature of the PLA occurred at lower temperature in the hybrid fibers than for the pure PLA ones (**Figure 3-6**, **Table 3-4**). The ORMOGLASS promoted an earlier PLA degradation which was even more anticipated when the ORMOGLASS content was increased. Under thermal-oxidative conditions (in air), the thermal stability of PLA was thus influenced by the content of the ORMOGLASS. This is in accordance with a study performed by Wen *et al.* who showed that an increase in titanium content in polymeric network decreased the degradation temperature of the polymer [37]. Other researchers also proved that addition of hydrophilic or organic specied (organosilicon compounds) in PLA resulted in a decrease in the decomposition temperature of the polymer [38,39]. Moreover, as observed on the derivative graphic and in comparison to the pure PLA fibers, two novel degradation peaks at lower temperatures appeared for the hybrid fibers. This indicated that compounds related to the glass additionally degraded before the PLA. According to the FTIR vapor phase analysis (performed under nitrogen flow for this kind of set-up), the infrared spectra associated to these two peaks were assigned to alkylphosphates (appendix A-4, A.4.4). The fact that such compounds were identified for the hybrid fibers suggested that not all the phosphate contained in the glass gel had reacted to form the glass network. Carta *et al.* also attributed these two peaks to unreacted alkylphosphate molecules [30]. Knowing that the phosphorous precursor is composed of mono and di-ethyl phosphate species (appendix A-1), the non reaction of these two species would explain that two peaks (i.e. two different compounds) are observed. Liang et *al.* suggested that such free molecules degraded because they are small and thus able to volatilize easily [29]. To enhance the incorporation of the phosphate to the ORMOGLASS, a modification of the hydrolysis parameters of the glass (i.e. catalyst used, hydrolysis rate...) will be needed to control this aspect. Finally, it may also be possible that part of the alkylphoshate molecules detected were not all resulting from the signal of unreacted molecules. Perhaps, some of them resulted from the chain scission of the phosphate groups located at the end of the glass chain network (backbone) [40]. These end groups need, in fact, less energy of activation to volatilize in comparison to phosphate groups well incorporated in the inside of the ORMOGLASS network.

Apart from this consideration, it can be fully understood that the alkylphosphates were part of the ORMOGLASS gel introduced into the polymeric solution and that its weight percentage should be taken into account when determining the weight percent of ORMOGLASS contained in the hybrid fibers. Accordingly, T5 10-90 fibers had a total ORMOGLASS content of 25.5% and the T5 20:80 ones of 40.8% (**Table 3-4**). It is also not excluded that other organic fragments contained in the ORMOGLASS network also degraded during the assay but that they were not accounted in that percentage if they did not appear clearly on the TGA curves (limit of detection for example). On the other hand, the weight percent

of the T5 20-80 fibers was not exactly the double of the T5 10-90 ones, as it would have been expected according to the v:v ratio defined. One explanation for this is the way of preparing the samples. Preparing the blends by v:v ratio introduced some imprecision regarding the quantification of the ORMOGLASS gel added to the polymeric solution. The gel was, in fact, difficult to take with a syringe because of its high viscosity. Some air bubbles might have been aspired in the syringe during the withdrawn of the gel. As the opaque color of the gel did not allow the detection of the bubbles, this might have resulted in a reduction of the measured ORMOGLASS quantity - in comparison to what was targeted. Another approach consisting of preparing the blends by m:m ratio has been also considered but this was not possible because the ORMOGLASS started to dry quickly and it was impossible to measure a stable weight value. Extract the gel using the syringe appeared to be the most suitable method to have a good compromise between gel quantity determination and experimental constraints. In any case, these results demonstrated that hybrid fibers have been successfully produced with two different ORMOGLASS contents. It can be also noticed that the ORMOGLASS contributed greatly to the mass of the final scaffold.

Regarding the mechanical properties of the whole constructs, tensile tests demonstrated that the Young's Modulus and the Yield strength of the hybrid fibers exhibited higher values than the PLA ones (**Figure 3-7**). This attested that tougher materials were produced. The mechanical behaviors of hybrids closely depend on the nature of the inorganic phase introduced into the polymeric matrix. As reported by Wen *et al.* for example [37], hybrids produced by the incorporation of inorganic phases containing metal alkoxides greatly improved the mechanical features of the pure polymeric material. They also showed that these mechanical properties can be tailored by modifying the content of the inorganic glass. Here, similar results were observed. Based on these statements and the fact that no increase in crystallinity was detected by DSC, it is assumed that the use of alkoxide precursors and sol-gel method is the main reason for the good mechanical properties measured for the hybrids. As a more general observation, it can be seen that aligned fibers exhibited the higher mechanical properties. This behavior is commonly observed when tensile tests are performed in parallel with the principal axis of the fiber alignment [41,42].

Protein adsorption on the surface of biomaterials is very important as this phenomenon constitutes the really first interactions that the material establishes with the biological fluid, and contributes to an efficient cell adhesion [15,43]. Bovine serum albumin (BSA) was shown to adhere better on the surface of the hybrid fibers than on the PLA ones (**Figure 3-8**). Several explanations can be given for that. The first one is the composition of the ORMOGLASS that contained a high amount of calcium and albumin is known as the major- calcium binding protein present in tissues and fluids [44]. Hybrid fibers may thus have a significant amount of binding sites available for the protein. In fact, for pure PLA substrates, a previous surface activation or functionalization is usually required to promote albumin adsorption [43]. Another reason may be the negative charge of the hybrid fiber surface. According to Klinger *et al.*, the electrostatic interactions between albumin and titanium surfaces are the main mechanism involved in the adsorption of the protein. BSA is a negatively charged protein in the range of pH in which the assay is

conducted (appendix A-4, A.4.8). As PLA fibers showed a generally more electronegative potential than the hybrid fibers, BSA had less affinity with the PLA fibers than with the hybrids (**Figure 3-4**). This may be also emphasized by the pH of the solution in which the assay is performed. As revealed by the pH measurements, when hybrid fibers are immersed in diverse solutions (medium, SBF, water), the pH of the solutions decreased (**Figure 3-9**). The complementary pH measurements reported in the appendix A-4 confirmed that the pH of the solution in which the albumin adsorption assay is performed was lower for the hybrids than for the PLA. This means that the electrostatic potential of the fibers was even more electropositive than the one of the PLA fibers in the conditions of the test. As a consequence, ZP and pH intimately affected together the adsorption efficiency. Zhu *et al.* and Krajewski *et al.* already described this ZP-pH dependence in the literature [45,46]. Finally, the lasts two factors that may have favored the adhesion of the BSA are the wettability and the reactive groups present at the fiber surface [43,47]. The wettability of the PLA fibers being lower than the one of the hybrids (**Figure 3-3**), this may have prevented the BSA to bind to the surface. It is also hypothesized that suitable reactive groups such as hydroxyl might be present at the fiber surface, providing additional binding-sites for the protein.

Biological response is of paramount importance in the success of scaffold implantation. Scaffolds are indeed aimed to act as a template for cell adhesion, proliferation, differentiation and migration. They should thus provide a suitable environment to the cells in order to direct their activity thanks to the materials features (for example, architecture, chemical composition, wettability) [48]. When cultured on the hybrid fibers for 1 day, MSCs attached and greatly spread on the substrate for both fibers compositions (**Figure 3-10**). EPCs also adhere on the fibers but their spreading appeared to be less efficient. After 10 days, MSCs significantly proliferated on all fiber types while EPCs seemed to have difficulties to proliferate on the T5 10-90 fibers especially (**Figure 3-11**). Quantification of the cell proliferation confirmed this tendency (**Figure 3-12**). Based on these results, hybrid fibers seemed to be a suitable substrate to culture MSCs. For EPCs however, the cellular response was more limited. As a general observation, the lower EPCs proliferation is observed not only on the hybrids but also on the pure polymeric mats. It is thus hypothesized that the fibrous structure of this scaffold might not be the most suitable topography for these cells [49,50]. It can be however specified that EPCs tent to proliferate better on the hybrid fibers than on the polymeric ones and that they proliferated slightly better on the T5 20-80 fibers than on the T5 10-90 ones. This suggested that the amount of ORMOGLASS contained in the fibers seemed to play a role in the proliferation of EPCs.

It can be additionally noticed that cells followed fibers distribution. On random fibers, cells spread in any direction whereas on aligned fibers, they aligned along the unique direction of the fibers. This is a common behavior well reported in the literature that shows how cells modulate their cytoskeleton shape depending on the substrate structure and how the cell-material interactions are influenced by the design of the material [51]. On the other hand, electrospun scaffolds are often described as suitable templates for cell infiltration due to their high porosity and high surface area [52]. In this *in vitro* study, cells did not seem to penetrate the scaffold according to the FESEM images. This may be

explained by the chosen cell types, as well as the porosity (small pores) of the produced scaffolds [53]. Even with less tortuosity (aligned fibers), cells did not penetrate efficiently into the membranes. Such behaviors have been also reported in *in vitro* assays with EPCs by Mobarakeh *et al*. who suggested that the small pore size of nanofibrous scaffolds was the reason of this non-infiltration [54]. Several methods can be used to promote cell penetration on electrospun mats, such as selective leaching or combination of eletrospraying with coelectrospinning [55,56]. For the produced hybrid fibers, an improvement regarding the cell infiltration would be required if cells are aimed to be cultured *in vitro* on the scaffolds and that infiltration is required for the application targeted [54]. However, when implanted in rats, cells surprisingly infiltrated the T5 20-80 fibers. Boland *et al.* also highlighted the lack of infiltration in *in vitro* conditions but the good cell migration after *in vivo* implantation [57]. It is hypothesized that the external forces applied by the animal activity/motion promoted the migration of the cells towards the center of the material and helped the cells to push individual fibers from their path during migration. In fact, assays reported in the previous chapter also demonstrated that cells infiltrated well into fibrous templates in *in vivo* conditions. Though, it is clear that the infiltration in fibrous mats was lower than in other materials having bigger pore size and interconnectivity [58]. The more interesting aspect from this *in vivo* test is the good vascularization potential of the hybrid fibers (**Figure 3-13**, **Figure 3-14**). Compared with PLA fibers, the efficiency of T5 10-90 and 20-80 fibers after four weeks was significantly good. Even though the T5 10-90 fibers did not seem to improve angiogenesis after one week, a great enhancement in blood vessel density was achieved between the first week and the end of the assay. This suggested that these fibers may be also a promising scaffold but that they may require more time than the T5 20-80 ones to induce angiogenesis. This may be attributed to the difference in ORMOGLASS content. What is sure is that the hybrid fibers possess a clear potential to induce vascularization. These encouraging results may be explained by the good hydrophilicity of these ORMOGLASS-containing scaffolds and the presence of the bioactive ORMOGLASS itself which has been demonstrated to have a chemical composition that enables cells chemotaxis and enhancement in cellular responses, partly due to its calcium release [9,59]. These hybrid fibers seem thus to be promising according to their bioactivity and biocompatibility. Nevertheless, further investigations such as differentiation tests are required to confirm the potential of these biomimicking materials for bone tissue regeneration.

Despite the additional biological assays that are required, the production of these titanium-based fibers represents a great progress for the development of artificial bioactive matrices. Indeed, up to date, most of the designed biomaterials focused on silica-based glasses. This is especially explained by the higher difficult preparation of phosphate-based glasses containing titanium in comparison to silicon-based ones [60]. Hence, only few reports concerning this system are found in the literature. Moreover, most of them involve the conventional melt-quenching method [61–64]. To the best of our knowledge, only Pickup *et al.* used the sol-gel method to prepare titanium-based glasses [65]. But, the drawback of their approach is that the preparation of their glass requires several weeks. In fact, ageing and drying were performed during 10 weeks at temperatures between 60°C and 350°C. For the sol-gel derived glass

described in this chapter, only three days are necessary to obtain the glass and low temperatures are involved in the process (4°C and ambient temperature). This enabled us also to conserve the organic fragments present in the glass and to work with ORMOGLASSES. On the other hand, titanium-based glasses have been rarely used to prepare composite materials and were rather investigated as isolated scaffolds [66,67]. Composite materials were mainly introduced by Navarro and coworkers [7,8,12] but another group started recently to work also on these materials [62]. However, as already mentioned, their glasses were prepared by the melt-quenching method. This is thus the first time that sol-gel derived glasses based on titanium were used to design composites (more precisely hybrids). Moreover, in the usual composites, the glasses were used as fillers for polymeric matrices (dispersion of microparticles) [7,12,62]. In our new material, the glass is used in the form of a sol, what enabled us to prepare a nanometric suspension of glass and to obtain a hybrid blend suitable for electrospinning. This is another advantage of the described material: the processing of the hybrid blend. Based on our literature review, no hybrid fibers (not even composite fibers) based on titanium glasses seemed to have been prepared up to date. Therefore, considering all these advances, the prepared fibers constitute a real novelty regarding the other titanium-based glasses and composite materials. Finally, the preparation of these fibers demonstrated that not only silicon-based glasses (see chapter 2) but also titanium-based ones could be prepared as ORMOGLASS and be used to produce hybrids. In particular, it confirmed that polymer-ORMOGLASS blends are suitable for electrospinning, enabling thus the production of a novel family of materials for the field of tissue engineering.

3.3.4. Conclusion

PLA-titanium based ORMOGLASS composites have been produced as fibrous mats. For the first time, the bioactive glass has been successfully obtained by applying the sol-gel method and has been efficiently used to prepare an electrospinnable polymer/glass blend. Electrospinning parameters (blend viscosity, voltage intensity, dispensing rate, distance tip-collector) were correctly set for this novel hybrid system and a continuous fiber deposition was achieved. Fibers, collected as random and aligned structures with two different glass contents, exhibited regular shapes, improved mechanical properties and good hydrophilicity. Globally, the addition of the ORMOGLASS into the polymeric matrix resulted in the enhancement of the physico-chemical properties of the pure polymeric scaffolds. On the other hand, the fibers induced promising biological responses. In particular, *in vivo* implantation demonstrated the potential of the hybrids to induce vascularization. Although further assays are required to assess more precisely the potential of these novel fibers (osteogenesis and angiogenesis promotion efficiency), this study represents a valuable step forward for the fabrication of biomimicking materials as potential functional cell-instructive scaffolds for vascularized bone regeneration.

3.4. *In vitro* degradation of the fibers

The second part of the chapter is dedicated to the assessment of the fiber degradation in simulated physiological conditions. The changes occurring during the material incubation were assessed in terms of morphology, topography, composition and dissolution profile. The aim of this study was to understand the *in vitro* degradation mechanisms of the novel fibers and to evaluate the duration for which the fibrous templates could serve as supports for cellular activity once implanted.

3.4.1. Materials and Methods

3.4.1.1. Incubation conditions

This *in vitro* assay was performed with T5 10-90 and T5 20-80 random fibers. 5 mm x 30 mm fiber strips were cut from the electrospun fibrous layer, rinsed during one hour in water and immersed in SBF at 37°C up to 28 days. Each fiber strip was introduced in an individual flask containing 30 mL c-SBF (conventional SBF [68]). The SBF preparation and determination of SBF quantity necessary for the study were selected according to the conditions reported by Kokubo *et al.* [69]. SBF was changed every 2 days. Fibers were removed from the SBF at different time points (1h, 1d, 3d, 7d, 21d, 28d), rinsed three times with ultra pure water and dried under vacuum for at least 3 days before characterization.

3.4.1.2. Fiber morphological characterization

Pieces were cut from the dried incubated fibrous layer and fixed on the metallic support used for SEM to assess the fiber morphology (Hitachi S-5500). Samples were coated with a thin layer of carbon in order to enhance the quality of the pictures. Pictures were taken at a 5 kV voltage and a height distance of 5 mm. FESEM (same device than previously) was also used to obtain a better resolution and achieve pictures with more details.

3.4.1.3. Fiber topography

To assess the topographical changes occurring at the fiber surface, atomic force microscopy (AFM) was used. Measurements were operated using an AFM MultiMode8, Bruker machine and the PeakForce QNM method in air under ambient conditions. Image processing and data analysis were performed with the Nanoscope Analysis software v1.2.

3.4.1.4. Chemical changes

Chemical composition of the fibers was assessed by Energy Dispersive XRay Spectroscopy (EDS, Quanta 200 XTE, FEI Co.) This technique enables the determination of the fiber composition by determining the relative molar ratio of the different element with regards to the other compounds

(percentage). Samples already used for FESEM observations were also used to perform the element quantification. Measurements were performed at the different time points at 3 arbitrarily selected locations on the samples.

Fourier Transform Infrared Spectroscopy in Attenuated Total Reflectance mode (FTIR-ATR, Nicolet 8700, Thermo Scientific) was also used to evaluate the chemical changes. No preliminary treatments were applied to the samples before performing these measurements.

3.4.1.5. Calcium dissolution and pH measurements

Given the importance that calcium ions seem to play regarding cellular activity, dissolution tests were carried out to monitor the release profile of the calcium contained in the hybrid fibers during their degradation. Pieces of 1 cm^2 were cut from the electrospun fibrous layer. Four replicates were prepared for each fiber type (T5 10-90 and T5 20-80, random). Each sample was placed in a well of a 24 well-culture plate. Deionized water was added to each well (1mL) and parafilm was used to seal properly the plate in order to avoid water evaporation. Following this, the plate was placed in an incubator at 37°C. After each time point (5 min, 1h, 1d, 2d, 3d, 6d, 7d, 8d, 9d, 10d, 13, 14d), the water was removed and 1 mL was again added to the wells. Calcium concentrations were measured using a Crison Ca^{2+} selective electrode and an Ag/AgCl reference electrode. pH was additionally measured using a Crison GLP22+ pH-meter and a Crison pH microelectrode. Initially, this assay was performed in SBF. However, it has been noticed that the buffering effect of SBF partially masked the real observation of the dissolution behavior of the material. Therefore, instead of SBF, deionized water was preferred to perform this assay in order to determine the real amount of calcium released by the material. The results with SBF are reported as complementary information in appendix A-4, A.4.9. The calcium concentration is reported as a cumulative value.

3.4.1.6. Polymer thermal properties

Differential Scanning Calorimetry (DSC) analysis was performed to check if changes in the organic phase occurred during the degradation assay. A DSC Q2000 TA device and 1.20 mg samples confined in hermetic aluminum pans were used. Samples (fibers not incubated and incubated at 1h, 3d, 7d, 21d) were heated at a rate of 10°C/min starting from -20°C up to 180°C. The same heating ramp was again applied to the samples after its cooling. Nitrogen was used as a purge gas.

Melting and crystallization properties were evaluated by analyzing the curve of the first heating ramp of the DSC assays. In this part of the study, the small bump associated to the melting peak of the hybrid fibers (not considered as significant in the previous part of the chapter) is particularly taken into account because it has been noticed that it changed during the degradation test. About the crystallization peak, even though not observed on the DSC curves previously shown, it is also taken into account here in order to verify if the degradation test influenced the crystallization behavior of the polymer over time.

The crystallinity of composite materials is given by the following equation [70,71]:

$$\chi(\%) = \frac{\Delta Hm - \Delta Hc}{\Delta Hm^{\circ}\,(1 - Wg)}$$

Where χ is the percentage of crystallinity, $\mathbf{\Delta}H_m$ is the heat of fusion, $\mathbf{\Delta}H_c$ is the heat of the cold crystallization, $\mathbf{\Delta}H_m^{\circ}$ the heat of fusion of a 100% PLA crystalline material (93.1 $J.g^{-1}$ [72]) and W_g the weight percent of glass contained in the hybrids. For this assay, the exact W_g is not known because the materials degraded over time. It is thus not possible to calculate precisely the crystallinity of each sample. However, even if an accurate value of crystallinity cannot be obtained, the heat of fusion and cold crystallization (if observed) can be determined and be used to discuss changes in the theoretical crystallinity of the fibers; even without knowing precisely the W_g values (see section **3.4.2.5** and **3.4.3**). This is possible thanks to mathematical considerations made in the equation above.

The glass transition temperature (T_g) was determined considering the second heating cycle and using the inflexion point method. The TA Universal Analysis software v4.7A was used to analyze all DSC curves.

3.4.1.7. Determination of glass loss

Incubated fibers were subjected to thermal degradation in order to compare the quantity of inorganic phase contained in the fibers before and after incubation. Small quantities of samples were placed in aluminum pans and heated from room temperature up to 700°C at a heating rate of 10°C/min in air. Thermograms were analyzed with the TA Universal Analysis software v4.7A. The weight percent remaining at the end of the thermal treatment corresponds to the amount of inorganic compound present in the studied material. However, if the inorganic material is not completely inorganic but contained some organic fragments (as the ORMOGLASS), the remaining weight does not exactly correspond to the amount of glass contained in the fibers. If detected by TGA, the weight loss due to the organic fragments of the ORMOGLASS should be also considered to quantify the glass content. Finally, the content of the glass is approximated by adding the remaining weight loss of the inorganic phase and the weight loss associated to the organic fragments of the ORMOGLASS.

3.4.1.8. Glass distribution in the fibers

TEM observations were also performed to assess the dispersion of the glass in the polymeric matrix before and after incubation (see appendix B-12). A few fibers were extracted from the layers and deposited on a carbon coated copper grid for analysis. A JEOL JEM 1200 EX instrument was used and the accelerate voltage was set at 120 kV.

3.4.2. Results

3.4.2.1. Fiber morphology

Figure 3-15 shows the morphology of the fibers as produced by electrospinning and the evolution of their aspect over the duration of the assay (1d, 7d and 21d of immersion in SBF). For PLA, no significant differences were observed except a small increase in roughness that appeared with time (wrinkles). For the hybrid fibers, more drastic differences occurred rapidly. Fibers collapsed and subsequently opened following the fibers length in two different ways. The first one looked like an instantaneous crack that revealed a cavity (**Figure 3-15, a**). The other seemed to be rather due to a slow process that induced the opening of the fibers (**Figure 3-15, b**). These two phenomena are described in more details in section **3.4.3**. After 21 days, hybrid fibers additionally showed a non smooth surface which seemed more obvious than for the PLA ones. This is especially well observed for the fibers that possessed the higher ORMOGLASS ratio (**Figure 3-15, c**).

Typical fiber morphological changes are presented with better resolution in **Figure 3-16** (representative images of the diverse "defects" that could have been seen). The appearance of wrinkles on PLA is clearly observed, as well as the surface modifications that occurred for the hybrid fibers. Images attested that fibers collapsed and underwent considerable surface changes. Finally, these pictures showed that PLA fibers maintained their cylindrical morphology during the immersion period while hybrid fibers lost their round fiber shape and were exposed to a faster degradation.

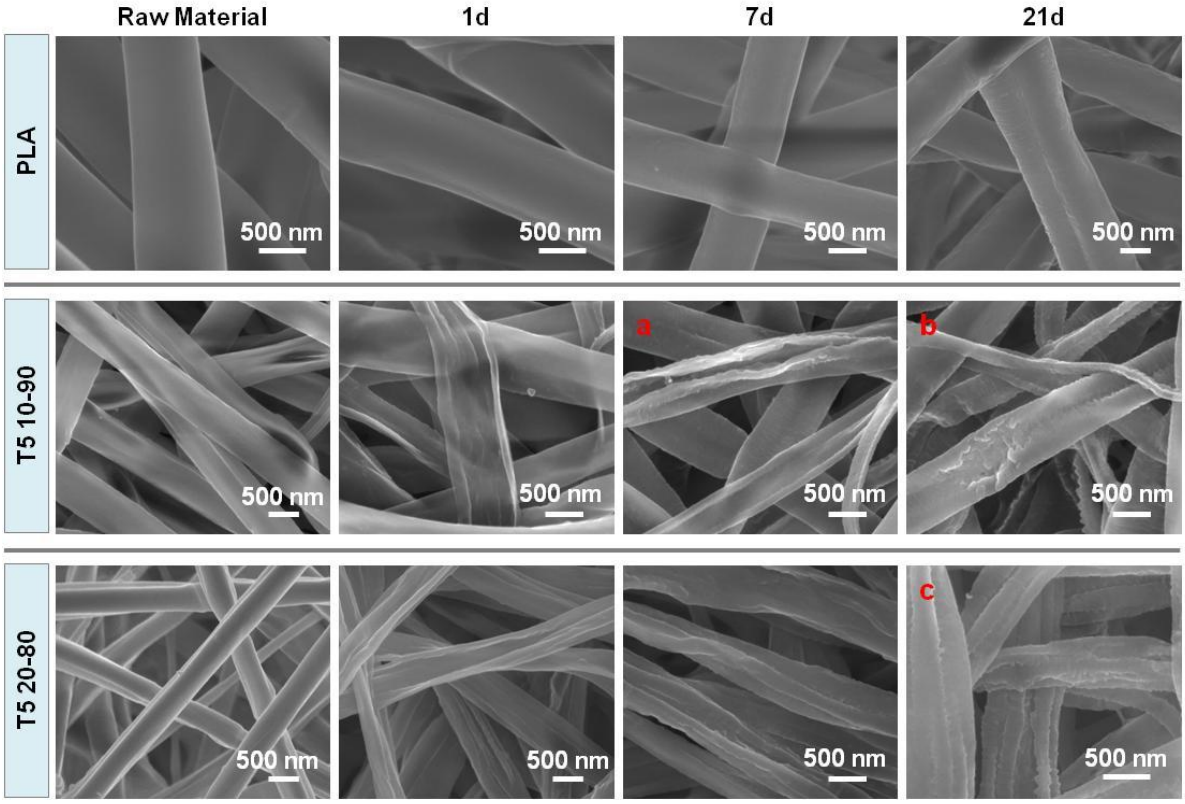

Figure 3-15. Morphology of PLA and hybrid fibers before and during the degradation assay (FESEM images).

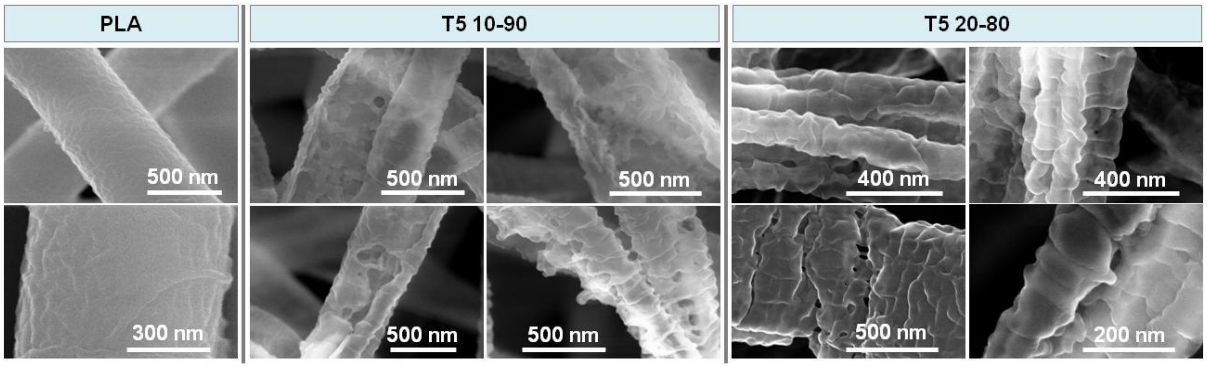

Figure 3-16. Aspect of typical defects observed on the PLA and hybrid fibers after 28d of incubation in SBF.

3.4.2.2. Fiber topography

During the degradation period, hybrid fiber topography considerably changed (**Figure 3-17**). Additional pictures can be found in the appendix A-4, A.4.10. After one hour immersion in SBF, hybrid fibers exhibited a uniform topography with a difference in height of around 30 nm. At 1 day however, the collapsing of the fibers was already clearly seen and more consequent changes in height profile were observed (120 nm height deflection). This suggested that the surface of the fibers was rather smooth at the beginning of the assay in comparison with the later time points. At 7 days, the cracks observed on FESEM pictures were also detected by the AFM. Finally, at 21 days, the surface of the fibers had significantly changed, as noticed with the profile undulations between 0 and 500 nm width. The change in height between 500 nm and 700 nm width was rather attributed to the part of the fibers that collapsed (see **Figure 3-17**).

The last behavior identified by AFM is the slow opening of the fibers. On the height profile, it can be seen how the slow cracking of the fibers tends to lower the height value between the two fiber walls.

Generally, AFM images are in accordance with the degradation behaviors identified with the FESEM pictures and evaluation of the topographical changes through the height profile determination confirmed these modifications.

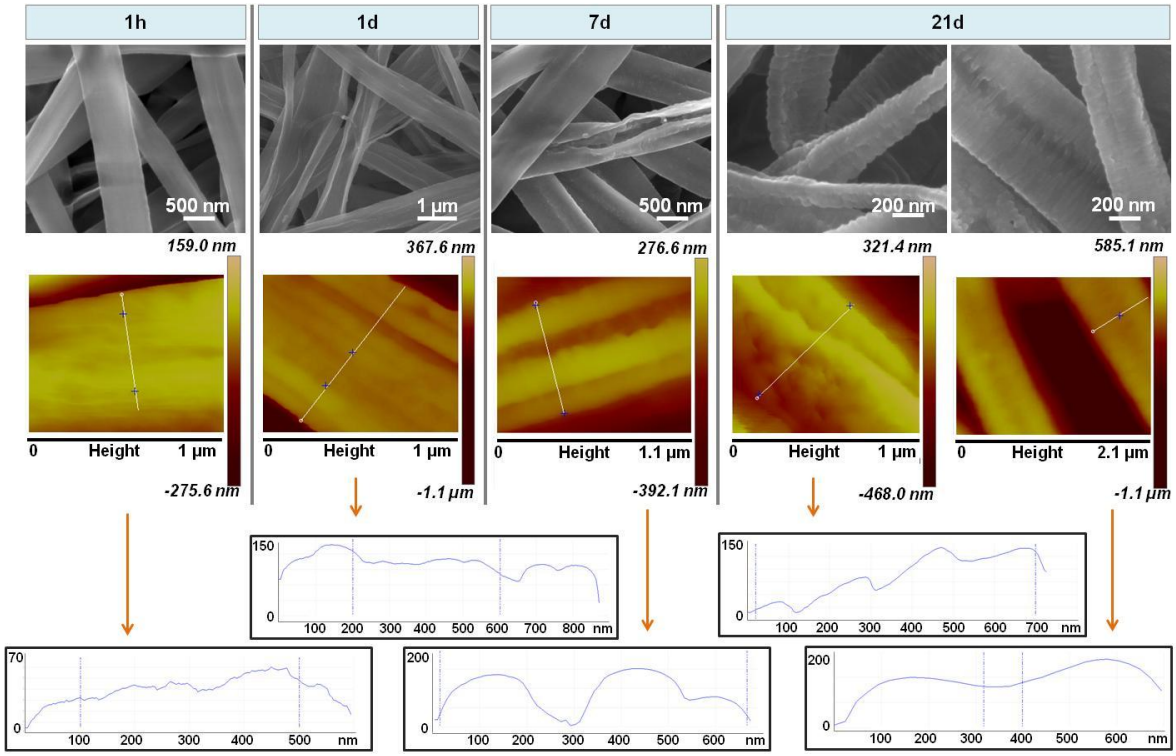

Figure 3-17. Correlation between the fiber morphology assessed by FESEM and AFM, and topographical changes (imaging and height profiles) observed for the hybrid fibers after 1h, 1d, 7d and 21d in SBF.

3.4.2.3. Chemical changes

Fibers were successfully produced with the targeted composition (G5). Fibers contained thus initially a high amount of phosphate and calcium, and a low amount of sodium and titanium **(Figure 3-18)**. EDS measurements on the fibers showed that after one hour in SBF, huge changes in ORMOGLASS composition had already occurred. The quantity of calcium dropped dramatically. The phosphate amount also decreased but in a more moderated manner. However, phosphate continued to decrease up to the first day, while the calcium percentage increased slightly. As a consequence of these changes, the titanium content increased. For the sodium, it is believed that it was already released at the early stage of incubation. For this reason, no significant changes were observed for the sodium (almost not detected by the device). After 3 days, the molar composition of the fibers remained stable up to the end of the assay but the initial G5 composition was not maintained. The same modifications were observed for the T5 10-90 and T5 20-80 fibers.

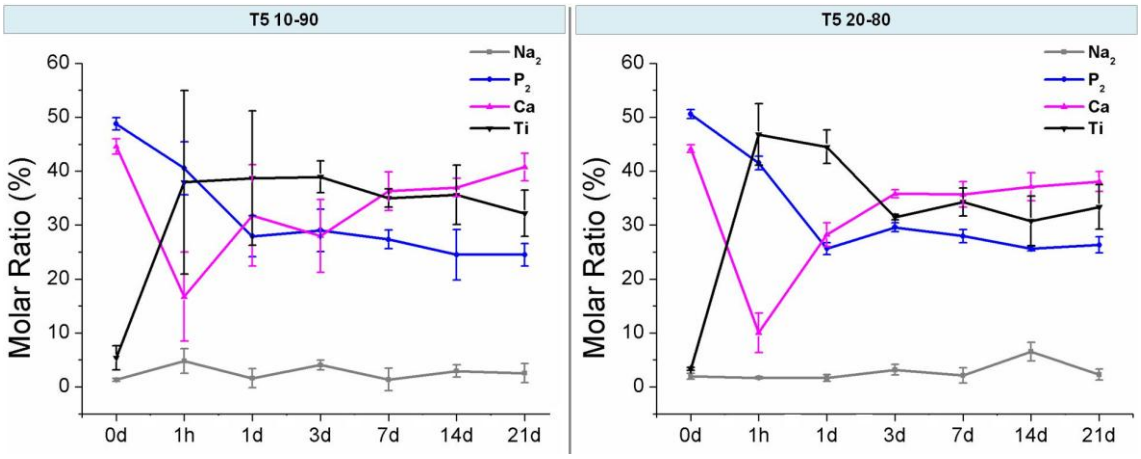

Figure 3-18. Evolution of the fiber composition during the incubation period (EDS measurements).

Figure 3-19 displays the infrared spectra collected on the fibers before and after degradation. The infrared spectra of the fibers obtained as produced by electrospinning exhibited the typical peaks of PLA and additional signals due to the presence of phosphate complexes: P=O stretching at 1223 cm^{-1} [73–76], PO_4^{3-} [7,76] and P-O stretch [77] at 1047 cm^{-1}, PO_4^{3-} 958 cm^{-1} [76,78], P-O-P asymmetric stretching at 910 cm^{-1} [74,79], P-O-P symmetric stretching 820 and 802 cm^{-1} [79], harmonics of bending O-P-O and O=P-O at 580-450 cm^{-1} [74,76,80]. Fibers with both ORMOGLASS contents showed similar infrared spectra. Though, the intensity of phosphate peaks of the fibers prepared with a 20-80 ratio appeared to be stronger than the ones of the T5 10-90 fibers, which is logical as they possessed a higher amount of glass. After one hour, most of the peaks assigned to phosphate disappeared. Only a small shoulder can be noticed in the 580-450 wavenumber region. No significant changes were observed afterwards and the spectra became similar to the one of the pure PLA fibers.

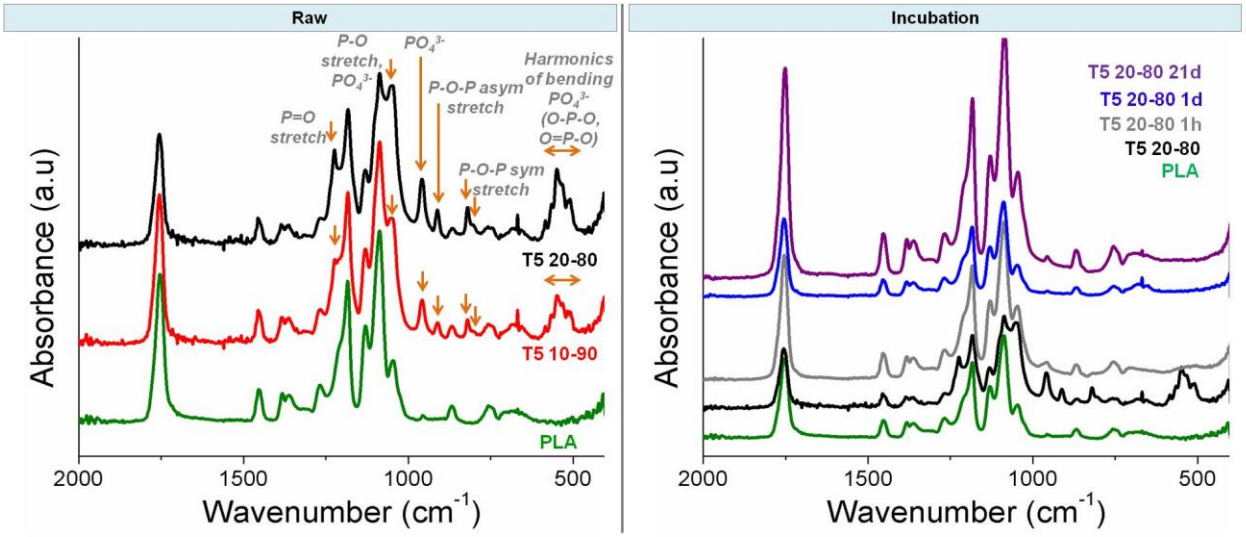

Figure 3-19. FTIR spectra of the PLA and hybrid fibers as produced by electrospinning (raw) and during the degradation test (PLA spectra is added for comparison).

3.4.2.4. Calcium dissolution and pH measurements

The dissolution profiles of calcium and the associated pH measurements are displayed in **Figure 3-20**. The main changes occurred during the first two days. A burst release of calcium was particularly observed immediately after the material immersion. Then, during these two days, calcium was released in a less drastic manner. After this time, the material did not seem to release calcium, or in a very low concentration. Regarding the pH of the extracts, it can be noticed that it increased over time. It can be moreover noticed that the T5 20-80 fibers released a higher amount of calcium than the T5 10-90 fibers.

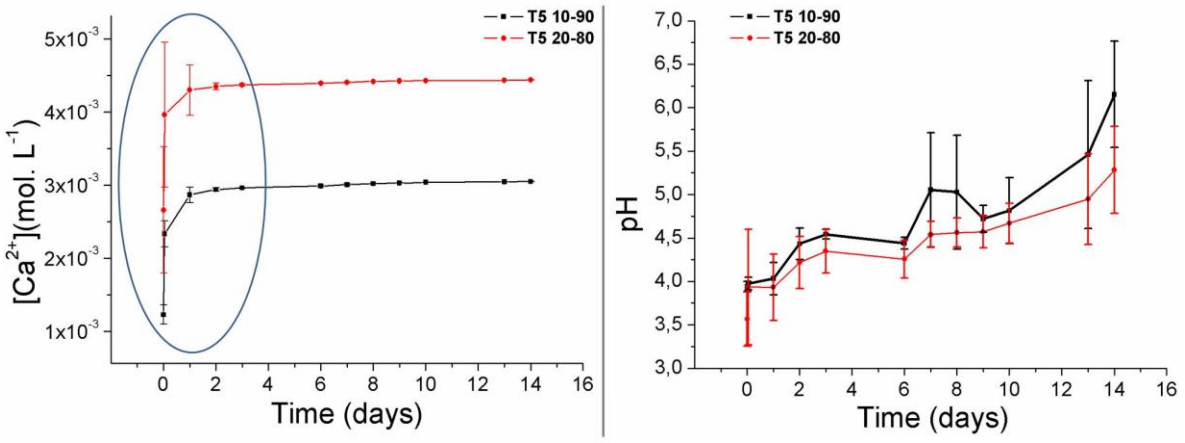

Figure 3-20. Calcium dissolution profiles of the hybrid fibers and pH measurements. Blue circles denote the main changes occurring in the solution.

3.4.2.5. Polymer thermal properties

DSC assay was performed to determine whether changes in the polymer occurred along with the material degradation. DSC curves obtained for the hybrid fibers before and after incubation period are displayed in **Figure 3-21**. **Table 3-5** summarizes the evolution of the heat of fusion ($\mathbf{\Delta}H_m$ – melting peak integration) and T_g during the assay. Analysis of curves showed that peaks (i.e. bumps) associated with melting processes slightly increased in intensity with incubation time. Values of the $\mathbf{\Delta}H_m$ confirmed these observations. No peak of crystallization was observed for any of the curves. For our hybrids, $\mathbf{\Delta}H_c$ is thus not involved in the calculation of crystallinity (see section **3.4.1.6**). Only $\mathbf{\Delta}H_m$ and W_g variables should be considered when evaluating fiber crystallinity. Determination of the T_g did not reveal any particular trends. The incubation did not seem to affect the glass transition temperature of the materials.

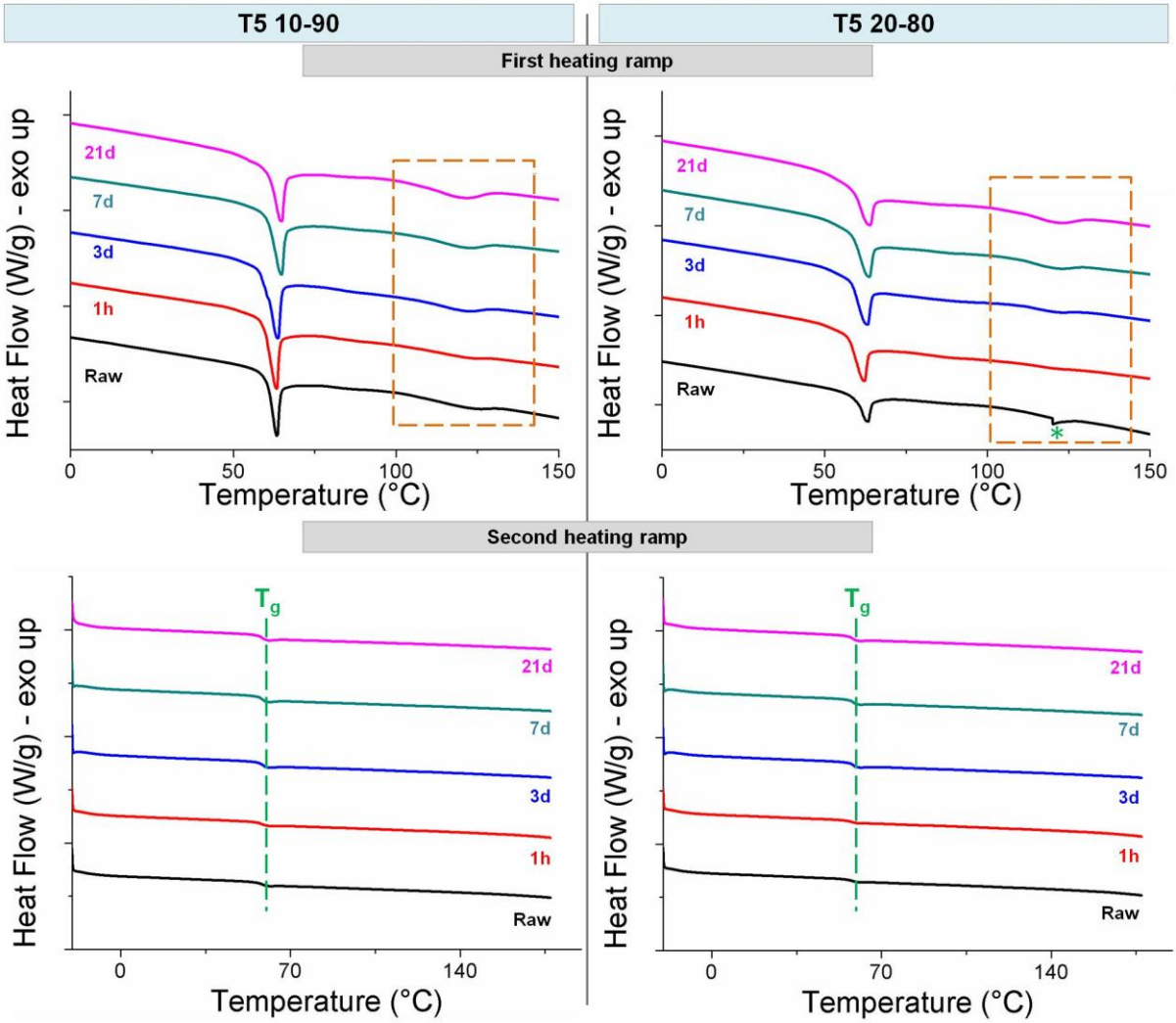

Figure 3-21. Thermograms of the hybrid fibers incubated in SBF at different time points (DSC measurements, *: measurement artifact).

Table 3-5. Evolution of T_g of the hybrid fibers during the degradation assay.

	T5 10-90		**T5 20-80**	
	ΔH_m (J/g)	**T_g**	**ΔH_m (J/g)**	**T_g**
Raw	1.84	58.13	0.65 (*)	58.11
1h	1.13	58.24	0.12	57.53
3d	2.11	58.22	0.36	58.78
7d	2.44	58.71	1.64	58.40
21d	3.71	58.38	2.83	58.53

3.4.2.6. Glass loss

The curves obtained by thermogravimetry analysis for the fibers, as electrospun and incubated (1 hour and 28 days in SBF), are presented in **Figure 3-22**. The remaining weights and calculated glass

contents obtained after the thermal treatment are summarized in the **Table 3-6**. Results showed that the T5 10-90 and T5 20-80 fibers, as produced, had an inorganic weight percentage equal to 26.09 and 35.28 respectively. After one hour in SBF, fibers lost an important quantity of inorganic phase, especially the T5 20-80 fibers for which the percentage was reduced of 50%. These fibers lost the higher quantity of inorganic phase after one hour in comparison to the T5 10-90 fibers which showed a less drastic loss (21%). However, after one hour and up to the end of the assay, the T5 10-90 fibers appeared to be the ones that lost the biggest amount of inorganic part. Equal to 20.56% after one hour, the weight percentage indeed dropped to 3.06% for the T5 10-90 fibers whereas the T5 20-80 ones showed a more reasonable decrease (from 16.4% to 8%). After the degradation period (28 days), the T5 20-80 fibers ended with the higher inorganic weight percentage (around 8% against 3% for the T5 10-90 fibers).

To obtain more information on the ORMOGLASS loss, particular attention should be given to the alkylphosphate. The peaks associated to these unreacted alkylphosphate molecules are, in fact, almost lost after one hour and completely disappeared after 28 days. The big weight loss observed at the early stage of immersion is probably due to their fast dissolution.

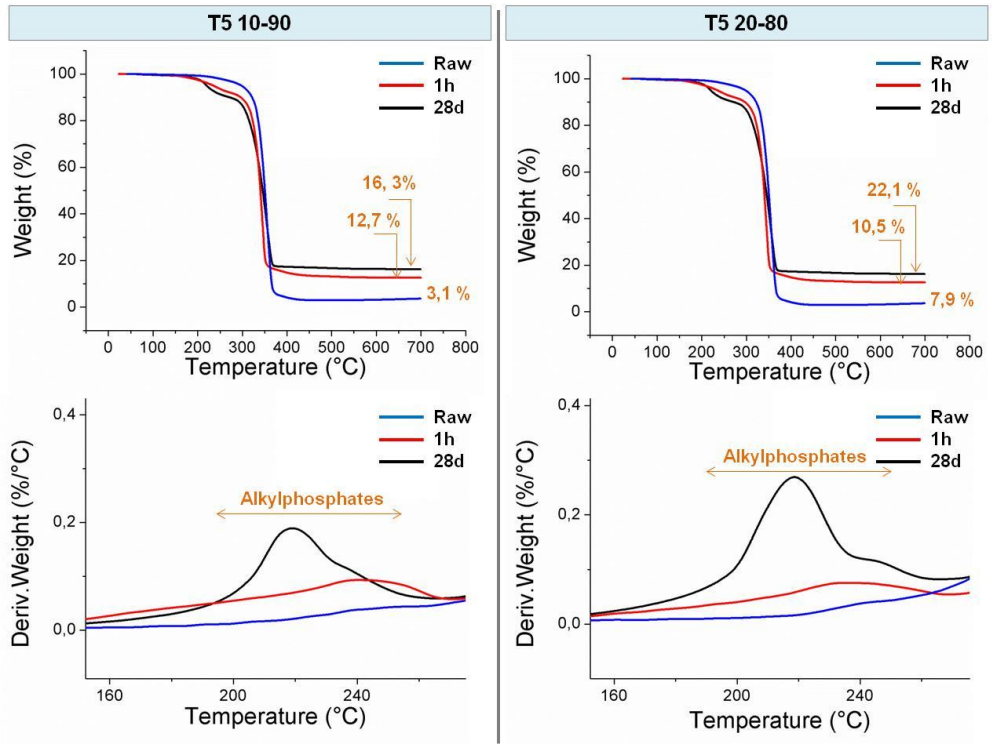

Figure 3-22. TGA curves of the hybrid fibers and their associated derivative curves (DTA), showing the remaining inorganic mass after the thermal treatment and the loss of alkylphosphate molecules.

Table 3-6. Summary of the data extracted from the TGA and DTA graphs used for the evaluation of the glass content in the fibers.

	Remaining weight (%)	**Weight attributed to alkylphosphates (%)**	**Glass content (%)**
T5 10-90	16.31	9.78	26.09
T5 10-90 1h	12.65	7.91	20.56
T5 10-90 28d	3.06	0	3.06
T5 20-80	22.09	13.19	35.28
T5 20-80 1h	10.47	5.97	16.44
T5 20-80 A 28d	7.92	0	7.92

3.4.2.7. Glass distribution in the fibers

TEM images revealed that the glass gel was incorporated in the PLA as continuous "bands" distributed along the fiber axis (**Figure 3-23**). But after 21 days of incubation, the PLA phase was less visible and "granules" and small holes appeared on the pictures. When manipulating the samples, it has been additionally noticed that incubated fibrous layers were more brittle than the ones as obtained by electrospinning. This can be observed on the TEM pictures on the areas where fibers broke. The fracture seemed to happen suddenly without previous elastic deformation (instantaneous breaking). When fibers were immersed in SBF for longer times than the duration of this presented study, they actually became extremely fragile up to a critical point where it was not possible to manipulate the scaffold anymore (see appendix A-4, A.4.11).

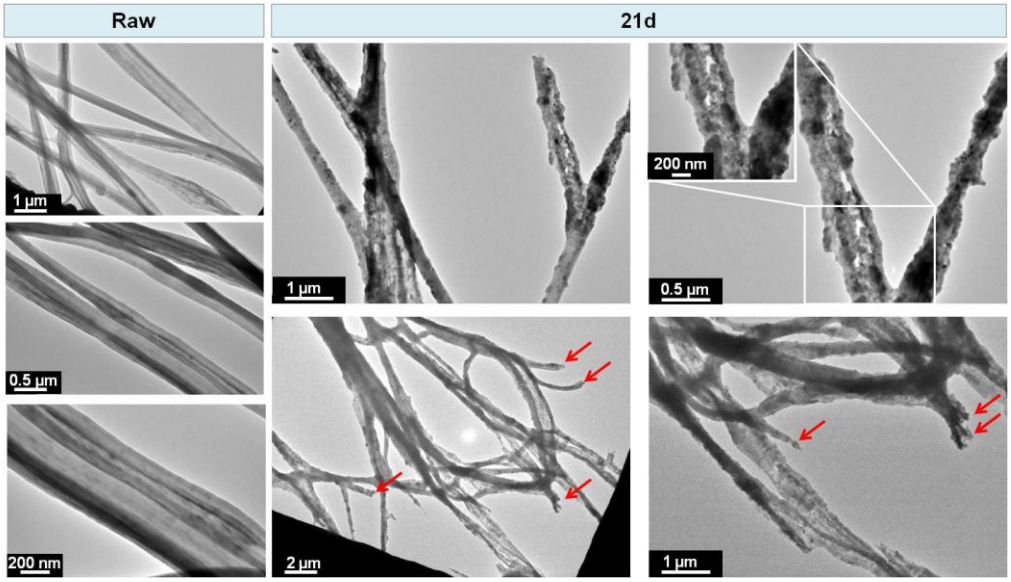

Figure 3-23. Distribution of the ormoglass in the hybrid fibers as collected by electrospinning (raw) and as obtained after 21d of incubation in SBF (TEM images). Arrows point the fractured fibers that show the brittleness of the structure.

3.4.3. Discussion

The degradation behavior of the novel fibrous PLA-titanium based ORMOGLASS scaffolds has been studied in terms of morphological, topographical and chemical modifications. The material was incubated for different periods of time in physiological conditions and diverse techniques such as FESEM, EDS, TEM, FTIR and TGA were used to monitor its evolution during immersion in SBF at 37°C. Results demonstrated that significant changes happened for the fibers over time.

SEM examinations showed that changes in the surface aspect occurred for both the pure polymeric and hybrid fibers (**Figure 3-15**, **Figure 3-16**). These changes were however more critical for the hybrid fibers than for the PLA ones. Only wrinkles were seen on PLA fibers while structural cracks were additionally noticed on the hybrids. Hybrid fibers also shortly collapsed after their immersion in SBF. The wrinkles of the PLA fibers might be the result of the material degradation process. In nature, the degradation of PLA can be induced, for example, by thermal activation, biological activity (enzymes), oxidation, photolysis or hydrolysis [81,82]. In this study, in which physiological conditions are simulated without the involvement of biological entities and other external factors (temperature, gases), hydrolysis is suggested to be the main phenomena that can degrade PLA. This process, called hydrolytic degradation, relies on the polymer chain scission that occurs through the nonspecific cleavage of the ester bonds of the main chain [83]. In contact with SBF, hydrolytic degradation induced modifications at the fiber surface with time. For the hybrid fibers, the incorporation of the ORMOGLASS significantly affected the degradation profile of the material. The first observed characteristic feature was the collapsing of the fibers. According to the contact angle values reported in the previous part of the chapter, the hybrid fibers exhibited a high hydrophilicity (contact angle on non-woven fibers: 82° for the T5 10-90 and 69° for the T5 20-80) (**Figure 3-3**). Thus, SBF can have rapidly infiltrated into the hybrid scaffolds;

unlike for the pure PLA fibers which were quite hydrophobic (contact angle: 133°). This fast fluid infiltration may have applied stress on the fiber walls which in turns made them collapse. Fibers, produced by electrospinning as hollow structures due to the Kirkendall effect [84], may have not supported this force and flattened. As a consequence, cracks might have sometimes formed because of this sudden fiber structural change. The fast fluid infiltration can be also an explanation for the slow opening of the fibers. If fibers did not instantaneously fracture by cracking, the change of fiber structure might have led to other stresses perpendicularly applied to the fibers axis which slowly may tend to open the fibers. This process may have been also amplified by the presence of the crack itself. A crack introduced 'weaknesses' on the fibers walls which could have acted as the starting point of this fiber opening process. A schematic representation of these possible processes can be seen in appendix A-4, A-4-12. Another phenomenon that could explain the formation of cracks could be an increase of crystallinity in the material during the incubation. In fact, when materials become more crystalline, the rearrangement of the polymer chains leads to the formation of space with low chain density and possibly facilitates the apparition of cracks. Previously reported DSC results demonstrated that the $\mathbf{\Delta}H_m$ of the hybrid fibers increased with the incubation time (**Figure 3-21** and **Table 3-5**). In a pure polymeric sample, this would have suggested that more crystalline phase was present in the fibers. But, in the case of hybrid samples, the percentage of the polymer crystallinity depends on the amount of inorganic phase present in the materials. Considering the usual equation for crystallinity determination (see section **3.4.1.6**), the percentage of crystallinity in our hybrids is calculated by dividing $\mathbf{\Delta}H_m$ by a factor inferior to one (calculated considering the percentage of the inorganic compounds in the studied material). The lower the amount of the inorganic phase, the higher this factor, and consequently, the lower the value of the quotient. In our case, the ORMOGLASS dissolved during the incubation. This means that the fibers, after 21 days incubation, contained less ORMOGLASS than the ones after 3 days, for example. Thus, for the 21d fibers, the $\mathbf{\Delta}H_m$ is divided by a higher factor than the 3d fibers. As a result, the $\mathbf{\Delta}H_m$ is more significantly lowered by the ORMOGLASS content for the 21d fibers than for the 3d fibers. In other words, these mathematical considerations mean that for our study, an increase in the $\mathbf{\Delta}H_m$ does not demonstrate an increase in crystallinity. It is possible that the higher $\mathbf{\Delta}H_m$ value of the 21d fibers was "compensated" by the introduction of the low value of the ORMOGLASS content for the determination of the crystallinity. Unfortunately, it has not been possible to calculate precisely the crystallinity of the fibers during this degradation study because the amount of ORMOGLASS was not known for each time point. TGA assays could have been carried out to approximate this data but after the other assays, insufficient samples for such destructive tests remained. Complementary XRD measurements were however performed to verify if the crystallinity was indeed increased or not (see appendix A-4, A-4-13). Ultimately, as no crystalline peaks were seen on the XRD spectra, it was assumed that the incubation did not increase the crystallinity of the polymeric constituent of the fibers (or at least, not above the detection limit of the device). For this reason, it was believed that crystallinity was not involved in the formation of cracks. Therefore, the hypothesis that stress on the fiber walls caused the defects was favored.

In addition to that, it might be also that the acidic pH caused by the presence of the ORMOGLASS promoted the degradation of the polymeric phase [85]. The hydrolyzed fragments may be removed from the surface and released in the SBF, what would explain the observation of holes on the FESEM and TEM pictures (**Figure 3-16**, **Figure 3-23**). The AFM analysis confirmed that the morphological changes resulted in topographical modifications (**Figure 3-17**). It demonstrated, for example, how the opening of the fibers induced a slight decrease in the height profile in the middle of the fiber width and how the roughness of the fibers increased after the degradation period.

Regarding the chemical composition of the fibers, most changes occurred during the first day of incubation (**Figure 3-18**). A high decrease in the calcium content was observed after the first hour while the phosphate amount continued decreasing till the first day. The dissolution of a high amount of calcium just after the material immersion was also confirmed by the calcium release assay. The increase of calcium observed between the first hour the first day on the EDS measurements should be interpreted as a result of the phosphate decrease and not as gain of calcium on the fibers; taking into account that percentages are relative values. This is what happened for the calcium and also for the titanium content which increased significantly because of both decrease of phosphate and calcium. After 3 days and up to 21 days, the composition of the fibers stabilized. This suggested that the degradation of the glass phase occurred in a homogeneous manner in terms of chemical molar ratios. This result is in accordance with a study performed by Melba *et al.* on different titanium based glasses that revealed a stable Ca/P_2 ratio after the first hours of incubation of micrometric glasses and a quasi stable ionic release along their slow dissolution [63]. However, the composition of the fibers after 3 days differs from the original G5 one as lot of phosphate and calcium are lost at the initial stage of the immersion. As the composition of titanium based glasses affects cellular response and that 5% mol of titanium appeared to be the optimal titanium content for an effective gene up-regulation and cellular activity [67], an improvement should be made regarding the material preparation in order to maintain the G5 composition after material immersion in fluid. In relation to the previous cellular assays reported in the chapter, this means that cells were not exactly cultured on the G5 composition. Given the potential of this G5 composition, it is believed that even better cellular responses could be achieved with these fibers if the dissolution of the glass was better controlled and the exact G5 composition maintained even after immersion.

FTIR analysis showed that infrared spectra of the hybrid fibers after their deposition by electrospinning exhibited the characteristic absorbance peaks of PLA and additional signals related to phosphate complexes (**Figure 3-19**). The PO_4^{3-} tetrahedron, the basic building block of phosphate based glasses [76,86], is present in the fibers as represented by the absorbance observed at numerous wavelengths. P-O-P stretching modes are also clearly visible on the spectrum. The presence of these signals is attributed to the P-O-P bonds involved in the glass forming network. The P=O bonds at the contrary did not contributed to the ORMOGLASS network creation due to their chemical stability. After one hour in SBF, phosphate signals almost disappeared, because an important quantity of phosphate was dissolved in this short time. Only a very slight shoulder between 580 and 450 cm^{-1} can attest of a small

phosphate remaining amount. But after one day, no signals from phosphate were noticed anymore. This is in accordance with EDS results: the dissolution of phosphates started as soon as the material was in contact with fluid and continued during the first day. In parallel to the calcium, the fibers seemed therefore to undergo a strong burst release of phosphates.

To quantify the ORMOGLASS loss, TGA measurements were performed. The decrease of the inorganic content weight which immediately dropped after one hour immersion in SBF confirmed that for both T5 10-90 and T5 20-80 fibers, a significant amount of ORMOGLASS was dissolved after this time (**Figure 3-22**, **Table 3-6**). As enounced before, the produced fibers contained a high amount of unreacted alkylphosphates. It was suggested that part of the monoethyl- and diethyl-phosphate molecules contained in the ORMOGLASS precursor mix did not all react to form the ORMOGLASS network or that they reacted but formed a very weak bond with the other species. According to the weight loss associated to alkylphosphates, it is clear that a significant amount of phosphate was not effectively incorporated and was rather found as free molecules in the ORMOGLASS gel (i.e fibers). As a consequence, it can easily be released in SBF. This could partially explain the results obtained by EDS, FTIR and TGA after 1 hour of immersion. However, even if only the loss of phosphate is observed on TGA thermograms, it should be stated that the diminution of the starting glass weight percentage was also due to the initial calcium release revealed by EDS measurements and the calcium release assay (**Figure 3-18**, **Figure 3-20**). In other words, it means that the amount of the ORMOGLASS in the fibers was not exactly the one determined by the TGA. The values should be a little bit higher. This is also true because an ORMOGLASS was studied. So, it is sure that organic fragments of the ORMOGLASS degraded during the assay, even if they were not revealed by TGA (probably under the detection limit or masked by other signals). In conclusion, TGA can give an idea on the ORMOGLASS amount contained in the fibers but it did not provide accurate values, unlike for other composites that contained a fully inorganic phase [87]. After 28 days, no alkylphosphate peaks were observed in the hybrid fibers (no peaks on the thermograms). Based on FTIR and EDS observations, this dissolution seemed in fact to have been already completely reached after the first day. This is why after 3 days and up to the end of the assay, the composition of the fibers showed less critical changes than at the beginning. Once the excess of non reacted compounds and a certain amount of glass gel have been released, the molar ratio stabilized and the glass maintained the same composition along its degradation. At the end of the assay, small amounts of inorganic were found in the fibers in comparison to their initial content. Considering that titanium based glasses degrade slowly because of the presence of titanium in the glass network, a logical conclusion would be that the changes in weight were mainly due to the fast initial dissolution described above. This slow degradation behavior has been shown for a micrometric solid bulk glasses [63]. Here, several factors may have promoted a faster degradation of the ORMOGLASS: the “gel” state of the ORMOGLASS, the high surface-to-volume ratio of the scaffold and its high hydrophilicity. Fast dissolution and subsequent degradation were therefore finally suggested to be both involved in the global weight changes determined by TGA.

Concerning specifically the critical high weight loss at the beginning of the assay, a similar behavior has been identified for other composites made of PLA and G5 glass. Prepared by the solvent casting-sol leaching method, these materials demonstrated a significant weight loss after the first week of immersion in SBF [7]. This was attributed to some morphological modifications and degradation of glass particles. The fact that in our case, the fast dissolution is already finished after one hour confirmed that this release might mainly be due to the release of residual compounds not involved in the ORMOGLASS structure and part of the ORMOGLASS gel. PLA and ORMOGLASS degradation was indeed not expected to happen in such a short time. To minimize or avoid this burst release, a better control on the ORMOGLASS network formation could be further performed in order to enhance the efficiency of the hydrolysis and thus obtain a better incorporation of calcium and phosphate. Changes in the catalyst or hydrolysis duration could be assessed, for example. If more calcium and phosphate reacted with the others reagents, a less drastic immediate release would be expected. However, G5 corresponds to a glass that contains a high amount of calcium and phosphate. It is therefore not easy to find the experimental conditions that induce an optimal hydrolysis of the compounds and therefore an efficient reactivity to form the glass network. Precise investigations involving NMR for example should be thus performed in the future to define accurate hydrolysis parameters and prepared an optimized ORMOGLASS gel.

Another possibility to prevent the burst release of ORMOGLASS would be to better control the interaction between the ORMOGLASS and the polymer [13]. As seen on TEM images, the ORMOGLASS and the polymer did not mix homogeneously when preparing the blends for electrospinning (**Figure 3-23**). ORMOGLASS "bands" were observed in the produced fibers independently from the polymeric phase. This may explain the DSC results obtained in the previous section of the chapter in which no significant differences in the T_g were reported for the PLA and hybrid fibers. Because the polymer did not properly interpenetrate with the ORMOGLASS, the mobility of the PLA chains was not affected. Indeed, if better interactions between the phase would be achieved, an increase in the T_g would be expected due to the diminution of flexibility and mobility of the polymer chains, their intermolecular interactions with the ORMOGLASS and the steric effect applied by the ORMOGLASS [88]. It is thus believed that the T_g remained quasi unchanged not only because the fibers are a class I material but also because the phases are not properly blended. Even though considered as not significant, the very slight decreases of the T_g observed after incorporation of the ORMOGLASS may suggest that the presence of the ORMOGLASS however affected the T_g to a very low extent. As observed for some composites [7,89], one hypothesis could be that the ORMOGLASS slightly decreased the molecular weight of the PLA, favoring thus the glass transition at lower temperature. Nevertheless, as the differences are too low, this comment is speculation and it is not possible to converge to a precise conclusion. More investigations are required in order to clearly determine the real effect of the ORMOGLASS on the thermal properties of the PLA in the hybrids. What is clear is that, unlike in the study performed by Navarro *et al*., the fibers did not undergo changes in the T_g during the degradation assay [7]; probably because of this non-homogeneous dispersion of the glass in the polymer matrix.

On the other hand, after 21 days, granule-like structures were observed inside the fibers and the ORMOGLASS bands lost their continuity during the fibers degradation. Such granules are typically observed when titanium based materials are assessed under TEM [90–92]. The loss of glass continuity is attributed to the drastic loss of compounds occurring just after the material immersion and the progressive dissolution of the glass remaining in the fibers. Moreover, holes were also observed on FESEM and TEM pictures, attesting that the compounds partially degraded. It has been also observed that along the material incubation, fibers became more and more brittle, whereas the mats were fully flexible before incubation. In hybrid materials, the inorganic phase promotes the bioactivity of the scaffold and the organic one supports the mechanical properties. It is thus hypothesized that in the case of the incubated fibers, PLA reached a critical point of degradation where it was not able to fulfill his function anymore. On the TEM pictures, the fragility of the scaffold is particularly evident. Moreover, the material 'defects' enumerated previously (holes, cracks, opened fibers) surely introduced weaknesses in the structure which might have directly led to the depreciation of the scaffold mechanical properties. Combined with the granules-like structures which did not seemed to have a proper cohesion between each other (discontinuity), all these morphological and structural modifications might have contributed to the low resistance of the material to collapse and decrease in toughness.

The degradation period of this study was rather short in comparison to some other *in vitro* degradation investigations reported in the literature [93,94]. However, the scaffolds presented here significantly degraded in 4 weeks and there was no reason for a longer incubation time; especially because of the brittleness and the difficulties to handle the material. It was evident that a lot of the glass gel is lost during the initial dissolution and its subsequent degradation. It was also clear on the TEM pictures that part of the polymeric phase was degraded. In fact, during the degradation of composites, the dissolution of each constituent influences the dissolution of the other phases. As explained previously, PLA resorbs following a hydrolytic degradation mechanism. The cleavage of the ester bonds leads to the formation of carboxylic (and hydroxyl) groups creating an acidic environment. This change in pH can catalyze the scission of more PLA chains (autocatalysis) but also favors the dissolution of the ORMOGLASS [7,72]. On the other hand, the dissolution of the ORMOGLASS can also accelerate the PLA degradation by modifying as well the pH of the surrounding fluid [95]. It has been demonstrated that when G5 glass is added to PLA, the molecular weight of the polymer is reduced [7]. The PLA used in our study was especially exposed to degradation as it was completely amorphous (no crystalline peaks detected by Xray – see appendix A-4, A-4-13). The degradation processes of both phases are therefore closely related and the material resorption cannot be fully interpreted following the degradation of the individual compounds. Moreover, the interplay of different factors such as hydrophilicity, fluid infiltration, scaffold structure (fibers thinness), porosity and interconnectivity additionally complicate the understanding of the degradation mechanism of hybrids and materials in general [17,81,96]. Without forgetting that in *in vivo* conditions, other biological parameters will influence the material resorption as

well (cell-material interactions, dynamic flow of body fluid, enzymes activity…) and consequently altered the scaffold integrity in a different way than the one reported herein.

Studies involving bioactive (mainly silicon-based) glasses often report the precipitation of calcium phosphate at the scaffold surface after incubation in SBF. Here, the SBF incubation did not promote the deposition of such compounds even it is a meta-stable solution designed for it. It is assumed that the fast dissolution of the glass at the beginning of the immersion removed so much glass that the content of phosphate and calcium was not suitable anymore for an effective deposition. Also, according to Lucacel *et al.*, the presence of titanium in the glass network (TiO_2) inhibits the formation of apatite type layer [74]. It is believed that titanium based glasses decrease the bioactivity of calcium phosphate samples because of their slow dissolution rate. These glasses however favor cell attachment, proliferation and differentiation [86]. It is thus already commonly accepted that such bioactive glasses should be rather used with cells than for an efficient mineralization [67,86]. Actually, Monem *et al.* demonstrated that bone growth does not necessary require a chemical bonding between calcium phosphate compounds and the host tissue because other properties of the material may also promote the bone growth [97]. In fact, the novel fibrous mats described in this chapter are aimed to be used as substrates for the triggering of specific cellular activity, either in cellular or acellular tissue engineering approaches and not be used for improving implant integration.

3.4.4. Conclusion

The *in vitro* degradation of PLA-G5 fibrous scaffolds has been assessed in simulated physiological conditions. This study revealed that the material resorption was first characterized by a burst release of calcium and phosphate at the beginning of the incubation, followed by a continuous PLA and ORMOGLASS degradation till the end of the assay. The fibers maintained a stable molar ratio over the incubation period which suggested that the ORMOGLASS dissolved homogeneously over time in terms of chemical composition. However, due to the high dissolution rate of the ORMOGLASS at the early stage of the immersion, the fibers did not possess the exact G5 composition during this assay.

Regarding the possible clinical application of this scaffold, improvement should be made on the ORMOGLASS preparation and on the organic-inorganic interactions in order to minimize the initial fast dissolution occurring the first day. Otherwise, tissues and cells could be immediately damaged by this burst release if no washing of the material is done before cell seeding (critical change in pH, see pH measurements above). Moreover, the degradation of the scaffold was rather fast according to the morphological changes observed. For bone regeneration however, templates that exhibit a slower degradation are usually preferred so that the graft gradually degrade at a speed that matches the formation of the natural bone. According to this assay, the fibers did not seem appropriate for long-term applications. But it should be kept in mind that the degradation behavior of a material generally differs between *in vitro* and *in vivo* assays and that its resorption rate might be reduced by the dynamic flow of

the body fluid (removal of the acidic species). Therefore, further investigations on the ORMOGLASS preparation (improvement of hydrolysis efficiency), phases interactions (homogeneous blending and creation of strong chemical bonding) and *in vivo* studies should be additionally performed to assess the real effective potential of PLA-T5 ORMOGLASS fibers for bone tissue engineering applications.

3.5. Chapter conclusion

PLA-ORMOGLASS bioactive fibers were produced for the first time with a titanium-based glass, thus providing a biomimicking substrate for cells. The homogeneous fibers exhibited a high hydrophilicity, improved mechanical properties compared to pure polymeric fibers and favored protein adsorption. Preliminary *in vitro* and *in vivo* assays demonstrated the potential of these fibers to support cellular adhesion, proliferation and to trigger angiogenesis. Osteogenesis has not been yet proved by using this material but results reported in the literature already demonstrated that titanium based glasses had a great osteogenic ability. The potential of such glasses is thus already accepted but the new fibrous structure described in this chapter still has to be validated. Regarding their degradation, significant changes in morphology, topography and composition were observed when fibers were incubated in SBF. The degradation behavior was first characterized by a burst release of unreacted compounds and/or fragments located at the backbone chain of the ORMOGLASS network. Subsequently, the material resorbed gradually. This study revealed the necessity to better control the hydrolysis of the glass, its incorporation into the polymeric matrix and also highlighted the importance of the phase interactions in hybrids. In conclusion, the fabrication of these novel fibers demonstrated that the sol-gel method can be used to prepare hybrid fibers containing titanium based ORMOGLASS by electrospinning. However, many improvements are still required regarding the material design in order to enhance the material degradation properties and reach the optimal cellular responses that could be hoped for an ORMOGLASS effectively conserving a G5 composition after immersion in fluids.

3.6. Acknowledgments

I kindly thank Prof. Joelle Amedee from INSERM (Bordeaux) and Prof. Lewandowska from the WUT (Warsaw) for accepting me as a guest in their laboratory. Reine Bareille, Robin Siadous, Dr. Sylvain Catros and Dr. Hugo Oliveira from INSERM are especially thanked for their teaching with cellular assays and rat implantation. From the WUT, Dr. Tomasz Brynk, Tomasz Jaroszewicz, Ewa Kijeńska, Emilia Choińska, Piotr Borychowski and Marcin Rasinski are also thanked for their assistance with tensile machine, DSC, FTIR, TGA, SEM-EDS and TEM devices, respectively. A particular thank for Dr. Agata Roguska who helped me to carry out the degradation study day by day in Warsaw. This work was also partially supported by a fellowship provided by the European Commission (European ERANET project PI11/03030 - NANGIOFRAC).

3.7. References

[1] Navarro M, Michiardi A, Castaño O, Planell JA. Biomaterials in orthopaedics. Journal of the Royal Society, Interface 2008;5:1137–58.

[2] Hench LL, Thompson I. Twenty-first century challenges for biomaterials. Journal of the Royal Society, Interface 2010;7:S379–91.

[3] Hench LL, Polak JM. Third-generation biomedical materials. Science 2002;295:1014–7.

[4] Xynos ID, Edgar AJ, Buttery LD, Hench LL, Polak JM. Gene-expression profiling of human osteoblasts following treatment with the ionic products of Bioglass 45S5 dissolution. Journal of Biomedical Materials Research 2001;55:151–7.

[5] Rhee S-H, Choi J-Y, Kim H-M. Preparation of a bioactive and degradable poly(ε-caprolactone)/silica hybrid through a sol-gel method. Biomaterials 2002;23:4915–21.

[6] Kanczler JM, Oreffo ROC. Osteogenesis and angiogenesis: the potential for engineering bone. European Cells & Materials 2008;15:100–14.

[7] Navarro M, Ginebra MP, Planell JA, Barrias CC, Barbosa MA. In vitro degradation behavior of a novel bioresorbable composite material based on PLA and a soluble CaP glass. Acta Biomaterialia 2005;1:411–9.

[8] Charles-Harris M, Koch MA, Navarro M, Lacroix D, Engel E, Planell JA. A PLA/calcium phosphate degradable composite material for bone tissue engineering: an in vitro study. Journal of Materials Science: Materials in Medicine 2008;19:1503–13.

[9] Aguirre A, Gonzalez A, Navarro M, Castano O, Planell JA, Engel E. Control of microenvironmental cues with a smart biomaterial composite promotes endothelial progenitor cell angiogenesis. European Cells and Materials 2012;24:90–106.

[10] Charles-Harris M, Navarro M, Engel E, Aparicio C, Ginebra MP, Planell JA. Surface characterization of completely degradable composite scaffolds. Journal of Materials Science Materials in Medicine 2005;16:1125–30.

[11] Charles-Harris M, del Valle S, Hentges E, Bleuet P, Lacroix D, Planell JA. Mechanical and structural characterisation of completely degradable polylactic acid/calcium phosphate glass scaffolds. Biomaterials 2007;28:4429–38.

[12] Serra T, Planell JA, Navarro M. High-resolution PLA-based composite scaffolds via 3-D printing technology. Acta Biomaterialia 2013;9:5521–30.

[13] Jones JR. New trends in bioactive scaffolds: the importance of nanostructure. Journal of the European Ceramic Society 2009;29:1275–81.

[14] Burg KJ, Porter S, Kellam JF. Biomaterial developments for bone tissue engineering. Biomaterials 2000;21:2347–59.

[15] Anderson JM, Rodriguez A, Chang DT. Foreign body reaction to biomaterials. Seminars in Immunology 2008;20:86–100.

[16] Rolfe B. The fibrotic response to implanted biomaterials: implications for tissue engineering. Regenerative Medicine and Tissue Engineering - Cells and Biomaterials, 2011.

[17] Cao Y, Mitchell G, Messina A, Price L, Thompson E, Penington A, et al. The influence of architecture on degradation and tissue ingrowth into three-dimensional poly(lactic-co-glycolic acid) scaffolds in vitro and in vivo. Biomaterials 2006;27:2854–64.

[18] Heidemann W, Jeschkeit S, Ruffieux K, Fischer JH, Wagner M, Krüger G, et al. Degradation of poly(D,L)lactide implants with or without addition of calciumphosphates in vivo. Biomaterials 2001;22:2371–81.

[19] Hong Z, Reis RL, Mano JF. Preparation and in vitro characterization of scaffolds of poly(L-lactic acid) containing bioactive glass ceramic nanoparticles. Acta Biomaterialia 2008;4:1297–306.

[20] Jones JR. Review of bioactive glass: from Hench to hybrids. Acta Biomaterialia 2013;9:4457–86.

[21] Sanzana ES, Navarro M, Ginebra M-P, Planell JA, Ojeda AC, Montecinos HA. Role of porosity and pore architecture in the in vivo bone regeneration capacity of biodegradable glass scaffolds. Journal of Biomedical Materials Research Part A 2013:1–7.

[22] Middleton JC, Tipton AJ. Synthetic biodegradable polymers as orthopedic devices. Biomaterials 2000;21:2335–46.

[23] Woodruff MA, Hutmacher DW. The return of a forgotten polymer -polycaprolactone in the 21st century. Progress in Polymer Science 2010;35:1217–56.

[24] Stevens MM. Biomaterials for bone materials tissue engineering. Materials Today 2008;11:18–25.

[25] Rasband WS. Image J. US National Institute of Health, Bethesda, USA, Http://imagej.nih.gov/ij/ 1997:2014.

[26] Hench LL. Genetic design of bioactive glass. Journal of the European Ceramic Society 2009;29:1257–65.

[27] Leu A, Stieger SM, Dayton P, Ferrara KW, Leach JK. Angiogenic response to bioactive glass promotes bone healing in an irradiated calvarial defect. Tissue Engineering Part A 2009;15:877–85.

[28] Gerhardt L-C, Widdows KL, Erol MM, Burch CW, Sanz-Herrera JA, Ochoa I, et al. The pro-angiogenic properties of multi-functional bioactive glass composite scaffolds. Biomaterials 2011;32:4096–108.

[29] Liang H, Shi W. Thermal behaviour and degradation mechanism of phosphate di/triacrylate used for UV curable flame-retardant coatings. Polymer Degradation and Stability 2004;84:525–32.

[30] Carta D, Pickup DM, Newport RJ, Knowles JC, Smith ME, Drake KO. Structural studies of bioactive sol-gel phosphate based glasses. Physics and Chemistry of Glasses 2005;46:365–71.

[31] Mahony O, Tsigkou O, Ionescu C, Minelli C, Ling L, Hanly R, et al. Silica-gelatin hybrids with tailorable degradation and mechanical properties for tissue regeneration. Advanced Functional Materials 2010;20:3835–45.

[32] Kim J, Cho J, Seidler PM, Kurland NE, Yadavalli VK. Investigations of chemical modifications of amino-terminated organic films on silicon substrates and controlled protein immobilization. Langmuir 2010;26:2599–608.

[33] Uo M, Mizuno M, Kuboki Y, Makishima A, Watari F. Properties and cytotoxicity of water soluble Na2O-CaO-P2O5 glasses. Biomaterials 1998;19:2277–84.

[34] Pham QP, Sharma U, Mikos AG. Electrospinning of polymeric nanofibers for tissue engineering applications: a review. Tissue Engineering 2006;12:1197–211.

[35] Geltmeyer J, Van der Schueren L, Goethals F, De Buysser K, De Clerck K. Optimum sol viscosity for stable electrospinning of silica nanofibres. Journal of Sol-Gel Science and Technology 2013;67:188–95.

[36] Ogoshi T, Chujo Y. Organic–inorganic polymer hybrids prepared by the sol-gel method. Composite Interfaces 2005;11:539–66.

[37] Wen J, Mark JE. Synthesis, structure, and properties of poly(dimethylsiloxane) networks reinforced by in situ-precipitated silica-titania, silica-zirconia, and silica-alumina mixed oxides. Journal of Applied Polymer Science 1995;58:1135–45.

[38] Petinakis E, Liu X, Yu L, Way C, Sangwan P, Dean K, et al. Biodegradation and thermal decomposition of poly(lactic acid)-based materials reinforced by hydrophilic fillers. Polymer Degradation and Stability 2010;95:1704–7.

[39] Pan H, Qiu Z. Biodegradable poly(l -lactide)/polyhedral oligomeric silsesquioxanes nanocomposites: enhanced crystallization, mechanical properties, and hydrolytic degradation. Macromolecules 2010;43:1499–506.

[40] Perng LH, Tsai CJ, Ling YC, Wang SD, Hsu CY. Thermal decomposition characteristics of poly[diethyl-2-(methacryloyloxy)ethyl phosphate] using thermogravimetric analysis/mass spectrometry. Journal of Applied Polymer Science 2002;85:821–30.

[41] Thomas V, Jose M V, Chowdhury S, Sullivan JF, Dean DR, Vohra YK. Mechano-morphological studies of aligned nanofibrous scaffolds of polycaprolactone fabricated by electrospinning. Journal of Biomaterials Science Polymer Edition 2006;17:969–84.

[42] Nerurkar NL, Elliott DM, Mauck RL. Mechanics of oriented electrospun nanofibrous scaffolds for annulus fibrosus tissue engineering. Journal of Orthopaedic Research 2007;25:1018–28.

[43] Athoff B, Hilborn J. Protein adsorption onto polyester surfaces: is there a need for surface activation? Journal of Biomedical Materials Research Part B 2007;80B:121–30.

[44] Fogh-Andersen N. Albumin/calcium association at different pH, as determined by potentiometry. Clinical Chemistry 1977;23:2122–6.

[45] Zhu X, Fan H, Li D, Xiao Y, Zhang X. Protein adsorption and zeta potentials of a biphasic calcium phosphate ceramic under various conditions. Journal of Biomedical Materials Research Part B 2007;82B:65–73.

[46] Krajewski A, Malavolti R, Piancastelli A. Albumin adhesion on some biological and non-biological glasses and connection with their Z-potentials. Biomaterials 1996;17:53–60.

[47] Arima Y, Iwata H. Effect of wettability and surface functional groups on protein adsorption and cell adhesion using well-defined mixed self-assembled monolayers. Biomaterials 2007;28:3074–82.

[48] Liu C, Xia Z, Czernuszka JT. Design and development of three-dimensional scaffolds for tissue engineering. Chemical Engineering Research and Design 2007;85:1051–64.

[49] Dalby MJ, Riehle MO, Johnstone H, Affrossman S, Curtis ASG. In vitro reaction of endothelial cells to polymer demixed nanotopography. Biomaterials 2002;23:2945–54.

[50] Le Saux G, Magenau A, Böcking T, Gaus K, Gooding JJ. The relative importance of topography and RGD ligand density for endothelial cell adhesion. PloS One 2011;6:e21869.

[51] Flemming RG, Murphy CJ, Abrams GA, Goodman SL, Nealey PF. Effects of synthetic micro- and nano-structured surfaces on cell behavior. Biomaterials 1999;20:573–88.

[52] Jang J-H, Castano O, Kim H-W. Electrospun materials as potential platforms for bone tissue engineering. Advanced Drug Delivery Reviews 2009;61:1065–83.

[53] Chang H-I, Wang Y. Cell responses to surface and architecture of tissue engineering scaffolds. Regenerative Medicine and Tissue Engineering - Cells and Biomaterials, 2011.

[54] Ghasemi-Mobarakeh L, Morshed M, Karbalaie K, Fesharaki M, Nasr-Esfahani MH, Baharvand H. Electrospun poly(e-caprolactone) nanofiber mat as extracellular matrix. Yakhteh Medical Journal 2008;10:179–84.

[55] Ekaputra AK, Prestwich GD, Cool SM, Hutmacher DW. Combining electrospun scaffolds with electrosprayed hydrogels leads to three-dimensional cellularization of hybrid constructs. Biomacromolecules 2008;9:2097–103.

[56] Agarwal S, Wendorff JH, Greiner A. Progress in the field of electrospinning for tissue engineering applications. Advanced Materials 2009;21:3343–51.

[57] Boland ED, Telemeco TA, Simpson DG, Wnek GE, Bowlin GL. Utilizing acid pretreatment and electrospinning to improve biocompatibility of poly(glycolic acid) for tissue engineering. Journal of Biomedical Materials Research Part B, Applied Biomaterials 2004;71B:144–52.

[58] Lu JX, Flautre B, Anselme K, Hardouin P, Gallur A, Descamps M, et al. Role of interconnections in porous bioceramics on bone recolonization in vitro and in vivo. Journal of Materials Science Materials in Medicine 1999;10:111–20.

[59] Navarro M, Engel E, Planell JA, Amaral I, Barbosa M, Ginebra MP. Surface characterization and cell response of a PLA/CaP glass biodegradable composite material. Journal of Biomedical Materials Research Part A 2008;85A:477–86.

[60] Abou Neel EA, Pickup DM, Valappil SP, Newport RJ, Knowles JC. Bioactive functional materials: a perspective on phosphate based glasses. Journal of Materials Chemistry 2009;19:690–701.

[61] Abou Neel EA, Knowles JC. Physical and biocompatibility studies of novel titanium dioxide doped phosphate-based glasses for bone tissue engineering applications. Journal of Materials Science: Materials in Medicine 2008;19:377–86.

[62] Chrzanowski W, Abou Neel EA, Lee K-Y, Bismarck A, Young AM, Hart AD, et al. Tailoring cell behavior on polymers by the incorporation of titanium doped phosphate glass filler. Advanced Engineering Materials 2010;12:B298–B308.

[63] Navarro M, Ginebra M, Clément J, Martinez S, Avila G, Planell JA. Physicochemical degradation of titania-stabilized soluble phosphate glasses for medical applications. Journal of the American Ceramic Society 2003;86:1342–52.

[64] Rajendran V, Gayathri Devi AV, Azooz M, El-Batal FH. Physicochemical studies of phosphate based P_2O_5–Na_2O–CaO–TiO_2 glasses for biomedical applications. Journal of Non-Crystalline Solids 2007;353:77–84.

[65] Pickup DM, Speight RJ, Knowles JC, Smith ME, Newport RJ. Sol–gel synthesis and structural characterisation of binary TiO2–P2O5 glasses. Materials Research Bulletin 2008;43:333–42.

[66] Lakhar NJ, Park J-H, Mordan NJ, Salih V, Wall IB, Kim H-W, et al. Titanium phosphate glass microspheres for bone tissue engineering. Acta Biomaterialia 2012;8:4181–90.

[67] Abou Neel EA, Mizoguchi T, Ito M, Bitar M, Salih V, Knowles JC. In vitro bioactivity and gene expression by cells cultured on titanium dioxide doped phosphate-based glasses. Biomaterials 2007;28:2967–77.

[68] Oyane A, Kim H-M, Furuya T, Kokubo T, Miyazaki T, Nakamura T. Preparation and assessment of revised simulated body fluids. Journal of Biomedical Materials Research Part A 2003;65:188–95.

[69] Kokubo T, Takadama H. How useful is SBF in predicting in vivo bone bioactivity? Biomaterials 2006;27:2907–15.

[70] Chow WS, Lok SK. Thermal properties of poly(lactic acid)/organo-montmorillonite nanocomposites. Journal of Thermal Analysis and Calorimetry 2009;95:627–32.

[71] Lee TH, Boey FYC, Khor KA. On the determination of polymer crystallinity for a thermoplastic PPS composite by thermal analysis. Composites Science and Technology 1995;53:259–74.

[72] Henton DE, Gruber P, Lunt J, Randall J. Polylactic acid technology. Natural Fibers, Biopolymers and Biocomposites, 2005.

[73] Ng S, Guo J, Ma J, Loo SCJ. Synthesis of high surface area mesostructured calcium phosphate particles. Acta Biomaterialia 2010;6:3772–81.

[74] Lucacel RC, Maier M, Simon V. Structural and in vitro characterization of TiO_2-CaO-P_2O_5 bioglasses. Journal of Non-Crystalline Solids 2010;356:2869–74.

[75] Schrotter J, Cardenas A, Smaihi M, Hovnanian N. Silicon and phosphorus alkoxide mixture: sol-gel study by spectroscopic technics. Journal of Sol-Gel Science and Technology 1995;4:195–204.

[76] Dayanand C, Bhikshamaiah G, Jaya Tyagaraju V, Salagram M, Krishna Murthy ASR. Structural investigations of phosphate glasses: a detailed infrared study of the x(PbO)-(1-x)P_2O_5, vitreous system. Journal of Materials Science 1996;31:1945–67.

[77] Pryce RS, Hench LL. Tailoring of bioactive glasses for the release of nitric oxide as an osteogenic stimulus. Journal of Materials Chemistry 2004;14:2303–10.

[78] Radev L, Hristov V, Michailova I, Samuneva B. Sol-gel bioactive glass-ceramics. Part II: Glass-ceramics in the CaO-SiO_2-P_2O_5-MgO system. Central European Journal of Chemistry 2009;7:322–7.

[79] ElBatal HA, Khalil EMA, Hamdy YM. In vitro behavior of bioactive phosphate glass–ceramics from the system P_2O_5–Na_2O–CaO containing titania. Ceramics International 2009;35:1195–204.

[80] Aguiar H, Serra J, González P, León B. Structural study of sol–gel silicate glasses by IR and Raman spectroscopies. Journal of Non-Crystalline Solids 2009;355:475–80.

[81] Yew GH, Mohd Yusof AM, Mohd Ishak ZA, Ishiaku US. Water absorption and enzymatic degradation of poly(lactic acid)/rice starch composites. Polymer Degradation and Stability 2005;90:488–500.

[82] Mochizuki M, Hirami M. Structural effects on the biodegradation of aliphatic polyesters. Polymers for Advanced Technologies 1997;8:203–9.

[83] Li S. Hydrolytic degradation characteristics of aliphatic polyesters derived from lactic and glycolic acids. Journal of Biomedical Materials Research 1999;48:342–53.

[84] Fan HJ, Gösele U, Zacharias M. Formation of nanotubes and hollow nanoparticles based on Kirkendall and diffusion processes: a review. Small 2007;3:1660–71.

[85] Lee W, Gardella JA. Hydrolytic kinetics of biodegradable polyester monolayers. Langmuir 2000;16:3401–6.

[86] Kiani A, Lakhkar NJ, Salih V, Smith ME, Hanna J V, Newport RJ, et al. Titanium-containing bioactive phosphate glasses. Philosophical Transactions of the Royal Society Series A, Mathematical, Physical, and Engineering Sciences 2012;370:1352–75.

[87] Patlolla A, Collins G, Livingston Arinzeh T. Solvent-dependent properties of electrospun fibrous composites for bone tissue regeneration. Acta Biomaterialia 2010;6:90–101.

[88] Lee JH, Park TG, Park HS, Lee DS, Lee YK, Yoon SC, et al. Thermal and mechanical characteristics of poly(l-lactic acid) nanocomposite scaffold. Biomaterials 2003;24:2773–8.

[89] Pluta M. Melt compounding of polylactide/organoclay: structure and properties of nanocomposites. Journal of Polymer Science Part B: Polymer Physics 2006;44:3392–405.

[90] Caruso RA, Schattka JH, Greiner A. Titanium dioxide tubes from sol-gel coating of electrospun polymer fibers. Advanced Materials 2001;13:1577–9.

[91] Chang G, Zheng X, Chen R, Chen X, Chen L, Chen Z. Silver nanoparticles filling in TiO_2 hollow nanofibers by coaxial electrospinning. Acta Physico-Chimica Sinica 2008;24:1790–6.

[92] Li D, Xia Y. Electrospinning of nanofibers: reinventing the wheel? Advanced Materials 2004;16:1151–70.

[93] Chouzouri G, Xanthos M. In vitro bioactivity and degradation of polycaprolactone composites containing silicate fillers. Acta Biomaterialia 2007;3:745–56.

[94] Blaker JJ, Nazhat SN, Maquet V, Boccaccini AR. Long-term in vitro degradation of PDLLA/bioglass bone scaffolds in acellular simulated body fluid. Acta Biomaterialia 2011;7:829–40.

[95] Li H, Chang J. pH-compensation effect of bioactive inorganic fillers on the degradation of PLGA. Composites Science and Technology 2005;65:2226–32.

[96] Choueka J, Charvet JL, Alexander H, Oh YH, Joseph G, Blumenthal NC, et al. Effect of annealing temperature on the degradation of reinforcing fibers for absorbable implants. Journal of Biomedical Materials Research 1995;29:1309–15.

[97] Monem AS, ElBatal HA, Khalil EMA, Azooz MA, Hamdy YM. In vivo behavior of bioactive phosphate glass-ceramics from the system P_2O_5-Na_2O-CaO containing TiO_2. Journal of Materials Science Materials in Medicine 2008;19:1097–108.

Chapter 4

Polylactic acid electrospun fibers covalently coated with silicon-calcium-phosphate bioactive ORMOGLASSES

In this chapter, a novel protocol to coat covalently polylactic acid electrospun fibers with silicon-calcium-phosphate ORMOGLASSES is presented. It also includes the assessment of the material features in terms of mechanical properties, mineralization potential and cellular adhesion (preliminary in vitro assay).

The fabrication of these fibers was conducted at the institute for Bioengineering of Catalonia (IBEC). All characterization methods used to develop the fabrication protocol were available at this research center. Once prepared, the obtained fibers were partially characterized at the IBEC and at the Warsaw University of Technology (WUT, Poland) (differential scanning calorimetry, Fourier transform infrared spectroscopy, thermogravimetry). The assays performed at the WUT were done in parallel to the work conducted during the 3-months research stay in Warsaw for the European Nangiofrac project (see chapter 3). Finally, measurements performed with dynamic light scattering device were obtained at the Wageningen University (WUT, the Netherlands) during a 3-months research stay, financed by a travel grant provided by the Catalan government. (nb: other results obtained during this stay concern the NMR studies conducted to characterize the precursors used in this thesis)

4.1. Chapter summary

The biological performance of ORMOGLASSES based on silicon-calcium-phosphate (abbreviated as Si-Ca-P_2[1]) and titanium-calcium-phosphate-sodium (abbreviated as Ti-Ca-P_2-Na_2[2]) systems has been demonstrated in chapter 2 and chapter 3 respectively. Despite their remarkable biological properties, materials involving blend preparation are class I hybrids. They do not possess strong chemical interactions between their constituents. Consequently, when their weak interactions are not highly optimized, their degradation is not well controlled. In fact, this was the case for the titanium-based hybrid blend, for example. A novel protocol has thus been developed to create class II hybrids, i.e. materials with strong interactions between their phases, to better control their degradation behavior and also produce materials with improved mechanical properties. The protocol is based on a coating approach that enables the functionalization of polymeric electrospun fibers with ORMOGLASSES by means of covalent bondings. It involves a succession of surface treatments such as hydrolysis, functional groups activation, and coupling agent and glass functionalization steps. Results showed that the protocol can be applied to different ORMOGLASS compositions and is perfectly reproducible. This study also demonstrated that the material surface properties (composition, roughness, wettability, stiffness…) can be tailored by changing the ORMOGLASS composition and its processing conditions (hydrolysis level). As

[1]The abbreviation was defined in accordance with the oxide based nomenclature (oxides used to prepare the ORMOGLASS system): Si in reference to silicon oxide SiO_2, P_2 in reference to phosphorous oxide P_2O_5, and Ca in reference to calcium oxide CaO *[Hench et al., Journal of Biomedical Materials Research 1971; 5, 117-141]*.

[2]The abbreviation was defined in accordance with the oxide based nomenclature (oxides used to prepare the ORMOGLASS system): Ti in reference to titanium oxide TiO_2, Ca in reference to calcium oxide CaO, P_2 in reference to phosphorous oxide P_2O_5, and Na_2 in reference to sodium oxide Na_2O *[Navarro et al., Journal of the American Ceramic Society 2003; 86, 1342-52]*.

cells modulate their behavior according to these surface properties, it is believed that the protocol developed could be used to produce scaffolds capable of triggering various cellular responses. The advantage of coating the polymeric fibers with ORMOGLASSES - instead of simply preparing a mix of the two phases having covalent interactions - is that the bioactive compound is directly exposed at the fiber surface. Cells can immediately detect the bioactive compound and there is no delay in the cellular response. In fact, a preliminary *in vitro* assay performed to evaluate adhesion and spreading of cells cultured on the material revealed that cells interacted with the scaffolds after a short time. As it is well known that glasses induce up-regulation of genes and favor mineralization, for examples, it appeared therefore essential to design a material, which has a bioactive phase that is not covered by the polymer. Even though further biological assays are obviously required to confirm the hypothesis that biological performance can be improved through the preparation of such coated hybrids, the protocol already represents considerable progress regarding material development. It is the first step towards the validation of novel materials, addressing three common problems regarding hybrids: the lack of strong interactions between the compounds, the limited bioactivity that can result from the embedding of the bioactive phase in the polymeric matrix, and the lack of material fabrication strategy to produce class II hybrids. On the other hand, this protocol seems particularly promising for the field as it can be transferred to other structure and also to other ORMOGLASS systems.

4.2. Introduction

In the two previous chapters, hybrid polymer-ORMOGLASSES fibers prepared by the sol-gel method efficiently promoted osteo and angiogenesis. In addition to the different studies found in the literature on hybrid biomaterials, there is no doubt that they have a promising potential for the development of bioactive tough scaffolds for bone tissue engineering [1–3]. Indeed, hybrids are of great interest for scientists working in the field as they exhibit the combined properties of their different constituents: bioactivity provided by the glass and toughness provided by the polymer. However, many of them present a major drawback: they degrade fast and non-homogeneously in body fluids. Although they possess chemical interactions at the nanoscale [4], these interactions are usually weak (i.e. Van der Waals, ionic, hydrogen bonding) and easy to break. As a consequence, this leads to non-homogeneous and rapid dissolution of the different phases. This was the case for the fibers presented in the chapter 3, due to phase segregation and a not properly blended material. However, to be recognized as a successful temporary implant, scaffolds should degrade at a rate that matches the formation of the new tissue. So a strong chemical interaction between the glass and the polymer is required to have a better control on the material degradation speed.

On the other hand, even though having recognized biological performance, many of the class I hybrids currently developed have their bioactive compound embedded inside the polymer matrix. This is a common issue in hybrids because both compounds are usually mixed without a proper control on their

respective dispersed positions [5,6]. In this case, the polymer often masks the glass, meaning that the cells cannot detect it properly. Generally, artificial biocompatible and biodegradable polymers do not have an intrinsic bioactivity. It is thus essential to produce materials that present a better exposure of the bioactive compound in order to be detected by the cells, and improve the cell-material interactions. As a result, no previous degradation of the polymer would be needed to uncover the glass, thus enhancing the adhesion efficiency and spreading of cells [7,8]. One of the reasons would be that all ions released from the glass during its degradation could be immediately perceived by the biological entities, promoting their faster migration, proliferation and differentiation [9].

Based on the main problems listed above, the need to design hybrid scaffolds using novel materials fabrication strategies appeared clear. A coating approach seemed to be the best option for the development of scaffolds having the bioactive compound exposed at their surface because it is the most direct way to reach that goal. As mentioned before, the coating protocol should also aim to create a strong bonding between the material compounds. Therefore, a novel coating protocol has been developed to overcome these two problematic aspects. Polymeric fibers have been covalently functionalized with ORMOGLASSES. More than overcoming common issues related to class I hybrids, it was believed that the achievement of a successful homogenous coating and the development of a reproducible protocol would provide new perspectives of work for the field of regenerative medicine. This protocol represents a significant progress in material fabrication.

4.3. Fiber preparation: protocol development

This part of the chapter describes the protocol developed to coat covalently polymeric electrospun fibers with silicon based ORMOGLASSES. These ORMOGLASSES were chosen because their hydrolysis was more controlled than the one of the titanium based ORMOGLASS. Given the complexity of developing a completely new protocol, it was more convenient to use the silicon based system. By developing such protocol, we aimed to produce a novel type of class II hybrid material able to induce immediate and specific cellular responses.

4.3.1. Materials and Methods

4.3.1.1. Electrospinning and glass preparation

The fibrous polymeric template used to perform the coating was obtained by electrospinning a solution of PLA (poly-l/dl lactic acid 95/5, Purasorb PLDL 9562, inherent viscosity midpoint 6.2 dl/g, Mw ≈ 125,000 g/mol) dissolved in TFE (2,2,2-trifluoroethanol, Sigma-Aldrich ≥ 99%). The solution was prepared according to a w/w ratio of 3% and around 15 mL of this polymeric solution was electrospun at a flow rate of 0.5 mL/hour, a voltage of 7.5 kV and a distance tip-to-collector of 13 cm. Fibers were collected on a flat metallic aluminum foil as a non-woven mat.

The ORMOGLASS precursor solution was prepared by mixing the same alkoxide reagents as those reported in chapter 2. Alkoxides precursors were also obtained in the same way as reported previously and characterized by NMR (see appendix A-1 and B-1). Two mix compositions were considered to perform the coating: S40 (40Si: 45Ca: 15P_2) and S60 (60Si: 30Ca: 10P_2). The final glass precursor mixes were kept under inert atmosphere until hydrolysis was performed. The setup can be seen in appendix A-2.

4.3.1.2. Surface treatments

A scheme representing the different reactions involved in the coating protocol is shown in **Figure 4-1**. The coating process is based on a 4-step surface treatment [10]: hydrolysis of the fibers surface to create carboxylic groups, activation of these groups, coupling agent functionalization (3-aminopropytriethoxysilane, APTES coupling molecule) and condensation process enabling the bonding of the glass to the PLA by means of APTES [10]. Once removed from the aluminum foil, fibrous sheets were thus hydrolyzed in a NaOH 0.1 M solution for 150 s. Fibers were then immersed in a 0.1M EDC/0.2M NHS (Aldrich, 97% / Aldrich, 98%) solution for 1 hour and placed afterwards in an APTES solution (Acros Organics, 99%, 10% v/v in ethanol) for 2 hours. At this point, ORMOGLASS precursor mixes were removed from the inert atmosphere and immediately partially hydrolyzed to obtain a suspension of glass nanoparticles (Si-Ca-P_2 network). Precursors were both hydrolyzed for 150 s but with different Silicon: water molar ratio: 1 to 1 for the S60 mix, 1 to 2 for the S40 mix. The chosen ratios were determined as the maximum quantity of water that can be introduced in each glass precursor solution without inducing a full gelation over 2 hours. This way, the particles were kept well dispersed, minimizing the apparition of possible aggregates. This was essential for the final coating stage during which single particles were aimed to be linked to the fibers with a homogeneous distribution. After hydrolysis, ethanol was moreover added to dilute the suspensions in order to avoid the alcoholysis degradation of the fibers that can occur when fibers are placed in contact with a so concentrated solution of alkaline compound such as alkoxides [11]. The dilution factor was fixed to 1 mL ethanol for 1 mL of S60 ORMOGLASS suspension and 4 mL ethanol for 1 mL of S40 ORMOGLASS suspension. The diluted ORMOGLASS suspensions were then added to the pre-APTES functionalized fibers to initiate the condensation process, creating a siloxane bond between the APTES molecules and the glass nanoparticles. To ensure that the glass particles were strongly attached to the fibers surface, fibers were finally placed in an ultrasonic bath for 5 minutes. All residual non-attached particles were expected to be eliminated. Fibers were left on a petri dish to dry at room temperature. The obtained templates were labeled as “coated S60” and “coated S40” fibers.

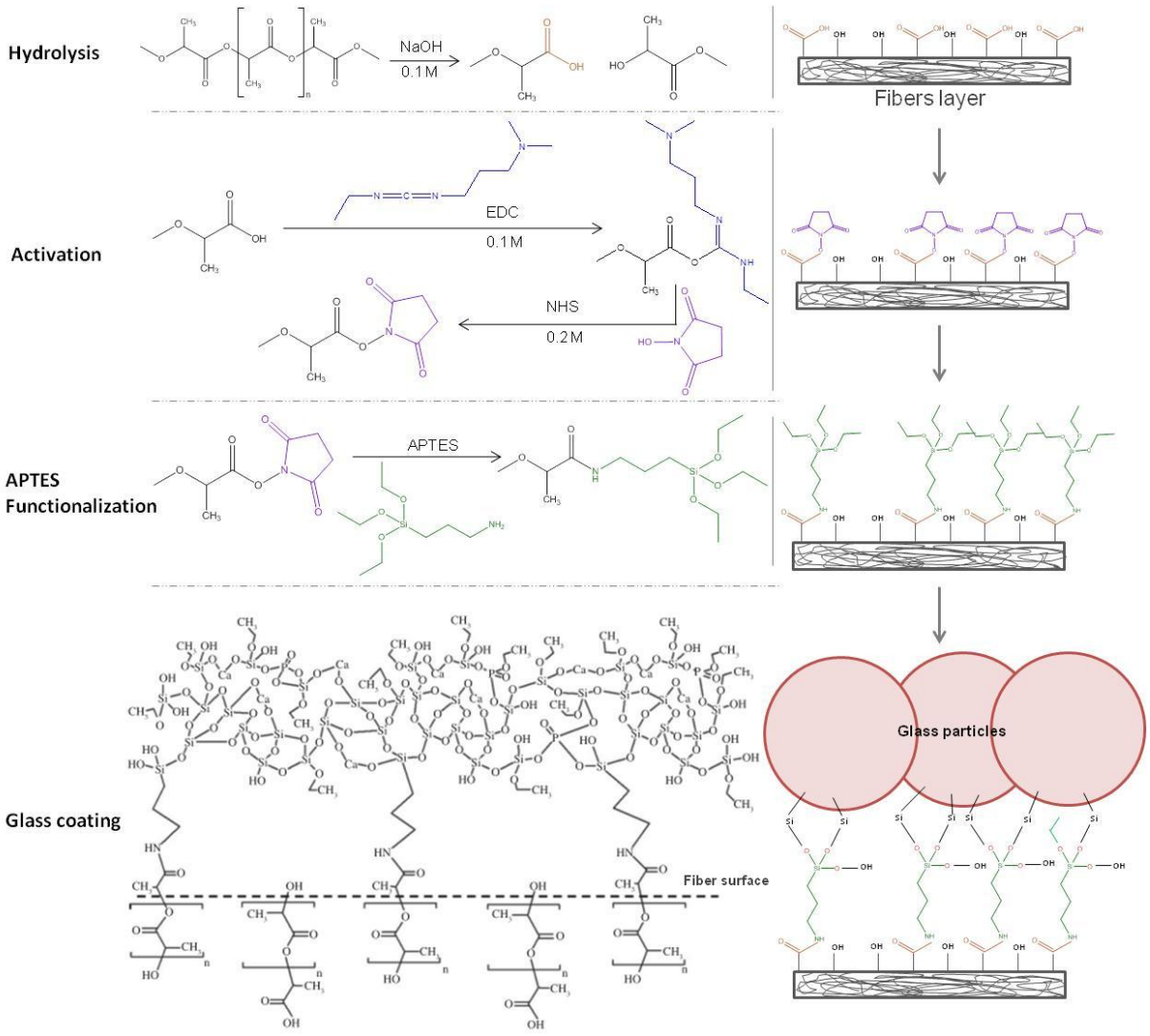

Figure 4-1. Schematic illustration of the chemical reactions involved in the coating process: hydrolysis, activation of reactive groups, functionalization with coupling agent and ormoglass bonding.

4.3.1.3. Surface modifications - characterization

Zeta potential (ZP) technique was used to confirm that each treatment step was efficiently achieved (see appendix B-5). In fact, each treatment was supposed to induce chemical changes at the fiber surface. These modifications should affect the surface charge of the template due to the creation (hydrolysis) or grafting of novel surface chemical groups. Using this technique, it is thus possible to evaluate if the chemical reactions occurred or not. In the case that the surface modifications did not clearly induce changes in the surface charge, Fourier Transform Infrared Spectroscopy (FTIR) and Energy X-ray Dispersive Spectroscopy (EDS) were used to make sure that these steps were indeed achieved (qualitative evaluations) (see appendix B-11 and B-2, respectively).

ZP measurements were performed in a 1 mM KCl electrolyte solution using the "adjustable gap cell" set-up (electrokinetic analyzer SurPASS, Anton Paar Ltd. Austria). The pH of the electrolyte was titrated from the basic region (pH ~ 9) to the acid one (pH ~ 2.5) by adding HCl 0.1 M using the device

pump. The electrolyte was forced to pass between two thin layers of fibers using a pressure program of maximum 300 mbar. The isoelectric points (IEP) and ZP values at pH = 7 were taken into account to compare the charge surface changes after the treatments.

Infrared measurements were carried out in attenuated total reflectance mode (Nicolet 8700 Thermo Scientific), placing the sample directly in contact with the ATR crystal without a preliminary special preparation. FTIR spectra were averaged from 64 scans at a resolution of 4 cm^{-1} and collected in the 4000-400 cm^{-1} wavenumber range.

EDS measurements were performed with an EDS detector coupled with a SEM device (Quanta 200 XTE 325/D8395; FEI Co.). Several spectra were acquired at different places of the treated samples (APTES functionalized and glass coated). The acquisition was done for 30s for each point.

4.3.2. Results

4.3.2.1. ZP assays

Changes in the surface electrostatic potential were evaluated by measuring the ZP. **Figure 4-2** shows the curves obtained. **Table 4-1** summarizes the isoelectric point values (IEP, pH value at ZP = 0) and ZP values after each treatment step at pH = 7 (indicative value chosen for comparison). Except for the last treatment, significant changes in the electrical potential attested that modifications at the surface of the fibers occurred. Pure PLA fibers produced by electrospinning showed an IEP equal to 3.06. After hydrolysis, this value decreased to 2.73. After activation, the fibrous layer became much less electronegative with a value of 6.07. Then, a significant drop in the IEP value was observed once APTES was grafted on the surface (IEP = 3.68). After the addition of glass, IEP values remained approximately unchanged compared to the ones obtained after APTES functionalization. For this reason, the efficiency of this final step remained unclear. FTIR and EDS were thus used to clarify this point.

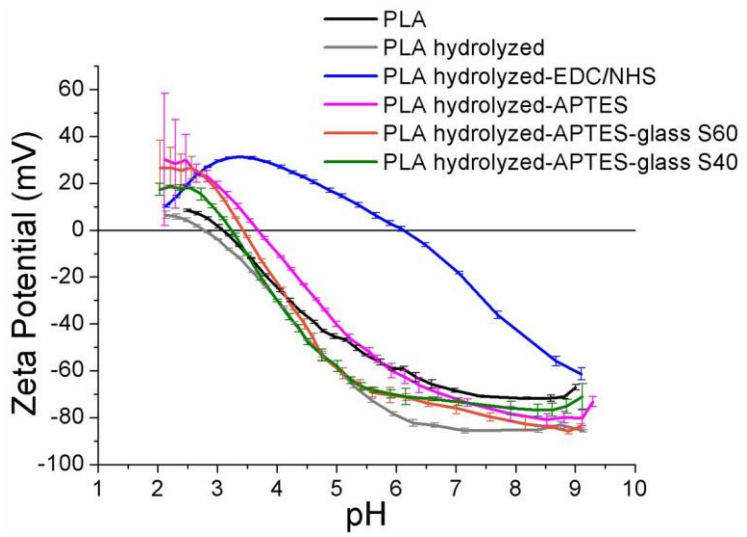

Figure 4-2. pH dependence of the zeta potential of the fibrous layer after the different surface treatments applied to perform the coating.

Table 4-1. Electrostatic potential (ZP) at pH = 7 and isoelectric point values of the fibers surface after each treatment.

	ZP at pH = 7 (mV)	IEP
PLA Fibers	-68	3,06
Hydrolysis	-85	2,73
Activation	-18	6,07
APTES Functionalization	-73	3,68
Coating - composition S60	-74	3,43
Coating - composition S40	-76	3,24

4.3.2.2. FTIR measurements

Figure 4-3 reports the FTIR spectra of the fibers acquired by ATR method before (raw material) and after APTES functionalization and ORMOGLASS coating. Spectra of both coating compositions were similar to each other. However, differences between the PLA fibers, APTES functionalized fibers and coated fibers spectra were observed. Most of these changes occurred in the fingerprint region. Only one difference can be noticed between 4000 cm^{-1} and 1600 cm^{-1}: a small peak located at 3446 cm^{-1} appeared after APTES functionalization and remained after the glass coating. In the fingerprint region, several changes that are observed coincide with peaks related to raw PLA. For example, the intensity of peaks located at 1213 and 1183 cm^{-1}, initially find on the raw PLA spectra, increased after APTES functionalization. The same behavior is observed for the peak situated at 756 cm^{-1}. At 919 cm^{-1}, however, a completely novel peak appeared. After the coating, numerous novel peaks appeared on the spectra of the coated fibers in comparison with the spectra of the APTES functionalized fibers: at 1026, 925, 776, 582 and 545 cm^{-1}. The increased peak observed on the APTES functionalized fiber spectra at 756 cm^{-1} is still observed, as well as the ones at 1213 and 1183 cm^{-1}. However, the one at 919 cm^{-1} seemed to have disappeared or significantly decreased, and it was not clearly visible anymore.

The peak assignments are summarized in **Table 4-2** and are discussed in details in the discussion section.

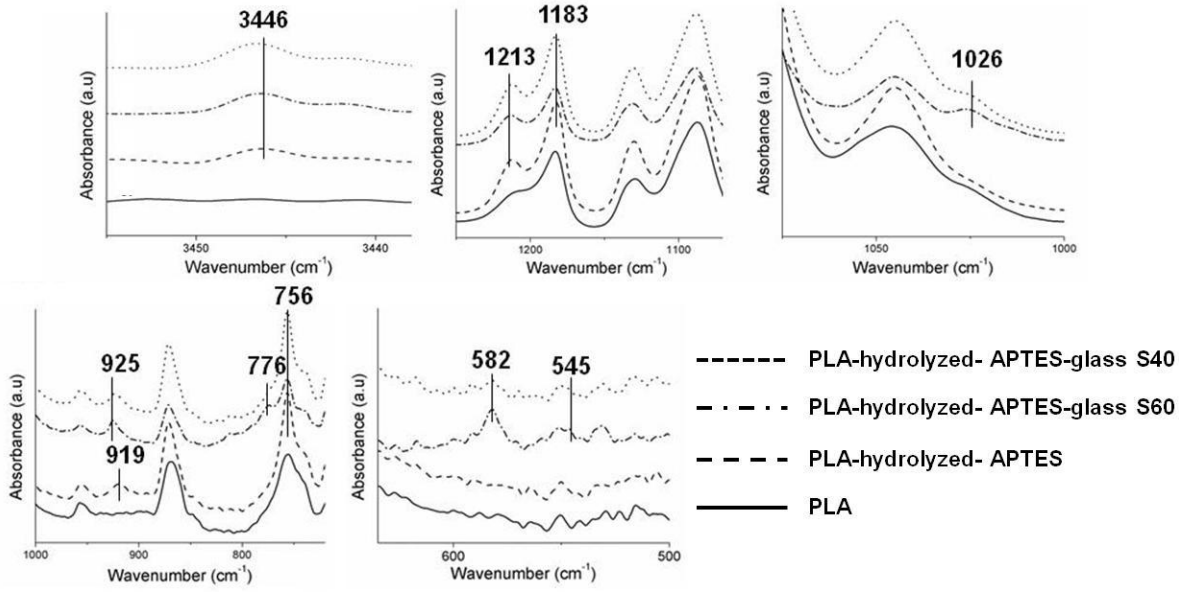

Figure 4-3. FTIR spectra of PLA, APTES-functionalized and coated fibers.

Table 4-2. FTIR bands assignment for APTES functionalized and coated fibers.

Wavenumber (cm^{-1})	**Assignement**	**References**	**Spectra**
3446	N-H stretching	[12]	All fibers except PLA
1213, 1183	Si-O-Si, Si-OCH_2CH_3	[13] [14] [15]	Coated fibers APTES functionalized fibers and coated fibers
1026	Si-O-Si asymetric stretching	[12] [16] [13] [17]	Coated fibers
919, 925	Si-OH stretching	[13] [18] [19]	APTES functionalized fibers Coated fibers
776	Si-O-Si symmetric stretching	[16] [19]	Coated fibers
756	N-H bending	[20]	All fibers except PLA
582, 545	P-O vibrations	[21] [22]	Coated fibers

4.3.2.3. EDS measurements

As an additional assay to FTIR results, EDS measurements were performed on APTES functionalized and coated fibers. **Figure 4-4** shows representative spectra of the elements detected on the fiber surfaces. The qualitative analysis revealed that only silicon was detected on the fiber surface after APTES functionalization (silane coupling agent). After glass coating, silicon, calcium and phosphate

were detected. It was also noticed that, from a quantitative point of view, the amount of silicon was increased after the glass coating in comparison to the one measured on APTES-functionalized fibers.

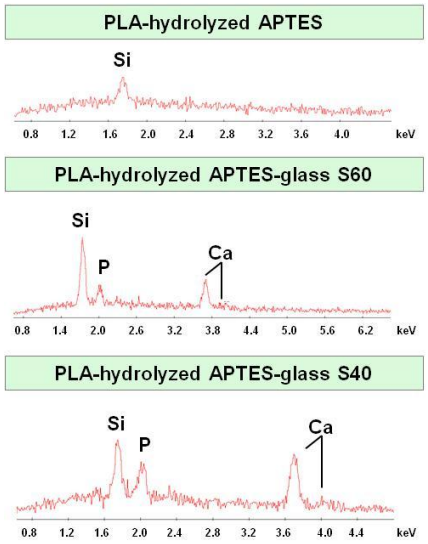

Figure 4-4. Qualitative EDS measurements performed on the APTES functionalized fibers and the coated ones.

4.3.3. Discussion

ZP (**Figure 4-2**, **Table 4-1**), FTIR (**Figure 4-3**, **Table 4-2**) and EDS (**Figure 4-4**) results demonstrated that surface properties of the fibers changed after each treatment of the applied protocol. Initially, at pH = 7, PLA fiber exhibited an IEP value equal to 3.06. This value decreased after hydrolysis due to the formation of reactive negatively charged carboxylic (COO-) at the fiber surface. After activation, the IEP value significantly increased. This was attributed to the positive surface charges related to the grafting of imide groups. After functionalization with the coupling agent, IEP value decreased again because of the bonding of the APTES molecule and the grafting of a silane group on the surface. Up to the APTES functionalization, ZP results made us inferred that the desired chemical reactions occurred after each surface treatment. Comparison of the IEP values measured for the fibers obtained after the last two treatments did not allow conclusions to be made regarding the efficiency of the final step of the protocol (glass coating).

FTIR however, clearly revealed that the fiber surface of the APTES functionalized fibers changed after the glass coating treatment. It also confirmed the ZP results: the activation and APTES functionalization steps were successfully achieved. **Table 4-2** summarizes the assignment of the peaks identified in the results section. The peak located at 3446 cm^{-1} was assigned to the secondary amine of PLA-linked APTES (NH stretching) which also resulted in the increase of the infrared signal at 756 cm^{-1} (NH wag) after APTES grafting. The increase of peak intensity observed at 1213 and 1183 cm^{-1} were found to correspond to characteristics peaks of Si-OCH_2CH_3 (ethyl) groups from APTES, inferring that APTES have been successfully attached on the fibers. The novel peak located at 919 cm^{-1} also confirmed the presence of APTES molecules on the fibers surface. This peak resulted from silanol groups (Si-OH)

of some grafted APTES molecules already partially hydrolyzed. It is assumed that these silanols groups formed during the APTES functionalization step because of the ambient humidity, or during the time that passed between the functionalization and the infrared measurements. Another possibility is that some of the APTES molecules were simply already hydrolyzed in the commercially purchased solution. After the coating, the new signals at 582 and 545 cm^{-1} were associated to phosphate species. The ones located at 1026 and 776 cm^{-1} were assigned to siloxane (Si-O-Si vibrations). According to the literature, siloxane bonds commonly give signal also around 1210 cm^{-1}. This means that an increase of the 1213 cm^{-1} peak would be expected after the coating. But it is actually not the case as this peak is also depending and associated to the ethyl groups of grafted APTES. This peak might thus be the result of a contributory effect between the decrease of this peak due to the hydrolysis of APTES (ethyl groups replaced by hydroxyl ones) and the increase of the peak due to the grafting of glass particles (Si-O-Si based network). Consequently, the fact that the intensity of this peak did not undergo apparent changes after APTES functionalization and glass coating can be explained by two possibilities: the first one implies that the signal is associated to a full substitution of the Si-OCH_2CH_3 groups from APTES by Si-O-Si groups from the glass coating network; the second one implies that the intensity is an addition of the intensity from some non-hydrolyzed Si-OCH_2CH_3 groups from APTES and Si-O-Si groups from the glass coating network. Notice that Si-O-Si signal can be both associated to Si_{glass}-O-Si_{glass} or to Si_{APTES}-O-Si_{glass} bondings, which can be inferred to a covalent bond between the polymeric fiber surface and the glass coating network. Finally, the peak located at 925 cm^{-1} on the coated fibers spectra was typically due to silanol groups and was assigned to the ones pertaining to the glass network. On the APTES-functionalized fibers, these groups raised signals at 919 cm^{-1}. This shift in wavenumber was attributed to the difference in chemical environment of the silanols. Our interpretation is that the 919 cm-1 peak might also appear in the spectra of the coated fibers but it is difficult to see it because of the diminution of its intensity due to the formation of Si_{APTES}-O-Si_{glass} bond (silanols of APTES replaced by Si_{APTES}-O-Si_{glass} bonds) and the presence of the 925 cm^{-1} peak. Indirectly, this suggested that the covalent bonding between the ORMOGLASS and the APTES efficiently occurred. Thus, in summary, FTIR results suggested that the glass coating step was successfully achieved.

FTIR results were, in fact, confirmed by EDS measurements. Indeed, the fact that silicon, calcium and phosphate were detected after the ORMOGLASS coating step demonstrated that APTES functionalized fibers had been successfully coated with the ORMOGLASS nanoparticles. Moreover, the high silicon content on the coated fibers, in comparison to the one of the APTES functionalized ones, is justified by the contribution to the measurement of the silicon-based network of the ORMOGLASS. As an ORMOGLASS particle possesses much more silicon atoms than an APTES molecule, it is understandable that silicon amount detected after coating was higher. This is especially true knowing that three glass particles can potentially link to the APTES molecules. It should be however noticed that this situation is not very probable because three glass particles may not attach to each APTES molecule as steric effects may hinder the bonding of three nanoparticles on each coupling agent molecule in the case

of full APTES hydrosysis. But this depends also on the nanoparticle size, and the determination of the number of particles linked to APTES molecules is not determined. These results simply confirmed that the fibers were coated with the ORMOGLASS.

4.3.4. Conclusion

Based on the results reported here above, the different treatments applied to the fibers seemed to have been successfully performed. The ZP analysis indicated that after hydrolysis, activation and coupling agent functionalization, the surface charge of the fiber surface was modified, demonstrating the efficiency of these first treatments. FTIR and EDS were used as complementary techniques to ZP analysis to demonstrate particularly that the final glass coating step was also achieved. The combination of these three methods enabled to conclude that a novel coating approach based on the sol-gel method can be implemented. The characterization of the material was however required to evaluate the potential of this new hybrid material.

4.4. Fiber characterization

The characterization of the materials produced by applying the protocol described in the previous section is reported in this part of the chapter. This study aimed to investigate the material physico-chemical properties in order to evaluate its potential for bone tissue engineering. Therefore, the material properties were first discussed in terms of material design improvement and furthermore in terms of relevance for biomedical applications and importance for cell-materials interactions. A preliminary *in vitro* test is also reported to assess the cellular response induced by the materials at the early stage of cell adhesion.

4.4.1. Materials and Methods

4.4.1.1. Fiber morphology

After drying at room temperature and carbon coating, fibers were loaded to a field emission scanning electron microscope (FESEM, Nova™-Nano SEM-230; FEI Co., the Netherlands) to observe their morphology (see appendix B-2). The pictures were taken at an accelerating voltage of 5 kV and a working distance of 5 mm. Pictures with cells fixed on the scaffolds were obtained in the same conditions. Using FESEM images and ImageJ Software [23], fibers thickness average was determined by measuring a minimum of 15 fibers diameters (before and after coating).

4.4.1.2. Coating composition

The same samples used for FESEM were loaded to an electron scanning microscope with an EDS detector (Quanta 200 XTE 325/D8395; FEI Co., the Netherlands) to determine the exact coating

composition (see appendix B-2). Three different places were arbitrarily selected on the scaffold to perform the measurements (30 s acquisition time for each point - silicon, calcium and phosphate quantification).

4.4.1.3. Fiber wettability

Fiber wettability was evaluated via contact-angle measurements using an OCA 20 system (Dataphysics, GmbH) and the sessile drop technique (see appendix B-3). This method consists in the measurement of the equilibrium angle formed between a 3 µL of an ultra high pure water drop and the surface of the fibrous sheet. Measurements were performed on three different points for each sample.

4.4.1.4. Mechanical properties

Fibers stiffness was investigated using Atomic Force Microscope (AFM MultiMode 8, Bruker and NanoScope Analysis, v1.2) in PeakForce tapping mode in air (see appendix B-4). Thin layer of fibers was deposited on an adhesive substrate and scanned along the fibers length (individual fiber measurements). Stiffness was assessed by evaluating the DMT modulus which is calculated by taking into account the load force and adhesion between the tip and the sample [24]. AFM analysis also enabled the determination of the surface roughness of the fibers (Root Mean Square roughness R_q).

Fibers strips of 50x10 mm were used to evaluate the Young's modulus and yield strength of the scaffolds by tensile tests (Adamel Lhomargy DY34 - see appendix B-10). Strips were clamped between the grips of the machine and then subjected to elongation (setting parameters previously defined). The thickness of the strips, needed for the calculation of the desired mechanical values, was determined by FESEM (see appendix A-5, A.5.1) and measured thanks to the ImageJ Software [23]. Results were considered statistically significant for $p < 0.05$ and highly significant for $p < 0.002$ (Student's t-test).

4.4.1.5. Thermal assays

Thermogravimetry analysis was used (TGA Q5000 TA) to determine the content of glass constituting the hybrid materials (see appendix B-9). Samples were heated at 10°C/min up to 700°C in air. In order to identify the gaseous products that degraded during this thermal treatment, an additional TGA analysis coupled FTIR was carried out under nitrogen flow (10ml/min) with the coated S60 fibers.

Differential scanning calorimetry analysis was performed to check if changes in the organic phase occurred after the coating protocol (see appendix B-8). A DSC Q2000 TA device and 5 mg samples confined in hermetic aluminum pans were used. Samples were heated at a rate of 10°C/min starting from 25°C up to 180°C. The degree of crystallinity was calculated as follows [25,26]:

$$\chi(\%) = \frac{\Delta Hm - \Delta Hc}{\Delta Hm^{\circ}\,(1 - Wg)} * 100$$

Where χ is the percentage of crystallinity, $\mathbf{\Delta}H_m$ is the heat of fusion, $\mathbf{\Delta}H_c$ is the heat of the cold crystallization, $\mathbf{\Delta}H_m^\circ$ the heat of fusion of a 100% PLA crystalline material (93.1 $J.g^{-1}$ [27]) and W_g the weight percentage of glass contained in the hybrids (values obtained from TGA assays).
The software used to analyze DSC and TGA results was TA Universal Analysis 2000 v4.7A.

4.4.1.6. Fiber morphology after thermal treatment

In order to observe the morphology of the fibers after thermal treatment (i.e once only the inorganic phase of the fibers remains), another thermal treatment was applied to the hybrid fibers in parallel to the thermogravimetry. This assay aimed to directly measure the thickness of the inorganic coated compound. The conditions of thermal treatment were set to enable a gradual and slow degradation of the organic phase. Coated fibers were placed in a furnace and slowly heated up to 600°C during 10 hours. This temperature was maintained for 5 hours and then decreased to ambient temperature during 5 hours. The remaining inorganic phase was fixed on a FESEM support, coated with a thin layer of carbon, and imaged using the same FESEM device than the one named previously. Ten measurements were performed on the shell using ImageJ software [23].

4.4.1.7. ORMOGLASS particle size

Dynamic Light Scattering (DLS) technique was used to measure the size of the glass nanoparticles prepared to coat the polymeric fibers (see appendix B-13). This assay was conducted to determine if the composition of the particles influenced the particles size, and consequently affected the thickness of the glass coated. As mentioned before, the S60 particles were prepared with a hydrolysis ratio $Si:H_2O$ of 1:1 and the S40 ones with a ratio of 1:2. It appeared thus interesting to investigate not only the influence of the glass precursor solution composition but also the degree of hydrolysis on the particles size. For this reason, particles were prepared with different compositions and with different ratio of hydrolysis. The hydrolysis of the glass precursor mix was performed according to the following $Si:H_2O$ molar ratios: 1:0.5, 1:1, 1:2, 1:3 for the S60 glass and 1:1, 1:2, 1:3, 1:4, 1:5 for the S40 glass. The ratio 1:0.5 was not considered for the S40 glass as only a tiny amount of particles was reached after this hydrolysis level and it was impossible to isolate them. On the other hand, the ratios 1:4 and 1:5 for the S70 could not have been applied as well as they induced a rapid gelation of the glass solution. No particles could have been obtained as the hydrolysis was too high and the ability of creating particles was therefore lost. After the 2.5 min of hydrolysis of the mix, 1 mL of absolute ethanol was added to 0.5 mL of particles suspension and vigorously shaken. This dilution was done to minimize the further hydrolysis during posterior centrifugation (4 minutes at 20°C and 4000 rpm), which was done to collect the particles. The supernatant was carefully removed and 1.5 mL of absolute ethanol was added to the deposit. Particles were homogeneously resuspended and centrifuged again. This step was performed twice to remove the excess of glass precursor mix (mix containing multiple solvents from the alkoxides) and, finally, to have

the particles in suspension in absolute ethanol. This was essential regarding the measurements of the particle size which required the use of a unique solvent as dispersant.

The glass particles suspension obtained was sonicated for 1 minute just before starting the DLS measurements and 1mL of that suspension was placed in the measurement "cuvette". Measurements were conducted using a Malvern Zetasizer Nano ZS device (laser wavelengths of 633 nm and detection angle of 173°) and were run three times with 2 minutes of intervals for each types of suspension. DLS results were analyzed in terms of particle number percentage using Malvern DTS software v5.1.

4.4.1.8. Calcium dissolution and pH measurements

Dissolution tests were carried out to monitor the release profile of the calcium contained in the glass network of the coated fibers. Pieces of 1 cm^2 were cut from the treated fibrous layer. Four replicates were prepared for each sample type and were placed in wells of a 24 culture plate. Deionized water was added to each well (1 mL) and parafilm was used to seal properly the plate in order to avoid water evaporation. Then, the plate was placed in an incubator at 37°C. After each time point (5 min, 1h, 1d, 2d, 3d, 6d, 7d, 8d, 9d, 10d, 13, 14d), the water was removed and 1 mL was again added to the wells. Calcium concentrations were measured using a Crison Ca^{2+} selective electrode and an Ag/AgCl reference electrode. pH was additionally measured using a Crison GLP22+ pH-meter and a Crison pH microelectrode. Instead of SBF, deionized water was preferred to perform this assay in order to determine the real amount of calcium released by the material. Otherwise, the buffering effect of SBF can mask the real observation of the dissolution behavior (see appendix A-5, A.5.2). The calcium concentration is reported as a cumulative value.

4.4.1.9. Mineralization potential

The mineralization potential of the fibers was assessed by immersing the fibers alternatively in concentrated calcium and phosphate solutions. The procedure was firstly reported by Yu *et al.* to induce mineralization on polycaprolactone fibers [28]. To achieve that, they applied an aggressive hydrolysis to the fibers prior to the calcium-phosphate (CaP) induction and subsequent mineralization. In the case of the coated fibers, this test is not used to force the CaP precipitation. It is simply used to check if the fibers can precipitate calcium phosphate compound by themselves in these conditions, without preliminary treatment. This way, the mineralization potential of PLA and coated fibers can be compared.

PLA and coated fibers were dipped 1 s in ethanol and washed with water. Afterwards, they were immersed alternatively in $CaCl_2$ aqueous solution (150 mM) for 30 s, washed 5 s with water and immersed in Na_2HPO_4 aqueous solution (150 mM) for 30 s. This succession of immersions was performed six times and was done under slight stirring. Finally, fibers were placed in the ultrasonic bath during 15 s and then dried at room temperature.

The obtained fibers were coated with a thin layer of carbon and were imaged using the same FESEM device than the one presented previously for the assessment of the non-coated and coated fibers morphology.

4.4.1.10. In vitro assay

4.4.1.10.1. Material conditioning and cell seeding

Mesenchymal stem cells (MSCs) and endothelial progenitor cells (EPCs) obtained from rat bone marrow were used for this study. These two types of cells were chosen according to published results that demonstrated the potential of this glass system to promote mesenchymal stem cell differentiation into osteoblastic cell lineage and endothelial progenitor cell differentiation towards phenotype involved in vascularization [29–31]. Squares were cut from the fibers layer produced to fit in a 24 well-plate, sterilized by immersion in ethanol for 15 min under UV radiation, pre-incubated for 2 hours in complete medium at 37°C and rinsed with PBS before seeding. Cells were seeded at a density of 10 000 cells/disc in 24 well-plates.

4.4.1.10.2. Fluorescence staining

After 24 hours, cells were fixed using a paraformaldehyde-sacarose-H_2O-PBS solution to observe them thanks to fluorescent staining. 4,6-diamidino-2-phenylindole (DAPI) was used to stain the nuclei and green phalloidin for the actin cytoskeleton. Fluorescent images were collected using a confocal microscope with a x63 objective lens (oil immersion).

4.4.1.10.3. Cell fixation for FESEM imaging

Cells were also fixed using a glutaraldehyde-PBS solution and then lyophilized before carbon coating to be observed under FESEM. Pictures with cells fixed on the scaffolds were obtained with the same device and under the same conditions than the images of the fibers without cells.

4.4.2. Results

4.4.2.1. Fiber morphology, thickness, composition and wettability

Results obtained regarding the fiber morphology, thickness and wettability are shown in **Figure 4-5**. Differences in the fiber surface morphology were observed before and after coating. Coated fibers showed a rough nanostructured topography, whereas PLA fibers exhibited a smoother one. Also, the roughness of the coated S40 fibers seemed to be lower than that of the S60 fibers.

Measurements of fibers diameters, before and after coating, were made to evaluate the increase in diameter obtained after the coating. In comparison to the PLA fibers diameter (686 ± 48 nm), coated fibers showed an increase in their thickness: 976 ± 84 nm and 770 ± 66 nm for the S60 and S40 fibers,

respectively, which corresponded to thicknesses of ~ 150 nm for the S60 coating and ~ 45 nm for the S40 one. The coating with the lower silicon content seemed thus to lead to a thinner layer of coating.

The exact composition of the coating was determined by EDS measurements (**Table 4-3**). The first composition of the coating (molar percent ratio) was 60Si: 32Ca: $8P_2$ (coated S60 fibers) and the second one 39Si: 46Ca: $15P_2$ (coated S40 fibers).

According to water contact angle measurements, both hybrid scaffolds showed excellent hydrophilic properties in comparison to the PLA ones. No significant difference was observed between the wettability of the coated S60 fibers and S40 ones.

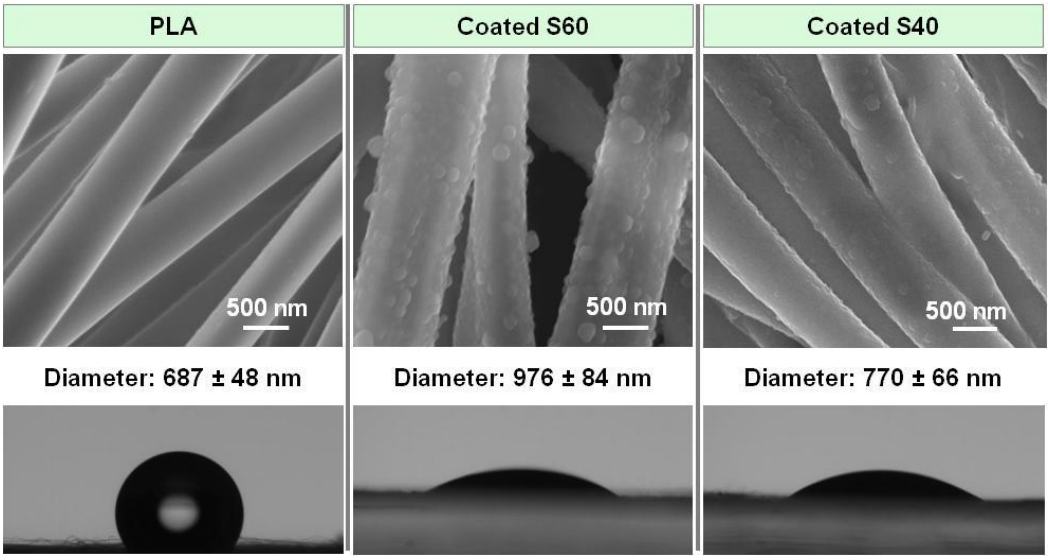

Figure 4-5. Surface morphology (FESEM images), thickness and wettability (contact angle pictures) of PLA and coated fibers.

Table 4-3. Composition of coated fibers (molar ratio) measured by EDS.

	Coating composition S60	**Coating composition S40**
Si %	59.71 ± 8.89	38.67 ± 2.78
Ca %	32.11 ± 6.20	45.85 ± 4.16
P_2 %	8.18 ± 4.85	15.47 ± 2.05

4.4.2.2. AFM measurements

According to AFM measurements, the DMT modulus of PLA scaffold as well as the roughness was significantly increased after coatings (**Figure 4-6**). The coated S60 fibers exhibited an average DMT modulus of 42.29 ± 4.24 MPa and the coated S40 ones of 60.63 ± 5.81 MPa, while PLA fibers showed a value equal to 3.84 ± 0.32 MPa. Comparing the coated fibers, the fibers with the lower silicon content exhibited the lower stiffness. As noticed on the FESEM pictures, coated S60 fibers seemed to be rougher than coated S40 ones. The measurements of the fiber surface roughness confirmed that after coating, the

roughness of the fibers was increased. R_q values revealed indeed that the roughness of PLA fibers was doubled after being coated with the S40 ORMOGLASS composition, while increasing five-fold after being coated with the S60 ORMOGLASS composition. The lower the silicon content, the higher the roughness.

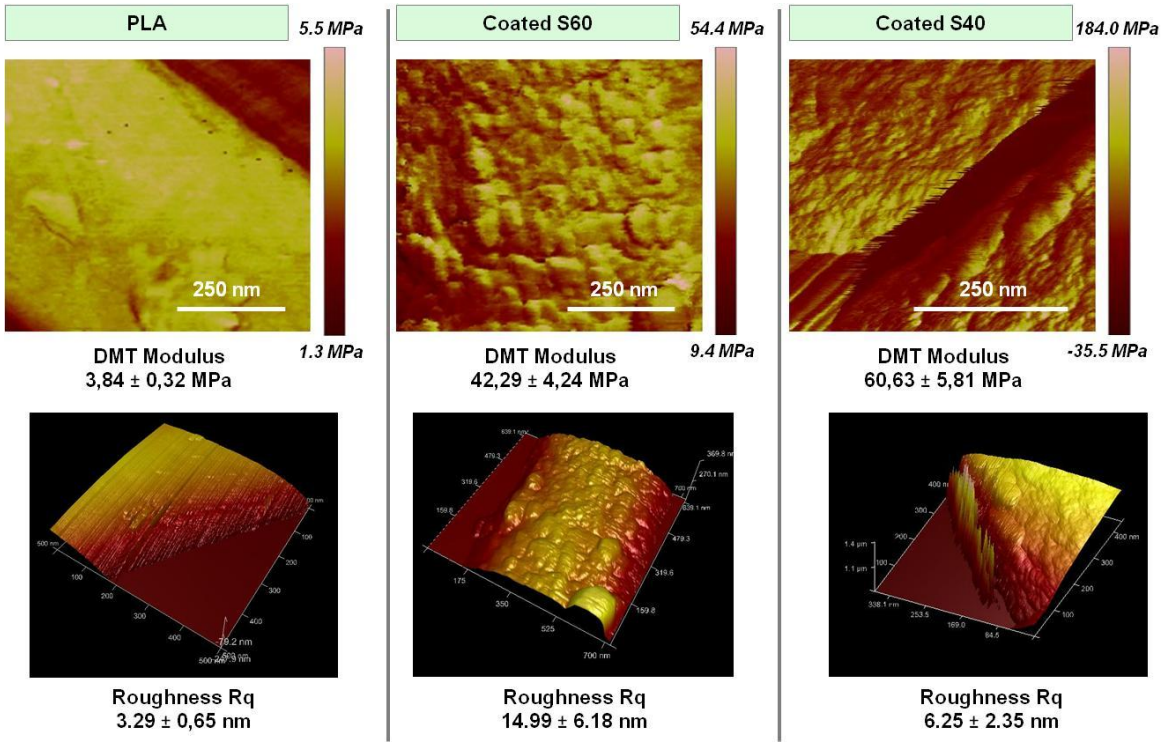

Figure 4-6. DMT Modulus and roughness (3D images) of PLA and coated fibers measured by AFM.

4.4.2.3. Tensile tests

While AFM measurements enabled to determine the local mechanical properties of the fibers, tensile tests enabled to evaluate the mechanical properties of the whole scaffold. Histograms in **Figure 4-7** displays the values of the Young's Modulus and Yield Strength obtained by this assay for the PLA and coated fibers (strain-stress curves are reported in appendix A-5, A-5-3). For both coating compositions, the Young's Modulus and the Yield strength were significantly increased in comparison to the pure PLA scaffold. S60 fibers had a Young's Modulus sixfold higher than non-coated ones. S40 fibers also exhibited a remarkable property: they reached almost fivefold the value of the PLA fibers. The coated fibers with the lower silicon content appeared to be the stiffer material of the study, in term of mechanical properties of the whole construct.

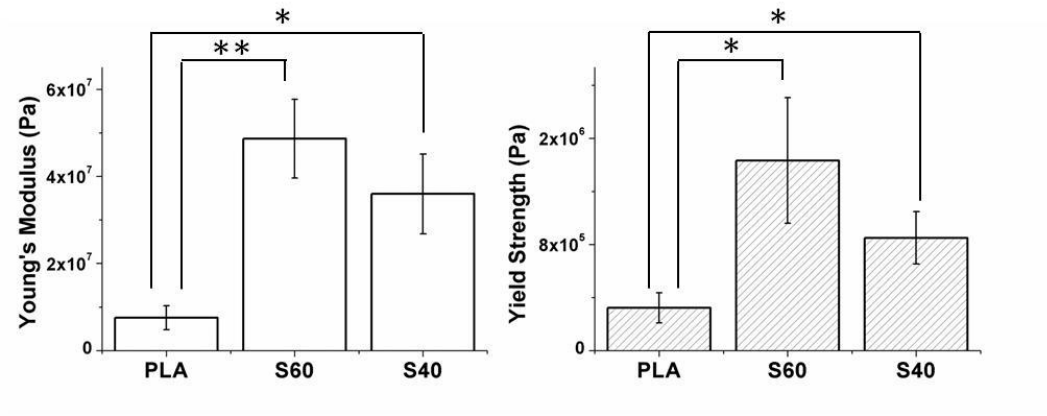

Figure 4-7. Histograms displaying the Young's Modulus and Yield Strength of PLA and coated fibers (tensile test measurements - *: statistical difference $p < 0.05$, **: statistical difference $p < 0.002$).

4.4.2.4. Thermogravimetry

In order to quantify the amount of coated ORMOGLASS, thermogravimetry analysis was performed. This technique is widely used to determine the percentage of inorganic phase contained in hybrid organic-inorganic materials and to assess material stability [32,33]. As organic compounds degrade at lower temperatures, it is possible to evaluate the quantity of the inorganic part of the glass that was grafted on the polymeric fibers when applying the proper heat treatment. As seen on **Figure 4-8**, the remaining glass mass percentage (non degraded phase) related to the coated S60 fibers was higher than the one of the coated S40 fibers (5.6 and 1.7% respectively). Correlated to the fibers' thickness measurements, this seemed to confirm that less glass has been coated for the low silicon content composition than the one with the higher silicon content.

From the TGA assay, information about the degradation byproducts can be also obtained. Indeed, differences on the derivative curve graphics were observed: peaks at ~ 77°C and ~ 270°C that were not observed on the PLA curve clearly appeared on the coated S60 fibers curve. The first peak is not observed for the coated S40 fibers, but a very small shoulder can be seen for the second one. To determine to which compounds these changes were related to, measurements with TGA coupled with FTIR were performed. The peak at lowest temperature was attributed to the presence of triethoxysilane molecules and the second one to the degradation of PLA, as well as the third peak common to all fibers samples (see appendix A-5, A.5.4). As the first peak was related to a compound contained in the ORMOGLASS (organosilane), it should be also considered to evaluate the real amount of ORMOGLASS coated. Taking into account the weight percentage loss of this compound, the amount of ORMOGLASS coated for the S60 fibers was finally equal to 7.7%, and not 5.6% as initially mentioned. For the coated S40 fibers however, the weight loss of the triethoxysilane was not considered as it was almost not detected by the TGA assay. Thus, S40 fibers were considered to have a remaining percentage of inorganic phase equal to ~ 1.7%.

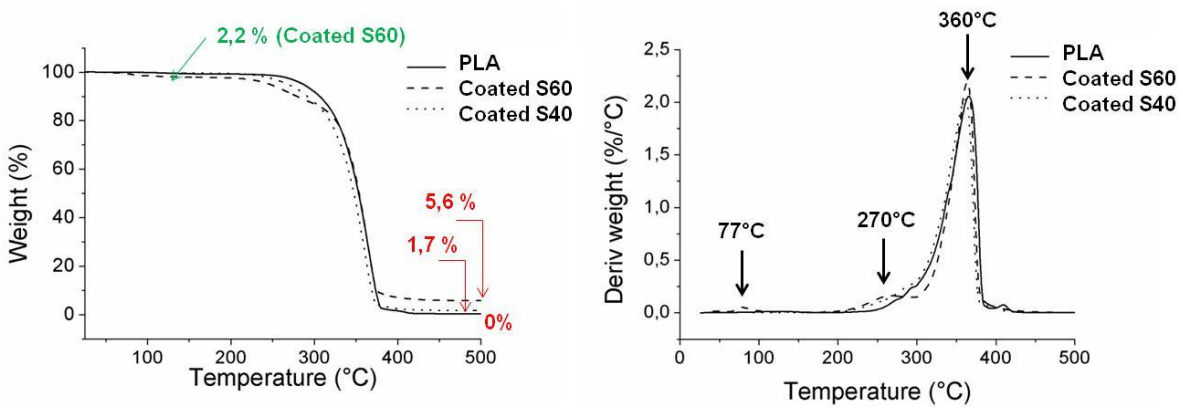

Figure 4-8. Thermogravimetry analysis of PLA and coated fibers (representation of TGA and DTA curves). The percentages in red represent the amount of inorganic ORMOGLASS remaining at the end of the assay. The percentage in green corresponds to the weight loss associated to the degradation of triethoxysilane molecules (peak at 77°C) in the coated S60 fibers. For the S40 fibers, this change is not significant and is therefore not shown.

4.4.2.5. Fiber morphology after thermal treatment

Figure 4-9 shows the morphology of coated S60 fibers after the applied thermal treatment to measure the thickness of the inorganic shell. A tubular structure was observed. Measurements of the thickness of this organic shell gave an averaged value of 72 ± 14 nm. These pictures also revealed that the coating seemed to be achieved as a monolayer of glass particles. Unfortunately, it has not been possible to obtain such pictures for the calcination of the coated S40 fibers. In fact, it seemed that this shell was too thin and that the tubular structure collapsed during the preparation of the samples for FESEM observations (appendix A-5, A.5.5). It is also highly probable that the tubular structure was already affected by the thermal treatment itself. If the thickness is very thin as suggested by the fiber diameter measurements, it might be that they cannot resist stresses provoked by the shrinkage of the glass network during the heating ramp, resulting in the collapse of the structure.

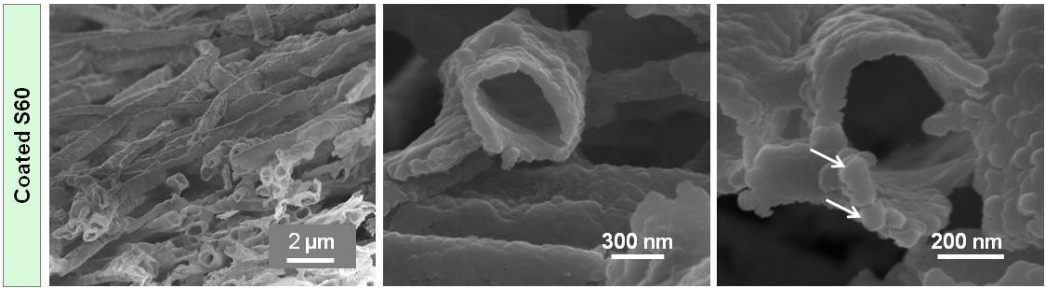

Figure 4-9. FESEM images of the remaining inorganic shell after the thermal treatment in the furnace of the coated S60 fibers.

4.4.2.6. DSC measurements

DSC curves are displayed in **Figure 4-10**. Thermal characteristics of the PLA and coated fibers extracted from these curves are summarized in **Table 4-4**. This assay was performed to determine whether changes in the polymer occur after applying the coating protocol. Curves analysis showed that

the melting onset (T_m onset) and crystalline onset (T_c onset) temperatures of both coating compositions are shifted towards higher values than the ones associated to pure PLA fibers (presenting the typical thermal curve of a semicrystalline polymer). For the coated fibers, the T_c onset is increased of ~ 12-13° and the T_m onset of ~ 2°. Also, it was noticed that the intensity of T_c exothermal peak was more intense and well defined for the pure PLA fibers than the one observed for the coated fibers. This was well reflected by the different dH_c values. On the other hand, the crystallinity of the coated fibers (around 44%) significantly increased in comparison to the one of the PLA fibers, which initially had a low crystalline percentage (10%).

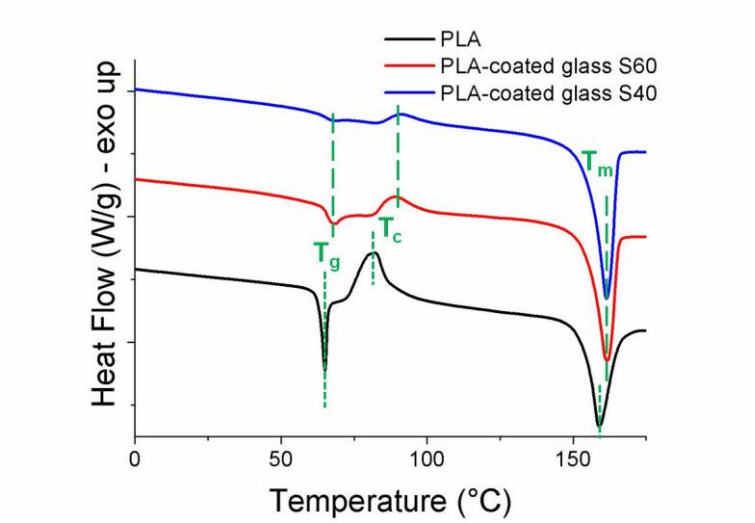

Figure 4-10. DSC thermograms (first heating ramp) of PLA and hybrid coated fibers (T_g: glass temperature, T_c: crystallization temperature, T_m: melting temperature).

Table 4-4. Thermal properties of PLA and coated fibers extracted from the DSC thermograms.

	T_m onset (°C)	T_m peak (°C)	ΔH_m (J/g)	T_c onset (°C)	T_c peak (°C)	ΔH_c (J/g)	Crystallinity (%)
PLA	153,44	159,08	34,51	72,42	82,23	24,55	10,70
S60	155,27	161,39	39,80	86,54	92,50	1,84	44,22
S40	155,36	161,29	43,89	85,07	91,85	4,01	43,57

4.4.2.7. DLS measurements

The measurements of particle size in function of the hydrolysis ratio for both ORMOGLASS compositions are presented in **Figure 4-11**. Results showed that the size of the particles prepared with the S60 composition was greatly influenced by the quantity of water introduced in the ORMOGLASS precursor mix to perform the hydrolysis. The higher the hydrolysis ratio, the bigger the particles. Size evolution seemed more precisely to follow an exponential increase. Modifying the hydrolysis ratios,

particles ranging from 100 nm to 1.5 µm in diameter could have been produced. For the S40 particles, results showed that the particle size was also influenced by the amount of water introduced in the ORMOGLASS precursor mix to perform the hydrolysis but that the changes were less drastic than for the S60 particles. In fact, only a slight linear increase of particle size was observed with the increase of the hydrolysis ratio for the S40 particles. Moreover, the particles appeared to be much smaller, ranging from 50 to 100 nm in diameter.

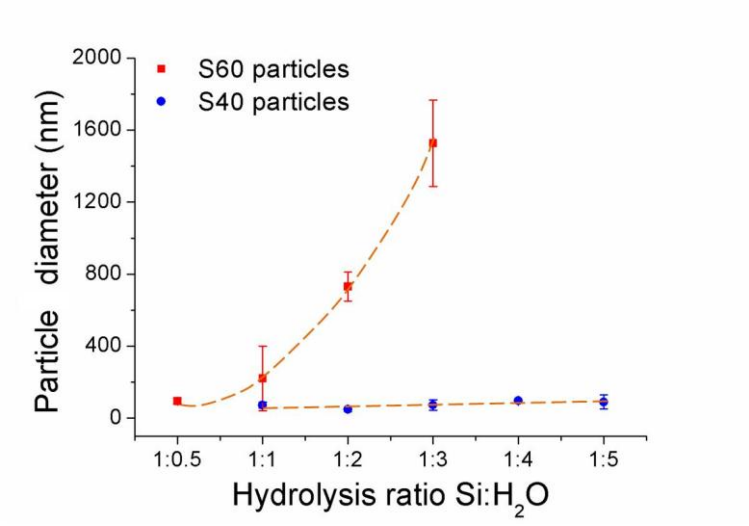

Figure 4-11. Influence of the hydrolysis level on the size of particles prepared with two different molar compositions (comparative graphic).

4.4.2.8. Calcium dissolution and pH measurements

The dissolution profile of calcium of the materials and the associated pH measurements are displayed in **Figure 4-12**. The main changes occurred during the first two days. A burst release of calcium was particularly observed immediately after the material immersion. Then, during these two days, calcium was released in a less drastic manner. After this time, the material did not seem to release calcium, or in a very low concentration. It can be moreover noticed that S60 fibers released a higher amount of calcium than the S40 fibers and that they exhibited the higher burst release during the first minutes. The pH measured in the extracts decreased significantly at the initial stage of the assay and tend to stabilize afterwards.

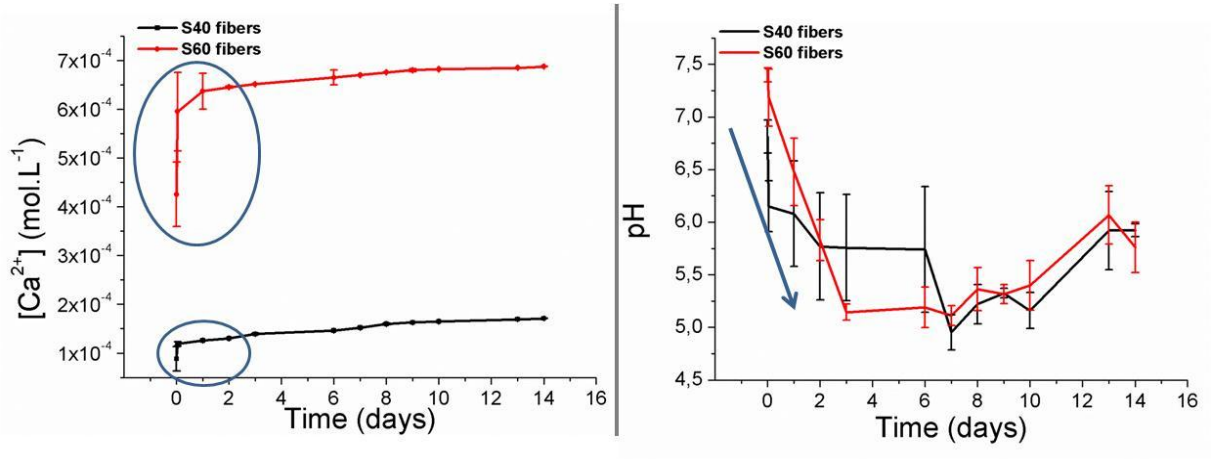

Figure 4-12. Calcium dissolution profiles of the coated fibers and pH measurements. Blue circles denote the main changes occurring in the solution and the blue arrow symbolizes the pH decrease at the beginning of the assay.

4.4.2.9. Mineralization potential

Figure 4-13 presents the FESEM pictures of the PLA and coated fibers after the successive immersions in calcium and phosphate solutions. It can be observed that for the PLA fibers, only few calcium phosphate particles deposited on the fibers surface. Actually, it seemed that these particles were not really deposited on the mat, but rather trapped in the template due to the tortuosity of the fibers. On the contrary, coated fibers clearly possessed calcium phosphate precipitated on their surface. The CaP induction homogeneously occurred over the fibrous mats and the calcium phosphate compound strongly attached to the fibers (not removed after the ultrasonic bath). X-ray diffraction performed on the CaP-induced coated fibers revealed that in the conditions used for this assay, brushite was deposited (see appendix A-5, A.5.6 and appendix B-14). Brushite ($CaHPO_4.2H_2O$, also known as dicalcium phosphate dihydrate) is a precursor for hydroxyapatite deposition and is commonly used to initiate the mineralization of scaffolds [34–36].

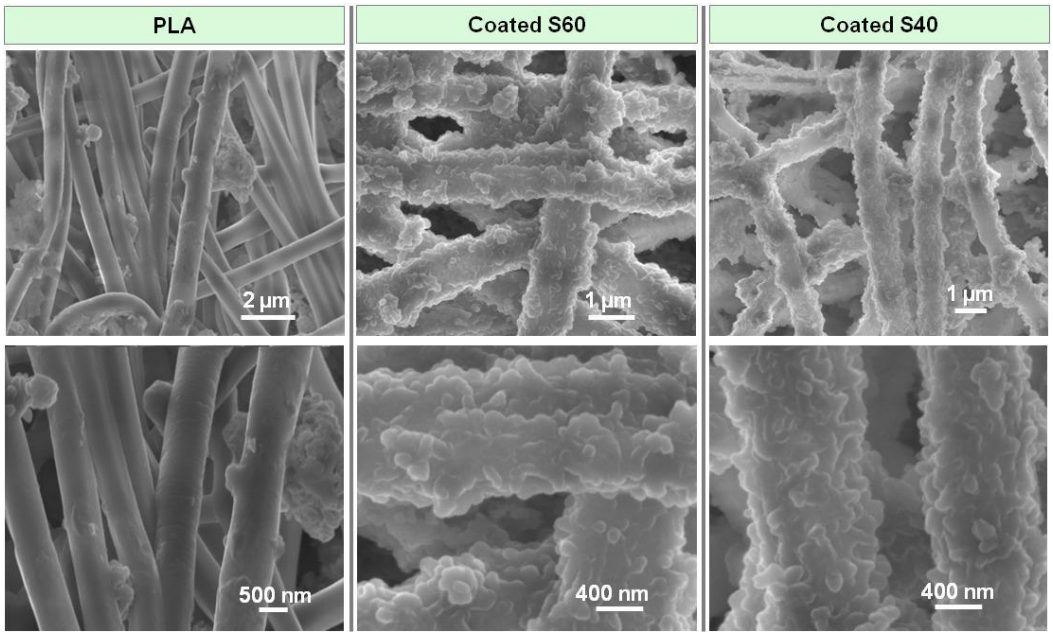

Figure 4-13. FESEM images of PLA and coated fibers after their immersion in calcium and phosphate solutions alternatively.

4.4.2.10. Cell adhesion and spreading

After 1 day of culture on the produced materials, EPCs and MSCs were fixed and stained with specific fluorophores to assess their morphology. Pictures obtained from confocal microscope imaging revealed that both cell types restricted their spreading on PLA fibers, whereas they spread significantly on the coated fibers for both coating compositions (**Figure 4-14**). Cells on polymeric scaffolds presented a round shape with only few branches, while on the coated ones cells tended to better ramify and extended their cytoskeleton. Stress fibers were even observed inside the cells.

Cells were also observed under FESEM in order to visualize the interactions between the cells and the scaffolds. The assessment of the FESEM pictures confirmed the observations made thanks to the fluorescent staining. Cells globally presented a rounder shape on PLA fibers than on the coated ones (**Figure 4-15**). Additional pictures at higher magnifications were taken to show better how the cells spread and attached to the coated fibers (**Figure 4-16**). Cells spread greatly on the fiber length and also extended cytoplasmic projections towards neighboring fibers (filopodia).

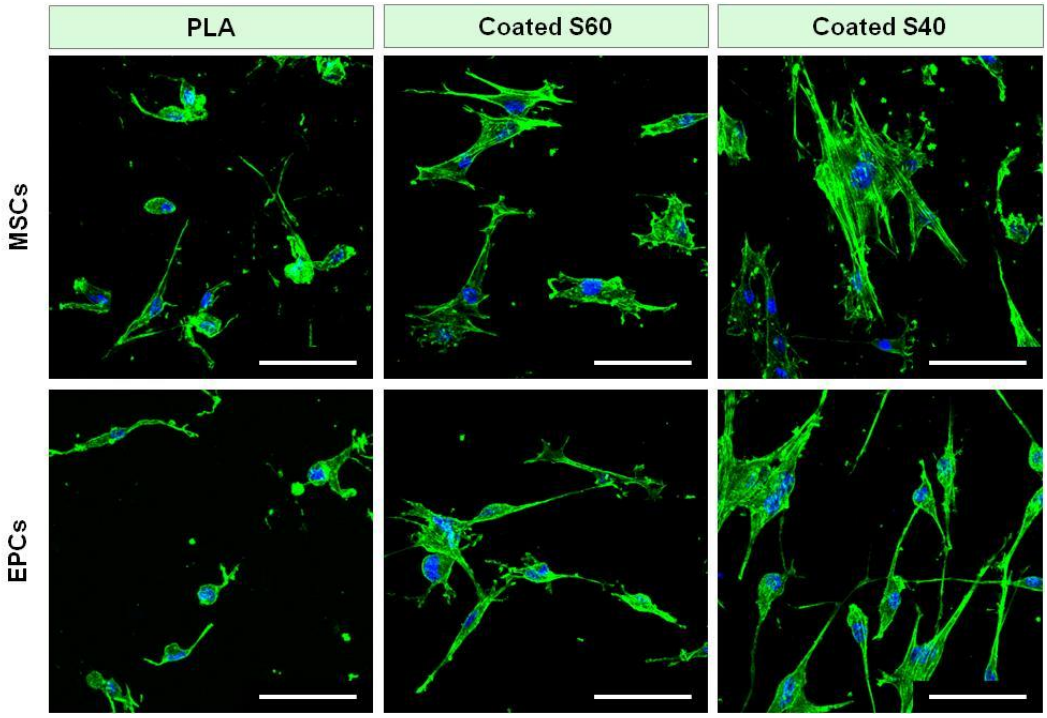

Figure 4-14. Pictures of cells adhered on non-coated and coated fibers after 1d of culture (confocal microscope images of fluorescence staining: blue for the nucleus, green for the cytoskeleton - scale bars: 75µm).

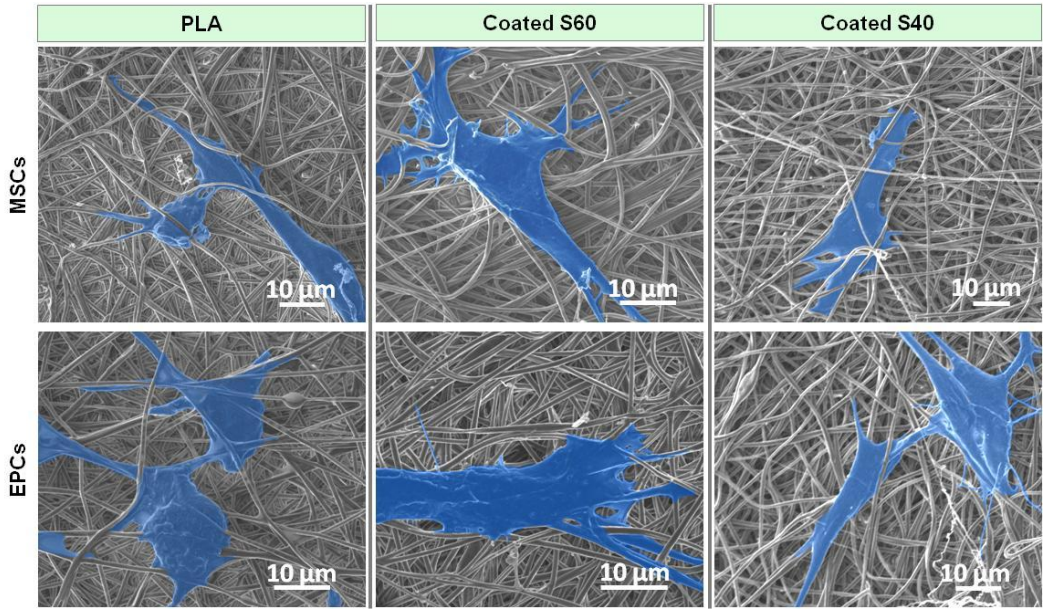

Figure 4-15. Pictures of cells adhered on non-coated and coated fibers after 1d of culture (FESEM images - cells artificially colored in blue to better visualize the cells on the scaffold)

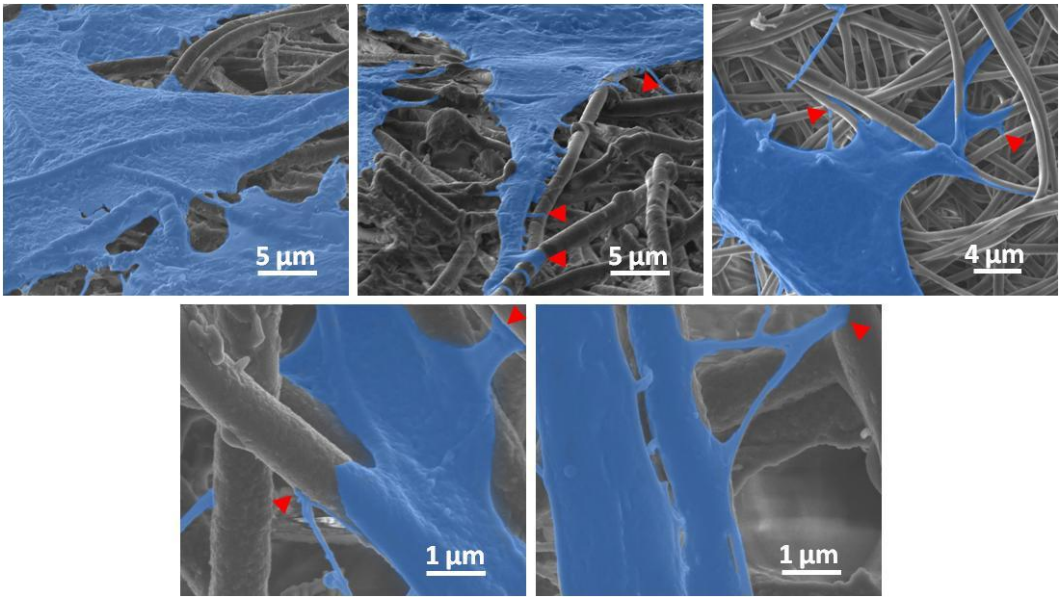

Figure 4-16. High magnification pictures of cells adhered on coated fibers after 1d of culture (FESEM images - cells artificially colored in blue to better visualize the cells on the material, red arrows point the filopodia).

4.4.3. Discussion

Novel hybrid fibers have been successfully produced by the sol-gel method and a succession of surface treatments. The fabrication of these fibers consists in the coating of polymeric fibers with ORMOGLASSES. The coating relies on the covalent bonding of ORMOGLASS nanoparticles to the fibers surface. FESEM images revealed that the fibers were homogeneously coated all along the fiber length (**Figure 4-5**). This attested that the protocol had been properly developed to avoid problems related to a non homogeneous coating such as partial coating of the fibers, coating of the first fibrous layer only or deposition of a dense coupling agent layer (see appendix A-5, A.5.7). The coated fibers exhibited a nanoroughness, a higher diameter than the pure PLA fibers and an improved wettability (**Figure 4-5**).

According to AFM measurements, the roughness of the fibers was higher on the fibers coated with particles having the higher silicon content (**Figure 4-6**). This suggested that there is an intimate relationship between the roughness and the glass particles composition, influencing ultimately the fibers' topography. As confirmed with the DLS measurements, the composition of the ORMOGLASS significantly affected the particles size. Particles with the higher silicon content (coated S60 fibers) were bigger than the ones prepared with the lower silicon content (coated S40 fibers) (**Figure 4-11**), and this, independently from the hydrolysis ratio considered to prepare the glass particles. Because bigger particles were used to produce the coated S60 fibers, these fibers exhibited the higher roughness [37]. It confirmed thus that roughness and ORMOGLASS composition were related. Using AFM, the stiffness of the fiber surface was also measured (**Figure 4-6**). Results clearly revealed that, after the coating, the stiffness of PLA fibers was significantly increased and that different ORMOGLASS particle compositions led to different stiffness. It can thus be concluded that the particles composition not only affected the roughness of the fibers but also its local mechanical properties.

About the whole mechanical properties of the templates, tensile tests showed that the coated fibers had higher Young's modulus and yield strength than non-coated ones (**Figure 4-7**). In particular, the coated S60 fibers were the fibers having the higher values. These results are in agreement with the other studies reported in the literature that showed the improvement of tensile properties in polymeric material containing a calcium phosphate compound such as hydroxyapatite or bioactive glass [38,39]. The differences between the coated S60 and S40 fibers may be attributed to the differences in coating thickness (revealed by the fiber diameter measurements and TGA assay) and also to the differences in their intrinsic composition. A particularly interesting point of these novel fibers is that, even though their stiffness and global toughness were enhanced, the hybrid scaffolds remained perfectly flexible (see appendix A-5, A.5.8). The material was indeed within an interesting working range, where it is ductile and has a low fragility. In comparison to other hybrids [3,40], this feature is particularly remarkable for a material that has glass as one of its constituents. This is due to the use of an ORMOGLASS rather than a fully inorganic one [41,42] and the continuity of flexibility maintained between the polymeric structure and its non-brittle coating. No delamination of the ORMOGLASS is observed when bending the material, and it can easily be manipulated to fill bone defects with any shape. The coating approach offers thus the possibility to enhance the stiffness of pure polymeric structures and to reach values closer to that of the calcified bone while remaining flexible.

Based on the diameter of the fibers, before and after coating, S60 fibers seemed to have a thicker layer of ORMOGLASS bonded on their surface (**Figure 4-5**). Thermogravimetry assay performed to assess the ORMOGLASS coatings validated these measurements. Indeed, the percentage of inorganic mass that remains after the TGA thermal treatment was higher for the coated S60 fibers than for the coated S40 ones (**Figure 4-8**). This attested that a higher amount of ORMOGLASS was bonded in the case of the coated S60 fibers. This can be explained by the bigger size of the S60 particles. As the coating appeared to be achieved as a monolayer of particles, the bonding of big particles rationally led to a thicker coated layer and consequently to a higher percentage of inorganic compound at the end of the TGA assay. However, the percentage of inorganic phase measured after the TGA thermal treatment did not represented the exact amount of ORMOGLASS coated; this was for two reasons. The first is that, based on the DTA curve of the TGA, triethoxysilane molecules degraded during the thermal treatment. As these organosilanes are related to the glass, the amount of these molecules should be also considered for the evaluation of the amount of glass coated. The detection of triethoxysilane compound can be associated to the presence of non reacted molecules that could have been trapped in the ORMOGLASS network during its formation [43]. As this peak is not observed for the coated S40 fibers, it was assumed that this coating possesses only residual silanes molecules, whose concentration are lower than the detection limit of the device. Complementary gas chromatography assay actually revealed that silanes were indeed found in the S40 fibers, although they were not clearly revealed by the TGA assay (see appendix A-5, A.5.9 and appendix B-15). These silanes molecules might remain in the coatings because of the fast formation of the colloidal suspension that could have led to the quick encapsulation of non reacted molecules [44]. The

second reason that can explain that the percentages of determined weight loss did not correspond to the exact amount of glass coated is that the particles were made of an ORMOGLASS. This means that organic fragments of the ORMOGLASS also degraded during the TGA assay. However, they were not directly accounted for the weight percentage of ORMOGLASS grafted as they were not revealed by the TGA. It is believed that the degradation of these organic fragments occurred at a concentration that did not enable their detection - as for the triethoxysilane molecules contained in the S40 particles covering PLA (coated S40 fibers) - or that their signals were possibly masked by peaks of the other reactions. Despite the inability to measure exactly the mass of the ORMOGLASS coated using TGA, it is assumed that the values determined can give an indication on the real weight percentage of ORMOGLASS coated. It is however recognized that, the real amounts of glass should be slightly higher than those identified by the TGA measurements. To have a direct evaluation of the amount of coated glass, one can reasonably think to use a balance and to quantify the increase of weight of PLA fibers after coating. Such "weight-monitoring" assessments are commonly used for example to control the degradation of macroscopic composites possessing a significant amount of inorganic phase (micrometer scale particles) [45,46]. However, in the case of the coated fibers, the coating is achieved at the nanoscale. It is therefore very difficult to measure weight changes with the usual balances present in the laboratory, given the thinness of the coating. Moreover, weighing the fibers is already a challenge as they are very light. A balance with an extremely high sensitivity would be thus required to perform such measurements.

The proof that the coated ORMOGLASS lost polymeric fragments during the thermal treatments, and that, as a result, the amount of inorganic compound weighted by TGA did not correspond to the exact mass of coated ORMOGLASS, is provided by several data: the fiber diameter measurements (before and after coating), the particle size measurements and the inorganic shell diameter measurements performed after calcinations. Indeed, according to the fiber diameter measurements, the thickness of the S60 coating was evaluated to 150 nm and the one of the S40 to 45 nm. These values were in quite good accordance with the DLS measurements that measured the S60 particles within the range of 100 nm and 300 nm (hydrolysis ratio 1:1) and the S40 ones within the range of 40 nm and 70 nm (hydrolysis ratio 1:2). These measurements corresponded to ORMOGLASSES particles (inorganic/organic glass). To the contrary, the measurements performed on the shell remaining after the calcination treatment in the furnace corresponded to pure inorganic glass particles. These measurements showed that size of the particles was reduced after the thermal treatment: the S60 particles had a diameter equal to 72 nm (**Figure 4-9**). The fact that the tubular structure was easily destroyed after the thermal treatment of the coated S40 fibers may suggest that the size of the inorganic remaining particles was very low. These differences in measurements before and after thermal treatments can be explained by the loss of the organic fragments contained in the ORMOGLASS particles during the heating. The glass which was prepared by the partial hydrolysis of a mix containing alkoxides possessed organic groups in the network (i.e non hydrolyzed organic ligands from alkoxides). Therefore, when these groups were degrading, a shrinkage of the ORMOGLASS may have occurred, resulting in a decrease of the layer thickness.

About the polymeric thermal properties, TGA assay revealed that for the coated fibers, a small part of the polymer decomposed before the degradation of the main part of the PLA (novel peak observed at 270°C for the coated fibers). This suggests that the coating influenced the thermal degradation of the polymer and favored the decomposition of some polymeric fragments before the usual PLA degradation temperature (characteristic peak at 360°C). This can be explained by the degradation of short polymeric fragments created by the hydrolysis of the fibers during the first surface treatment (chain scission-depolymerization) and the formation of OH chain ends. This promoted the earlier thermal decomposition of some polymeric fragments as lactide or oligolactides by favoring the backbiting ester interchange reaction occurring during thermal decomposition of PLA [47,48]. On the other hand, DSC results also showed that the thermal properties of the polymer were affected by the coating. It revealed, for example, a significant increase in the onset crystallization temperature (**Figure 4-10**, **Table 4-4**), meaning that more energy was needed to make crystallize the amorphous PLA phase. This reflected the mobility limitations of the polymer chains after coating. One explanation can be that the bonding between the glass and the polymer prevents the rearrangement of the polymer chains in a well-ordered phase by restricting their mobility ability. This suggests that strong interactions between the polymer and the glass might have been efficiently created. This affirmation is supported by a study performed by Pluta *et al.* that showed that an increase in the crystallization temperature is observed when the interactions between the composites' constituents are improved [32]. The fact that the crystallization peak is also less intense for the coated fibers (lower dH_c values) possibly means that less amorphous phase can be ordered after the coating protocol. Regarding the melting temperature, a small increase of ~ 2°C was revealed. This demonstrated a slight improvement in the thermal stability of the crystalline phase of the composites. This suggested that even if PLA was hydrolyzed during the first coating treatment and a decrease of the T_m could be expected [27], the strong interactions between the polymer and the ORMOGLASS may have compensated this possible decrease. Moreover, the crystallinity of the coated fibers was significantly higher than the one of pure PLA fibers. Complementary X-ray data confirmed that after the coating process, a crystalline phase attributed to the PLA compound was formed (see appendix A-5, A.5.10). This can explain that less amorphous phase can be ordered after the coating, as part of it seemed to already have undergone crystallization during the coating treatments. The ORMOGLASS coating seemed thus to act as a nucleating agent that induced a partial PLA crystallization. This increase of crystallinity could have been also interpreted as a result of the hydrolysis applied on the polymer fibers (first treatment step of the protocol) and a chain auto-rearrangement process. This option has been however discarded based on additional DSC assays. In fact, no difference in crystallinity was observed between raw PLA fibers and hydrolyzed PLA fibers, meaning that the applied hydrolysis had almost no effect on the polymer crystallization (see appendix A-5, A.5.11). Also, in their study on PLA-nanocomposites, Pluta and coworkers demonstrated that PLA crystallization was mainly influenced by the interactions between the compounds rather than the molecular weight of PLA [32]. These two facts tend to show that the coating indeed induced partial crystallization of the PLA. This increase of crystallinity could be moreover an

additional explanation for the shift observed in the crystallization temperatures associated to the coated fibers. The already ordered parts might have hindered the organization of the potentially structurable chains. According to this crystallinity level, it can finally be concluded that the mechanical properties previously assessed by tensile tests are not only due to the presence of the glass but also to this crystallinity gain [49]. Both aspects might contribute to the modifications of the mechanical properties of the scaffold. To summarize, except that a small part of PLA vaporized before the usual decomposition temperature of PLA (TGA), thermal properties of PLA were globally increased after the coating. This represents a good advantage over other hybrids as many of them commonly have lower melting and crystallization temperatures than pure polymeric material [25,50].

The size of the ORMOGLASS particles is clearly determined by the precursor mix composition and the degree of hydrolysis of that mix (**Figure 4-11**). This is especially true for the S60 particles, which size was significantly affected by the amount of water introduced to the mix to prepare the particles. The higher the silicon:water ratio, the bigger the particles. This demonstrated that the particles size can be controlled by selecting specific hydrolysis ratios. Kim *et al.* also described this ability [51]. Consequently, based on these observations, it is believed that this experimental parameter can be used to tune the fiber roughness and coating thickness. The fact that smaller particles are obtained for the S40 ORMOGLASS than for the S60 ones can be explained by its lower TEOS content. Silicon from TEOS is indeed expected to be the main building block network of the glass in which calcium and phosphate are incorporated. If less TEOS molecules are available in the glass precursor mix, it may have reduced the extent of condensation process (Si-O-Si based network) and resulted in the formation of smaller particles. Finally, the fact that the increase in the hydrolysis ratios did not induce significant changes in the S40 particle size may signify that the nucleation process already reached a critical point that did not enable a further significant growth of the particles [52].

As demonstrated in the literature and in the chapter 2, calcium release is essential for the regulation of cell behaviors. A higher amount of calcium was released for the coated S60 fibers than for the coated S40 ones (**Figure 4-12**). Taking into account the higher calcium content of the coated S40 fibers (intrinsic composition of the ORMOGLASS), a higher calcium release was expected for these fibers. Though, as described above, the coating of the S60 fibers was much thicker than the one of the S40 fibers. It is therefore possible that after the coating, a higher amount of calcium is measured for the coated S60 fibers in comparison to the S40 ones. It can be also that calcium was less well incorporated in the ORMOGLASS network and that consequently, it was released in a more drastic manner immediately after immersion. Globally, the burst release and subsequent stable calcium concentration is a typical dissolution behavior observed for melt and sol-gel derived glasses [53]. The dissolution profiles obtained with these fibers are particularly in good accordance with the ones reported by Yu *et al.*, who assessed the *in vitro* dissolution in water of sol-gel Si-Ca-P_2 glasses also prepared with calcium methoxyethoxide: the major changes in the calcium release profile occurred during the first two days. Afterwards, in the longer term, the calcium concentration remained stable. The direct comparison with other studies is however

difficult and not always relevant as the materials are usually prepared through different fabrication method, using different constituents and assessed in different solutions [53–55]. Concretely, as these fibers constitute a novel class II material, it would have been interesting to compare the obtained results with another class II material, as for example the one prepared by Poologasundarampillai *et al.* [56]. But in their study, they assessed the dissolution behavior of the material in SBF (not in water) and the material is prepared with calcium chloride. Therefore, when the ion release profile is assessed and compared, it should be always kept in mind that differences in assessment conditions between the studies exist and that it influences the final material dissolution behavior. This is especially true in the long term because buffering solutions (such as SBF) regulates the pH changes, and consequently may slow down the degradation rate of the material in comparison with using water. This means that the ion release profile of the materials is affected by the selection of the solution in which the assay is conducted. Consequently, in the long term, a comparison is not adequate in such conditions. The only comparison that can possibly be considered as relevant should be done shortly after the material immersion; during the time that the buffering solution has not reached its equilibrium yet. Considering that, the coated fibers exhibit the same behavior than the material developed by Poologasundarampillai *et al.*: a burst release of calcium occur immediately after the material immersion. From a general point of view, the coated fibers have thus a similar calcium release profile than materials potentially comparable described in the literature (i.e. containing calcium methoxyethoxide, being sol-gel derived glasses and being a class II material).

The bioactivity of a material in bone tissue engineering is commonly approached by assessing its ability to deposit calcium phosphate on its surface when incubated in simulated physiological fluid. Bioactivity is an essential property for bone tissue engineering as it enables to improve the integration of the scaffold with the host tissue. Common inorganic bioactive glasses based on Si-Ca-P_2 system are well-known for that purpose. They indeed induce the precipitation of a calcium phosphate layer at the material-body interface, favoring the strong anchoring of the implant. In the case of the coated fibers, CaP induction assay revealed that these hybrids exhibited an excellent mineralization potential (**Figure 4-13**). In fact, compared to pure PLA fibers, they were homogeneously covered with brushite; a compound known as a precursor for hydroxyapatite deposition under physiological conditions [35] (appendix A-5, A.5.6). This suggested that the coated fibers initiated the mineralization process more efficiently than pure polymeric fibers. This behavior was attributed to the direct exposure of the ORMOGLASS at the fibers' surface and the presence of silanol groups in the glass network (see FTIR results, first part of the chapter). Silanols groups act as nucleation sites for the deposition of calcium phosphate compounds [57]. According to the literature, calcium and phosphate also play a role in the deposition of minerals because they promote the supersaturation of the fluid in which the assay is conducted [58,59] (SBF or DMEM for examples [34]). However, this is observed in experiments performed over several days or hours. In the case of the alternate soaking method, the immersion is performed in a very limited time (30 sec for each immersion). It is therefore not very probable that calcium and phosphate contributed significantly to the

deposition of brushite. Also, the CaP induction was done under stirring. It is thus believed that the supersaturation mechanism that could have hypothetically occurred even during this short time of immersion may be disturbed by the solution movement. Consequently, the silanols are supposed to be the main responsible factor that promoted the efficient mineral deposition. Regarding this assay, it should be finally specified that this test was performed to evaluate the potential of the new hybrid scaffold to mineralize in comparison to the pure PLA one. However, the results obtained do not prove that fibers would mineralize under milder conditions (solutions with lower calcium and phosphate concentration). For this reason, other tests such as long immersion in SBF [60] or implantation in bone cavity defects [38,61] should be performed to validate the observations done thanks to this preliminary mineralization assay.

As described previously, the materials developed in this study aimed to improve interactions between the cells and the material. To verify that the exposure of the bioactive phase directly at the material surface had a positive effect on cellular response, a preliminary *in vitro* assay was performed with EPCs and MSCs. After one day, the spreading of the cells was better on the coated fibers than on the PLA ones (**Figure 4-14**, **Figure 4-15**, **Figure 4-16**). Stress fibers were even observed inside the cells. Moreover, numerous filopodia were observed on the FESEM pictures of cells cultured on the coated fibers, what demonstrated the good health and adhesion of cells on the scaffold [62,63]. Filopodia act as points of attachment on the extracellular matrix but also enable the cells to probe the environment for chemical cues for example that regulate their behavior [64]. These cell cytoplasmic protrusions represent thus a great benefit regarding the triggering of specific cellular responses as cells may used these filopodia to detect efficiently the signals provided by the coated glass. This preliminary assay thus demonstrated that even after a short time, cells immediately modulated their attachment spreading according to the fibers' surface properties of the materials. The rapid and consequent spreading of the cells on the coated fibers can be explained by several factors. The first is the direct exposure of the bioactive ORMOGLASS at the material surface which can be immediately perceived by biological entities; the second is the focal adhesions that are promoted by the existence of the nanoroughness of the coating [65,66] and finally, the significant hydrophilicity of the scaffold [67]. The nanofeatures (nanofibers, nanoroughness) of these scaffolds represent moreover significant advantages over macro or microstructured materials as they play an important role for implantation success of scaffolds in many applications for tissue engineering [68]. On the other hand, the developed material is intended to act as an ion release agent that will promote cell migration, adhesion, proliferation and differentiation by delivering the appropriate chemical cues and acting as a chemotactic agent [29,69–71]. Based on the remarkable properties achieved with the hybrid fibers presented in chapter 2, good cellular responses are also expected to be reached by using this novel hybrid containing the same ORMOGLASS system. In parallel, these novel fibers could also serve as a drug delivery system to enable the release of therapeutic agents (molecules or particles, for example). The formation of hollow fibers during the electrospinning process [72] (see appendix A-5, A.5.12) provides a supplementary surface- to-volume ratio that would enhance

the degradation rate of the scaffold, as well as an inner surface that could be functionalized with other bioactive or antimicrobial agents [73]. In summary, although further investigations such as proliferation and differentiation assays are needed to confirm these scaffolds as efficient materials for bone tissue engineering, these first cellular results showed that the coating enabled an immediate positive interaction of the cells with the material and that this hybrid deserves attention for future assays.

On the other hand, achieving the coating with different compositions demonstrated the versatility and potential of this approach for the production of materials with different features. As chemical and physical cues received by cells from the material are essential for the triggering of specific cellular responses, the ability to change material properties simply by changing the ORMOGLASS composition and/or the experimental working conditions reflects the great potential of this valuable protocol for the development of multifunctional grafts for biomedical applications.

Finally, in bone repair, coating is a concept introduced first for the development of metallic prostheses as it helps to improve the integration of the implant with the host tissue. This commonly involves calcium phosphate compounds such as hydroxyapatite - among others (brushite, tricalcium phosphate…) [74,75]. Hydroxyapatite is considered as a good coating material because it has a similar chemical composition to that of the mineral component of natural bone. It is additionally stable under physiological conditions (as crystalline and stoichiometric phase) and is biocompatible. However, hydroxyapatite coatings often lack of strong cohesion with the metallic surface, leading to cracks, delamination of the coating and release of particles in the bloodstream [76,77]. Moreover, their processing conditions have to be precisely controlled to achieve a suitable composition, structure, and therefore dissolution [78]. This is however a difficult task because complicated procedures that require several preliminary steps of preparation and high temperatures are generally involved [77,79]. In addition, such calcium phosphate coated materials are still not bioactive. Therefore, growth factors, proteins and/or biomimetic compounds (chitosan, gelatin…) need to be incorporated in the coatings to promote a good material mineralization after implantation and to trigger specific cellular responses [79,80]. However, such approaches are also delicate to implement because only cold processing techniques can be used in this case [81]. Another possibility to produce bioactive coating is the use of bioactive glasses. Bioactive glasses are indeed able to trigger these responses without the incorporation of additional agents. However, bioactive glasses are brittle and there is a risk of cracks and delamination (as for hydroxyapatite coatings), especially if the metal/bioactive glass interface is weak [82–84]. Also, when used as particles, the bioactive glass is not always covering homogeneously the overall surface of the material (particles dispersed on the surface) [85]. Given all these drawbacks, the coating approach described in this chapter presents several significant advantages:

- The coating protocol is applied to polymeric materials, while coatings are mainly focused on metallic implants. The benefit of that is that the protocol can be used for biodegradable materials, and not only for implants used for permanent substitutions.

- The coating involves an ORMOGLASS and a covalent bonding between the ORMOGLASS and the polymer. Consequently, the obtained material is flexible and no delamination is observed under mechanical stimulation.
- The ORMOGLASS is coating the overall surface of the material homogeneously
- Due to its ion release ability, ORMOGLASSES, as the conventional bioactive glasses, trigger the desired cellular responses and favor mineralization. ORMOGLASSES satisfy by themselves these two requirements; no additional agents are necessary.
- The protocol does not imply high temperatures processes and is based on simple surface functionalization steps.

In summary, the coating approach described in this chapter constitutes a great alternative to other coating materials and methods developed in the last years.

4.4.4. Conclusion

The hybrid fibers produced by applying the protocol developed in the first part of the chapter have been characterized. These fibers presented a great potential to be used as an engineered material for bone tissue engineering. It exhibited a nanostructured topography, excellent hydrophilic properties, promising mineralization potential, remarkable mechanical features and showed, as first encouraging *in vitro* assay, a great ability to support cell spreading. The coating was moreover homogeneously achieved along the fiber length and its features (roughness, stiffness, thickness) have been shown to be controllable by changing the glass particle composition and/or the degree of hydrolysis considered to prepare these particles. This protocol is therefore a valuable tool to produce hybrid materials with well-defined surface properties. Such possibility is particularly interesting as most of the material fabrication techniques currently available do not enable such a precise control.

4.5. Chapter conclusion

A novel coating protocol that allows the fabrication of materials with tailorable surface properties (topography, chemical composition, stiffness was successfully developed. This approach, involving the sol-gel method, is an efficient, reproducible, cost-effective and versatile option to produce hybrid materials that possess the bioactive phase fully exposed at their surface and strong interactions between their constituents. The materials produced showed excellent instantaneous cellular response and improved mechanical properties. Moreover, the ability to easily modify their surface properties by changing the glass composition or the glass hydrolysis ratio, for example, highlighted the potential of this promising protocol. As materials' surface properties influence cell functionalities, a wide range of biomaterials that could possibly trigger different cellular response could be produced. This functionalization method

therefore represents an essential improvement towards the design of functional materials for the regenerative medicine field.

4.6. Acknowledgments

I kindly thank Prof. Lewandowska from the WUT for providing the DSC, FTIR and TGA devices. Tomasz Jaroszewicz, Ewa Kijeńska and Emilia Choińska are also thanked for their help with these techniques (DSC, FTIR and TGA respectively). Finally, Prof. Velders is thanked for providing the DLS device and Dr. Junyou Wang for introducing me to this technique. The European Commission and the Agencia de Gestio d'Ajusts Universitaris I de Recerca (AGAUR) are also acknowledged for funding (European ERANET project PI11/03030 – NANGIOFRAC and BE fellowship, respectively).

4.7. References

[1] Wang M. Developing bioactive composite materials for tissue replacement. Biomaterials 2003;24:2133–51.

[2] Chen Q, Roether JA, Boccaccini AR. Tissue engineering scaffolds from bioactive glass and composite materials. Tissue engineering, vol. 4, 2008.

[3] Martin RA, Yue S, Hanna J V, Lee PD, Newport RJ, Smith ME, et al. Characterizing the hierarchical structures of bioactive sol-gel silicate glass and hybrid scaffolds for bone regeneration. Philosophical Transactions of the Royal Society - Series A, Mathematical, Physical, and Engineering Sciences 2012;370:1422–43.

[4] Poologasundarampillai G, Ionescu C, Tsigkou O, Murugesan M, Hill RG, Stevens MM, et al. Synthesis of bioactive class II poly(γ-glutamic acid)/silica hybrids for bone regeneration. Journal of Materials Chemistry 2010;20:8952–61.

[5] Niemela T, Niiranen H, Kellomaki M, Tormala P. Self-reinforced composites of bioabsorbable polymer and bioactive glass with different bioactive glass contents. Part I: Initial mechanical properties and bioactivity. Acta Biomaterialia 2005;1:235–42.

[6] Tong H-W, Wang M, Li Z-Y, Lu WW. Electrospinning, characterization and in vitro biological evaluation of nanocomposite fibers containing carbonated hydroxyapatite nanoparticles. Biomedical Materials 2010;5:054111 (13pp).

[7] Charles-Harris M, Koch MA, Navarro M, Lacroix D, Engel E, Planell JA. A PLA/calcium phosphate degradable composite material for bone tissue engineering: an in vitro study. Journal of Materials Science: Materials in Medicine 2008;19:1503–13.

[8] Serra T, Planell JA, Navarro M. High-resolution PLA-based composite scaffolds via 3-D printing technology. Acta Biomaterialia 2013;9:5521–30.

[9] Hoppe A, Güldal NS, Boccaccini AR. A review of the biological response to ionic dissolution products from bioactive glasses and glass-ceramics. Biomaterials 2011;32:2757–74.

[10] Sachot N, Castaño O, Mateos-timoneda MA, Engel E, Planell JA. Hierarchically engineered fibrous scaffolds for bone regeneration. Journal of the Royal Society, Interface 2013;10:20130684.

[11] Gryglewicz S. Alkaline-earth metal compounds as alcoholysis catalysts for ester oils synthesis. Applied Catalysis A: General 2000;192:23–8.

[12] Coates J. Interpretation of infrared spectra, a practical approach. Encyclopedia of analytical chemistry, 2000.

[13] Swann GEA, Patwardhan S V. Application of fourier transform infrared spectroscopy (FTIR) for assessing biogenic silica sample purity in geochemical analyses and palaeoenvironmental research. Climate of the Past 2011;7:65–74.

[14] Launer PJ. Infrared analysis of organosilicon compounds: spectra-structure correlations. Silicone Coumpounds Register and Review, 1987.

[15] Vandenberg ET, Bertilsson L, Liedberg B, Uvdal K, Erlandsson R, Elwing H, et al. Structure of 3-aminopropyl triethoxy silane on silicon oxide preparation of APTES surfaces. Journal of Colloid and Interface Science 1991;147:103–18.

[16] Manzano M, Salinas AJ, Gil FJ, Vallet-Regí M. Mechanical properties of organically modified silicates for bone regeneration. Journal of Materials Science Materials in Medicine 2009;20:1795–801.

[17] Ravarian R, Wei H, Dehghani F. Improving the bioactivity of bioglass/(PMMA-co-MPMA) organic/inorganic hybrid. 33d Annual International Conference of the IEEE Engineering in Medicine and Biology Society 2011;2011:3593–6.

[18] Peña-Alonso R, Rubio F, Rubio J, Oteo JL. Study of the hydrolysis and condensation of γ-aminopropyltriethoxysilane by FT-IR spectroscopy. Journal of Materials Science 2007;42:595–603.

[19] Costa VC, Costa HS, Vasconcelos WL, Pereira MDM, Oréfice RL, Mansur HS. Preparation of hybrid biomaterials for bone tissue engineering. Materials Research 2007;10:21–6.

[20] Stewart JE. Vibrational spectra of primary and secondary aliphatic amines. The Journal of Chemical Physics 1959;30:1259–65.

[21] Vallet-Regi M, Salinas AJ, Ramirez-Castellanos J, Gonzalez-Calbet JM. Nanostructure of bioactive sol-gel glasses and organic-inorganic hybrids. Chemistry of Materials 2005;17:1874–9.

[22] Ribeiro CC, Gibson I, Barbosa MA. The uptake of titanium ions by hydroxyapatite particles - structural changes and possible mechanisms. Biomaterials 2006;27:1749–61.

[23] Rasband WS. Image J. US National Institute of Health, Bethesda, USA, Http://imagej.nih.gov/ij/ 1997:2014.

[24] Derjaguin B V, Muller VM, Toporov YP. Effect of contact deformations on the adhesion of particles. Journal of Colloid and Interface Science 1975;53:314–26.

[25] Chow WS, Lok SK. Thermal properties of poly(lactic acid)/organo-montmorillonite nanocomposites. Journal of Thermal Analysis and Calorimetry 2009;95:627–32.

[26] Lee TH, Boey FYC, Khor KA. On the determination of polymer crystallinity for a thermoplastic PPS composite by thermal analysis. Composites Science and Technology 1995;53:259–74.

[27] Henton DE, Gruber P, Lunt J, Randall J. Polylactic Acid Technology. Natural Fibers, Biopolymers and Biocomposites, 2005.

[28] Yu H-S, Jang J-H, Kim T-I, Lee H-H, Kim H-W. Apatite-mineralized polycaprolactone nanofibrous web as a bone tissue regeneration substrate. Journal of Biomedical Materials Research Part A 2009;88:747–54.

[29] Hench LL. Genetic design of bioactive glass. Journal of the European Ceramic Society 2009;29:1257–65.

[30] Leu A, Stieger SM, Dayton P, Ferrara KW, Leach JK. Angiogenic response to bioactive glass promotes bone healing in an irradiated calvarial defect. Tissue Engineering Part A 2009;15:877–85.

[31] Gerhardt L-C, Widdows KL, Erol MM, Burch CW, Sanz-Herrera JA, Ochoa I, et al. The pro-angiogenic properties of multi-functional bioactive glass composite scaffolds. Biomaterials 2011;32:4096–108.

[32] Pluta M. Melt compounding of polylactide/organoclay: structure and properties of nanocomposites. Journal of Polymer Science Part B: Polymer Physics 2006;44:3392–405.

[33] McLauchlin AR, Thomas NL. Preparation and thermal characterisation of poly(lactic acid) nanocomposites prepared from organoclays based on an amphoteric surfactant. Polymer Degradation and Stability 2009;94:868–72.

[34] Mandel S, Tas AC. Brushite ($CaHPO_4 \cdot 2H_2O$) to octacalcium phosphate ($Ca_8(HPO_4)_2(PO_4)_4 \cdot 5H2O$) transformation in DMEM solutions at 36.5°C. Materials Science and Engineering: C 2010;30:245–54.

[35] Roop Kumar R, Wang M. Biomimetic deposition of hydroxyapatite on brushite single crystals grown by the gel technique. Materials Letters 2001;49:15–9.

[36] Dorozhkin S V. Biocomposites and hybrid biomaterials based on calcium orthophosphates. Biomatter 2011;1:1–54.

[37] Lüthen F, Lange R, Becker P, Rychly J, Beck U, Nebe JGB. The influence of surface roughness of titanium on beta1- and beta3-integrin adhesion and the organization of fibronectin in human osteoblastic cells. Biomaterials 2005;26:2423–40.

[38] Jo J-H, Lee E-J, Shin D-S, Kim H-E, Kim H-W, Koh Y-H, et al. In vitro/in vivo biocompatibility and mechanical properties of bioactive glass nanofiber and poly(ε-caprolactone) composite materials. Journal of Biomedical Materials Research Part B, Applied Biomaterials 2009;91:213–20.

[39] Kim H-W, Song J-H, Kim H-E. Nanofiber generation of gelatin-hydroxyapatite biomimetics for guided tissue regeneration. Advanced Functional Materials 2005;15:1988–94.

[40] Ravarian R, Wei H, Dehghani F. Improving the bioactivity of bioglass/(PMMA-co-MPMA) organic/inorganic hybrid. 33d Annual International Conference of the IEEE Engineering in Medicine and Biology Society 2011;2011:3593–6.

[41] Valliant EM, Jones JR. Softening bioactive glass for bone regeneration: sol–gel hybrid materials. Soft Matter 2011;7:5083–95.

[42] Vallet-Regí M, Salinas AJ, Arcos D. From the bioactive glasses to the star gels. Journal of Materials Science Materials in Medicine 2006;17:1011–7.

[43] Pickup DM, Wetherall KM, Knowles JC, Smith ME, Newport RJ. Sol-gel preparation and high-energy XRD study of $(CaO)_x(TiO_2)_{0.5}$-$(P_2O_5)_{0.5}$ glasses (x = 0 and 0.25). Journal of Materials Science Materials in Medicine 2008;19:1661–8.

[44] Wen J, Mark JE. Synthesis, structure, and properties of poly(dimethylsiloxane) networks reinforced by in situ-precipitated silica-titania, silica-zirconia, and silica-alumina mixed oxides. Journal of Applied Polymer Science 1995;58:1135–45.

[45] Navarro M, Ginebra MP, Planell JA, Barrias CC, Barbosa MA. In vitro degradation behavior of a novel bioresorbable composite material based on PLA and a soluble CaP glass. Acta Biomaterialia 2005;1:411–9.

[46] Niemelä T, Niiranen H, Kellomäki M. Self-reinforced composites of bioabsorbable polymer and bioactive glass with different bioactive glass contents. Part II: In vitro degradation. Acta Biomaterialia 2008;4:156–64.

[47] Kopinke F, Remmler M, Mackenzie K, Möder M, Wachsen O. Thermal decomposition of biodegradable polyesters - II. Poly(lactic acid). Polymer Degradation and Stability 1996;53:329–42.

[48] McNeill IC, Leiper HA. Degradation studies of some polyesters and polycarbonates - 2. Polylactide: degradation under isothermal conditions, thermal degradation mechanism and photolysis of the polymer. Polymer Degradation and Stability 1985;11:309–26.

[49] Perego G, Cella GD, Bastioli C. Effect of molecular weight and crystallinity on poly(lactic acid) mechanical properties. Journal of Applied Polymer Science 1996;59:37–43.

[50] Bang G, Kim SW. Biodegradable poly(lactic acid)-based hybrid coating materials for food packaging films with gas barrier properties. Journal of Industrial and Engineering Chemistry 2012;18:1063–8.

[51] Kim KD, Kim HT. Formation of silica nanoparticles by hydrolysis of TEOS using a mixed semi-batch/batch method. Journal of Sol-Gel Science and Technology 2002;25:183–9.

[52] Guo J, Liu X, Cheng Y, Li Y, Xu G, Cui P. Size-controllable synthesis of monodispersed colloidal silica nanoparticles via hydrolysis of elemental silicon. Journal of Colloid and Interface Science 2008;326:138–42.

[53] Yu B, Turdean-Ionescu CA, Martin RA, Newport RJ, Hanna J V, Smith ME, et al. Effect of calcium source on structure and properties of sol-gel derived bioactive glasses. Langmuir 2012;28:17465–76.

[54] Sepulveda P, Jones JR, Hench LL. In vitro dissolution of melt-derived 45S5 and sol-gel derived 58S bioactive glasses. Journal of Biomedical Materials Research 2002;61:301–11.

[55] Prabhakar RL, Brocchini S, Knowles JC. Effect of glass composition on the degradation properties and ion release characteristics of phosphate glass-polycaprolactone composites. Biomaterials 2005;26:2209–18.

[56] Poologasundarampillai G, Ionescu C, Tsigkou O, Murugesan M, Hill RG, Stevens MM, et al. Synthesis of bioactive class II poly(γ-glutamic acid)/silica hybrids for bone regeneration. Journal of Materials Chemistry 2010;20:8952–61.

[57] Jones JR, Gentleman E, Polak J. Bioactive glass scaffolds for bone regeneration. Elements 2007;3:393–9.

[58] Rhee S-H. Effect of calcium salt content in the poly(ε-caprolactone)/silica nanocomposite on the nucleation and growth behavior of apatite layer. Journal of Biomedical Materials Research Part A 2003;67:1131–8.

[59] Kokubo T, Kushitani H, Ohtsuki C, Sakka S, Yamamuro T. Chemical reaction of bioactive glass and glass-ceramics with a simulated body fluid. Journal of Materials Science: Materials in Medicine 1992;3:79–83.

[60] Hong Z, Reis RL, Mano JF. Preparation and in vitro characterization of scaffolds of poly(L-lactic acid) containing bioactive glass ceramic nanoparticles. Acta Biomaterialia 2008;4:1297–306.

[61] Wheeler DL, Jenis LG, Kovach ME, Marini J, Turner AS. Efficacy of silicated calcium phosphate graft in posterolateral lumbar fusion in sheep. The Spine Journal 2007;7:308–17.

[62] Buckley IK, Porter KR. Cytoplasmic fibrils in living cultured cells. Protoplasma 1967;64:349–80.

[63] Oakes PW, Beckham Y, Stricker J, Gardel ML. Tension is required but not sufficient for focal adhesion maturation without a stress fiber template. The Journal of Cell Biology 2012;196:363–74.

[64] DeLisser HM. Modulators of endothelial cell filopodia: PECAM-1 joins the club. Cell Adhesion & Migration 2011;5:37–41.

[65] Ross AM, Jiang Z, Bastmeyer M, Lahann J. Physical aspects of cell culture substrates: topography, roughness, and elasticity. Small 2012;8:336–55.

[66] Arnold M, Cavalcanti-Adam EA, Glass R, Blümmel J, Eck W, Kantlehner M, et al. Activation of integrin function by nanopatterned adhesive interfaces. ChemPhysChem: A European Journal of Chemical Physics and Physical Chemistry 2004;5:383–8.

[67] Dalton BA, Mcfarland CD, Thomas RG, Griesser HJ, Steele JG. Polymer surface chemistry and bone cell migration. Journal of Biomaterials Science, Polymer Edition 1998;9:781–99.

[68] Zhang L, Webster TJ. Nanotechnology and nanomaterials: promises for improved tissue regeneration. Nano Today 2009;4:66–80.

[69] Gough JE, Jones JR, Hench LL. Nodule formation and mineralisation of human primary osteoblasts cultured on a porous bioactive glass scaffold. Biomaterials 2004;25:2039–46.

[70] Bosetti M, Cannas M. The effect of bioactive glasses on bone marrow stromal cells differentiation. Biomaterials 2005;26:3873–9.

[71] Aguirre A, González A, Planell JA, Engel E. Extracellular calcium modulates in vitro bone marrow-derived Flk-1^+ $CD34^+$ progenitor cell chemotaxis and differentiation through a calcium-sensing receptor. Biochemical and Biophysical Research Communications 2010;393:156–61.

[72] Fan HJ, Knez M, Scholz R, Hesse D, Nielsch K, Zacharias M, et al. Influence of surface diffusion on the formation of hollow nanostructures induced by the Kirkendall effect: the basic concept. Nano Letters 2007;7:993–7.

[73] Li D, Xia Y. Direct fabrication of composite and ceramic hollow nanofibers by electrospinning. Nano Letters 2004;4:933–8.

[74] Biemond JE, Eufrásio TS, Hannink G, Verdonschot N, Buma P. Assessment of bone ingrowth potential of biomimetic hydroxyapatite and brushite coated porous E-beam structures. Journal of Materials Science: Materials in Medicine 2011;22:917–25.

[75] Tisdel CL, Goldberg VM, Parr JA, Bensusan JS, Staikoff LS, Stevenson S. The influence of a hydroxyapatite and tricalcium-phosphate coating on bone growth into titanium fiber-metal implants. Journal of Bone and Joint Surgery 1994;76:159–71.

[76] Lynn AK, DuQuesnay DL. Hydroxyapatite-coated Ti-6Al-4V part 1: the effect of coating thickness on mechanical fatigue behaviour. Biomaterials 2002;23:1937–46.

[77] Habibovic P, Barrère F, Van Blitterswijk CA, De Groot K, Layrolle P. Biomimetic hydroxyapatite coating on metal implants. Journal of the American Ceramic Society 2002;85:517–22.

[78] Ducheyne P, Radin S, Heughebaert M, Heughebaert JC. Calcium phosphate ceramic coatings on porous titanium: effect of structure and composition on electrophoretic deposition, vacuum sintering and in vitro dissolution. Biomaterials 1990;11:244–54.

[79] Shah NJ, Hong J, Hyder N, Hammond PT. Osteophilic multilayer coatings for accelerated bone tissue growth. Advanced Materials 2012;24:1445–50.

[80] Huang Z-M, Qi Y-Y, Du S-H, Feng G, Unuma H, Yan W-Q. Promotion of osteogenic differentiation of stem cells and increase of bone-bonding ability in vivo using urease-treated titanium coated with calcium phosphate and gelatin. Science and Technology of Advanced Materials 2013;14:055001 (10pp).

[81] Schmidmaier G, Wildemann B, Stemberger A, Haas NP, Raschke M. Biodegradable poly(D,L-lactide) coating of implants for continuous release of growth factors. Journal of Biomedical Materials Research 2001;58:449–55.

[82] Pazo A, Saiz E, Tomsia AP. Silicate glass coatings on Ti-based implants. Acta Materialia 1998;46:2551–8.

[83] Schrooten J, Helsen JA. Adhesion of bioactive glass coating to Ti6Al4V oral implant. Biomaterials 2000;21:1461–9.

[84] Lopez-Esteban S, Saiz E, Fujino S, Oku T, Suganuma K, Tomsia AP. Bioactive glass coatings for orthopedic metallic implants. Journal of the European Ceramic Society 2003;23:2921–30.

[85] Gomez-Vega JM, Saiz E, Tomsia AP, Marshall GW, Marshall SJ. Bioactive glass coatings with hydroxyapatite and Bioglass particles on Ti-based implants. 1. Processing. Biomaterials 2000;21:105–11.

Chapter 5

General discussion and conclusion

In this final chapter, the results and discussions reported in this thesis will be commented on and the achievements will be correlated to the state of the art of the current research performed on hybrid biomaterials. The limitations of each material, as well as the different studies conducted to characterize and assess the potential of these materials, will be also summarized. Finally, the future perspectives of work that this thesis provides will be described.

5.1. Achievements, contributions to the field and limitations of the studies

The aim of this thesis was to develop and to characterize novel hybrid materials for bone tissue engineering. The work especially focused on the fabrication of biodegradable and bioactive scaffolds made of synthetic polymers and organically modified glasses (ORMOGLASSES). The materials chosen for this study were polycaprolactone and polylactic acid for the organic phase, and silicon and titanium based ORMOGLASSES for the inorganic one. The sol-gel method and the electrospinning technique were used to produce fibrous mats. These mats were analyzed in terms of physico-chemical properties and biological performance.

Three types of new material were successfully produced. These materials relied on the combination of polymers and glasses that contained organic fragments in their network. This represents a new concept in the field as most of the materials currently developed are prepared with pure inorganic compounds [1,2]. To the best of the author's knowledge, only one inorganic material that contained organic groups has been reported in the literature up to date. This kind of material, named "star gel", was prepared by the sol-gel method and was introduced for bone tissue engineering by Manzano *et al.* in 2006 [3]. However, star gels were first described in 1995 by the DuPont Corporation [4,5], but Manzano and coworkers rendered these materials bioactive, making them suitable for osseous regeneration. In fact, they incorporated calcium alkoxide during the polycondensation process of the precursor. The produced materials successfully induced the deposition of an apatite layer on their surface and exhibited better mechanical properties than other conventional glasses due to the inherent molecular composition of the glass. Moreover, the presence of the organic groups in the gel provided flexibility to the material, a property that conventional glasses did not possess (brittle). According to the author's literature research, star gels and other possible organically modified inorganic networks did not seem to have been investigated afterwards; neither as a single material (as Manzano *et al.*), nor to prepare composites. Their resorption characteristics as well as their ability to induce cellular response and to interact properly with the biological environment also did not seem to have been assessed [6]. In this thesis, novel materials that contained ORMOGLASSES have been successfully developed and characterized. These materials did not only have calcium incorporated in their network but also phosphate. This work represents a valuable progress in the field as it demonstrated that polymer-ORMOGLASSES templates can be produced, that they can be prepared with different ORMOGLASS compositions and that they can trigger specific

cellular responses involved in osteo and angiogenesis. Thus, they appeared to be promising for bone tissue engineering and constitute a new family of material for the field. Moreover, these materials allowed us to introduce in the literature an acronym for organically modified glasses (ORMOGLASSES); as other researchers did for organically modified silanes (ORMOSILS) and ceramics (ORMOCERS) for example [7].

The first material presented in this thesis was based on the association of polycaprolactone and silicon-calcium- phosphate (Si-Ca-P_2) ORMOGLASSES (blends). This scaffold represented a proof of concept for the fabrication of novel hybrids and served to demonstrate the ability of such materials to positively influence cellular behavior towards responses required for tissue regeneration. *In vitro* and *in vivo* assays revealed the potential of such hybrids. The intrinsic material properties such as calcium release, stiffness and surface properties were suitable for the targeting of the desired biological responses. Given the efficiency of the material, an optimization study was carried out to facilitate the production of the fibrous templates. In fact, to perform additional studies on the fibers, a significant amount of material is required. Therefore, an improvement in the fiber deposition was needed to achieve a fluid fiber deposition. On the other hand, this study enabled the determination of the experimental working conditions that allowed the deposition of nanofibers. This way, from now on, materials that better mimic the fibrous structure of native bone can be prepared. However, despite the promising results obtained with these fibers, other aspects still need to be investigated. First, no degradation assay was conducted and it is well known that the degradation of a material is essential regarding the targeted application. Based on the *in vivo* subcutaneous tests, the materials started to be replaced by fibrous tissue already after 4 weeks of implantation. This may suggest that the material dissolved rather fast in the body. So, even if it did not seem to be problematic for vascularization (according to the results), it is possible that it will be for osteogenesis *in vivo* as the formation of bone usually requires more time [8,9]. However, no more comment can be made on that because the material was only implanted subcutaneously and not in a bone defect. In fact, this underlines another limitation of the study. Even though promising results were obtained regarding osteogenesis *in vitro* (ALP production, gene expression…), no study was conducted *in vivo* to directly assess the potential of the fibers to generate bone. Further assays should thus be performed in this direction. Finally, the last problematic consideration about the assessment of these fibers is the cells used for the *in vitro* tests. As explained in chapter 2, MC3T3-E1 cells are osteoblast precursors (cell line) [10,11]. For this reason, they may not be the most relevant cells to investigate, in a "neutral" way, the potential of the materials to trigger osteoblast differentiation. Instead, multipotent cells, i.e. mesenchymal stem cells (primary cells) [12], are strongly recommended. Consequently, the *in vitro* studies reported in the other chapters were afterwards conducted with these cells and not with cells having a natural tendency to differentiate into osteoblasts, for example. Despite this statement, it should be specified that results achieved with MC3T3-E1 cells are considered reliable by the scientific community [11,13]. The conclusions drawn from *in vitro* assays in chapter 2 were thus accepted as valid. The nature

of these cells made us question ourselves on the use of cell lines to assess biological responses and enabled us to establish more relevant material *in vitro* testing conditions for the hybrids characterized afterwards.

The second material presented in the thesis relied on the same concept that the first material but with other compounds. Polylactic acid and a titanium-calcium-phosphate-sodium (Ti-Ca-P_2-Na_2) ORMOGLASS were blended to create the fibers. The development of this material was aimed to demonstrate that ORMOGLASSES can efficiently be used to prepare scaffolds with different constituents and compositions. It was also intended to validate the use of ORMOGLASSES-containing hybrids for bone tissue engineering. The fabrication of these fibers showed that the combination of polymer with ORMOGLASSES is a versatile approach for the fabrication of biomaterials. Fibers with different ORMOGLASS contents were produced with two different fiber arrangements (random and aligned). *In vitro* tests performed with mesenchymal stem cells (MSCs) and endothelial progenitor cells (EPCs) (two types of primary cells) showed that cells attached and proliferated on the scaffolds, especially the MSCs. However, the degradation study revealed that, immediately after the fiber immersion in fluid, the fibers lost a significant amount of ORMOGLASS and unreacted compounds. This suggested that the hydrolysis of the ORMOGLASS precursor mix was still not well controlled, even if it enabled to prepare a suitable blend for electrospinning. This was not the only problem with this material. In fact, the phases were not homogeneously mixed. This may have contributed to the burst release of the ORMOGLASS compounds occurring at the early stage of the degradation assay. This had significant consequences on the assays that were performed in solution. In fact, this important loss of compounds surely influenced the cellular behavior. Initially, the material was prepared with the G5 composition, the optimal glass composition for osteo and angiogenesis [14,15]. After few minutes of immersion, the material lost a big amount of calcium and phosphate, in particular. This means that the results obtained with these fibers (*in vitro* and *in vivo*) were actually not related to the exact G5 composition. This may have affected the cellular response in comparison to what could be expected when using the real G5 composition. When this will be optimized, other cellular assays, in particular differentiation ones, will be also needed because such assays could not have been carried out in the time scale of the thesis and that it is essential to assess this aspect. On the other hand, as for the previous material, one limitation of that study is that the fibers were subcutaneously implanted in rats. In this case, the choice of this approach may be more relevant than for the first material as the composition of the ORMOGLASS used in that study was mainly selected for its ability to induce vascularization. Subcutaneous implantation was thus a good option for a preliminary assay. Additional assays are however required to monitor the formation of blood vessels and bone in other conditions. Performing assays in conditions as close as possible to the final targeted application is essential to properly evaluate the potential of the material for its specific use. Finally, the last comment about these fibers may be made on the use of SBF to assess the degradation of the material. Usually, SBF is used to assess the bioactivity of materials, i.e. its ability to promote calcium phosphate deposition on its

surface. If the material presents this capability, it is therefore not very appropriate to use SBF to monitor its dissolution behavior; in particular if the degradation is assessed by morphological observations for example. For such bioactive materials, it is better to use water as alternative to SBF. However, for titanium-based glasses, it is accepted that they do not efficiently induce mineralization and are more efficient to trigger specific cellular responses [16]. Therefore, the use of SBF, in this case, is not a drawback as the degradation can be assessed under simulated physiological conditions without that the deposition of calcium phosphate disturbing the degradation. This is mainly accepted when morphological and topographical observations are considered to evaluate the degradation behavior. However, if the degradation is assessed by means of calcium release measurements using an ion selective electrode, for example, SBF is not suitable. The reason is that SBF contains HPO_4^{2-} ions and that $CaHPO_4$ can easily precipitate when calcium ions are released by the material. As a result, the calcium electrode is not able to detect the amount of calcium released because calcium is not free in solution and that $CaHPO_4$ has a very low solubility under simulated physiological conditions. This is one of the reasons why the assays of calcium release reported in the chapters were performed in water. Depending on the properties to be assessed, the solution used for degradation test should be carefully selected, and for some assays such as calcium release measurements, it is not recommended to use SBF or other phosphate buffer solutions. If a buffering effect is desired, organic buffers such as HEPES (as in chapter 2) may be more suitable as they will not induce the precipitation of calcium phosphate species. If no buffering effect is desired, pure water can be used (see chapter 3 and 4). Finally, the only real problem of this degradation test is actually due to the material itself. As most of the ORMOGLASS is dissolved at the beginning of the assay, no degradation mechanism could have been explained. Hence, there is a need to enhance the material preparation to better analyze its ultimate biological and degradation behaviors.

The material last developed was another type of material involving polylactic acid and Si-Ca-P_2 ORMOGLASSES. Its fabrication relied on the coating of polymeric fibers with ORMOGLASS particles. This material was developed for several reasons. The first reason is that the dissolution of the composites is often not well controlled and occurs fast; especially if the blending of the material needs to be further optimizes, for example. The second reason is that the bioactive phase of the composites (ORMOGLASS in our case) is usually not directly exposed to the cells. This is a very common concern with the usual hybrid materials developed to date. The development of the novel protocol implemented to produce the new fibers demonstrated that hybrid materials satisfied two important criteria: the formation of strong covalent bonding between the constituents and the total exposure of the ORMOGLASS to biological entities (for the targeting of cellular responses) and fluid (for the mineralization process). This material is especially groundbreaking for the field because, up to date, only few class II materials were developed and they did not consider the problem of exposing the bioactive phase. The produced material exhibited a rough nanostructured surface, good hydrophilicity, suitable mechanical properties, promising mineralization potential and cellular spreading. Moreover, the surface properties of the materials could be

tailored by changing the ORMOGLASS composition and controlling the preparation of the particles (size). This ability to easily change the surface properties of materials is a valuable point for the triggering of specific cellular responses as cells modulate their behavior depending on the physical and chemical cues provided by the scaffolds. Even if this material appears promising for some regenerative medicine applications, there is still a long way to go. Now that the protocol has been properly set and that its versatility has been demonstrated, further *in vitro* and *in vivo* assays should be performed to definitely validate this material for bone tissue engineering. Also, a deep degradation study should be performed. According to the literature [17,18], materials that possess improved interactions between their constituents degrade in a more homogeneous manner and at a lower rate than other conventional materials. This still has to be proven for the coated fibers. Another limitation of this study is that the covalent bonding between the two phases could not have been directly revealed. In fact, the polymer and particles were linked between each other through siloxane bonds (by means of the coupling agent). Siloxanes were also building the ORMOGLASS network. It is therefore difficult to precisely distinguish in the FTIR spectra to which bonding correspond the siloxane signals. The high number of siloxanes present in the ORMOGLASS may mask the signal of the other siloxane bondings (in a much lower quantity). Researchers usually use NMR to clearly demonstrate the presence of covalent bondings [17]. However, such analysis requires time and precise investigation. Unfortunately, the research stay performed at the University of Wageningen to use NMR technique could not have been profitable for such investigation as no silicon probe was available. However, this stay enabled to set the basis for future NMR assays that should be performed to have direct proof of the covalent bonding, to analyze the structure of the ORMOGLASS network and to understand how calcium and phosphate are incorporated in the ORMOGLASS network. The final limitation of this study is the lack of a mineralization test. The mineralization potential of the coated fibers was assessed by the alternate soaking method, but its bioactivity was not tested in SBF. As this test is the commonly accepted way to demonstrate calcium phosphate deposition, this test should be also performed in the future.

From a general point of view, the assessment of the fibrous membranes revealed a main problem regarding the use of electrospun mats in *in vitro* conditions: the lack of cell infiltration. It is often mentioned in the literature that electrospun materials are suitable for cell culture because they possess a high surface area and high porosity. This is commonly believed to facilitate cell migration towards the center of the scaffold. However, high porosity does not systematically mean that cells have enough space to penetrate the template. The size of the pores and the interconnectivity are critical in that process [8,19,20], as well as the tortuosity of the fibers, their size and also the size of the cells used. In this thesis, no cell infiltration was observed when culturing the cells on the membranes in culture. Cell penetration was only observed in *in vivo* conditions. *In vivo* implantation seemed thus to favor cell infiltration. Consequently, it is suggested that electrospun templates may not be the best template to culture cells *in vitro* (static conditions) if the colonization of the templates is required. Otherwise, an improvement in the

material structure should be made to provide more space for the cells (macropores). One possibility is to create cotton-like electrospun scaffolds in order to bypass the problem of tightly packed nanofiber layers [21]. It can be also achieved by electrospinning different compounds at the same time and subsequently suppressing some of the fibers [22]. Other strategies such as decreasing the fibers diameter have also been reported but their efficiency is more limited because they did not significantly increase the pore size. Another possibility could be also to culture the cells under dynamic conditions or in a bioreactor [23,24]. If the novel fibers developed in this thesis are aimed to be efficiently used to culture cells in 3D *in vitro*, the cell infiltration should be imperatively enhanced. For *in vivo* however, the dense packing of the nanofibers does not seem to be critical.

The characterization of electrospun mats can also be a problem sometimes, as for example, the measurement of the porosity of the scaffolds. Studies found in the literature commonly report the measurement of the porosity and pore size by mercury intrusion or capillary flow porosimetry [25,26]. However, electrospun grafts are not rigid materials. When a force is applied to the material, the fiber arrangement immediately changes. Both of the enounced techniques require high pressure to perform the measurements. This means that the techniques do not measure the initial pore size and porosity of the material as produced, but rather measure these data as the fibers reorganized under pressure. Consequently, even if they are extensively used, these techniques are not very reliable. This problem was also described by Rutledge *et al.* but scientists continue using these devices without taking particular cautions when interpreting the results [27]. Because of the possible erroneous conclusions that can be made by measuring pore size and porosity with these techniques, the author preferred not to perform such assays and searched for more suitable device or technique. For example, the Brunauer-Emmett-Teller (BET) analysis was also considered because it involves gas pressure, in principle, lower than the ones used for mercury intrusion and capillary flow porosimetry [28,29]. To perform this assay, a preliminary degasification process that involves temperatures over T_g is required. Thus, this method cannot be used with the developed fibers as the polymer would degrade and consequently, BET analysis would also lead to the loss of the initial structure of the scaffold, as the other two cited techniques. Computed tomography was also taken into account as it enables to scan the object as it is produced. This way, images of the structure can be obtained to further calculate the porosity. Unfortunately, the fibers were too thin and it was not possible to obtain data. The resolution of the machine available for this test was not suitable for nanofibers. In fact, computed tomography is usually used for micrometric materials [30]. At the end, the last option considered to measure properly the porosity was the development of a novel approach that does not implies modifications of the intrinsic structure of the fibrous material. Hence, since last year, the "Biomaterials for Regenerative Therapies" and "Biomechanics and Cellular Biophysics" groups of IBEC collaborate in order to develop a confocal imaging method using fluorescent agents. Hence, the 3D structure of the template could be reconstructed and the porosity could be determined without the problems associated to conventional porosity measurements. This method is currently still being

developed. No other reliable methods were found to measure effectively porosity and pore size. For these reasons, no data were presented in the thesis about these properties; except SEM images that enabled the observation of the fibers packing density.

5.2. Improvements and Perspectives

Given the novelty of the developed materials, further investigations should be undertaken to confirm the use of polymer-ORMOGLASS scaffolds for bone tissue engineering. Improvements in the material design are necessary, as well as additional extensive *in vitro* and *in vivo* studies. However, their development is already a significant progress for the fabrication of advanced materials and they worth a particular attention for future research lines. Therefore, the main weaknesses of the hybrid fibers are summarized here along with the possible research directions and work perspectives that could be followed to overcome the different design problems or studies' limitations:

- Concern 1: drastic loss of unreacted compounds and ORMOGLASS after fiber immersion
  Suggested studies: improve the ORMOGLASS hydrolysis, better control of the hydrolysis and the incorporation of calcium and phosphate using NMR technique

- Concern 2: fast degradation of the fibers
  Suggested studies: improve the interactions between the ORMOGLASS and polymer by modifying the hydrolysis of the ORMOGLASS, mix the polymer and the ORMOGLASS for a longer time under very strong stirring

- Concern 3: lack of biological results
  Suggested studies: differentiation tests, gene expression evaluation, in vivo implantation in bone cavity, adaptation of in vitro tests to fibrous mats

- Concern 4: lack of degradation and mineralization tests
  Suggested studies: incubation in pure water, water containing HEPES, SBF or other phosphate buffer solutions (to select depending on the properties to assess)

- Concern 5: lack of cell infiltration *in vitro*
  Suggested studies: production of cotton-like structures, culture in bioreactor

- Concern 6: no direct proof of covalent bonding
  Suggested studies: NMR, XPS or AFM adhesion resistance investigation

In addition to these possible studies, the blends prepared for the electrospinning could be used to prepare other types of structure. It could serve to fabricate well ordered architectures, as for example the ones drawn by 3D printing techniques [31]. Some features such as viscosity of the blend may have to be

adapted to satisfy experimental requirement associated with the technique but it worth considering that this may be a good approach to take advantage of the development of these novel blends.

The most interesting perspectives of work that are provided by this thesis concern the coating protocol. To precisely control the surface properties of scaffolds has become in fact a substantial objective for scientists working for regenerative medicine as it influences cell functionalities. The novel coating approach developed in this thesis possesses a great potential for that purpose as it was demonstrated that surface properties of the fibers can be tailored by changing the molar composition of the particles. This offers, for example, the possibility to produce materials with a tailored ion release. This is especially interesting given that, based on chapter 1 and other recent results obtained by the group, calcium release is suggested to have a key role for the triggering of osteo and angiogenesis. Moreover, it was also shown that the particle size can be controlled by modifying the degree of hydrolysis of the ORMOGLASS precursor mix. This suggested that, by grafting small or big particles, different roughness and surface morphology could be achieved. As a proof of concept, coatings with different particles size were prepared. The results are reported in **Figure 5-1**. The images clearly revealed that the surface properties (roughness, morphology, topography) of the fibers can be tuned by selecting a specific particle size, offering thus a wide range of possible perspectives of work for the developed materials.

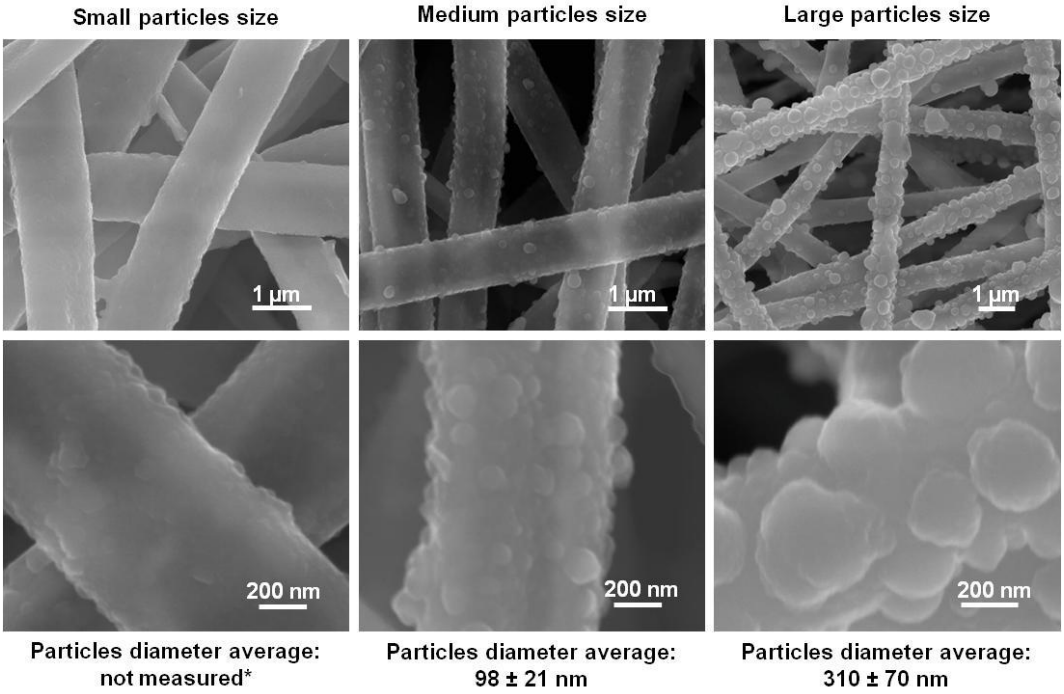

Figure 5-1. Fibers morphology of coated fibers obtained with different particle sizes (FESEM pictures - particles size measured using ImageJ Software - *: the pictures did not enable the measurement of the particle size).

Moreover, to demonstrate the versatility of this protocol, other structures have been coated. Thin films and rapid prototyping structures have been successfully coated with the ORMOGLASS particles (**Figure**

5-2). This demonstrated that the protocol can be transferred to other structures simply by adapting the protocol. This also means that other applications could be targeted depending on the architecture required.

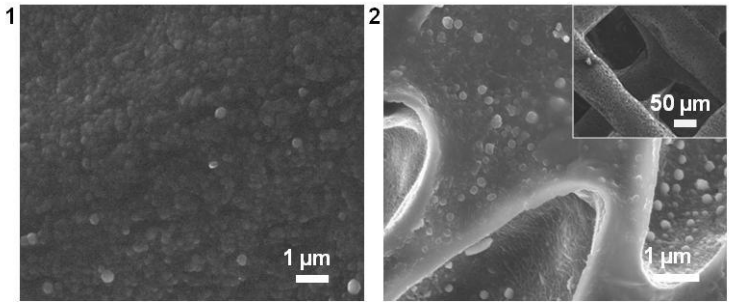

Figure 5-2. Morphology of thin film and rapid prototyping structure coated with ORMOGLASS particles.

On the other hand, it is also assumed that this protocol could be applied to other glass systems and that is not only relevant for the Si-Ca-P_2 one. For example, it could be transposed to the titanium based ORMOGLASS. Some preliminary tests were conducted to verify this hypothesis. Results are presented in **Figure 5-3**. Some ORMOGLASS particles attached on the fiber surface but, in a heterogeneous manner and not on all the fiber length. This assay also revealed that the particles were not spherical but rather looked like flakes. Apart from this inhomogeneous distribution of the particles, another problem was observed: particles seemed to aggregates at some places of the fibrous membranes. As a proof of concept, these tests showed that it is possible to bond particles to the fibers but that a significant effort should be made to obtain a homogeneous coating and avoid particles aggregations. In any case, all these preliminary assays clearly demonstrated the potential of the developed protocol and the working perspectives that it provides.

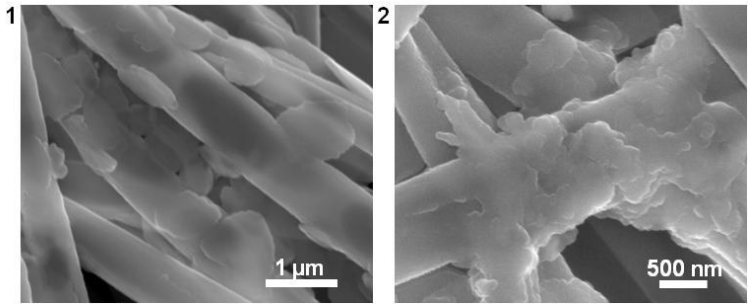

Figure 5-3. Morphology of the fibers after coating with titanium based ORMOGLASS particles.

Finally, all the perspectives of work provided by the development of ORMOGLASS-polymer blends and the coating protocol seem very promising for the development of various scaffolds for the regenerative medicine. This is especially interesting because each specific application has specific needs. In particular, bone tissue engineering requires a bioactive material that is able to support mechanical load without failure (among other criteria). This material needs to be tough enough to fill properly the defect and to maintain its initial shape even under body activity/every day stress. With the knowledge acquired during

researching of the thesis, it appeared that electrospun fibrous mats may not be the most suitable structure to regenerate significant bone defects. In fact, fibrous mats are rather soft when considered as a whole template. Simply by compressing fibrous mats (rolled or folded fibrous layer) with the fingers, it can be noticed that the mats do not support compression and immediately flatten. This means that, along with the implantation of fibrous mats in critical defects, screws and plates would be necessary to maintain the body structure and ensure the good regeneration process. However, this is not a satisfactory approach as a second surgery would be necessary to remove the screws and plates after complete bone healing. Thus, in regard to the concept of 'minimal invasive surgery procedure', this is not a good strategy. A solution would be to use other tougher constructs such as rapid prototyping scaffolds or calcium phosphate cements to fill the defect. Associated to these materials, the fibrous layer could be used to cover the implanted material. Hence, the fibrous layer would mimic the structure of bone periosteum. Bone periosteum is the dense fibrous membrane covering the surface of bone (long part). It is essential for the health of bone as it contains many blood vessels and contributes to the supply of the nutrients and oxygen to the bone cells through the Volkmann and Haversian canals (see chapter 1). It also directly contributes to the formation of bone as it contains osteoblasts. Concerning bone tissue engineering, fibrous layers seem thus to be more appropriate to facilitate bone healing through the association with other materials (in the case of critical defects) rather than to be used as single substitutes. Instead, for minimal damages, as for example damages of periosteum, the fibrous layer could be used to directly cover the damaged area and help to the tissue repair. Knowing that such damages are painful due to the presence of nerves in the periosteum, it is important to consider these problems for the patients, even if the damages may look minimal in comparison to critical defects. Hence, it is clear that fibrous layers cannot be used to treat all problems related to bone and that materials should be designed according to the requirements of a targeted application. If this strategy is not respected, not all the requirements needed for a precise application may be fulfilled. It is therefore essential to first establish the criteria that a scaffold should satisfy and then design a material among the different experts involved in the research, instead of developing a material and to try to adapt it to an *ad hoc* application. Fibrous membranes constitute a typical example of this problem: even though they mimic the structure of natural bone and are therefore presented in the literature as a good scaffold for bone regeneration, they do not satisfy all the needed criteria to repair critical defects for example. Based on these observations, it may be wondered if other applications may be more suitable for the use of fibrous layers. They seem particularly adapted for wound healing, for example. In fact, they can act as barrier protection against bacteria, while enabling oxygen flow. In this case, the compression properties of the fibrous membranes would not be a problem. Wound healing is thus an example of application for which electrospun fibers may be more appropriate.

In conclusion, fibrous layers may be used for bone tissue engineering to treat some precise problems but they may find better use for other applications. Given the necessity to specifically design implants for defined application, in addition, we should remark that the main benefit of the work

presented in this thesis is not the production of fibers itself (i.e. material processing with electrospinning) but the development of the blends and the versatility of the coating protocol. Indeed, the possibility to use the blends with other processing methods and to transfer the protocol to other structures is thought to be the principal advance for the regenerative medicine field, as it offers numerous perspectives of work and the ability to produce improved scaffolds for specific applications (requiring osteo and/or angiogenesis).

5.3. Summary

Overall, this thesis reports the development of three novel hybrid materials for bone tissue engineering. This work constitutes the starting point for the design of other materials and for further biological studies. From a general point of view, the main contributions of this thesis to the state of the art and to the advances achieved for the medicine regenerative field are:

- Fabrication of polymer-ORMOGLASS hybrids: a novel family of smart biomaterials
- Development of two class I materials (blends) exhibiting good biocompatibility
- Preparation of polymer-ORMOGLASS blends for a successful electrospinning process
- Development of a new protocol to prepare class II materials (coating approach) that possess the bioactive phase exposed at their surface
- Implementation of the sol-gel method to silicon- and titanium-based ORMOGLASSES, whose compositions may be used to modulate calcium release behavior of the final hybrid materials
- Validation of polymer-ORMOGLASS hybrids for the triggering of specific cellular responses
- Introduction of concepts and groundwork for the development of hybrid materials, providing valuable perspectives of work for the future

5.4. References

[1] Pereira MM, Jones JR, Hench LL. Bioactive glass and hybrid scaffolds prepared by sol–gel method for bone tissue engineering. Advances in Applied Ceramics 2005;104:35–42.

[2] Dorozhkin S V. Biocomposites and hybrid biomaterials based on calcium orthophosphates. Biomatter 2011;1:1–54.

[3] Manzano M, Arcos D, Rodriguez Delgado M, Ruiz E, Gil FJ, Vallet-Regi M. Bioactive star gels. Chemistry of Materials 2006;18:5696–703.

[4] Michalczyk MJ, Sharp KG. Single component inorganic/organic network materials and precursors thereof, 1995.

[5] Sharp KG, Michalczyk MJ. Star gels: new hybrid network materials from polyfunctional single component precursors. Journal of Sol-Gel Science and Technology 1997;8:541–6.

[6] Jones JR. New trends in bioactive scaffolds: the importance of nanostructure. Journal of the European Ceramic Society 2009;29:1275–81.

[7] Judeinstein P, Sanchez C. Hybrid organic-inorganic materials: a land of multidisciplinarity. Journal of Materials Chemistry 1996;6:511–25.

[8] Lu JX, Flautre B, Anselme K, Hardouin P, Gallur a, Descamps M, et al. Role of interconnections in porous bioceramics on bone recolonization in vitro and in vivo. Journal of Materials Science Materials in Medicine 1999;10:111–20.

[9] Simon JL, Roy TD, Parsons JR, Rekow ED, Thompson VP, Kemnitzer J, et al. Engineered cellular response to scaffold architecture in a rabbit trephine defect. Journal of Biomedical Materials Research Part A 2003;66:275–82.

[10] Sudo H, Kodama H-A, Amagai Y, Yamamoto S, Kasai S. In vitro differentiation and calcification in a new clonal osteogenic cell line derived from newborn mouse calvaria. The Journal of Cell Biology 1983;96:191–8.

[11] Gibon E, Batke B, Jawad MU, Fritton K, Rao A, Yao Z, et al. MC3T3-E1 osteoprogenitor cells systemically migrate to a bone defect and enhance bone healing. Tissue Engineering Part A 2012;18:968–73.

[12] Caplan AI. Mesenchymal stem cells. Journal of Orthopaedic Research 1991;9:641–50.

[13] Jo J-H, Lee E-J, Shin D-S, Kim H-E, Kim H-W, Koh Y-H, et al. In vitro/in vivo biocompatibility and mechanical properties of bioactive glass nanofiber and poly(ε-caprolactone) composite materials. Journal of Biomedical Materials Research Part B: Applied Biomaterials 2009;91B:213–20.

[14] Sanzana ES, Navarro M, Ginebra M-P, Planell JA, Ojeda AC, Montecinos HA. Role of porosity and pore architecture in the in vivo bone regeneration capacity of biodegradable glass scaffolds. Journal of Biomedical Materials Research Part A 2013:1–7.

[15] Vila OF, Bagó JR, Navarro M, Alieva M, Aguilar E, Engel E, et al. Calcium phosphate glass improves angiogenesis capacity of poly(lactic acid) scaffolds and stimulates differentiation of adipose tissue-derived mesenchymal stromal cells to the endothelial lineage. Journal of Biomedical Materials Research Part A 2013;101:932–41.

[16] Kiani A, Lakhkar NJ, Salih V, Smith ME, Hanna J V, Newport RJ, et al. Titanium-containing bioactive phosphate glasses. Philosophical Transactions of the Royal Society Series A, Mathematical, Physical, and Engineering Sciences 2012;370:1352–75.

[17] Mahony O, Tsigkou O, Ionescu C, Minelli C, Ling L, Hanly R, et al. Silica-gelatin hybrids with tailorable degradation and mechanical properties for tissue regeneration. Advanced Functional Materials 2010;20:3835–45.

[18] Poologasundarampillai G, Yu B, Tsigkou O, Valliant E, Yue S, Lee PD, et al. Bioactive silica–poly(γ-glutamic acid) hybrids for bone regeneration: effect of covalent coupling on dissolution and mechanical properties and fabrication of porous scaffolds. Soft Matter 2012;8:4822–32.

[19] Kim G, Kim W. Highly porous 3D nanofiber scaffold using an electrospinning technique. Journal of Biomedical Materials Research Part B 2007;81B:104–10.

[20] Rnjak-Kovacina J, Wise SG, Li Z, Maitz PKM, Young CJ, Wang Y, et al. Tailoring the porosity and pore size of electrospun synthetic human elastin scaffolds for dermal tissue engineering. Biomaterials 2011;32:6729–36.

[21] Blakeney BA, Tambralli A, Anderson JM, Andukuri A, Lim D-J, Dean DR, et al. Cell infiltration and growth in a low density, uncompressed three-dimensional electrospun nanofibrous scaffold 2012;32:1583–90.

[22] Baker BM, Gee AO, Metter RB, Nathan AS, Marklein RA, Burdick JA, et al. The potential to improve cell infiltration in composite fiber-aligned electrospun scaffolds by the selective removal of sacrificial fibers. Biomaterials 2008;29:2348–58.

[23] Nerurkar NL, Sen S, Baker BM, Elliott DM, Mauck RL. Dynamic culture enhances stem cell infiltration and modulates extracellular matrix production on aligned electrospun nanofibrous scaffolds. Acta Biomaterialia 2011;7:485–91.

[24] Fromstein JD, Zandstra PW, Alperin C, Rockwood D, Rabolt JF, Woodhouse KA. Seeding bioreactor-produced embryonic stem cell-derived cardiomyocytes on different porous, degradable, polyurethane scaffolds reveals the effect of scaffold architecture on cell morphology. Tissue Engineering Part A 2008;14:369–78.

[25] Li W-J, Laurencin CT, Caterson EJ, Tuan RS, Ko FK. Electrospun nanofibrous structure: a novel scaffold for tissue engineering. Journal of Biomedical Materials Research 2002;60:613–21.

[26] Frey MW, Li L. Electrospinning and porosity measurements of nylon-6/poly(ethylene oxide) blended nonwovens. Journal of Engineered Fibers and Fabrics 2007;2:31–7.

[27] Rutledge GC, Lowery JL, Pai C. Characterization by mercury porosimetry of nonwoven fiber media with deformation. Journal of Engineered Fibers and Fabrics 2009;4:1–13.

[28] Brunauer S, Emmett PH, Teller E. Adsorption of gases in multimolecular layers. Journal of the American Chemical Society 1938;60:309–19.

[29] Tsakiroglou CD, Burganos VN, Jacobsen J. Pore-structure analysis by using nitrogen sorption and mercury intrusion data. AIChE Journal 2004;50:489–510.

[30] Serra T, Planell JA, Navarro M. High-resolution PLA-based composite scaffolds via 3-D printing technology. Acta Biomaterialia 2013;9:5521–30.

[31] Yeong W-Y, Chua C-K, Leong K-F, Chandrasekaran M. Rapid prototyping in tissue engineering: challenges and potential. Trends in Biotechnology 2004;22:643–52.

Appendix A

Complementary information

A.1. Appendix A – Alkoxide precursor characterization (Nuclear Magnetic Resonance, NMR)

All the single alkoxide precursors prepared in our laboratory were characterized by NMR (see appendix B-1) to make sure that they were suitable for the sol-gel process. The acquired spectra are presented in **Figure A-1** and the assignment of the peaks in **Table A-1**. ^{1}H NMR measurements were performed using a Bruker AMX 500-MHz device. Alkoxides were dropped in small quantities (few µL) in deuterated solvents (around 500 µL). All measurements were run at ambient temperature (~ 25°C) using CD_3CD_2OD or CD_3OD. The solvent was selected according to its compatibility with the alkoxide precursor. For example, calcium 2-methoxyethoxide was not compatible with CD_3OD as it induced the instantaneous gelation of the solution (unknown reason). However, CD_3OD was preferred when its use did not represent a problem. The integration of the different peaks observed in the spectra was done by choosing the peak for normalization according to the stability of the associated compounds (peak of NMR solvent or peaks associated to a stable peak of the sample).

Calcium precursor was prepared by dissolving calcium metallic in 2-methoxyethanol [1]. The precursor showed 2 triplets centered at 3,68 and 3,48 ppm respectively. These triplets were attributed to the resonance of the two CH_2 groups found in calcium 2-methoxyethoxide, as well as the singlet located at 3,37 ppm assigned to the terminal CH_3 group of the molecules. The attribution of the peaks was confirmed by the integrated peak-area values. When considering the peak at 3.37 ppm as the peak for normalization (value "3" for CH_3), the area of the other peaks gave values almost equal to 2, attesting that these peaks were related to two CH_2 groups.

Phosphorous precursor was prepared by refluxing P_2O_5 in ethanol [2]. Ethanol (precursor's solvent) was observed at 3.62 ppm (quadruplet, CH_2 group) and 1.19 ppm (triplet, CH_3 group). The ratio of the integration values between the two peaks confirmed that the peak attribution was correct (125.49/83.95~1.5 as for the theoretical one 3/2=1.5). Other signals at higher shifts were also assigned to ethanol: the set of peaks located at around 4.05 ppm (overlay of two triplets) and 1.32 ppm (overlay of two quadruplets) (**Figure A-2**). As for the first enounced triplet and quadruplet, the ratio of peak-area values demonstrated that these overlays were indeed related to ethanol molecules.

The fact that ethanol signals are observed at different places suggested that ethanol molecules did not all interact with P_2O_5 in the same manner. It was even expected that some of them did not interact with P_2O_5 because ethanol was introduced in excess for the reflux. To assess that, DOSY NMR was performed (**Figure A-3**). The DOSY diagram clearly showed that the peaks at 3.62 ppm and 1.24 ppm were indeed resulting from free ethanol molecules (low diffusion coefficient as the free CD_3OD NMR solvent molecules) and the overlapping of the triplets and quadruplets was resulting from the interactions of ethanol with "big" molecules (i.e. P_2O_5 ones). The diffusion of these molecules was, in fact, slower. The overlapping of two triplets and the quadruplets suggested that two kinds of P_2O_5-ethanol interactions

occurred. In other words, at least two different species were found in the precursors. This observation was in accordance with other published results that demonstrated the formation of mono and diethyl phosphate when P_2O_5 is refluxed in ethanol [3,4]. Some other species might be also present but, if they are in smaller quantities than these two species, their signal might be masked by these two strong sets of triplets and quadruplets. Based on the peak-area values, it can be also concluded that the ethanol molecules that interacted with P_2O_5 represented approximately 50% of the total ethanol molecules (125.49/68.47 ~ 83.95/44.33 ~ 0.5). The quantification of the two species individually is, however, not possible due to the overlapping of the signals.

The sodium precursor was obtained by dissolving sodium metallic in 2-methoxyethanol [5]. It exhibited similar spectra than the calcium precursor. This is consistent as they were prepared with the same solvent and in the same way. The two triplets and the singlet are therefore observed in both precursors at the same positions.

The titanium precursor was prepared by dissolving commercial titanium isopropoxide in ethanol [6]. The precursor showed a septet centered at 3.95 ppm. This septet was attributed to the coupling between the CH groups of the isopropyl group with its neighboring CH_3 groups (coupling with 6 other H atoms = 7 peaks according to the Pascal's triangle, see appendix B-1). Reciprocally, the doublet at 1.17 ppm was assigned to the coupling between the CH_3 groups of the isopropyl group with the CH of that group. The two other signals located at 1.20 and 3.6 ppm were due to the presence of ethanol (precursor's solvent).

In summary, all the data obtained by NMR tend to show that the precursors were properly prepared.

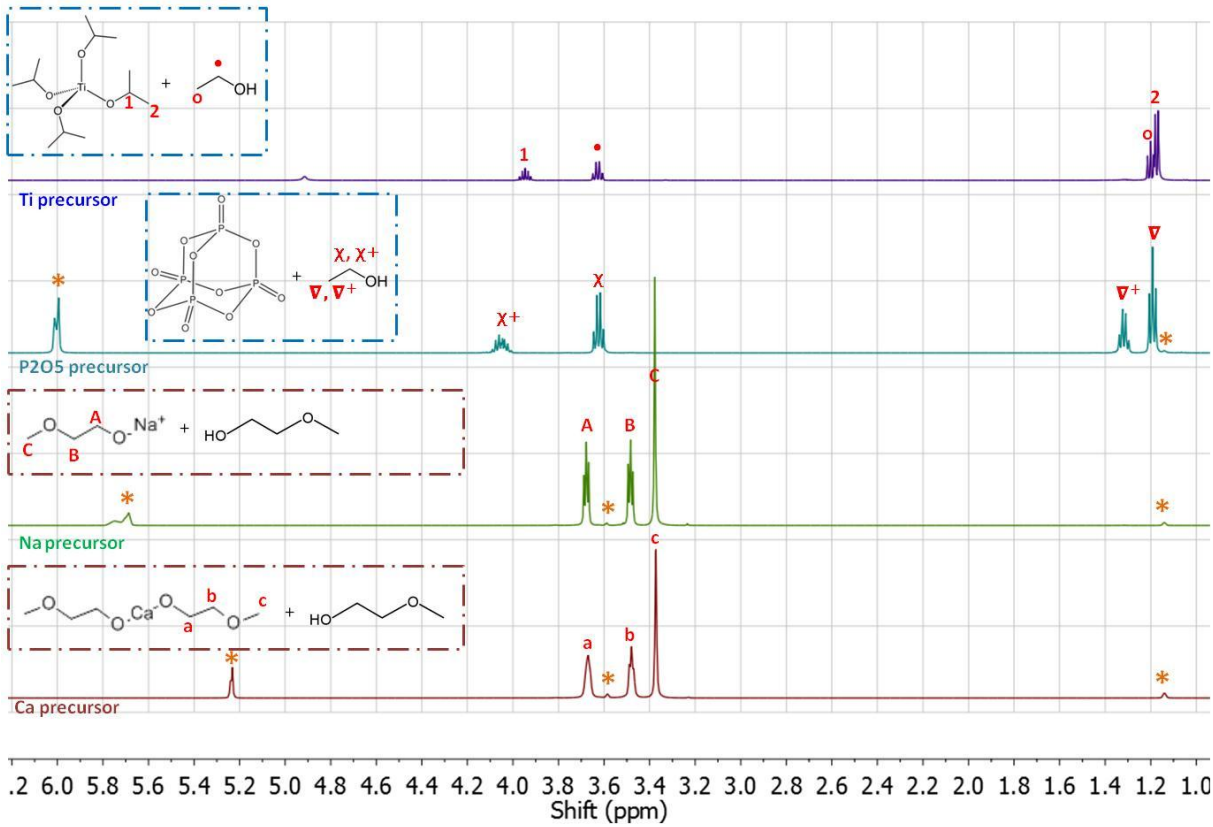

Figure A-1. ^{1}H NMR spectra obtained for single Ca, Na_2, P_2, and Ti precursors.

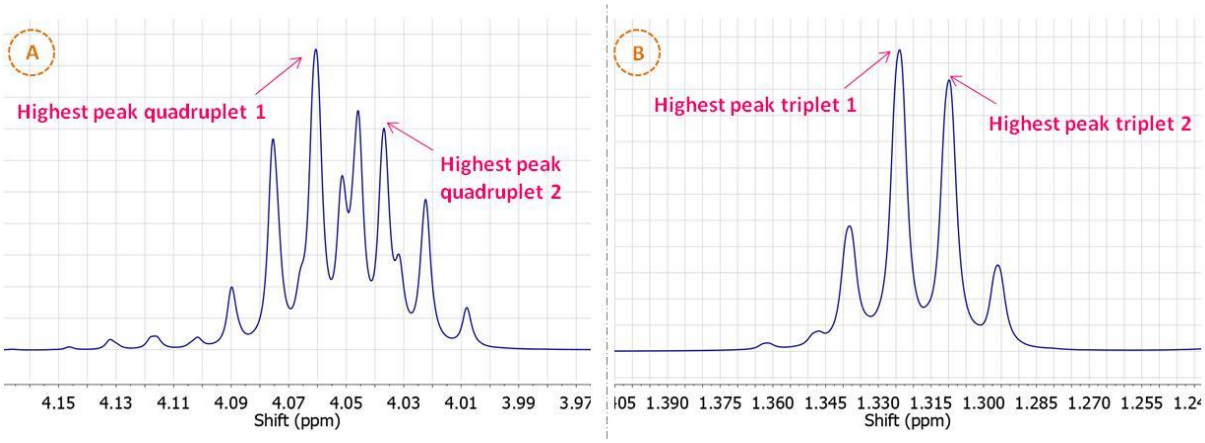

Figure A-2. Zoom of the ^{1}H NMR spectra obtained for P_2 where the overlays of the triplet and the quadruplet occured.

Table A-1. Summary of the peak assignments and their integration values. (*: value considered for integrals normalization)

Precursor (deuterated solvent)	Peak's label (chemical group associated)	Multiplet type	Shift (ppm)	Normalization peak considered for integration	Peak Area (integration)
Ca (CD_3CD_2OD)	a (CH_2)	triplet	3.67		2.17
	b (CH_2)	triplet	3.48	c	2.20
	c (CH_3)	singlet	3.37		3*
Na (CD_3CD_2OD)	A (CH_2)	quadruplet	3.68		1.98
	B (CH_2)	triplet	3.48	C	1.98
	C (CH_3)	singlet	3.38		3*
P (CD_3CD_2OD)	χ+ (CH_2)	overlay of 2 triplets	4.05		44.33
	χ (CH_2)	quadruplet	3.62	Solvent peak	83.95
	∇$^+$ (CH_3)	overlay of 2 triplets	1.32	(1.14ppm, 3*)	68.47
	∇ (CH_3)	triplet	1.19		125.49
Ti (CD_3OD)	1 (CH)	septuplet	3.95	1	1.00*
	2 (CH_3)	doublet	1.17		5.99
	• (CH_2)	quadruplet	3.63		1.41
	O (CH_3)	triplet	1.20		2.66

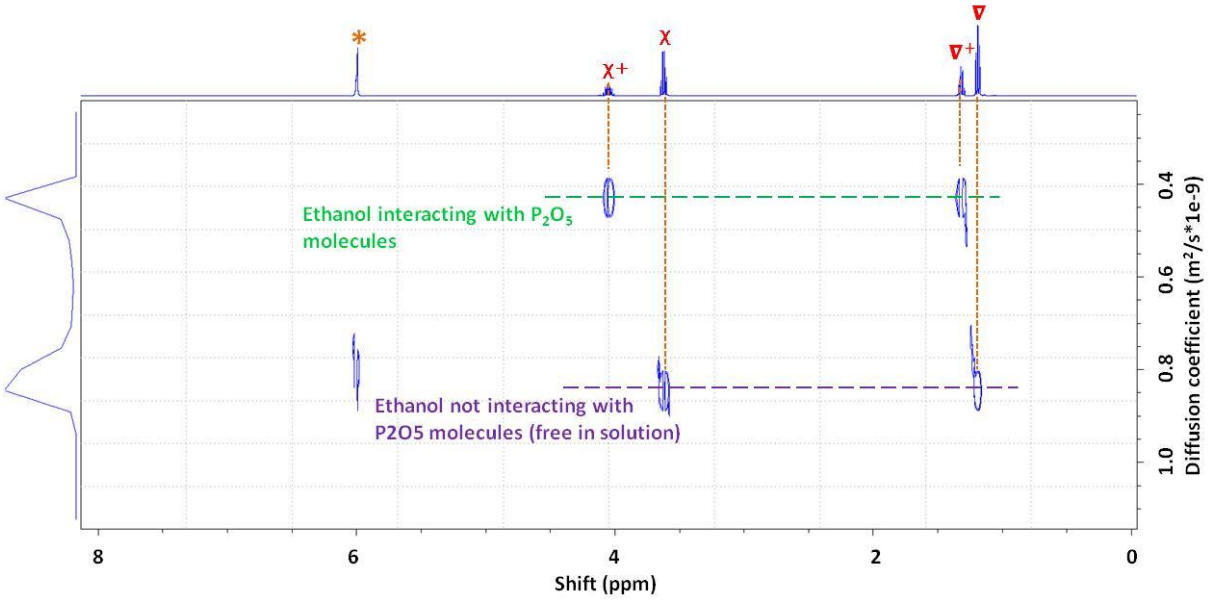

Figure A-3. DOSY NMR spectra obtained for phosphorous precursor showing the different diffusion coefficient of the molecules.

A.2. General Information

A.2.1. Precursor solutions – preparation

When alkoxide precursors were not commercially available (as the silicon one) to prepare the ORMOGLASS precursor mixes, they were prepared in the laboratory following procedures already established elsewhere. Calcium, phosphorous, titanium and sodium precursors were thus prepared by refluxing or dissolving independently the reagents under inert atmosphere in the desired solvent. The setup is presented in **Figure A-4**.

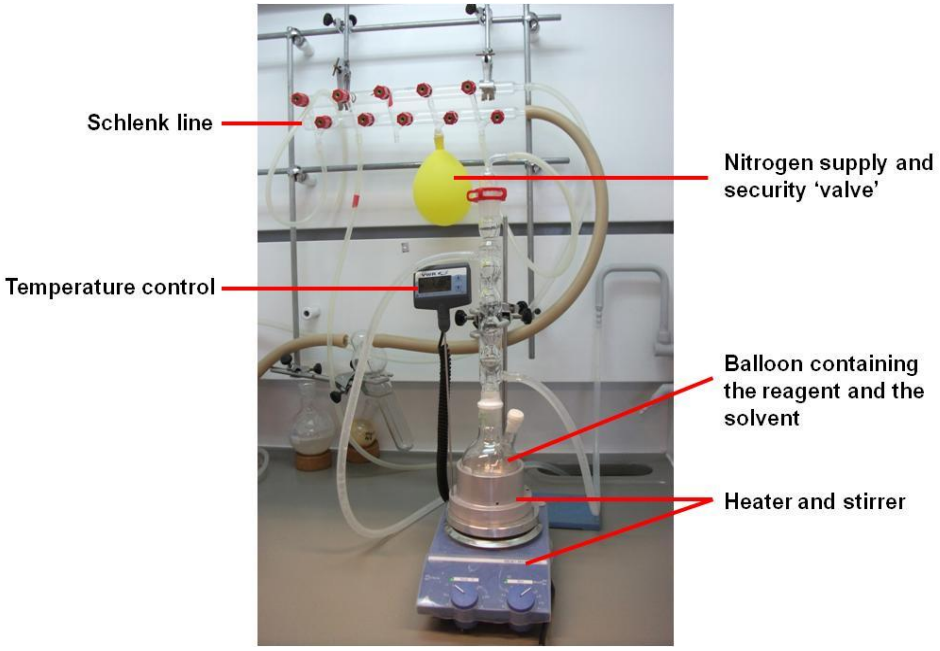

Figure A-4. Setup used to prepare the different alkoxide precursors by reflux method.

A.2.2. Blend preparation

The blends presented in the thesis, either based on Si-Ca-P_2 or Ti-Ca-P_2-Na_2 ORMOGLASS system, were prepared as described in the representation of the protocol in **Figure A-5**.

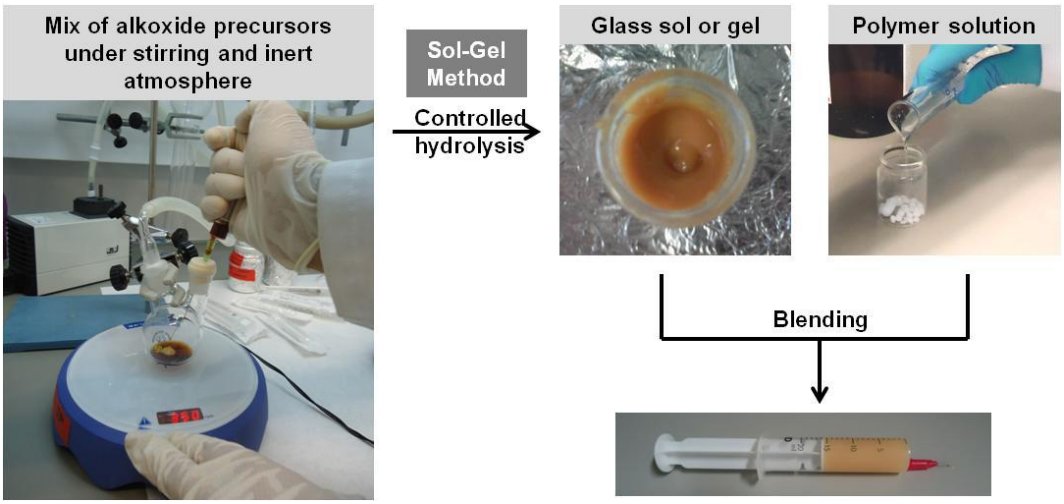

Figure A-5. Schematic representation of the preparation of the blends used for electrospinning.

A.2.3. <u>Electrospining device:</u>

The different blends were electrospun using a conventional electrospinning set-up which is shown in **Figure A-6**. Static flat collector was used to collect randomly distributed fibers and rotary collector was used to collect aligned fibers.

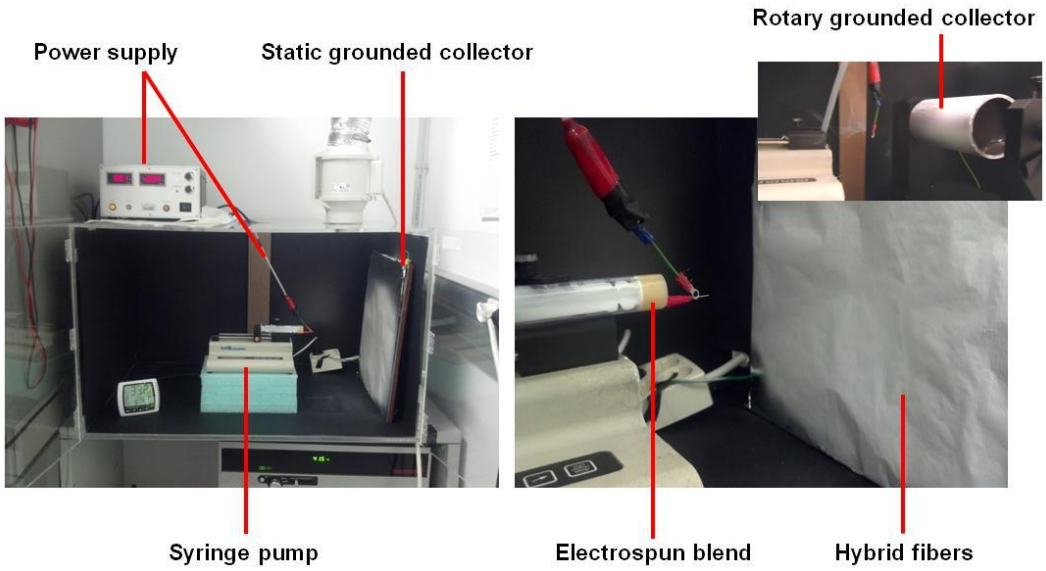

Figure A-6. Pictures of the electrospinning device used for the fabrication of the polymeric and hybrid fibers presented in the thesis.

A.3. Appendix A - Chapter 2

Assessment of the osteogenic potential by quantitative real-time polymerase chain reaction:

Table A-2. Primer sequences of the genes considered for the real-time PCR.

Gene	**Primer sequence**
ALP	(F) 5'-ACACCTTGACTGTGGTTACT-3' (R) 5'-CCTTGTAGCCAGGCCCGTTA-3'
COL I	(F) 5'-GCAACTCTGAAATCTCTCAA-3' (R) 5'-GCATCCATAGTACATCCTTG-3'
OPN	(F) 5'-GTGAAAGTGACTGATTCTGG-3' (R) 5'-TTGGAAGAGTTTCTTGCTTA-3'
OCN	(F) 5'-AGGGCAATAAGGTAGTGAAC-3' (R) 5'-ATACCGTAGATGCGTTTGTA-3'
GAPDH	(F) 5'-TGTTCCAGTATGACTCCACT-3' (R) 5'-TGGTGAAGACACCAGTAGAC-3'

A.4. Appendix A – Chapter 3

A.4.1. Contact angle measurements

When anisotropic materials are studied, the contact angle measurements should be performed in a well defined position for all the samples. In fact, when isotropic materials such as random fibers are analyzed, the positioning of the material in relation to the camera of the device does not affect the measured angle. The water drop spreads without any preferential direction. On the contrary, for anisotropic materials such as aligned fibers, the spreading of the drop is influenced by the topography of the material. In this case, the drop spreads preferentially along the fiber length. Therefore, it is important to place the samples always in the same position (transversal or cross section) to be able to compare the hydrophilicity of the different aligned mats. **Figure A-7** shows the effects of material anisotropy on the determination of the contact angle.

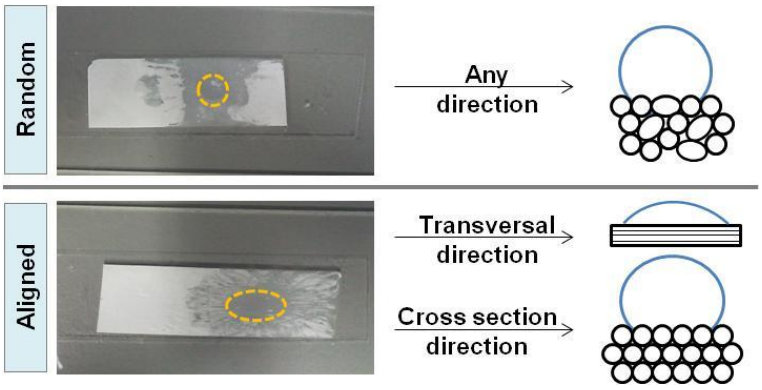

Figure A-7. Pictures and schematic representation of the water drop behavior on random and aligned fibers depending on the positioning of the sample.

A.4.2. Fibrous layer thickness

In order to determine the Young's Modulus and Yield strength of the fibrous mats (tensile tests), the thickness of the tested samples has to be known. This data was obtained from the FESEM pictures, imaging the mats in the transversal section. A typical example of such images is presented in **Figure A-8**.

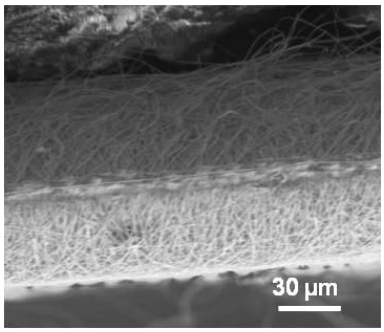

Figure A-8. Typical example of FESEM picture used for the determination of the fibrous mat thickness.

A.4.3. Differential scanning calorimetry

To verify that the sharp peak observed on the graphic of the T5 20-80 fibers (first heating ramp) was related to a measurement artifact, the DSC measurement was repeated for this sample. Because the device (DSC Q2000 TA, available in Warsaw) initially used for the assay was not available anymore, the measurement was repeated with another device in Barcelona (DSC Q20 TA). As seen on **Figure A-9**, the sharp peak observed with the first measurement is not observed on the graphic of the second measurement. This confirmed that the sharp peak was not related to the sample itself but to an artifact.

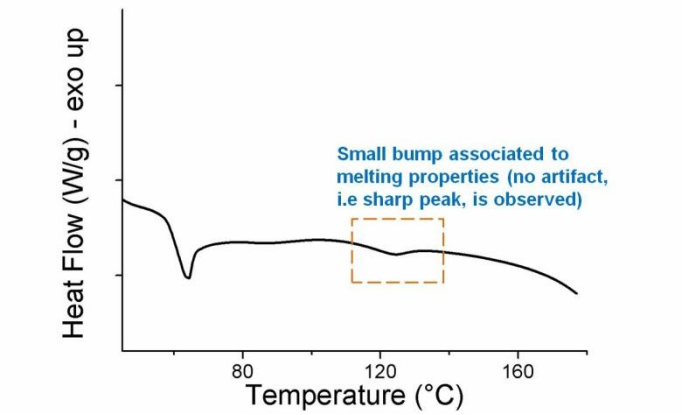

Figure A-9. DSC thermogram of T5 20-80 fibers.

A.4.4. Thermogravimetry analysis coupled Fourier Transform Infrared Spectroscopy

FTIR was coupled with TGA analysis in order to determine which compounds were degrading during the TGA assay (Peak 1 around 220°C, peak 2 around 245°C and peak 3 around 360°C). The spectra related to the decomposition of the compounds are presented in **Figure A-10**. Based on the literature [7,8], the peaks 1 and 2 observed for the hybrid fibers were both assigned to alkylphosphate molecules. The presence of two peaks associated to the same kind of molecules can be explained by the nature of the species found in the phosphorous precursor (mono and diethyl phosphate) (see appendix A-1). The third peak is typically due to the decomposition of PLA (lactide and other compounds associated to the degradation of PLA: carbon dioxide, carbon monoxide, acetaldehyde…) [9,10].

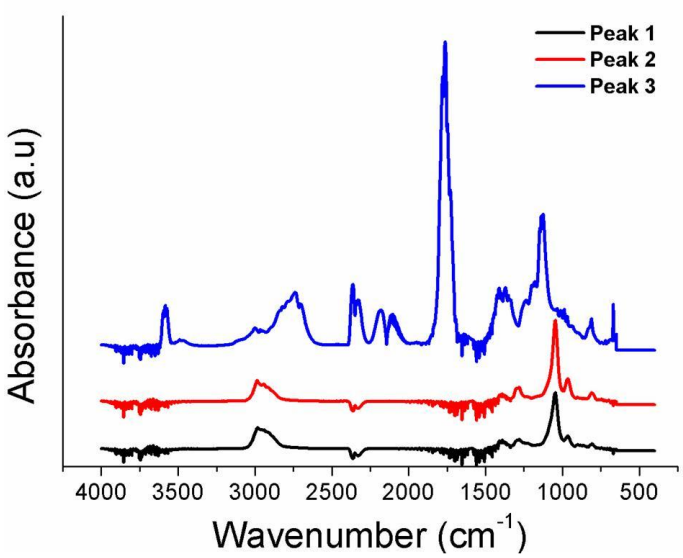

Figure A-10. FTIR spectra of compounds vaporizing during the thermal degradation of hybrid fibers.

A.4.5. Tensile tests

Although the Young's modulus and Yield strength were improved for the hybrid fibers, their fracture occurred under a lower strain value than PLA. As seen in **Figure A-11**, scaffolds fracture depended on the glass content. The random T5 10:90 fibers conserved some plastic deformation (from PLA) before breaking while the random T5 20:80 ones did not show this intermediate phase and simply breaks. This is typically related to a glass behavior [11]. The more ormoglass is introduced into the polymeric matrix, the more brittle becomes the material. For the aligned fibers, this behavior is also observed. Aligned T5 10-90 fibers did not even showed plastic deformation as they did as random mats.

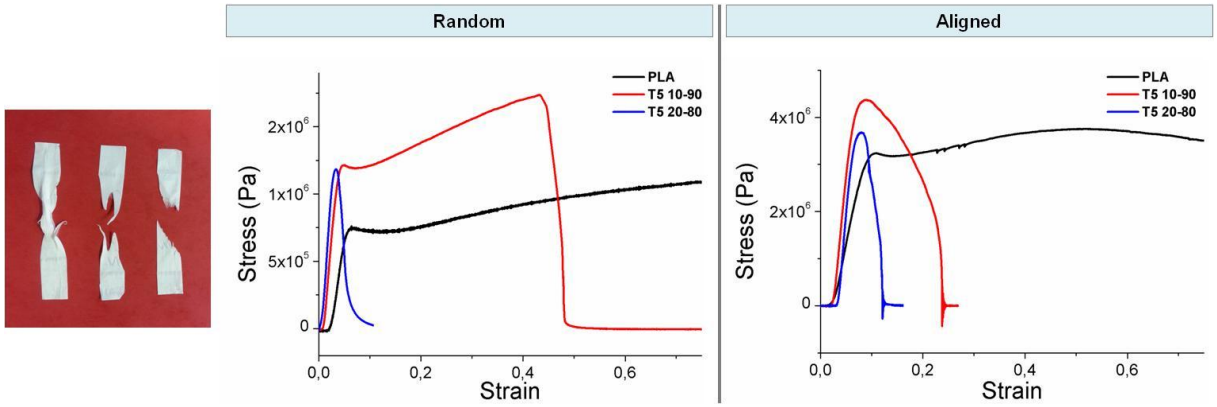

Figure A-11. Pictures of random hybrid fibers after tensile tests and strain-stress curves obtained for the random and hybrid mats.

A.4.6. In vitro assays:

Figure A-12 shows the FESEM pictures of MSCs and EPCs cultured on the hybrid fibers. Low magnification pictures confirmed the fluorescent images: cells proliferated well after 10d of culture and were found over the whole membranes.

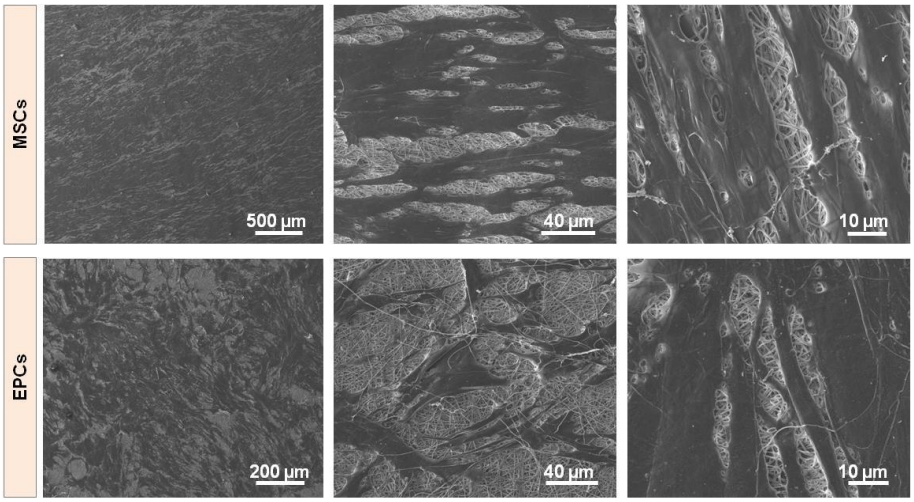

Figure A-12. FESEM images of cells cultured on the hybrid fibers.

A.4.7. Fiber preparation - Protocol improvement:

Numerous processing parameters have to be controlled to produce homogeneous fibers without imperfections. **Figure A-13** presents the typical problems that occurred during the elaboration of the fiber fabrication protocol. Picture 1 shows the presence of glass aggregates and picture 2 the bimodal distribution of the fiber thickness and presence of "spider web". These pictures pointed the importance of preparing a proper blend and setting correctly the electrospinning working conditions in order to produce homogeneous fibrous templates.

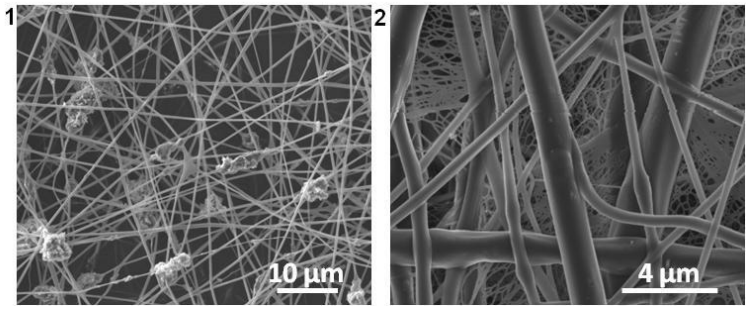

Figure A-13. Problems overcame during the elaboration of a protocol to fabricate homogeneous hybrid fibers (FESEM pictures).

A.4.8. Protein adsorption:

Depending on the pH of the solution in which a protein is contained, proteins can be negatively or positively charge [12]. pH measurements of the solution in which the adsorption assay was conducted

revealed that the pH was between 7.38 and 7.27 (**Figure A-14**). In this range of pH, bovine albumin serum (BSA) is negatively charged [13]. Moreover, these measurements showed that even after 1h of incubation before starting the test, the pH still slightly decreased the pH of water, especially the hybrid fibers. It confirmed thus that during this assay, the ZP of the hybrid fibers was more electropositive (but still negative) than PLA fibers and thus enhanced the affinity of the protein with the hybrids.

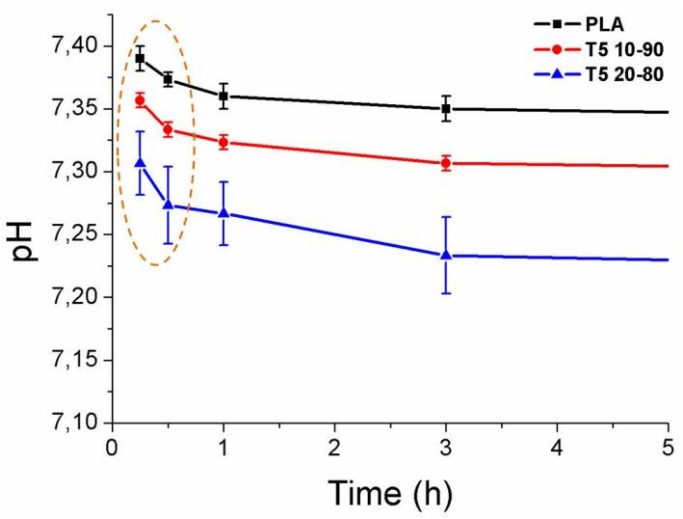

Figure A-14. pH measurements of the solution in which the BSA adsorption test was performed (orange circle denotes the range of pH of the solution during the time of the assay: 30min).

A.4.9. Calcium dissolution and pH measurements:

The assessment of ion dissolution by materials is often carried out in SBF or in culture medium [14]. Performing such assay in these solutions is interesting as it enables to determine the changes in ion concentration closely as they occur in *in vitro* and *in vivo* tests. However, these solutions act as buffers and can prevent these modifications to be clearly seen. Therefore, to assess precisely the ion release behavior, it is more appropriate to use deionized water as it does not temper the effects of the ion release. A study performed with the hybrid fibers incubated in water and in SBF demonstrated these affirmations (**Figure A-15**). While the difference in calcium concentration and release rate was obvious in water, it was difficult to be observed in SBF. The pH changes were also less important in SBF than in water. Moreover, the supply of calcium ion from the SBF rapidly masked the slight changes caused by the material. Differences in ion release profiles were also observed by other researchers when the studied materials were immersed in different solutions [15].

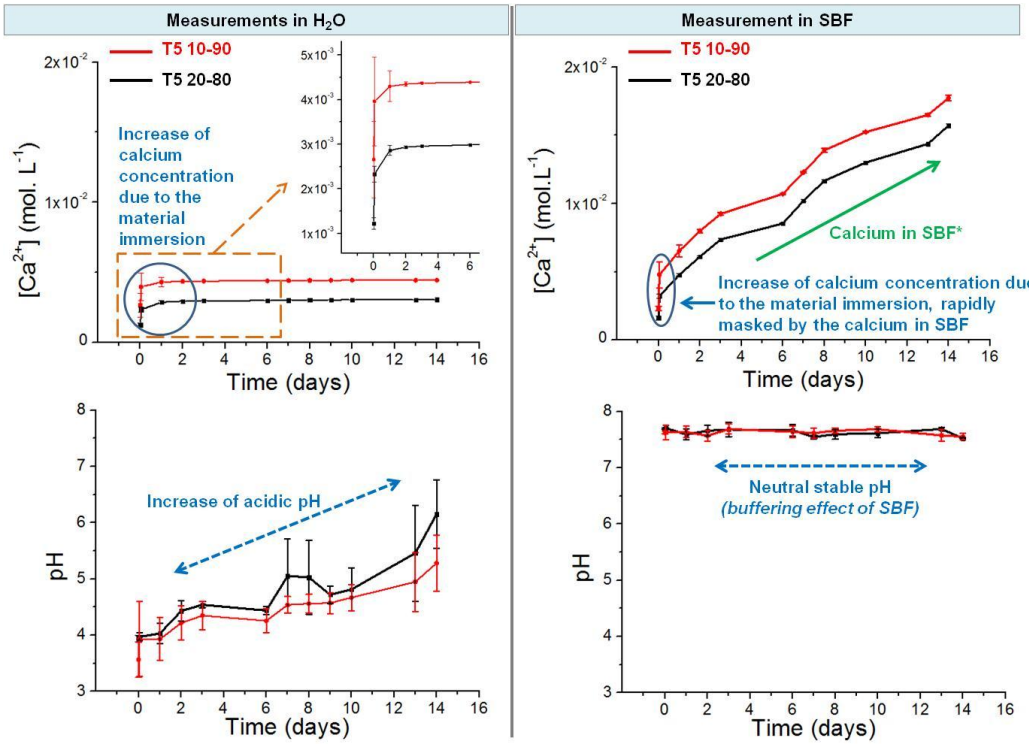

Figure A-15. Differences between a dissolution assay performed in water and in SBF. Blue circles point the area where the main changes occurred due to the material immersion (*: contained in the SBF solution itself – results are presented as cumulative ion concentration) and blue arrows denote the tendency of the pH variations.

A.4.10. Fiber morphology:

Additional pictures of the fibers morphology are shown in **Figure A-16**. These images demonstrated the good correlation between images obtained by FESEM and the ones obtained by AFM. All the typical fiber defects that occurred during the material incubation were seen with both techniques.

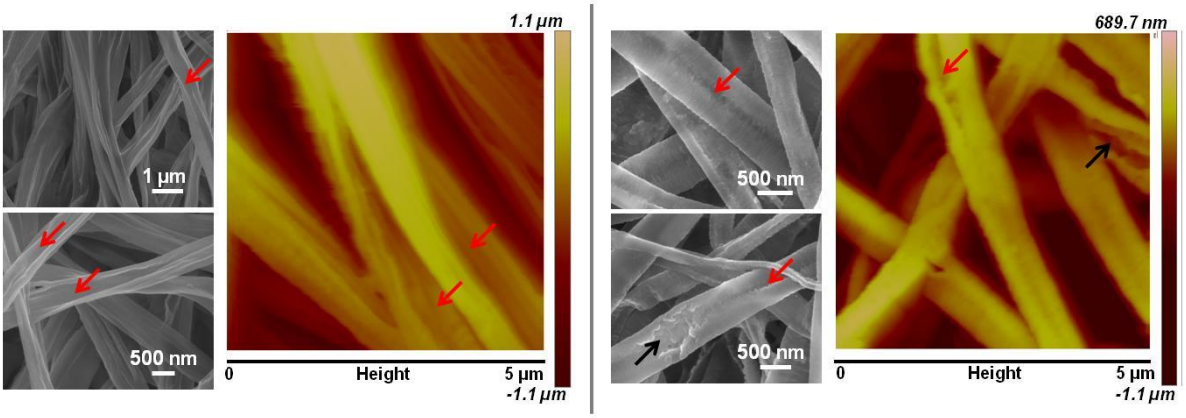

Figure A-16. Fiber morphology after 21 d of incubation in SBF. Red arrows point the flattening of the fibers and black ones show the opening and cracking of the fibers.

A.4.11. Scaffold integrity:

When hybrid fibers are incubated in SBF, they became extremely brittle with time. At some point, it was even impossible to handle the mats (**Figure A-17**).

Figure A-17. Pictures of the hybrid fibers after several weeks of incubation in SBF.

A.4.12. Fiber flattening and defects:

As represented in **Figure A-18**, when water infiltrated the fibers, the water may have originated zones of high strain on the fiber walls due to the fiber flattening (hollow fibers). To release this strain, fibers may have cracked instantaneously (***path 1***). Another possibility can be that fibers did not crack immediately and that the flattening led to additional forces applied perpendicularly to the fiber length. Consequently, fibers may have slowly opened in the middle of the fibers (***path 2***). The last explanation may be that the presence of the crack may have itself induced the opening on the fibers by introducing other forces on each side of the crack (***path 3***). These three options might explain the aspect of the different defects observed during the fiber degradation.

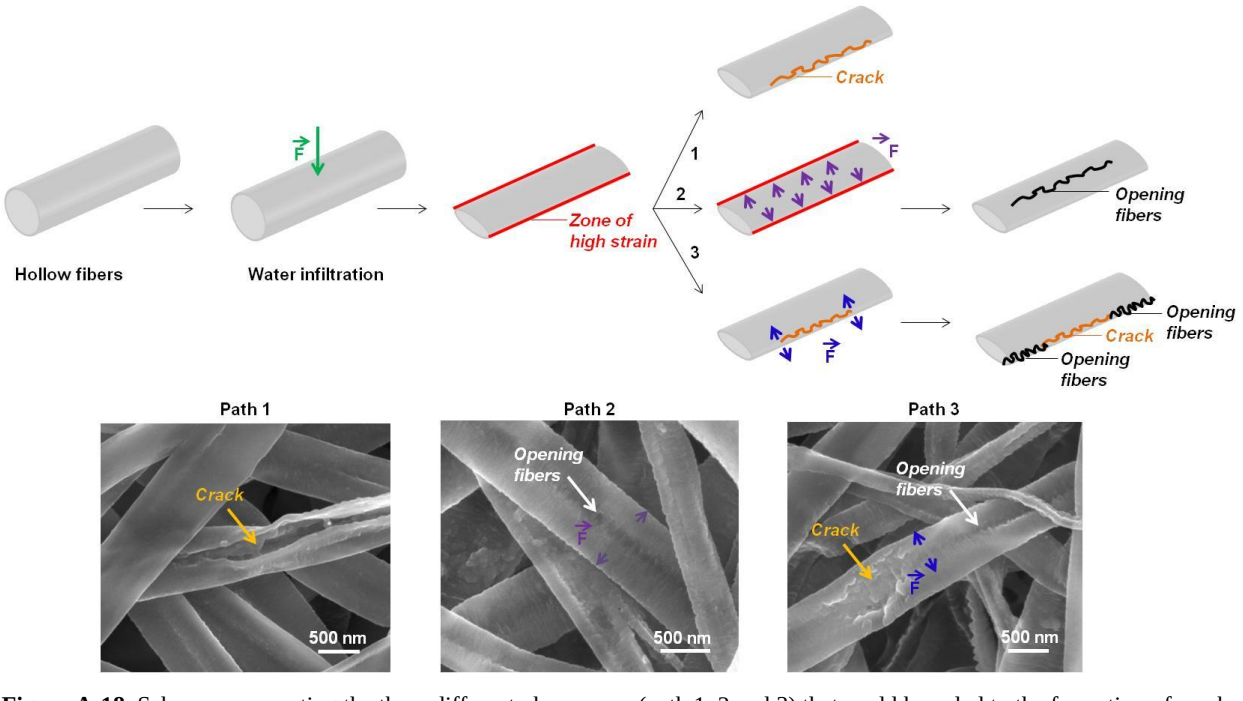

Figure A-18. Scheme representing the three different phenomena (path 1, 2 and 3) that could have led to the formation of cracks and opening on the fibers' surface, and correlation with FESEM images.

A.4.13. Fibers crystallinity

Because it was not possible, using DSC, to define if the crystallinity of the fibers increased along with the incubation, X-ray measurements were carried out as complementary tests with the T5 20-80 fibers. PLA pellets and PLA fibers were used as controls. The measurements were conducted using a PANalytical X'Pert PRO MPD diffractometer and measuring from 2 to 30° (2θ). Results are reported in **Figure A-19**. As seen on the spectra, crystalline phases were detected on the hybrid fibers, as produced by electrospinning. According to the literature [16,17] and the "International Center for Diffraction Data" XRay database (PCPDFWIN software), the associated peaks may correspond to hydrated titanium-phosphate species, containing or not sodium (for example, $Ti(HPO_4)_2.2H_2O$, $Na_2Ti(PO_4).4H_2O$ and other possible species). After 1h immersion, these peaks disappeared, suggesting that these compounds were dissolved in the SBF. Also, it was hypothesized that these compounds were present in a small quantity in comparison to the total amount of ORMOGLASS and were considered as "residual" species. After 1h immersion and up to the end of the assay, fibers did not seem to crystallize. All the samples appeared to be amorphous. This attested that the incubation did not favor the crystallization of the compounds in the fibers (or at least, not enough to be detected). As a consequence, it is highly probable that crystallinity did not cause the formation of cracks on the fibers.

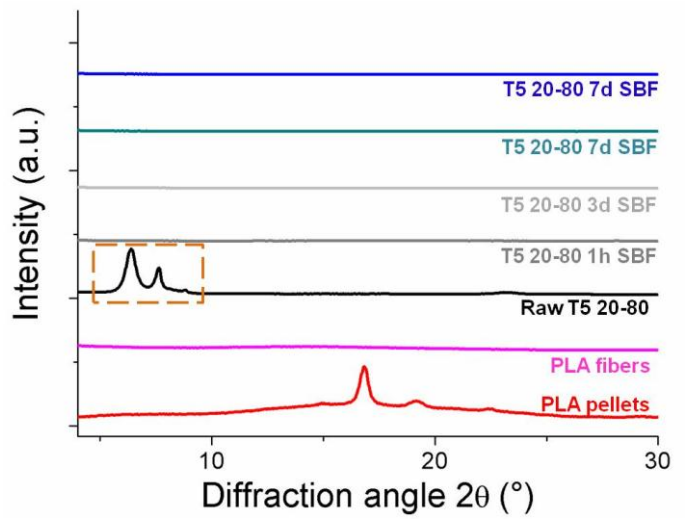

Figure A-19. X-Ray diffraction spectra of PLA pellets, PLA and T5 20-80 hybrid fibers (the orange square denotes the presence of crystalline compounds present in the hybrid fibers just after electrospinning).

A.5. Appendix A – Chapter 4

A.5.1. Fibrous layer thickness

In order to determine the Young's Modulus and Yield strength of the fibrous mats, the thickness of the tested sample should be determined. This data was obtained from the FESEM pictures, imaging the mat in the transversal section. A typical example of such images is presented in **Figure A-20**.

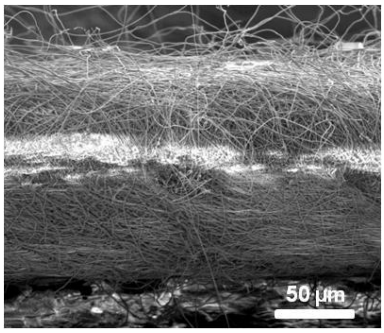

Figure A-20. Typical example of FESEM picture used for the determination of the fibrous mat thickness.

A.5.2. Calcium dissolution and pH measurements

The assessment of ion dissolution by materials is often carried out in SBF or in culture medium [14]. Performing such assay in these solutions is interesting as it enables to determine the change in ion concentration closely as they occur in *in vitro* and *in vivo* tests. However, these solutions act as buffers and can prevent these modifications to be clearly seen. Therefore, to assess precisely the ion release behavior, it is more appropriate to use deionized water as it does not temper the effects of the ion release. A study performed with the coated fibers incubated in water and in SBF demonstrated these affirmations (**Figure A-21**). While the difference in calcium concentration and release rate was obvious in water, it was difficult to be observed in SBF. The pH changes were also less important in SBF than in water. Moreover, the supply of calcium ion from the SBF rapidly masked the slight changes caused by the material.

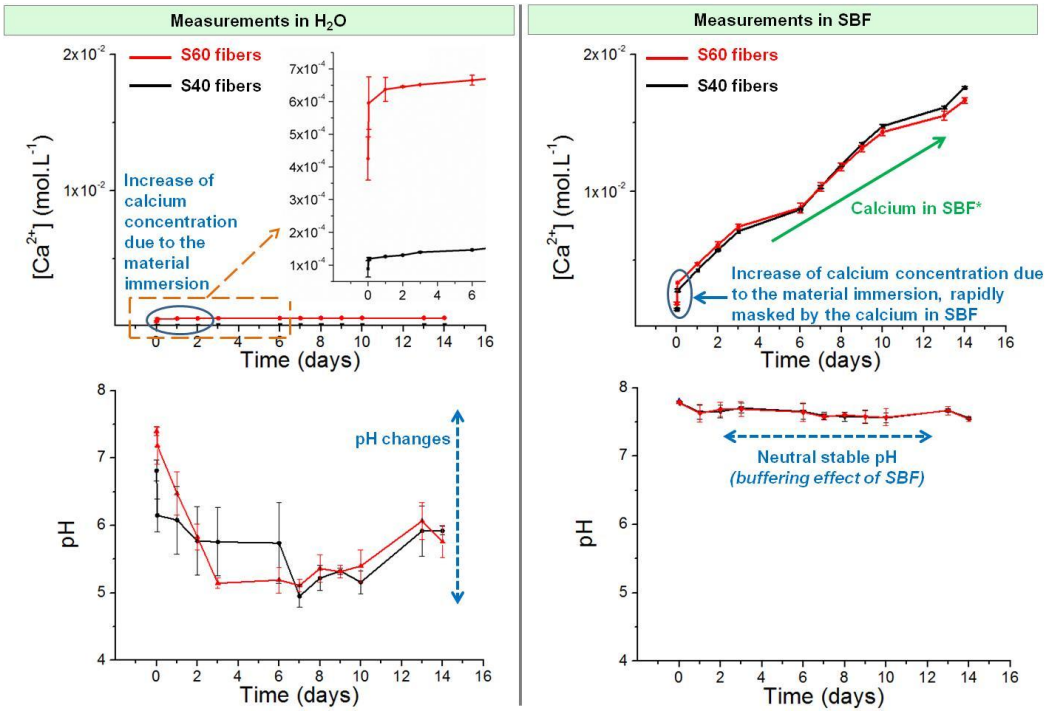

Figure A-21. Differences between a dissolution assay performed in water and in SBF. Blue circles point the area where the main changes occurred due to the material immersion (*: contained in the SBF solution itself – results are presented as cumulative ion concentration) and blue arrows denote the intensity of the pH variations.

A.5.3. Tensile tests

Tensile tests were performed to evaluate the mechanical properties of the whole PLA and coated fibrous mats. **Figure A-22** shows the representative strain-stress curves used to determine the Young's Modulus and Yield Strength reported in histograms in the thesis.

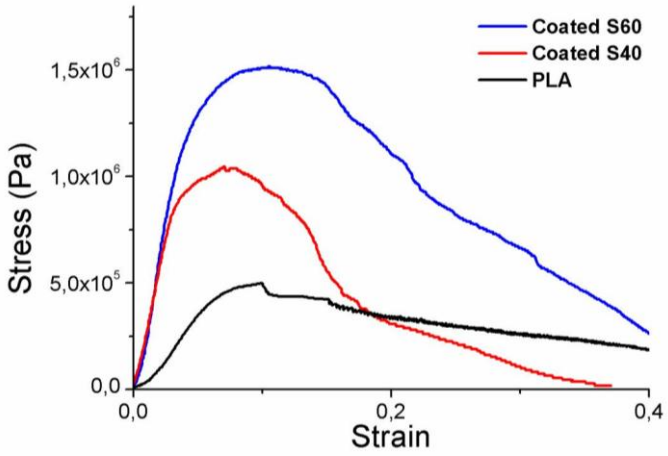

Figure A-22. Typical strain-stress curves obtained for the PLA and coated fibrous mats.

A.5.4. Thermogravimetry analysis coupled Fourier Transform Infrared spectroscopy:

FTIR was coupled with TGA analysis in order to determine the different compounds that degrade during the heating temperature program applied to fibers coated with the S60 glass composition. This method enabled the acquisition of the FTIR spectra of the gaseous products that vaporized at different temperatures to be used for compound identification. The spectra related to the decomposition of the three compounds seen with TGA (77°C, 270°C and 360°C) are presented in **Figure A-23**. Based on spectral database of the literature [18,19], the peak at 77°C was attributed to the presence of triethoxysilane compounds. This is due to the use of TEOS for the preparation of the glass and possible residual remaining molecules not incorporated in the glass network. Peaks at 270°C and 360°C were both assigned to the decomposition of different PLA fragments (lactide and other compounds associated to the degradation of PLA: carbon dioxide, carbon monoxide, acetaldehyde…) [9,10].

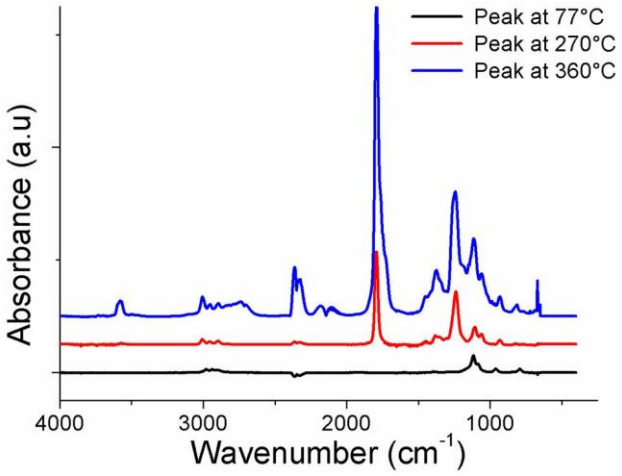

Figure A-23. FTIR spectra of compounds vaporizing during the thermal degradation of S60 fibers at 77°C, 270°C and 360°C.

A.5.5. FESEM images of the inorganic shell:

Figure A-24 shows the pictures of the inorganic shells obtained after thermal treatment of the coated fibers in the furnace. Images of the remaining inorganic shell of the S60 fibers showed the monolayer of glass particles forming the coating. Images of the S40 revealed that no well-defined tubular structure was found and the inability to measure the thickness of this layer in a reliable manner.

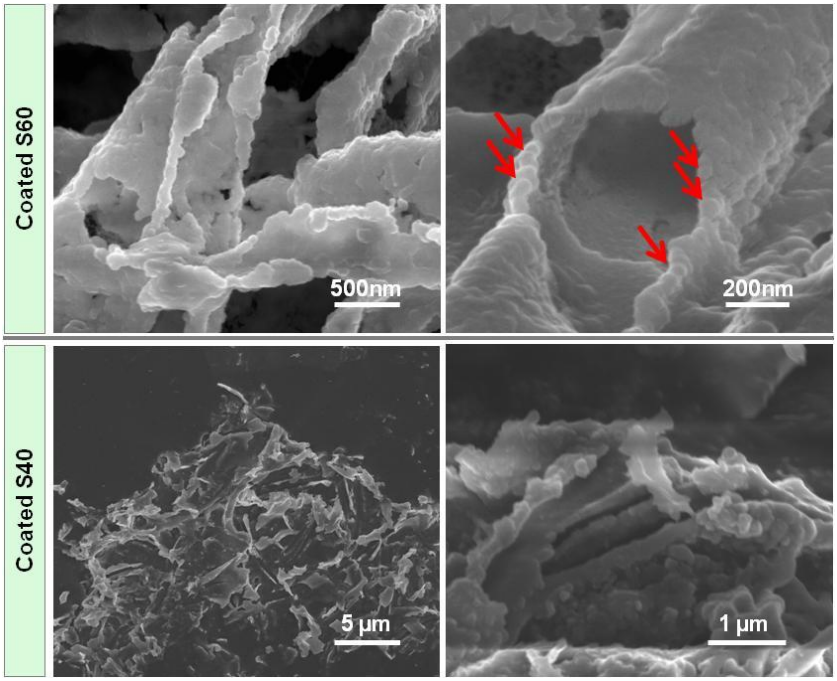

Figure A-24. FESEM picture of the inorganic shell obtained after calcinations of S60 and S40 fibers. (arrows point the particles where the monolayer can clearly be seen)

A.5.6. Mineralization potential – X-ray diffraction:

X-ray diffraction technique was used to determine the nature of the calcium phosphate compound precipitated on the fiber surface after the immersion procedure them in calcium and phosphate solutions (CaP induction). The assay was conducted using a PANalytical X'Pert PRO MPD diffractometer and measuring from 2 to 40° 2θ. After CaP induction, the spectra showed typical peaks of the brushite compound (**Figure A-25**) [20].

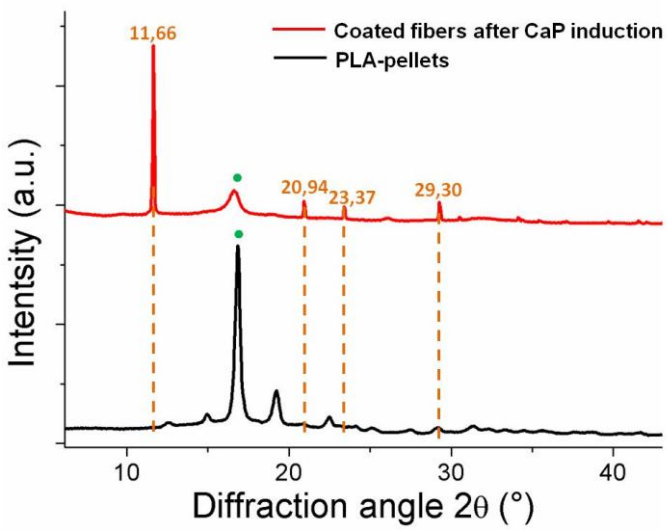

Figure A-25. X-Ray diffraction spectra of PLA pellets (pellets dissolved to obtain the polymeric solution for electrospinning – raw material) coated fibers after CaP induction.

A.5.7. Protocol development:

Figure A-26 presents the typical problems that occurred during the development of the coating protocol for the achievement of a homogeneous coating. Picture 1 shows the covering of the fibrous membrane by a layer of coupling agent. Picture 2 shows the aggregation of glass "blocks" on the fibrous layer. Picture 3 shows the non homogeneous distribution of the glass particles along the fiber length. Picture 4 shows the homogeneous distribution of the particles along the fiber length but only on the upper layers of fibers. These pictures pointed out the importance of carefully setting the different protocol steps to satisfy many essential requirements:

- To find the optimal treatments conditions that enables the different chemical reaction to occur
- To properly clean the fibrous membrane after each treatment
- To precisely control the hydrolysis of the glass precursor mix to have the particles
- To define a protocol that does not alter the fiber morphology
- To develop a reproducible protocol that enables the coating of the fibers in a homogeneous manner (fiber length and scaffold depth)

Based on the images of the coated fibers ultimately obtained with the protocol described in chapter 4, it can be concluded that the protocol has been finally successfully developed.

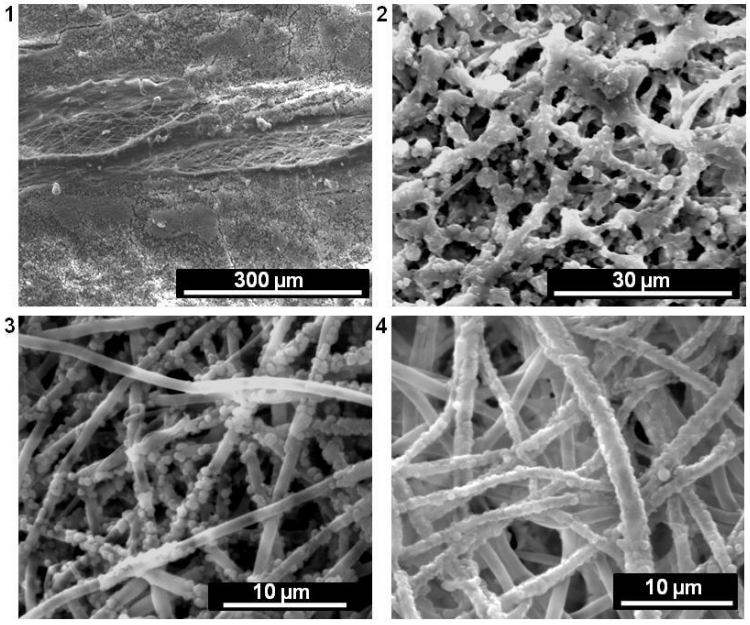

Figure A-26. Problems overcame during the development of the coating protocol to reach a homogeneous coating (FESEM pictures).

A.5.8. Coated fibers - flexibility:

Despite the increase in stiffness and toughness, PLA fibers coated with ORMOGLASSES showed a remarkable flexibility (**Figure A-27**). This is interesting especially for the manipulation of the material

during clinical assays and the conservation of the material structural integrity after implantation, for examples.

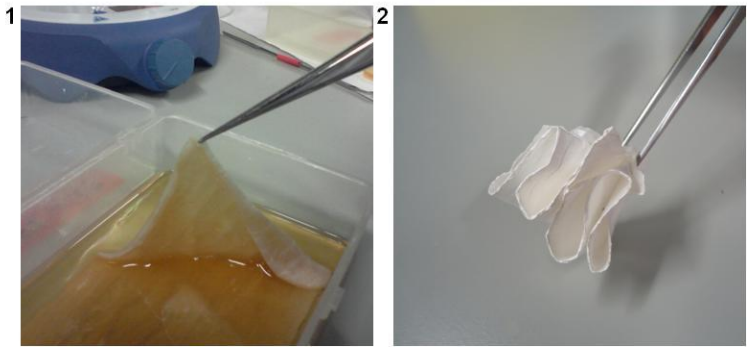

Figure A-27. Pictures of the coated fibers showing the good flexibility of the hybrid membranes in wet and dry conditions.

A.5.9. Gas chromatography:

Although it was evident that fibers possessed residual TEOS molecules in the case of the S60 fibers, TGA did not allow their detection for the S40 ones. Gas chromatography was therefore used to see if silane molecules could be however detected by using another technique, hypothesizing that they were present in the ORMOGLASS particles. Sample of 1*1 cm was incubated for 48h in highly pure water and the supernatant was analyzed using a Trace GC Ultra device (Thermo Scientific ITQ 900). The results shown in **Figure A-28** confirmed that residual TEOS molecules were also found in the S40 coated fibers. Triethoxypropylsilane molecules were detected as well, but in a smaller amount than TEOS.

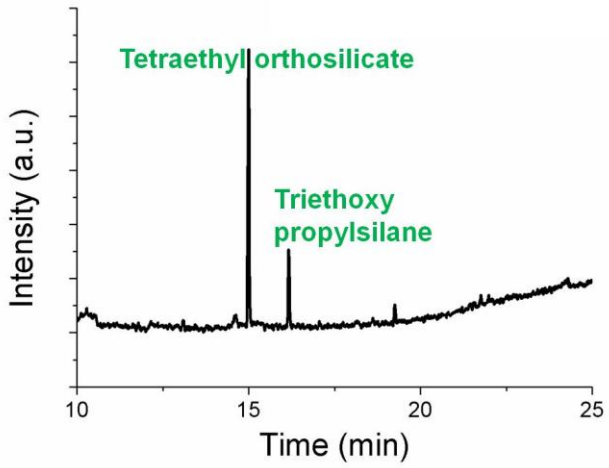

Figure A-28. Gas chromatography spectra obtained for the fibers coated with S40 glass composition.

A.5.10. Fiber crystallinity – X-ray diffraction:

X-ray diffraction technique was used to confirm the increase of crystallinity of the PLA fibers after their coating. A PANalytical X'Pert PRO MPD diffractometer was used. Measurements were acquired between 2 and 40° (2θ) (**Figure A-29**). According to DSC quantification, pristine PLA fibers

exhibited a low crystallinity level that was not detected by X-ray diffraction. On the contrary, for the coated fibers, a characteristic peak of the polymeric phase appeared. X-ray diffraction assay confirmed thus the DSC measurements and the increase of crystallinity after coating. Moreover, it demonstrated that the ORMOGLASS particles prepared by the sol-gel method were indeed amorphous and the crystallinity was not due to an eventual crystalline residual phase present in the ORMOGLASS. The bump observed at low diffraction angles on the spectra of the ORMOGLASS does not reveal any crystallinity [21,22]. Finally, it showed that the processing of the PLA influenced its structural organization: as pellets, PLA was a little bit crystalline, whereas after being electrospun, it is almost completely amorphous. One explanation to that phenomenon can be that the solidification of the liquid jet during the electrospinning process is too fast to enable a possible phase arrangement.

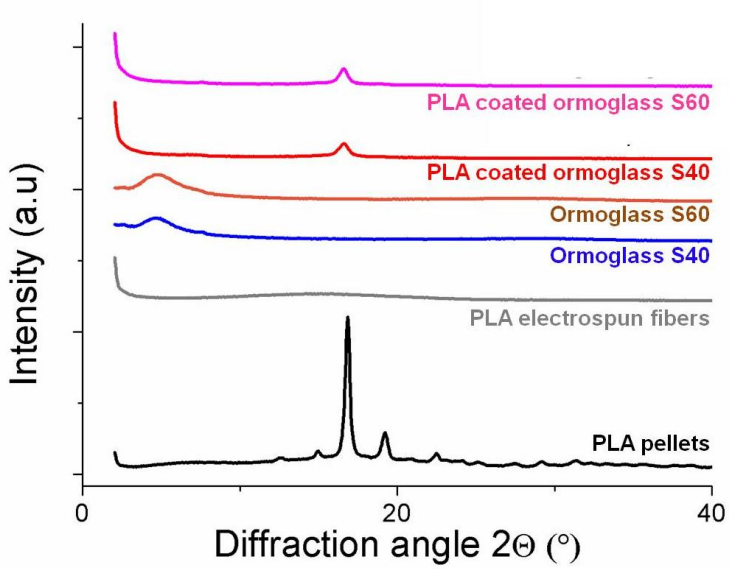

Figure A-29. X-Ray diffraction spectra of PLA pellets (pellets dissolved to obtain the polymeric solution for electrospinning – raw material), PLA electrospun fibers, glasses S40 and S60, and PLA fibers coated with both glass compositions.

A.5.11. Influence of hydrolysis on crystallinity – differential scanning calorimetry:

To explain the increase of crystallinity observed for the fibers before and after coating, it was hypothesized that the hydrolysis of the PLA fibers may have induced these changes. To verify if the hydrolysis was indeed responsible, the crystallinity of PLA fibers and PLA hydrolyzed fibers was determined. The applied hydrolysis conditions were the same than the ones reported in the coating protocol (2min30 in NaCl 0.1M aqueous solution). A Mettler Toledo DSC822e device was used. Samples were heated from 0 to 210°C and crystallinity was calculated according to the following equation [23]:

$$\chi(\%) = \frac{\Delta Hm - \Delta Hc}{\Delta Hm^{\circ}} * 100$$

Where χ is the percentage of crystallinity, $\mathbf{\Delta}H_m$ is the heat of fusion, $\mathbf{\Delta}H_c$ is the heat of the cold crystallization, $\mathbf{\Delta}H_m^{\circ}$ the heat of fusion of a 100% PLA crystalline material (93.1 $J.g^{-1}$ [23]).

The results are reported in **Figure A-30**. The crystallinity of hydrolyzed PLA fibers seemed slightly higher than the one of PLA ones (~ 2%). Knowing that coated fibers exhibited approximately 30% more crystallinity than PLA fibers, it was concluded that the hydrolysis was not the main cause that made crystallize the polymer.

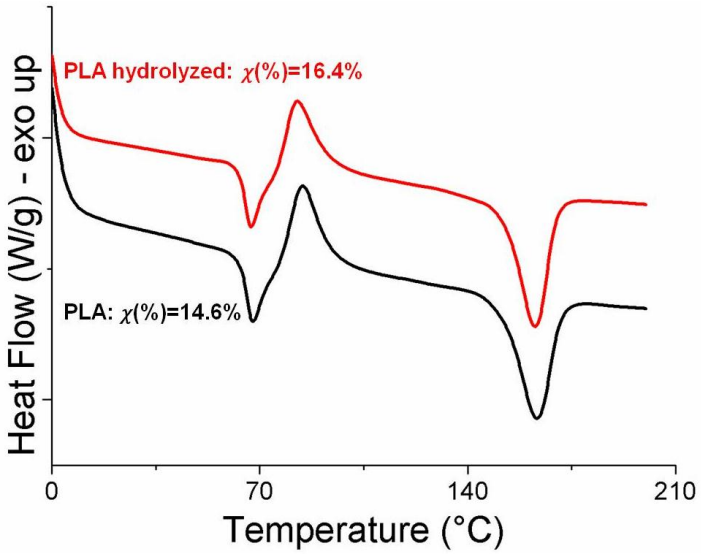

Figure A-30. DSC thermograms and percentage of crystallinity of PLA and hydrolyzed PLA fibers.

A.5.12. Focus ion beam:

Focus ion beam technique was used to observe the tubular structure of the fibers produced by electrospinning. The sample was coated with carbon as for FESEM imaging and loaded to a focus ion beam apparatus (Strata DB235; FEI Co., the Netherlands). Thanks to ions ablation, a square hole was created in the fiber mat in order to obtain a cross section of the tubular structure. Pictures were taken using an accelerating voltage of 5 kV, a working distance of 5 mm and a tilted angle of 45º (**Figure A-31**).

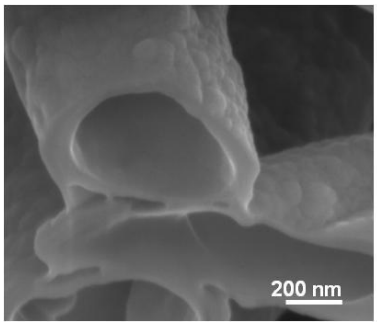

Figure A-31. Fiber cross section obtained by focus ion beam technique showing the tubular structure of the fibers.

A.6. References:

[1] Pickup DM, Valappil SP, Moss RM, Twyman HL, Guerry P, Smith ME, et al. Preparation, structural characterisation and antibacterial properties of Ga-doped sol–gel phosphate-based glass. Journal of Materials Science 2009;44:1858–67.

[2] Ali AF, Mustarelli P, Magistris A. Optimal synthesis of organo-phosphate precursors for sol-gel preparations. Materials Research 1998;33:697–710.

[3] Livage J, Barboux P, Vandenborre MT, Schmutz C, Taulelle F. Sol-gel synthesis of phosphates 1992;148:18–23.

[4] Carta D, Pickup DM, Newport RJ, Knowles JC, Smith ME, Drake KO. Structural studies of bioactive sol-gel phosphate based glasses. Physics and Chemistry of Glasses 2005;46:365–71.

[5] Chowdhury A, Bould J, Londesborough MGS, Milne SJ. The effect of refluxing on the alkoxide-based sodium potassium niobate sol–gel system: thermal and spectroscopic studies. Journal of Solid State Chemistry 2011;184:317–24.

[6] Barringer EA, Bowen K. Formation, packing, and sintering of monodisperse $Ti0_2$ powders. Journal of the American Ceramic Society 1982;65:199–201.

[7] George L, Sankaran K, Viswanathan KS, Mathews CK. Matrix-isolation infrared spectroscopy of organic phosphates. Applied Spectroscopy 1994;48:7–12.

[8] Bagalawis RL, Carlson J, Walsh J. Qualitative method for the detection of triethylphosphate in aqueous solutions. 2003.

[9] Vogel C, Siesler HW. Thermal degradation of poly(ε-caprolactone), poly(L-lactic acid) and their blends with poly(3-hydroxy-butyrate) studied by TGA/FT-IR spectroscopy. Macromolecular Symposia 2008;265:183–94.

[10] Kopinke F, Remmler M, Mackenzie K, Möder M, Wachsen O. Thermal decomposition of biodegradable polyesters - II. Poly(lactic acid). Polymer Degradation and Stability 1996;53:329–42.

[11] Lewandowski JJ, Wang WH, Greer AL. Intrinsic plasticity or brittleness of metallic glasses. Philosophical Magazine Letters 2005;85:77–87.

[12] Antosiewicz J, McCammon JA, Gilson MK. Prediction of pH-dependent properties of proteins. Journal of Molecular Biology 1994;238:415–36.

[13] Böhme U, Scheler U. Effective charge of bovine serum albumin determined by electrophoresis NMR. Chemical Physics Letters 2007;435:342–5.

[14] Sepulveda P, Jones JR, Hench LL. In vitro dissolution of melt-derived 45S5 and sol-gel derived 58S bioactive glasses. Journal of Biomedical Materials Research 2002;61:301–11.

[15] Pereira MM, Clark a E, Hench LL. Calcium phosphate formation on sol-gel-derived bioactive glasses in vitro. Journal of Biomedical Materials Research 1994;28:693–8.

[16] Norlund Christensen A, Krogh Andersen E, Krogh Andersen I, Alberti G, Nielsen M, Lehmann MS. X-ray powder diffraction study of layer compounds. The crystal structure of alpha-$Ti(HPO_4)2.H_2O$ and a proposed structure for gamma-$Ti(H_2PO_4)(PO_4).2H_2O$. Acta Chemica Scandinavica 1990;44:865–72.

[17] La Ginestra A, Massucci MA. Titanium and zirconium acid phosphate dihydrates: thermal behaviour and phase changes of their hydrogen, sodium and strontium forms. Thermochimica Acta 1979;32:241–56.

[18] Šimon I, McMahon HO. Infrared spectra of some alkyl silanes and siloxanes in gaseous, liquid, and solid phases. The Journal of Chemical Physics 1952;20:905–7.

[19] Kurosawa K, Miyano J, Maezono Y, Toshikawa K, Yokotani A. Characterization of SiO_2 films by photo-CVD using a Xe_2 excimer lamp. 203 Meeting Symposia - The Electrochemical Society 2003.

[20] Mandel S, Tas AC. Brushite ($CaHPO_4 \cdot 2H_2O$) to octacalcium phosphate ($Ca_8(HPO_4)_2(PO_4)_4 \cdot 5H_2O$) transformation in DMEM solutions at 36.5°C. Materials Science and Engineering: C 2010;30:245–54.

[21] Manzano M, Arcos D, Rodriguez Delgado M, Ruiz E, Gil FJ, Vallet-Regi M. Bioactive star gels. Chemistry of Materials 2006;18:5696–703.

[22] Carta D, Pickup DM, Knowles JC, Smith ME, Newport RJ. Sol–gel synthesis of the P_2O5–CaO–Na_2O–SiO_2 system as a novel bioresorbable glass. Journal of Materials Chemistry 2005;15:2134–40.

[23] Henton DE, Gruber P, Lunt J, Randall J. Polylactic acid technology. Natural Fibers, Biopolymers and Biocomposites, 2005.

Appendix B

Characterization techniques and methods

B.1. Nuclear magnetic resonance

Developed in 1946, the nuclear magnetic resonance spectroscopy (NMR [1]) is nowadays a very important analytic chemistry technique. It can be used to get information on the molecular structure of known compounds but also to determine the nature of unknown compounds present in a sample by using spectral libraries and interpreting the acquired data carefully. Diverse NMR techniques are available, what enables the analysis of a variety of sample types (solid, liquid, organic, inorganic…) and the investigation of numerous sample features such as its chemical structure, molecule hydrodynamic radius, phase changes or reaction kinetic for examples.

Nuclear magnetic resonance is a physical phenomenon that occurs when the nuclei of some atoms are placed in a strong magnetic field (several Tesla) (**Figure B-1**). Protons and neutrons have an angular moment called "spin". Depending on the number of these nucleons, a nucleus may exhibit an overall spin or not. If the number of protons plus neutrons is odd or that number of protons and number of neutrons are both odd, the nucleus possesses an overall spin. At the contrary, if both of these numbers are even, the nucleus has no spin. NMR principle being based on these spinning properties, nucleus without spin cannot be assessed using NMR technique. However, charged particles such as nuclei with spin generate a magnetic dipole along the spin axis. This represents a fundamental nuclear property that refers to the nuclear magnetic moment of the nucleus. In the presence of an external magnetic field, the magnetic moment of nuclides with spin quantum number 1/2, initially randomly oriented, lines up parallel to the applied field because of the interactions of the nuclear magnetic moment with the field (**Figure B-2, a**). The spin can orientate in the same direction as the field (parallel alignment) or in the opposite one (anti-parallel alignment). Two spin states with different energy can therefore be obtained (**Figure B-2, b**). The difference in energy between these two states depends on the magnetic field strength and the specific studied nucleus. The lower energy level, i.e. the one corresponding to the parallel spin alignment, is the slightly more populated state (Boltzmann distribution). By exciting with electromagnetic radiation (Radiofrequency), it is possible to induce transitions of these nuclei between the energy states. The frequency of radiation necessary to achieve this corresponds to the difference of energy between the two energy levels. The net absorption of energy during the transitions due to the unequal Boltzmann distribution constitutes the basis of the NMR technique.

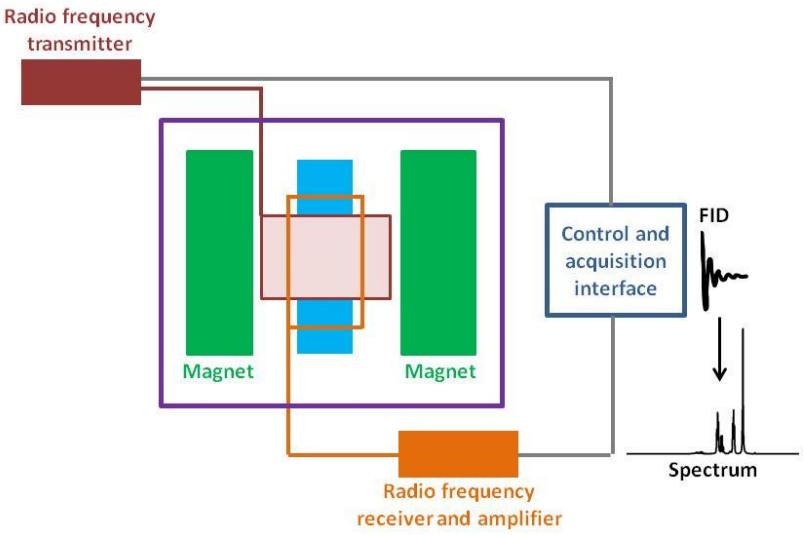

Figure B-1. Schematic NMR set-up.

Nowadays, 1D Fourier transform (FT) NMR instruments are the most widespread approach to collect NMR spectra (frequency domain). FT-NMR enables the excitation of numerous radiation frequencies at the same time and the acquisition of a signal called Free Induction Decay (FID). This FID is characteristic of the relaxation process of the nuclei magnetic moments by which they return back to thermal equilibrium with the magnetic field after the equilibrium perturbation induced by the radio frequency pulse. This signal contains the sum of the frequency of all nuclei present in the sample and is therefore specific of the sample. By applying a Fourier Transformation, this signal can be transposed as a frequency domain spectrum. This obtained spectrum is commonly expressed with reference to a standard compound (tetramethylsilane) to provide a so called "chemical shift" spectra specific of the sample and the atom targeted (H-NMR, C-NMR, Si-NMR…). A signal in the spectra refers to as a resonance frequency. A resonance frequency can be shifted from its initial position (i.e. the one defined by the applied magnetic field) depending on the solvent used, the temperature and the surrounding of other atoms (electronegativity) for examples. The analysis of the chemical shift spectra is therefore a particularly delicate task that requires a lot of knowledge, time and interpretation.

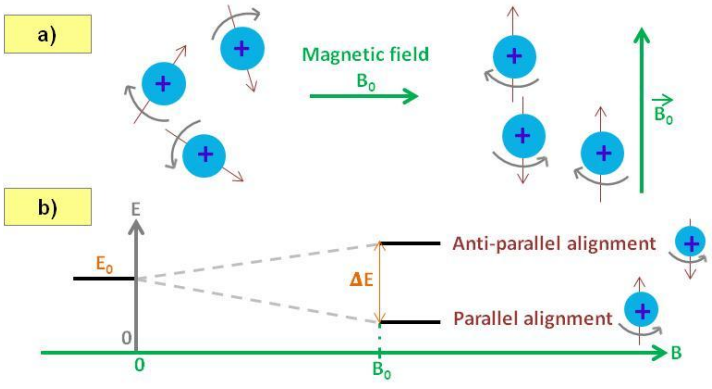

Figure B-2. a) Effect of a strong magnetic field on nuclear magnetic moment and b) energy splitting.

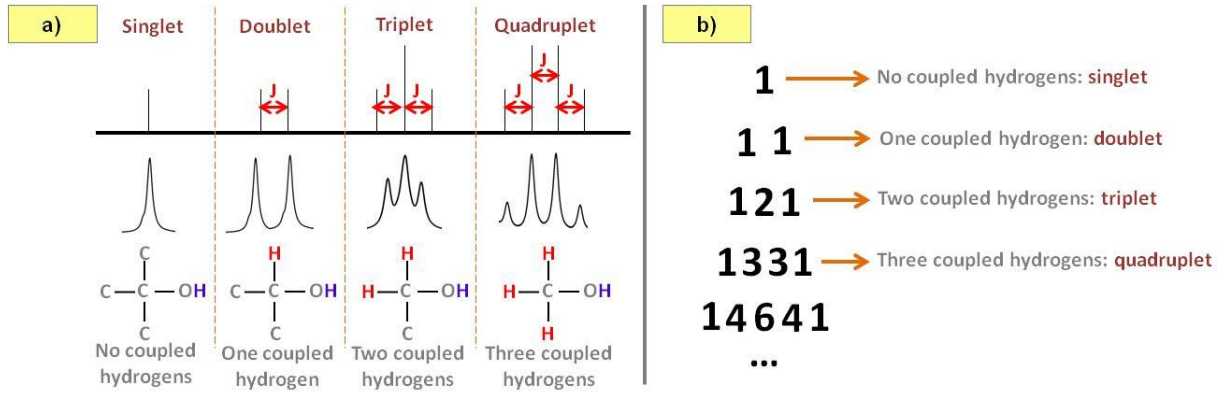

Figure B-3. a) Spin-spin coupling effect and b) relationship between Pascal's triangle and coupling determination.

Another phenomenon that complicates the analysis of the spectra by affecting the chemical shift spectra is the spin-spin coupling effect occurring between neighboring nuclei of the same nature. This happens for sets of interacting nuclei bonded in relatively close proximity and leads to the apparition of signal splitting at the resonance frequency of the given nuclei (**Figure B-3, a**). The coupling constant J is used to define the different existing coupling interactions and the Pascal's triangle to evaluate the exact number of splitting peaks expected to be observed on the spectra of a known molecule. Reversely, the number of splitting can indicates the number of chemically bonded nuclei according to the Pascal's triangle (**Figure B-3, b**) (NB: the Pascal's triangle rule is strictly only true for coupling to a number of identical spins). This is how information on the chemical structure of a sample can be reached.

In order to obtain additional information on a system, pseudo-2D and 2D NMR techniques have been also developed. One of the most popular pseudo-2D is the diffusion ordered NMR spectroscopy (DOSY NMR). It is used to determine the size of a compound or identify independent molecules by assessing the diffusion constants of the different chemical species present in a liquid sample. The measurement of diffusion is carried out by observing the attenuation of the NMR signals when a sequence of radio frequency pulses with delay periods between them is applied to the sample. The degree of attenuation is a function of the magnetic gradient pulse amplitude and occurs at a rate proportional to the diffusion coefficient of the molecule. The spectra acquired by DOSY displays the chemical shift spectra of the sample in correlation with the determined diffusion constants. Another well known 2D technique is the correlation NMR spectroscopy (COSY NMR). It is used to determine which spins are coupled to each other. The measurement is carried out by observing the resonance signal of the sample after applying an initial radio frequency pulse and a second pulse, each other separated by a well defined time called evolution time. The signal acquired is influenced by the coupling of the spins. COSY diagram displays the chemical shift spectra of the sample in correlation with the coupling of the spins.

Although NMR constitutes a powerful analytical tool for numerous scientists, it usually requires a large amount of sample (typically more than tens of micrograms). With too low concentrations (liquids) or sample quantities (solids), the sensitivity of the technique can be indeed a limitation to its profitable use. This is explained by the very small magnitude of energy changes that are involved in the

excitation/relaxation processes of the nuclear magnetic moments and the significant amount of molecules necessary to detect these changes. This is especially true for liquid NMR for which solvent already raise strong signals in the NMR spectra and can thus overlap the eventual signals raising from the molecules their selves. The availability of the studied sample is thus essential to perform this kind of assay.

B.2. Field Emission Scanning Electron Microscopy and Energy Dispersive X-ray Spectroscopy

Introduced by Manfred von Ardenne in the late 30's, the Scanning Electron Microscopy (SEM [2]) is now one of the most used techniques to evaluate surface morphology of materials. Information on the aspect of a sample but also on its structural properties (phase organization, fibers size determination, porosity evaluation…) can be obtained. Images from the macroscopic to the nanometric scale can easily be acquired for almost all solid materials.

The principle of the SEM relies on the interactions between electrons and matter. A schematic representation of the SEM setup is shown **Figure B-4, a**. A source of electrons (typically a tungsten filament) is used to generate an electron beam - usually called primary electron beam. This beam is accelerated through a high voltage and condensed in a thin beam by using electromagnetic lenses. When the sample is struck by the beam, diverse particles are ejected: secondary electrons, backscattered electrons, Auger electrons, X-ray, photons… These particles are the result of the beam penetration in depth what leads to the ejection of particles from a well defined volume directly depending on the accelerating voltage (Monte-Carlo simulation, **Figure B-4, b**). But only the secondary electrons are detected by the SEM device as they usually yield the best resolution. The selection of these electrons is achieved thanks to the suitable positioning of a particles detector. Depending on the topography of the sample, the number of electrons collected changes. It is thus possible to obtain an imaging of the sample by correlating the detected raster to a raster of grey scale.

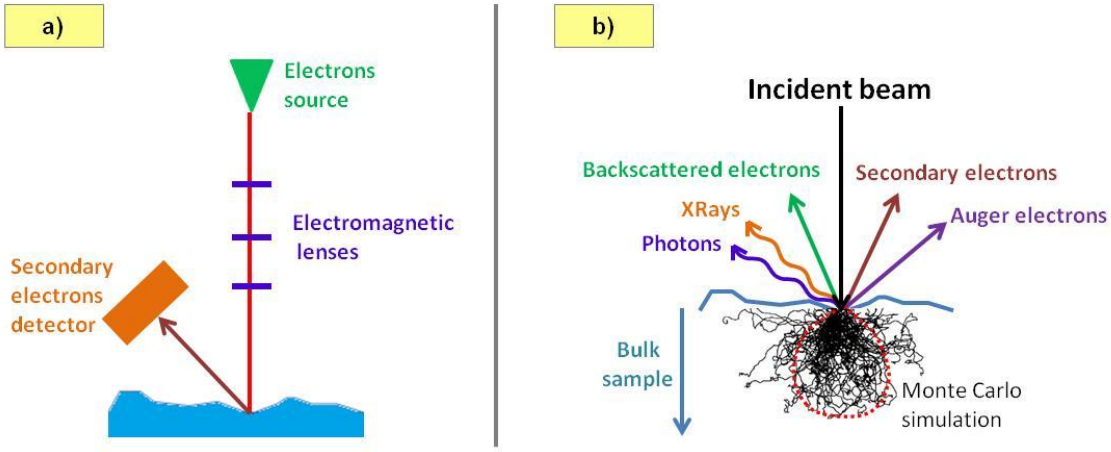

Figure B-4. a) Schematic SEM setup and b) representation of the interactions electrons-matter.

The SEM observations are preferentially operated in high vacuum to obtain pictures with high resolution. But to improve even more the quality of imaging and be able to do observations at greater magnifications, a field emission gun can be used instead of a heated filament. It enables the production of a thinner beam with a greater intensity than the conventional thermionic emitters, and consequently

improves the signal-to-noise ratio. It additionally possesses a better emission life duration and is more reliable.

Another interesting point regarding the use of SEM/FESEM is the possibility to couple the set-up with the Energy Dispersive X-ray Spectroscopy technique (EDS [3] – detection limit: 0.1 weight %). In this case, a specific spectrometer is mounted on the device to detect the emitted X-ray. When an electron beam hits a material surface with enough energy, the electron distribution of the atoms present at the material surface is disturbed (**Figure B-5.** Representation of the processes involved in the emission of X-rays.In fact, an electron of the inner electron shell of the atom (low energy electron) is ejected, consequently leaving a vacancy. An atom from an outer electron orbital (high energy electron) fills then this empty space. The difference of energy between the high and the low energy levels is released in the form of X-rays (relaxation process). This is precisely the difference of energy that is used to identify the atoms present in the material. As each element possesses a unique structure (atomic number), each element emits X-rays with characteristic energies. Hence, based on X-ray energy measurements and database, it is possible to determine the nature of the elements that were excited. But, the acquired spectrum of energy does not only serve for the identification of the material constituents (qualitative method), it is also used for the quantification of the material elemental composition (semi-quantitative method). This is possible because, in addition to the energy, EDS also determines the number of X-rays. The percentage of each element can thus be calculated as a relative value to the other elements.

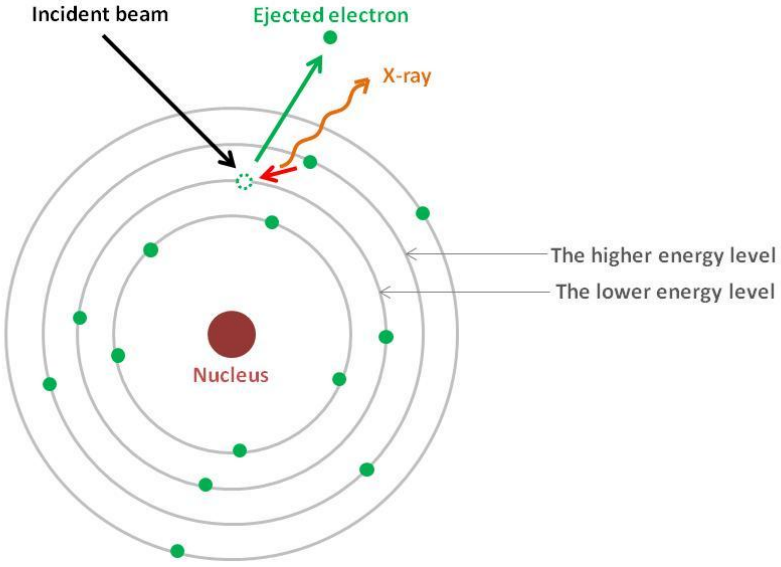

Figure B-5. Representation of the processes involved in the emission of X-rays.

Finally, in addition to that, SEM can be also monitored to allow the visualization of more delicate samples such biological entities. Usually, to be observed using SEM, samples should be completely dried which is generally not the case for samples containing cells for example. With the environment SEM (ESEM), the imaging of wet samples becomes possible thanks to the fixation of the sample using a cryogenic cooling process. The other alternative is to lyophilize carefully the system.

Also, pictures from non conductive samples can even be achieved thanks to this machine. For such samples, a preliminary treatment is nevertheless required: a thin coating of the material surface with a conductive compound (carbon or gold for example). In some cases, low vacuum can be used to image the surface of non conductive material but images with less resolution are achieved due to the low signal to noise ratio mentioned previously.

The high resolution imaging obtained by sequential scanning of the sample and the overlap in the functions of this instrument make this technique one of the most powerful tool for the surface characterization of materials.

B.3. Contact angle measurements

Contact angle measurements are commonly used in tissue engineering to evaluate the wettability of scaffolds [4]. Depending on the measured values, materials can be classified as hydrophilic or hydrophobic templates and also served as a comparative parameter when assessing different scaffolds.

Contact angle measurements can be performed in different ways. The most common one (sessile drop method) consists in the deposition of a small liquid drop on a material and the determination of the angle formed between the drop and the material surface (typically of few mm^2) (**Figure B-6, a**). Any types of liquids can potentially be used. Each measurement corresponds thus to a specific system that implies the material itself (nature, structure, composition), the liquid used (nature and drop volume), and the ambient atmosphere in which the assay is conducted (temperature, pressure). For high-energy surfaces or hydrated samples, another technique is used (captive air bubble). This method relies on the deposition of an air bubble beneath the studied sample surrounded by a liquid phase (**Figure B-6, b**). The contact angle within the bubble shape is measured and subtracted to 180° to obtain the final contact angle result. For medical applications, pure water is usually used but cellular medium can be also considered for that assay. The fluid infiltration is essential regarding the nutrients supply for example and it is thus important to produce a material with good hydrophilic properties.

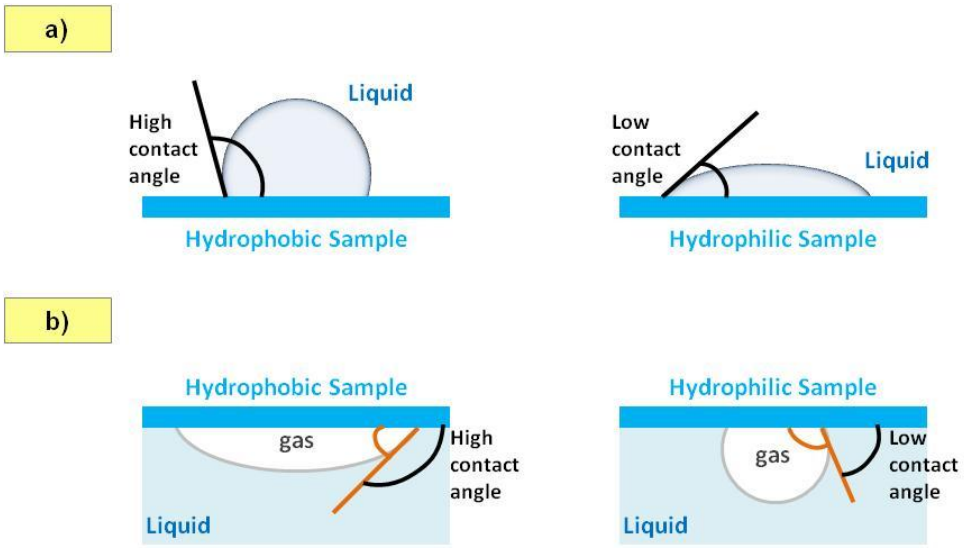

Figure B-6. Contact angle measurements performed on hydrophobic and hydrophilic samples with a) the sessile-drop and b) the captive-bubble methods (the orange angles represent the measured angles and the black ones the complementary angle to the orange ones, i.e values used for interpretation).

Even though several methods have been developed to perform contact angle measurements, the static sessile drop approach is the most widespread. A set up involving a goniometer is used to capture images and it is generally easy and fast to use. It enables the acquisition of images in which the equilibrium contact angle can be observed and measured by using the software provided by the company or external one such as ImageJ with the "Snake" plug-in [5], for example. If the sample is too hydrophilic,

however, no equilibrium contact angle might be reached as the drop immediately penetrates the material. In this case, a video can be recorded instead of a fixed image. The contact angle can then be evaluated by extracting the first image of the drop in contact with the scaffold. Though, this constitutes an indicative contact angle value rather than an accurate measure. But associated to the video, the high hydrophilicity of a scaffold can be demonstrated. Another possibility is the dynamic sessile drop method. It involves the gradual dispensing of a drop on the material surface (up to a determined volume) and the gradual decrease of this volume. Along with the increase and decrease of the drop volume, contact angles (advancing and receding) are measured as a function of time. This is particularly interesting as a range of contact angles can be measured and be used to evaluate the hydrophilicity of the substrate. Though, this approach has not been used in the thesis because of the high velocity that the drop spreads on the developed fibrous mats. In fact, this technique is suitable only when the motion of the liquid on the material occurs at appreciable speed.

Based on the liquid/solid and liquid/vapor interface principles, contact angle measurements give thus an efficient idea of the material wettability. However, it should be pointed out that these measurements are generally done by considering the material as a completely flat and having a smooth surface, which is actually not the case. Several models that introduce these real experimental deformations (for example for rough materials) in the contact angle calculations can thus be found in the literature. Nevertheless, they do not seem to be extensively used by scientists who may consider or not the effect of these deformations for the contact angle determination [6,7].

B.4. Atomic Force microscopy

Invented in the early 80's, the atomic force microscopy (AFM [8]) is used to form images of materials at a very small scale (up to the nano- and atomic-scale), providing precious information on its surface characteristics. It enables for example the determination of the roughness, grain size, phase distribution, topography, and mechanical properties.

Imaging by AFM relies on the physical interactions, namely the interatomic forces (i.e. Van der Waals, capillary, electrostatic, magnetic forces…), which occur when a sharp tip and a solid material are in contact. The tip is fixed to a flexible support called cantilever. When the tip scans the material surface, a cantilever deflection appears due to the forces between the tip and the sample. By measuring the vertical deflection of the cantilever, it is then possible to calculate these forces. The deflection is typically measured by using a laser beam focused on the cantilever and a photodetector placed over the cantilever surface (**Figure B-7**). The reflection of the beam changes depending on the topography of the material. The photodetector converts these changes into electrical signals and a data processor creates then an image according to this electronic feedback. The use of a piezoelectric material (named scanner) controls the movements of the sample in x, y and z directions, enabling thus the scanning of the material surface.

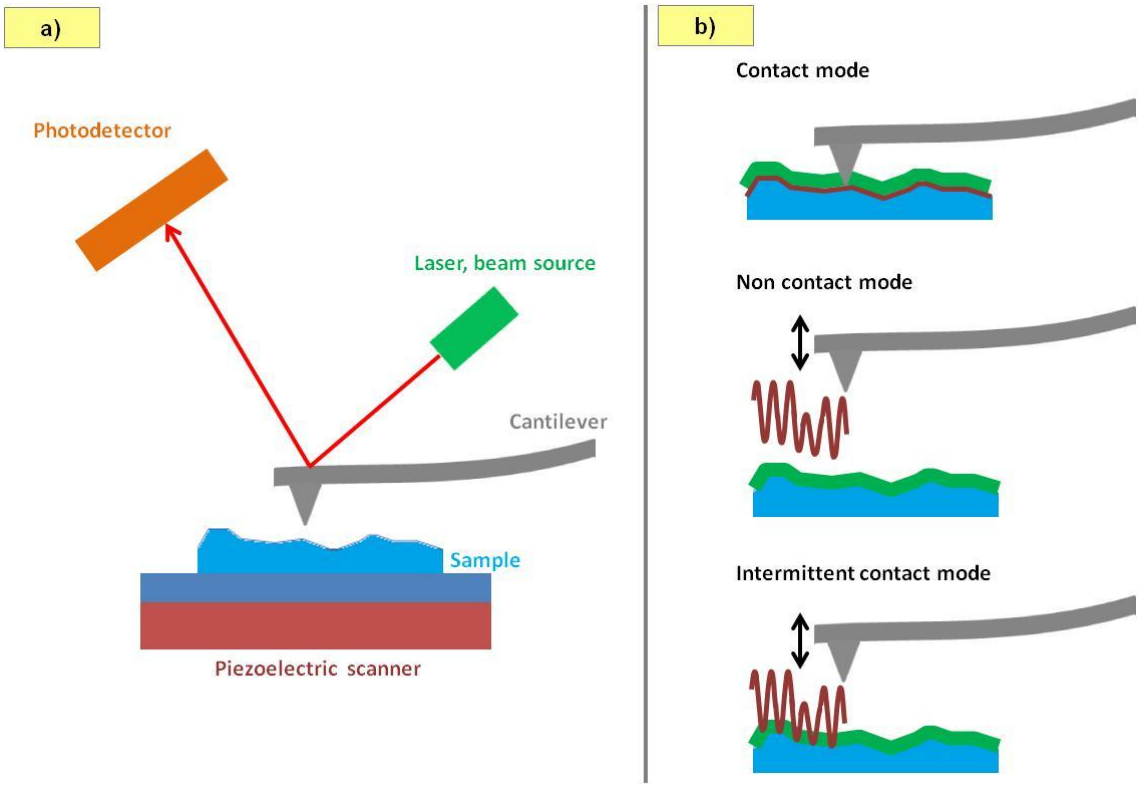

Figure B-7. a) Scheme of an AFM set-up and b) representation of the different AFM operating modes.

AFM can be operated in two different main modes: the contact mode and the non contact mode (both known as static modes) (**Figure B-7, b**). In the contact mode, the tip is in direct contact with the sample and a constant cantilever deflection (i.e. constant height above the sample) is maintained in order

to keep the force between the tip and the sample constant. Motion in z-direction is thus recorded. In the non contact mode, the cantilever is oscillating over the sample. The tip is quite close to the sample but remains in an attractive regime where it does not directly touch the material surface. For this mode, measurements of the changes in resonant frequency or amplitude of the cantilever are performed to obtain the imaging. Drawbacks have been however pointed by scientists regarding the artifacts caused by the use of these two modes. For examples, deformation of the samples due to significant forces between the tip and the samples for the contact mode and detection of the liquid contamination layer usually present on material surfaces in air for the non contact mode. To bypass these problems, intermittent contact mode (i.e. dynamic tapping mode) has been developed. With this approach, the tip does not touch continuously the surface, reducing thus the material degradation. Moreover, the real underlying material surface can be detected without being influenced by the meniscus of the adsorbed fluid. Nowadays the tapping mode is extensively used to assess numerous solid and soft materials.

Unlike SEM, this scanning probe microscopy is a very valuable technique which allows the 3D imaging of the material surfaces. The operating AFM mode closely depends on the surface characteristics of a sample and its hardness. But if the appropriate working conditions are met, all kinds of material can be assessed by AFM.

B.5. Zeta potential measurements

The zeta potential (ZP [9]) is commonly used to assess the electrical potential of colloidal suspension but it can be also used for films, fibers or plates (solid stationary samples). This characteristic of a material is determined by experimental investigations and indirect calculations based on theoretical models.

The ZP process relies on the electrokinetic effects that occur when a material is placed in aqueous medium and an external force is applied to the system (electric field, pressure). Briefly, when a solid material is in contact with an aqueous solution, the material surface charges due to its ionic and dipolar features. This causes a rearrangement of the local free ions in the liquid (**Figure B-8, a**). Depending on the surface charge, ions of the opposite charge will be attracted by the material surface and strongly bonded to it. This increased concentration of ions at the material surface forms an ionic layer called "Stern layer". Outside this layer, a layer named "diffuse layer" resulting from a balance between electrostatic forces and random thermal motion of ions is also formed. In this region, ions (counterions) are less attached to the material surface than the ions of the Stern layer and are therefore susceptible to move if external forces are applied (**Figure B-8, b**). Even though the interfacial boundary between the material and its surrounding environment is constituted by a so called "double layer ", only the diffuse layer is thus specifically used to evaluate the zeta potential.

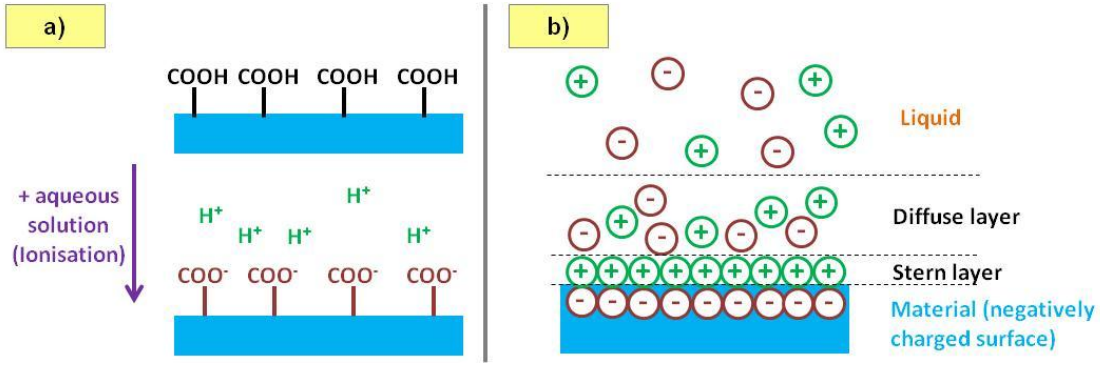

Figure B-8. a) Formation of charges at a material surface in contact with aqueous solution and b) "Double layer" representation.

The determination of the ZP can be achieved by using two main methods: the electrophoresis and the streaming potential. In the first case, an electric field is applied to a colloidal suspension inducing the migration of the charged particles with double layer towards the electrode of opposite polarity. As the mobility of the particles is proportional to the zeta potential, it is then possible to correlate the velocity to the zeta potential by means of the Smoluchowski theories. But for bulk materials, the streaming potential approach is more suitable. In this case, two stationary pieces of the material are organized to form a small channel in which fluid is forced to flow (**Figure B-9**). Consequently, counterions separate at the fluid-solid interface, creating a net motion of unbalanced charge in the solution (ions redistribution). The

transport of these counterions induce therefore an electric current, the streaming current, which can be used to calculate the zeta potential depending on the considered theory.

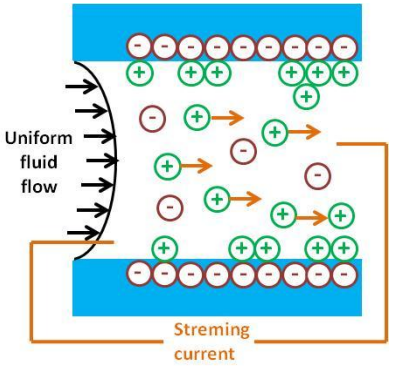

Figure B-9. Schematic representation of the ZP determination involving the streaming current approach.

The value of the zeta potential differs depending on several parameters: the material surface itself (ionization efficiency of surface groups, fluid ions adsorption ability, ion exchange mechanisms with the liquid...), the pH of the solution, the temperature and the nature and the composition of the surrounding medium. Modifying the pH for example, it is possible to determine the isoelectric point of the system; the pH value for which no electrical potential is detected. Initially, the Zeta potential assessment mainly found applications in microfluidics, but it rapidly became essential for tissue engineering and material science (determination of material electrical potential for cellular adhesion and evaluation of surface modification efficiency, respectively). It should be however kept in mind that this method provides information on the surface of the material depending on the nature and composition of the surrounding medium and not on the material surface potential itself. ZP values are indeed calculated regarding the slipping plane of the diffuse layer and not the exact material surface potential. Moreover, the zeta potential cannot be considered as a representative characteristic of the bulk material as the material surface might significantly differs from the bulk.

B.6. Cellular methods

B.6.1. Staining/Fluorescent staining

Biological samples are often difficult to observe under optical microscopes due to their lack of contrast and the non ability of researchers to distinguish the different parts of the specimen. Cells embedded in a gel can be for example particularly delicate to locate in a matrix if the contrast between the cells and the gel is not sufficient. Fluorescent [10] and non fluorescent [11] stainings are often done to tackle this problem and to improve phase contrast for microscope imaging. By selecting the appropriate dye, specific parts of the sample can be treated. Cells and tissues are currently the most stained samples but it can be also helpful for materials. Staining can thus be used to identify the location of biological entities in a matrix, serve as a tool for cell quantification based on imaging, evaluate the cellular morphology and highlight the distribution of some specific proteins but also provide information on the structure of the material (fibers, flakes, lamellaes…) or follow material mobility under dynamic conditions (tracking of nanoparticles in drug delivery for example). Histology, cytology, immunochemistry and material science are the main research areas that daily perform such staining.

B.6.2. Confocal microscope

Samples that are not completely flat and possess a rough surface cannot be properly observed with conventional fluorescent microscope (wide field) due to out-of-focus plane problems and inappropriate imaging. To overcome this, confocal microscope is regularly used [12]. It enables to acquire pictures from planes located at different heights in the sample (up to some micrometers) to obtain a three dimensional reconstructed image of the sample. This way, the morphology of cells cultured on fibrous scaffolds (rolling surface) for example can be assessed without difficulties. It can also provide information on the depth profile of a material (surface) or be used to determine the depth penetration of cells in a template. Apart from the imaging of fixed materials, it also allows the monitoring of biological reactions occurring in living tissues. It is therefore an extremely valuable method for scientists, especially for the ones who aim to investigate biological mechanisms *in vivo* or cellular behavior on 3D templates.

B.6.3. WST and Alamar blue®, proliferation methods

Proliferation assays are commonly used in biology and tissue engineering to evaluate the proliferation of cells on scaffolds and cellular health [13,14]. It implicitly enables the assessment of the material cytotoxicity. Several methods such as WST, LDH and Alamar blue® (commercial name) can be considered for that purpose. Alamar blue® is however the best option to perform this kind of assays because it requires less material than the other two. The same set of replicates is indeed used along the complete experiment whereas for WST and LDH, other sets are needed for each measurement (systematic

destruction of the cell-material system for each time point). Thus, this approach is particularly interesting if the availability of the material is limited.

Proliferation quantification by Alamar blue® is based on an oxidation-reduction reaction which occurs when living cells are in contact with a molecule called rezasurin. Rezasurin is a blue, almost non fluorescent, non toxic and cell permeable dye that is naturally reduced into a fluorescent molecule (resorufin, pink color) inside the cells and then released in the extracellular medium. Resorufin is continuously converted by viable cells due to their metabolic activity. Its extracellular concentration is proportional to the number of healthy cells. The quantification of the living cell number is therefore possible by using a calibration curve preliminary experimentally determined and the measurement of the fluorescence absorption intensity of the cellular medium (supplemented with Alamar blue® at the desired time point). WST relies on the same principles but it involves the reduction of soluble tetrazolium salts (slight red) into formazans (dark red) outside the cells. Cell number is thus also determined by colorimetric measurements. The incubation time is determined specifically for each experiment and cell types. The proliferation of animal but also human cell lines, and bacteria and fungi can be assessed using this method.

B.6.4. Alkaline phosphatase activity, differentiation assay

In vitro differentiation assays are extensively carried out in the field of tissue engineering in order to evaluate the potential of scaffolds to trigger specific cellular responses. For bone regeneration, osteogenic and angiogenic differentiation are targeted. Many methods are used to assess the degree of cell differentiation. Considering the thesis, the description of these methods will be restricted to the tests presented in the manuscript, i.e. alkaline phosphatase (ALP) activity, Western Blot and quantitative real-time polymerase chain reaction.

ALP is an enzyme located at the external membrane of cells, involved in the process of calcification [15]. It is therefore used as a marker for osteogenic activity at the early stages of mineralization. As for the proliferation tests, the measurement of the ALP activity is based on colorimetry. ALP reacts with p-nitrophenyl phosphate (colorless) to form p-nitrophenol (yellow). The level of ALP is directly proportional to the rate of formation of this yellow compound. The results obtained are commonly normalized to cell number or total protein to evaluate the level of cell differentiation.

Western blot is a technique used to detect proteins [16]. This technique is based on protein ability to bind to specific antibodies and electrophoresis principles. A protein can be identified in the cell lysate because antibodies bind to specific amino-acids sequences which are different for each protein. The proteins are separated depending on their size and the antibodies are then used to target the protein of interest. To visualize the complex protein-antibody, a chromogenic substrate, that reacts with the enzyme

attached to the antibody, is utilized. The amount of studied protein can be determined by chemiluminescent detection for example.

Polymerase chain reaction (PCR) is a technology used to determine the levels of gene expression [17]. It is based on the amplification of a very few number of DNA fragments to generate a huge amount of a particular DNA sequence. This is achieved through several successive replications steps of the generated DNA, hence the name of "chain reaction". Quantitative PCR allows the evaluation of the amount of a given sequence present in a sample and the use of specific primers enables the targeting of the desired DNA region to investigate. This selectivity enables, thus, the amplification of DNA regions where bone-associated genes, such as collagen, osteopontin and osteocalcin for examples, are located.

B.6.5. *In vivo* test, biocompatibility assay

For tissue engineering, biocompatibility tests can be performed by implanting artificial matrices in living organisms. The biocompatibility is evaluated by the immunological response induced, the presence of fibrous capsule and the presence of functional cells. In this thesis, the studied materials were subcutaneously implanted in rats. The presence of blood vessels, as well as the infiltration of cells, was additionally assessed. In order to estimate these criteria, histological studies were conducted. These assays consist in the sectioning and staining of tissue extracts to examine them under a light microscope, for example. After extraction from the implantation site, the tissue is prepared for subsequent staining. It is chemically fixed, dehydrated, embedded, frozen and sectioned in thin cuts. It is then stained with different stains depending on what is aimed to be assessed. Hematoxylin and Eosin are used to color the nucleus of cells in blue and cytoplasm in pink, respectively [18]. Masson's Trichrome stain is used to identify connective tissue [19]. The cuts can be immunostained as well. Immunostaining are utilized to detect the presence of a specific protein by using antibodies. For example, von Willebrand factor (protein present in blood vessel basement membranes) can easily be targeted by applying this method [11]. Thus, based on such histological and immuno/-staining assays, it is possible to evaluate biological responses to biomaterials.

B.7. Vibrational Viscometer

Vibrational viscometers are currently considered as one of the most efficient method to determine the viscosity of fluids [20]. Fluids of different natures and within a wide range of viscosity (from 0.3 to 100 000 cP depending on the used device) can be assessed with this technique.

The determination of the viscosity consists in the immersion of a vibrational resonator in a fluid for which the viscosity has to be assessed and the measurement of the resonator's damping when it oscillates (**Figure B-10**). As the viscosity of the fluid influences the resonator's damping, a correlation between the damping and the fluid viscosity can be made. The higher the viscosity, the faster the damping. Several methods involving the measurement of the power supply input, decay time of oscillation or resonator's frequency can be used to determine this damping. The measurement is fast and accurate. The high sensitivity, the continuous readings and the general practical use of this device have surely contributed to its popularity for the measurement of rapid and reliable viscosity.

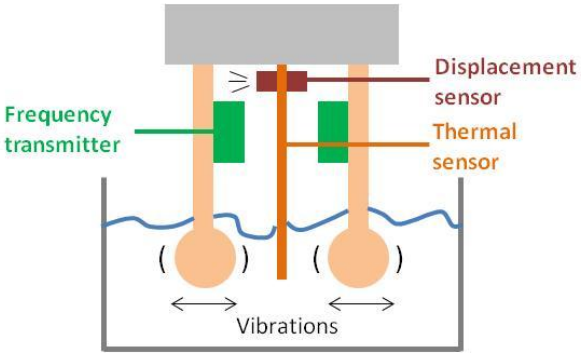

Figure B-10. Schematic vibrational viscometer.

B.8. Differential Scanning Calorimetry

Developped in 1960 by E. S. Watson and M. J. O'Neil, the Differential Scanning Calorimetry (DSC [21]) is the number one thermoanalytical method for the study of the thermal effects and determination of some properties of polymers such as crystallization, cross-linking, glass transition, specific heat or thermal stability-oxidation. It is also nowadays often used for composite materials to assess the influence on these properties of the incorporation of an inorganic phase into an organic one.

This technique measures the heat flow necessary to compensate the thermal effects between a sample and a reference when these two elements are submitted to the same temperature program (detection limit: < 1% volume). The device is constituted by a furnace and an acquisition interface. Basically, one aluminum pan containing the sample and another considered as reference (usually empty pan) are placed in the furnace on a metallic conductor base (**Figure B-11**). The temperature of both pans is continuously measured along the defined program. As long as the temperature difference between the capsules remains equal to zero, the heat flow is constant. When the sample undergoes a phase transition, heat is absorbed (endothermic process) or released (exothermic process) by the sample making vary the difference of temperature between the pans. In order to compensate that temperature difference, an additional heat flow proportional to this difference is sent. The variation of the heat flow is then quantified by means of a thermocouple and recorded by the acquisition interface. DSC measurements provide thus the representative curve of the heat flow in function of the temperature or time. The curve is entirely defined by the thermal characteristics of the sample, what enable to access to its thermal properties by analyzing and interpreting the graphic.

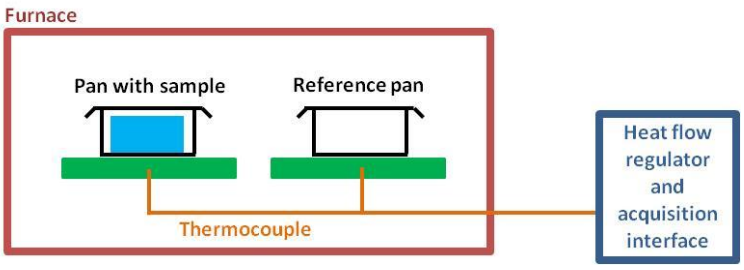

Figure B-11. Schematic DSC set-up.

Even though DSC is mainly used to assess the thermal transitions of polymeric or glass materials, it can also give precious information on the material history and physical aging. It can be moreover combined with another thermoanalytical method: the thermogravimetry analysis which measures the evolution of the sample mass in function of a temperature program. This way, thermal and degradation properties are determined in the exact same working conditions and can therefore be directly compared. It is then possible for example to correlate the thermal effects identified by DSC with the mass changes detected by TGA.

B.9. Thermogravimetry analysis

Thermogravimetric analysis (TGA [21]) is another thermoanalytic method often used parallely or simultaneously to DSC to assess the chemical and physical changes that occur in a sample when it is heated through a controlled temperature program. But unlike DSC which records heat flow data, TGA monitors the material weight loss. It is extensively used to characterize materials for pharmaceutical, petrochemical, environmental, food science and biomedical applications. In the case of tissue engineering for example, it is especially useful to determine the exact amount of the different compounds contained in hybrid scaffolds as the amount of each phase will significantly influence the final mechanical properties and biological response of the produced material.

TGA measures the amount and rate of weight changes associated with transitions and thermal degradation (detection limit: < 1% volume). It consists in placing the sample on a pan which is supported by a precision balance in a furnace (**Figure B-12**). A gas purge is used to control the atmosphere in the device during heating. Depending on what is intended to be assessed (oxidation, dehydratation, decomposition…), reactive or inert gas can be used. The collected results are in the form of a curve that displays the weight percent of the sample as a function of time or temperature. To better observe the different transitions, the relative derivative curve is often used. The observed transitions represent a unique serie of physico-chemical reactions related to the studied material. The two obtained curves are therefore characteristic of each material, what allows the determination of the specific thermal properties of the specimen assessed. To perform such assay, small amount of sample are needed (at least 1 mg) but samples between 2 and 50 mg are preferred. Liquids, powders, films, solids, crystals and fibers for example can be assessed using this method.

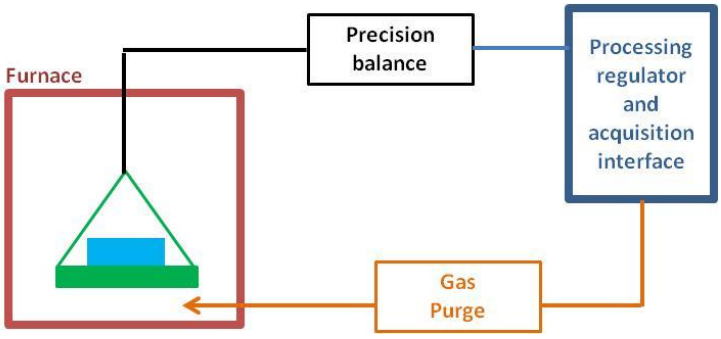

Figure B-12. Schematic TGA set-up.

An interesting advantage regarding the use of TGA is the possibility to combine this device with other techniques such as gas chromatography, mass spectrometry or Fourier transform infrared spectroscopy to identify which compounds decompose, sublimate or vaporize during the material degradation. This approach is known as the TGA-EGA method (Evolved Gas Analysis) and enables thus to correlate the sample weight loss with the different volatile coumpounds or combustion components

released as the material burns. Moreover, because of the high sensitivity of the technique, even very small changes in the weight of the sample can be detected by TGA. It is therefore extensively used to characterize materials containing macro and micro domains as well as nanosized ones. It has however one drawback: it is a destructive technique. This means that after TGA, the sample cannot be re-used for further analyses with other technique. This is also a reason why TGA is often coupled with other techniques and a maximum of information is intended to be collected simultaneously by the use of several devices at once.

B.10. Tensile testings

Tensile tests are fundamental in material science [22]. They enable the determination of the mechanical properties of a material when it is subjected to progressive deformation. Usually, an external uniaxial force is applied following the sample length to place the material in tension (**Figure B-13, a**). Material is then continuously elongated, possibly up to its failure. This measurement provides a curve representing the stress perceived by the material in function of the strain (**Figure B-13, b**). Thanks to this curve, information on the plastic and elastic properties of the specimen can be collected such as Young's Modulus and Yield strength for examples.

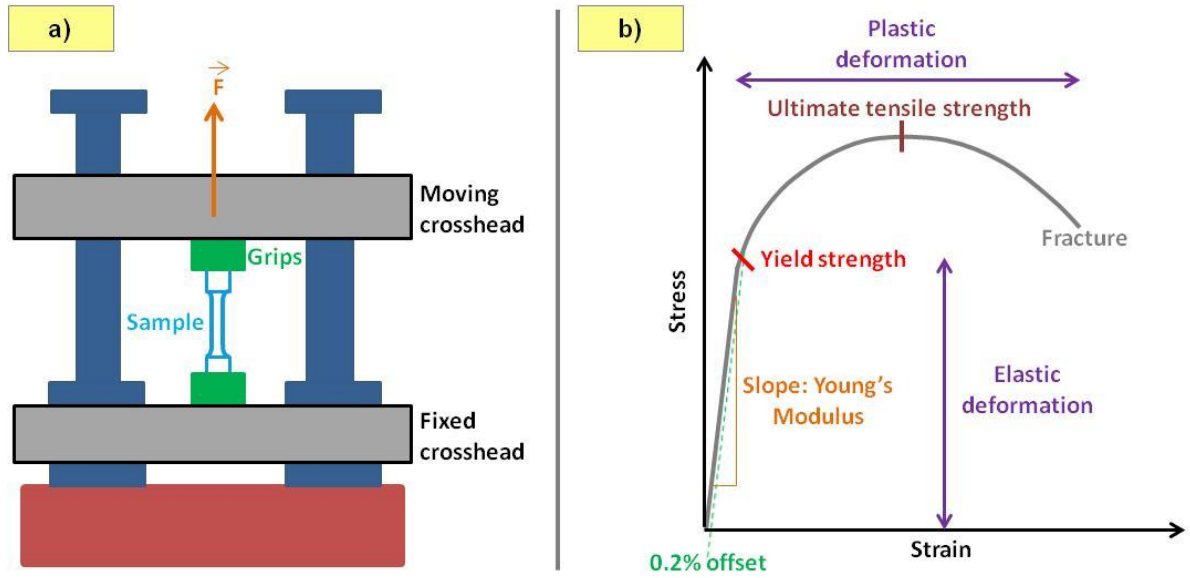

Figure B-13. a) Schematic tensile tests setup and b) example of curve obtained by tensile tests.

Although this method is widely used to evaluate material quality and to help in the design process, several cautions should especially be considered when performing such tests. The first one is the sample alignment which is critical because it can influence the recorded tensile profile of the material. The second one is the possible anisotropy of the material. If the tested specimen is isotropic, then the measurement will not be influenced by the positioning of the sample. But if it is not the case, like for aligned fibers, different results will be obtained depending on the orientation of the material. Before doing tensile assays, the isotropy of the material should be therefore investigated or it should be kept in mind that the determined mechanical properties are specific to a well defined orientation in the case of anisotropic specimens. Finally, the last problem is related to the standardization of the measurements. Even though many materials can be tested following homologated procedures, they are not always simple to satisfy. For hard materials, the gauge shape for example is quite easy to obtain (metals melting into molds, block material cutting and polishing…). However, for softer or brittle samples, producing the exact shape of the gauge can be complicated because of the loss of the structural integrity when handling

the material. For fibers for example, the fibrous organization of the scaffold can be damaged when shaping the layer. Therefore, it is very delicate to prepare the sample without affecting the initial arrangement of the template. This can also have consequences on the information extracted from the curve. Other simpler shapes selected by the operator may be used (stripes) to limit these drawbacks. Results cannot however be presented as standardized values but can be used as indicative data to compare mechanical properties between materials prepared with the same shape.

When all these requirements are met and the assays properly conducted, tensile tests provide useful information for industries which aim to develop materials for specific applications and thus with specific mechanical features. Among others, this includes materials for packaging, aerospace, textile, construction, leisure and biomedical material industries (examination of gloves, suture materials, dressings, bandages…).

B.11. Fourier Transform Infrared Spectroscopy

Fourier transform infrared spectroscopy (FTIR [23]) is a common method used to collect information on the chemical structure of materials. This technique is non-destructive, qualitative and quantitative.

FTIR is based on the absorption of electromagnetic IR radiations by materials. When IR radiations are sent to a sample, some of them are transmitted through the material and others are absorbed at different wavelengths depending on the chemical groups that it possesses. The signal obtained after transmission is called optical interferogram. By measuring the transmitted light intensity and converting it using an algorithm named "Fourier transform", the absorption spectra of the studied material can be obtained (**Figure B-14**). Each functional chemical group has typical absorption wavelengths (nature and vibrational modes), so it is possible to determine the composition and chemical structure of the sample by referring to the tables of the literature. If quantitative analysis is aimed to be done, the peak intensities are the relevant information to assess. The degree of absorption is indeed directly related to the number of absorbing molecules.

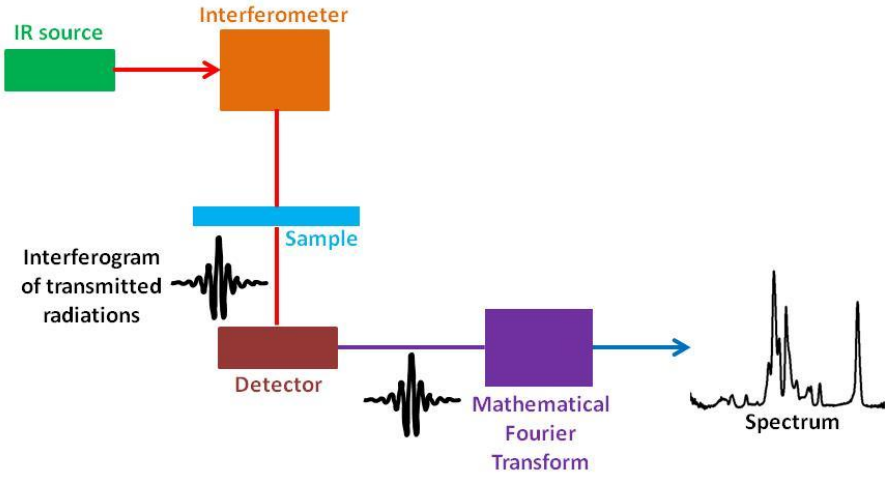

Figure B-14. Schematic representation of a FTIR set-up.

The transmission approach described above is commonly used, for example, for thin films or gases in order to enable the transmission of the incident radiations and their subsequent detection. But for solid or liquid samples, the attenuated total reflectance (ATR-FTIR) is more suitable as it implies the detection of reflected beam instead of the transmitted one. Moreover, it does not require preliminary sample preparation. The material is placed in direct contact with a crystal in which an infrared light passes through. When the beam passes through the crystal, the beam is reflected due to the presence of the sample (**Figure B-15**). This beam is usually named 'evanescent wave' and depends on the angle of beam incidence (penetration depth of the beam < 2µm). To use this method, the refractive index of the crystal should however be higher than the one of the material in order not to 'lose' the light in the sample.

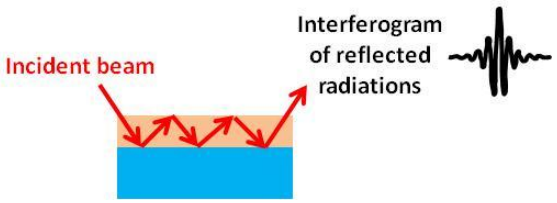

Figure B-15. Beam reflection in ATR-FTIR mode.

The advantages of FTIR spectroscopy are its high sensitivity, accuracy and rapid acquisition. The analysis of the obtained spectra provides valuable information on the elements present in the material as well as their structure. Multi-compounds samples can even be assessed by FTIR for the identification and amount determination of its different constituents. This method is thus very useful for the monitoring of the chemical modifications that occur in hybrids during their degradation, for example. For all these reasons and cost effectiveness, FTIR is nowadays the most used optical spectroscopy for numerous researchers.

B.12. Transmission electron microscopy

Transmission electron microscope (TEM [2]) is one of the most powerful microscopes operated to obtain morphological, compositional and crystallographic information on materials at the nano and angstrom-scale. It is extensively known in material sciences and is regularly used for the determination of particle size, phase composition, phase distribution and crystals organization in composites, for examples.

The principle of this technique relies on the interactions between electrons and the matter. The apparatus is made of a high vacuum chamber in which a beam source is condensed on a sample by electromagnetic lenses (**Figure B-16, a**). But unlike SEM/FESEM, the sample needs to be very thin (typically few nanometers) to allow the transmission of some incident electrons as they should pass through the sample to be detected (**Figure B-16, b**). In fact, when a beam travels through a thin specimen, the amount of scattered electrons directly depends on the density of the material. The presence of multiple phases in a material lead thus to different amount of scattered electrons. The detection of these differences is achieved through a fluorescent screening obtained when the scattered electrons hit a fluorescent screen placed on the bottom of the microscope. Images with different darkness contrasts are thus obtained, revealing the different parts of the material. Images can be directly observed on the machine 'in live' and acquired using a CCD camera.

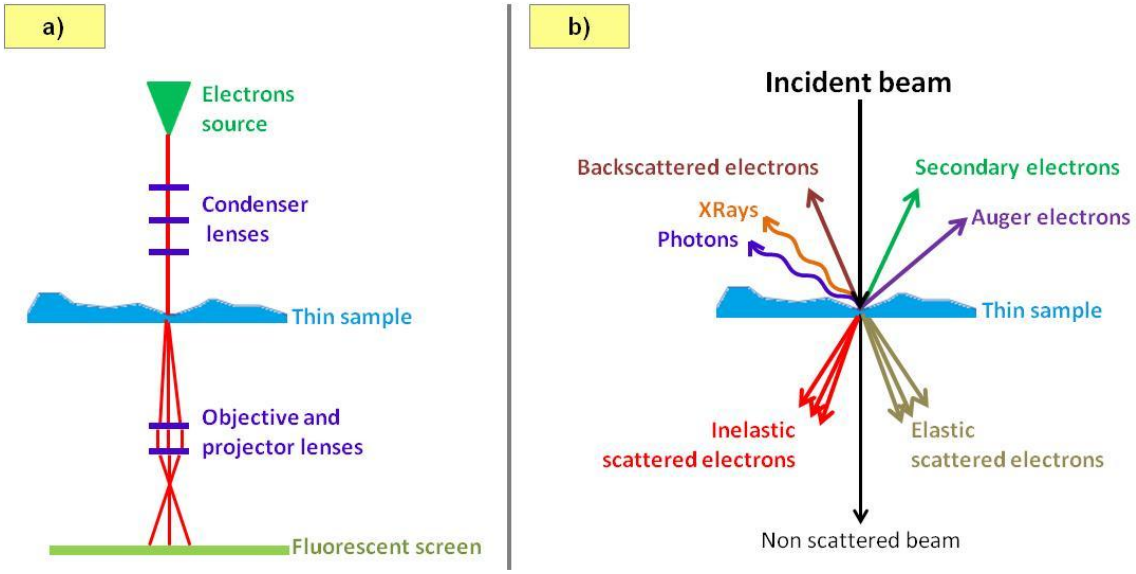

Figure B-16. a) Schematic TEM set-up and b) Schematic representation of the interactions between electrons and a very thin sample.

The operating mode described above is called "bright field mode" and is the most common mode used to perform TEM as it enables the imaging of nanometric phases/compounds with high magnification and the analysis of materials microstructure. The high resolution TEM can even provide data on the structure with atomic scale resolution. But the diffraction mode can also be used to collect precise information on the crystallographic structure of the phases, as well as the nanoanalytical mode to

determine their composition (energy dispersive spectroscopy). Images, diffraction pattern and elemental quantification can thus be correlated to achieve a complete understanding of the material features and general organization/arrangement.

The preparation of samples for TEM differs from one material to another. Materials such as nanofibers or nanoparticles do not generally require specific preparation due to their small dimensions and usual inherent electron transparency. They can thus simply be deposited on the TEM support grid and introduced in the apparatus. For biological samples however, it is more delicate because of the instability of their macromolecular structure under vacuum. Therefore, specimens must be first dehydrated, fixed and then embedded in vitreous ice or resin for examples. Like this, thin slices of the specimen can be obtained. In addition to that, a final staining is often necessary for these kinds of samples in order to improve their electron optical contrast.

In summary, diverse materials can be observed in TEM if a proper sample preparation is done. The ability to collect structural information for a broad range of sample types has consequently raised a significant interest for scientists of numerous research areas. This technique is currently an extremely valuable tool for the assessment of the inner/internal properties/structure of a material and is nowadays often used as a complementary technique to SEM (surface observations). Nanotechnology research and development have been especially improved thanks to this revolutionary device.

B.13. Dynamic light scattering

Particles are currently extensively investigated regarding their potential for drug/cells delivery and composites preparation, for examples. The size of the particles is of paramount importance as different fluid and materials properties can be achieved depending on their size (tribology, rheology, mobility, aggregations, mechanical properties…). The assessment of particle size is mostly performed by using light scattering techniques, especially dynamic light scattering (DLS [24]), which allows the determination of particles up to the nanometric level (typically up to 1 nm).

The principle of DLS relies on the interactions between light and particles in suspension in a liquid. When a laser beam passes through a solution containing particles, the incident light is scattered by these particles (**Figure B-17, a**). This scattering fluctuates because of the Brownian motion of the particles (random collision between the particles and molecules from the liquid) and the constructive and destructive interferences created because of the other surrounding particles. Consequently, this leads to changes in the light intensity. DLS measures these modifications as a function of time using a photon detector placed at a fixed scattering angle. With some elaborated equipment, the detection can also be performed at multiple angles. It is well known that small particles diffuse faster than big ones. By analyzing the time scale intensity fluctuations, it is then possible to evaluate the size of the particles as the diffusion rate of the particles is directly related to their size (**Figure B-17, b**). More than the average size of the particles, DLS can additionally provide information on the size distribution, the diffusion coefficient (Stoke-Einstein relation) and the polydispersity of a suspension. It can moreover be used for molecules or micelles and not only particles.

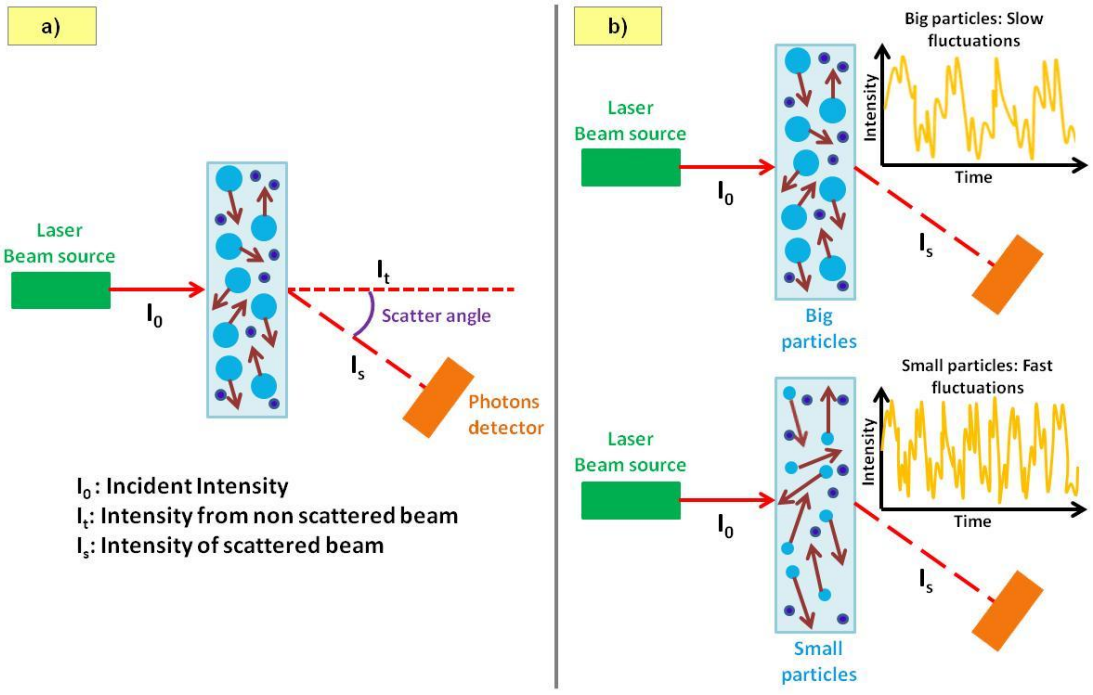

Figure B-17. a) Schematic DLS set-up and light scattering phenomenon and b) influence of particle size on the intensity fluctuations.

This technique presents however some limitations. Many problematic sample features can negatively affect the size measurements and lead to non reliable information: the shape of the particle, their color, their possible important polydispersity and the purification of the suspension. For example, big dust particles present in the suspension would scatter much more light than the small sample particles. As a result, an additional intensity peak which would not be representative of the sample itself would be obtained. The analysis of the data is therefore critical, as a wrong interpretation would result in an incorrect size determination or false evidence of polydispersity. The sample preparation and the analysis should be performed with extreme care and results well discussed because many factors influence the exact particle size determination. For non ideal samples, the data collected with this technique should thus rather be considered as informative data on the system and not as accurate size evaluation method.

Despite these drawbacks, DLS is often used by scientists because it provides useful dynamic information on the sample by the evaluation of the time scale of fluctuations of the beam scattering. However, it is clear that the obtained data should be analyzed with attention and that they might not be easy to interpret in some systems. Lot of reflection and time are usually required to extract the proper information.

B.14. X-ray diffraction

X-ray diffraction is the technique number one to determine the crystalline structure of materials with an atomic resolution and a penetration depth of around 100-200 μm [25]. In material sciences, it is extensively used to assess the arrangement of atoms in a sample, evaluate their size, investigate the chemical bonds or even identify unknown constituents present in multiple phase crystalline samples. It is also used in biology, mainly to determine the structure of proteins.

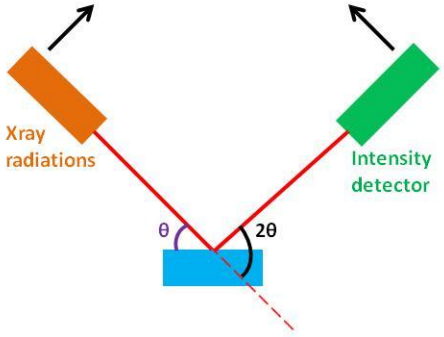

Figure B-18. Schematic XRay diffraction set-up.

The principle of X-ray diffraction is based on the scattering of X-ray electromagnetic radiations by the atoms of a sample (**Figure B-18**). The cloud of electrons is responsible for the diffraction of the incident beam. Its density influences the amplitude of the scattered wave proportionally and the angular dependence of the diffraction depends on the shape of the cloud (electron density probability). However, electron cloud is usually approximated as a symmetric sphere and the effect of a possible dissymmetry is not considered. In this approach, each atom also has a proper characteristic cloud of electrons. The scattering of the incident wave by atoms will thus result in the apparition of different waves that can either be destructive or constructive between each other. The total scattered intensity is the sum of all the waves scattered by the individual atom. Although the main part of the interferences in most directions are destructive, for materials with a periodic arrangement in three dimensions (i.e. crystal lattice), they add in some specific directions constructively. The presence of these interferences is defined by the Bragg's law, which relates the set-up beam features (wavelength and incident angle θ) to the spacing between the diffracting planes (**Figure B-19**). Experimentally, these interferences are observed as spots on a diffraction pattern and are therefore representative of the regular array that repeats in a crystal (unit). However, one pattern is not sufficient to extract global information on a crystal structure and numerous patterns should thus be acquired by rotating the sample step by step. For this reason, the measurement of the scattered intensity in function of different diffraction angle (2θ) is often preferred. This way, a diffraction diagram that contains all information on the sample structure (unique characteristic fingerprint) is directly obtained and it can be compared with database and literature to identify compounds in polycrystalline phases. The locations of the peaks provide for examples information on the

nature of the phase present in the sample whereas the peak heights reflect the phase concentrations. Obviously, this kind of assay cannot be achieved for amorphous materials (disordered structure) as intensity peaks are only due to well-organized arrangement of atoms. X-ray crystallography (diffraction) can however be used for numerous materials such as metals, minerals, salts, organic and inorganic compounds, offering thus a broad range of utilities for diverse fields.

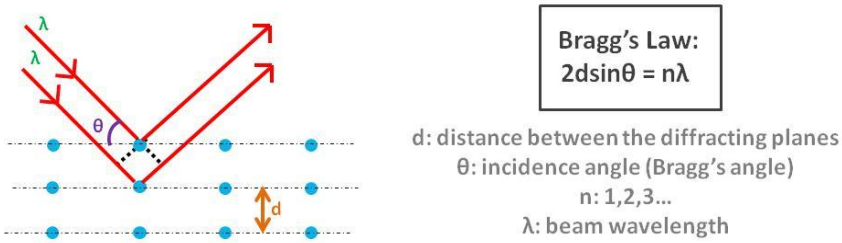

Figure B-19. Crystalline structure-Bragg's law correlation.

B.15. Gas-liquid partition chromatography

Gas-liquid partition chromatography (GLPC [26]) is a common analytical technique used to separate and analyze compounds from a mixture in a gas phase. It can be utilized for a variety of sample types as long as the compounds are volatile and do not degrade with temperature. It enables for example the determination of toxic products in water, detect the presence of contaminants in oils and more generally ensure the quality of substances in the chemical industry.

In gas chromatography, the separation of the compounds relies on the interactions between a liquid stationary phase and vaporized compounds of a sample carried out by an inert gas mobile phase. The set-up is constituted by an injection port, a column, an oven and a detector (**Figure B-20**). The sample, initially in the liquid form, is injected through a chamber that is heated up to a temperature allowing the vaporization of the sample's compounds. The volatile molecules are then carried in the column by a gas stream (carrier gas called mobile phase and passing through the column). The inside of the column is coated with a non volatile liquid phase (called stationary phase). Depending on the affinity of each vaporized molecule with this stationary phase, a separation of the compounds is possible. Indeed, the presence of this stationary engenders the adsorption of the molecules on the walls of the column. The rate at which the molecules progress along the column is directly influenced by the interactions of the compounds with the stationary phase. Molecules with low affinity with the stationary phase will reach the end of the column before compounds more strongly adsorbed on the column walls. The time at which each molecule is detected at the outlet stream of the column is called retention time (i.e. time at which molecules take to travel from the injection chamber to the detector placed at the end of the column) and is characteristic of the compound (**Figure B-21**). Thus, molecules can be identified based on the measured retention time. Thanks to a processing unit, the information collected by the detector is transformed in electrical signals and series of intensity vs retention time peaks are provided to the operator. This graphic is called chromatogram and is analyzed to identify the compounds. Based on the areas under the peaks, it can be also used to determine the relative quantities of the compounds. Another advantage of using GLPC is the possibility to couple this device with other techniques such as mass spectrometry to complete the information collected by GLPC. Combined together, these techniques enable the detection of compound even in a very small amount (up to 2 µg/L approximately). It is highly effective and sensitive and allows the identification of a huge range of compound without having to know their retention time. In fact, in the case that the compound has never been analyzed by GLPC as a pure compound and the retention time is not known, the MS become an extremely useful complement that provide the nature of the compounds based on its ionization and the measurement of its mass to charge ratios.

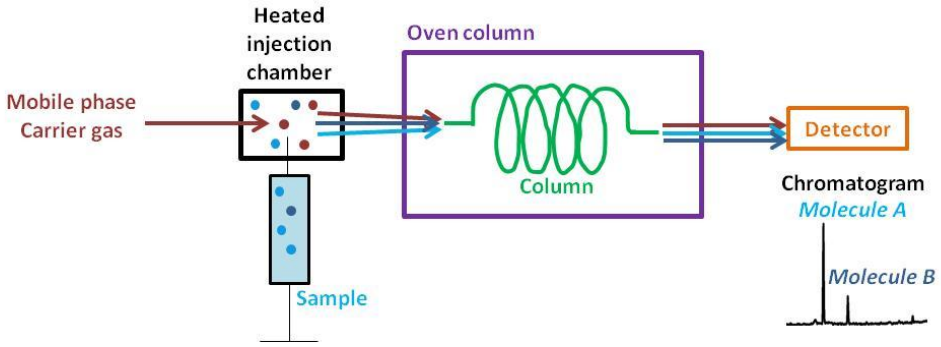

Figure B-20. Schematic GLPC set-up.

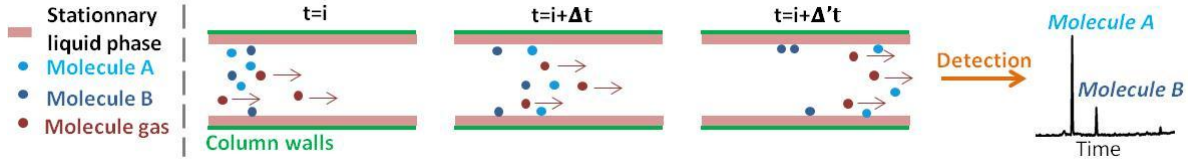

Figure B-21. Principle of particles retention using a stationary liquid phase coating the column walls. Influence of the affinity between the compounds and the stationary phase.

B.16. References

[1] James TL. Fundamentals of NMR. Nuclear Magnetic Resonance, 1998.

[2] Bozzola JJ, Russell LD. Electron microscopy: principles and techniques for biologists. 1999.

[3] Bertin EP. Introduction to X-ray spectrometric analysis. 1978.

[4] Yuan Y, Lee TR. Contact angle and wetting properties. Surface Science Techniques, vol. 51, 2013.

[5] Rasband WS. Image J. US National Institute of Health, Bethesda, USA, Http://imagej.nih.gov/ij/ 1997:2014.

[6] Han D, Steckl A. Superhydrophobic and oleophobic fibers by coaxial electrospinning. Langmuir 2009;25:9454–62.

[7] Drelich J, Miller JD, Good RJ. The effect of drop (bubble) size on advancing and receding contact angles for heterogeneous and rough solid surfaces as observed with sessile-drop and captive-bubble techniques. Journal of Colloid and Interface Science 1996;179:37–50.

[8] De Oliveira RRL, Albuquerque DAC, Cruz TGS, Yamaji FM, Leite FL. Measurement of the nanoscale roughness by atomic force microscopy: basic principles and applications. Atomic force microscopy - Imaging, measuring and manipulating surfaces at the atomic scale, 2012.

[9] Kirby BJ, Hasselbrink EF. Zeta potential of microfluidic substrates: 1. Theory, experimental techniques, and effects on separations. Electrophoresis 2004;25:187–202.

[10] Beutner EH. Immunofluorescent staining: the fluorescent antibody method. Bacteriological Reviews 1961;25:49–76.

[11] Pusztaszeri MP, Seelentag W, Bosman FT. Immunohistochemical expression of endothelial markers CD31, CD34, von Willebrand factor, and Fli-1 in normal human tissues. The Journal of Histochemistry and Cytochemistry 2006;54:385–95.

[12] Pawley JB (Ed.). Handbook of biological confocal microscopy. 2006.

[13] Uo M, Mizuno M, Kuboki Y, Makishima A, Watari F. Properties and cytotoxicity of water soluble Na_2O-CaO-P_2O_5 glasses. Biomaterials 1998;19:2277–84.

[14] Boland ED, Telemeco TA, Simpson DG, Wnek GE, Bowlin GL. Utilizing acid pretreatment and electrospinning to improve biocompatibility of poly(glycolic acid) for tissue engineering. Journal of Biomedical Materials Research Part B, Applied Biomaterials 2004;71B:144–52.

[15] Golub EE, Boesze-Battaglia K. The role of alkaline phosphatase in cartilage mineralization. Current Opinion in Orthopaedics 2007;18:444–8.

[16] Burnette WN. "Western blotting": electrophoretic transfer of proteins from sodium dodecyl sulfate-polyacrylamide gels to unmodified nitrocellulose and radiographic detection with antibody and radioiodinated protein A. Analytical Biochemistry 1981;112:195–203.

[17] Arya M, Shergill IS, Williamson M, Gommersall L, Arya N, Patel HRH. Basic principles of real-time quantitative PCR. Expert Review of Molecular Diagnostics 2005;5:209–19.

[18] Monem AS, ElBatal HA, Khalil EMA, Azooz MA, Hamdy YM. In vivo behavior of bioactive phosphate glass-ceramics from the system P_2O_5-Na_2O-CaO containing TiO_2. Journal of Materials Science Materials in Medicine 2008;19:1097–108.

[19] Li Z, Ramay HR, Hauch KD, Xiao D, Zhang M. Chitosan-alginate hybrid scaffolds for bone tissue engineering. Biomaterials 2005;26:3919–28.

[20] Viswanath DS, Ghosh TK, Prasad DHL, Dutt NVK, Rani KY. Viscometers. 2007.

[21] Menczel JD, Bruce Prime P. Thermal analysis of polymers, fundamentals and applications. 2009.

[22] Soboyejo W. Mechanical properties of engineered materials mechanical engineering 2007:2007.

[23] Stuart B. Infrared spectroscopy: fundamentals and applications. 2004.

[24] Pecora R. Dynamic light scattering: applications of photon correlation spectroscopy. 1985.

[25] Stanjek H, Häusler W. Basics of X-ray diffraction. Hyperfine Interactions 2004;154:107–19.

[26] McNair HM, Miller JM. Basic gas chromatography. 1997.

Appendix C

Work dissemination

C.1. Publications

• April 2014: ACS Applied Materials & Interfaces – published
(http://pubs.acs.org/doi/full/10.1021/am500885v)
"Angiogenesis in bone regeneration: tailored calcium release in hybrid fibrous scaffolds"
(O. Castano, **N. Sachot**, E. Xuriguera, E. Engel, J. A. Planell, J-H Park, G-Z Jin, T-H. Kim, J-H. Kim, H-W. Kim)

August 2013: Journal of the Royal Society, Interface – published
(http://dx.doi.org/10.1098/rsif.2013.0684)
"*Hierarchically engineered fibrous scaffolds for bone regeneration*"
(**N. Sachot**, O. Castano, M. A. Mateos-Timoneda, E. Engel, J. A. Planell)

• Submitted articles
"Novel hybrid materials for tissue engineering: a coating approach"
(**N. Sachot**, O. Castano, M. A. Mateos-Timoneda, A. Velders, E. Engel, M. Lewandowska, J. A. Planell)

"Optimization of blend parameters for the fabrication of polycaprolactone-silicon based ormoglass nanofibers by electrospinning"
(**N. Sachot**, O. Castano, J. A. Planell, E. Engel)

"*Hybrid scaffolds for Tissue Engineering*", Review
(**N. Sachot**, O. Castano, E. Engel)

• In preparation
"*PLA/bioactive glass blends to produce fibers for vascularized bone regeneration*"
(**N. Sachot**, O. Castano, J. A. Planell, E. Engel)

"*In vitro degradation behavior of PLA/bioactive glass fibers: a characterization study*"
(**N. Sachot**, A. Roguska, O. Castano, M. Lewandowska, J.A Planell, E. Engel)

C.2. Presentations

• September 2013: European Materials Research Society (eMRS) Fall Meeting, Warsaw, Poland
Poster presentation: "*In vitro degradation study of hybrid PLA-bioactive glass fibers intended for bone tissue engineering applications*"
(**N. Sachot**, A. Roguska*, M. Lewandowska, O. Castano)

• May 2013: eMRS Spring Meeting, Strasbourg, France
Oral presentation 1: "*Engineered electrospun polymeric scaffolds: a bioactive coating aiming to control cell fate*"
(**N. Sachot***, O. Castano, M. A. Mateos-Timoneda, E. Engel, M. Lewandowska, J. A. Planell)

Oral presentation 2: "*Towards hybrid PLA-organic bioactive glass fibers inducing vascularized bone regeneration*"
(**N. Sachot***, O. Castano, E. Engel, M. Lewandowska, J. A. Planell)

• September 2012: eMRS Fall Meeting, Warsaw, Poland
Oral presentation: "*Engineered electrospun polymeric scaffolds: a bioactive coating approach*"
(**N. Sachot***, O. Castano, E. Engel, J. A. Planell)

• June 2012: 5th IBEC Symposium, Barcelona, Spain
Flash oral and poster presentation: "*Engineered polymeric surfaces: a new protocol to coat electrospun nanofibers with bioactive glasses*"
(**N. Sachot***, O. Castano, M. A. Mateos-Timoneda, E. Engel, J. A. Planell)

• November 2011: Bioceramics 23 - International Society for Ceramics in Medicine, Istanbul, Turkey
Oral presentation: "*Electrospun polylactic acid fibers covalently coated with a Silicon-based bioactive glass: a nanostructured composite scaffold for bone tissue engineering*"
(**N. Sachot***, O. Castano, M. A. Mateos-Timoneda, E. Engel, J. A. Planell)
Award second best oral presentation

• October 2011: 4th IBEC Symposium, Barcelona, Spain
Poster presentation: *"Hybrid osteogenic and angiogenic electrospun fibers for bone tissue engineering*"
(**N. Sachot***, O. Castano, J. A. Planell, T. H. Kim, J. H. Kim, H. W. Kim)

• June 2010: 3d IBEC Symposium, Barcelona, Spain
Poster presentation: "*Bioactive hybrid fibers for bone regeneration*"
(**N. Sachot***, O. Castano, J. A. Planell, H.-W. Kim)